CM63-12914
Code 1

TECHNICAL MEMORANDUM
X-182

SOME EFFECTS OF VARIATIONS IN DENSITY AND AERODYNAMIC

PARAMETERS ON THE CALCULATED FLUTTER CHARACTERISTICS

OF FINITE-SPAN SWEPT AND UNSWEPT WINGS AT

SUBSONIC AND SUPERSONIC SPEEDS

By E. Carson Yates, Jr.

Langley Research Center
Langley Field, Va.

Declassified February 6, 1962

NATIONAL AERONAUTICS AND SPACE ADMINISTRATION

WASHINGTON   January 1960

copy

Codd 1

NATIONAL AERONAUTICS AND SPACE ADMINISTRATION

TECHNICAL MEMORANDUM X-182

SOME EFFECTS OF VARIATIONS IN DENSITY AND AERODYNAMIC

PARAMETERS ON THE CALCULATED FLUTTER CHARACTERISTICS

OF FINITE-SPAN SWEPT AND UNSWEPT WINGS AT

SUBSONIC AND SUPERSONIC SPEEDS

By E. Carson Yates, Jr.

L
4
6
4

SUMMARY

Subsonic and supersonic flutter calculations have been made by the method of NACA Research Memorandum L57L10 for 12 swept and unswept wings in order to evaluate the effects on calculated flutter characteristics of variations in aerodynamic parameters and flow density. Results are compared with experimental flutter data. With linearized-theory aerodynamic parameters used as the basis, the variations of aerodynamic parameters consisted of systematic constant-percent-chord changes in local aerodynamic center and systematic changes in the magnitude (but not in the distribution) of section lift-curve slope. These calculations indicated that when local aerodynamic centers are close to local centers of gravity, flutter calculations become extremely sensitive to small changes in aerodynamic-center position and calculations based on linearized-aerodynamic theory are likely to be considerably in error. If the local aerodynamic centers move rearward of the elastic axis, it is possible to have flutter speed increasing with increasing lift-curve slope. When local aerodynamic centers are sufficiently forward of the elastic axis and of the local centers of gravity, calculated flutter speed for a given wing varies approximately as the inverse square root of the lift-curve slope and as the inverse square root of the distance between aerodynamic center and center of gravity.

Flutter calculations made for the 12 wings at several values of flow density indicated that flutter at constant dynamic pressure was indicated only for unswept wings for which local aerodynamic centers were not close to local centers of gravity.

INTRODUCTION

Reference 1 presented a strip-theory type of flutter calculation procedure for finite-span swept and unswept wings based on spanwise distributions of lift and pitching moment derived from distributions of aerodynamic parameters associated with the undeformed wing in steady flow.[1] In references 1 and 2 comparisons of experimental flutter data for several wings with flutter characteristics calculated for these wings by the modal-analysis method of reference 1 indicated that the method yielded accurate flutter results for a broad range of wings at subsonic, transonic, and supersonic speeds. However, for some of the unswept wings of reference 1, calculated flutter speeds were high compared with those obtained by experiment at supersonic Mach numbers. Since these calculations utilized steady-flow aerodynamic parameters obtained from linearized-aerodynamic theory, it was hypothesized that for these unswept wings the absence of close agreement between experimental flutter speeds and those calculated from linearized-theory aerodynamics was related to the close proximity of the local aerodynamic centers to the local centers of gravity at supersonic speeds and to the fact that linear theory predicts too-far-rearward aerodynamic centers. This hypothesis was supported in reference 2 by the greatly improved agreement between experimental flutter characteristics and those calculated by using steady-flow aerodynamic parameters obtained from flight test. (See figs. 16 and 18 of ref. 2.) The local aerodynamic centers obtained from the flight-test load distributions were characteristically forward of those predicted by linear theory.

In view of this demonstrated inadequacy of linearized-aerodynamic theory and in view of the apparent sensitivity of some flutter calculations to small changes in aerodynamic parameters, it was considered desirable to obtain some quantitative indications of the effect on calculated flutter characteristics of variations in the aerodynamic parameters used. Accordingly, flutter calculations are presented herein for some of the swept and unswept wings of references 1 and 2 in which systematic modifications have been applied to the linearized-theory aerodynamic parameters of reference 1. Specifically, two sets of subsonic and supersonic flutter calculations have been made for three wings of aspect ratio 4.0, taper ratio 0.6, quarter-chord sweep angle 45°, and varying chordwise center-of-gravity positions and for four unswept wings of aspect ratios 4.0 and 7.4

L
4
6
4

---

[1]In the method of reference 1, spanwise distributions of steady-flow section lift-curve slope and local aerodynamic center for the undeformed wing are used in conjunction with the "effective" angle-of-attack distribution resulting from the assumed vibration modes in order to obtain values of section lift and pitching moment. Circulation functions modified on the basis of loadings for two-dimensional airfoils oscillating in compressible flow are employed to account for the effects of oscillatory motion on the magnitudes and phase angles of the lift and moment vectors.

and taper ratios of 0.6 and 1.0. The first set of calculations employed spanwise distributions of section lift-curve slope obtained from linear theory and spanwise distributions of linear-theory local aerodynamic center to which various constant-percent-chord increments had been added. The second set of calculations employed distributions of linear-theory section lift-curve slope which had been multiplied by various constant factors and distributions of linear-theory local aerodynamic centers. The first set of calculations thus indicates the sensitivity of calculated flutter characteristics to arbitrary constant-percent-chord changes in local aerodynamic center, whereas the second set indicates sensitivity to arbitrary changes in the magnitude (but not in the distribution) of local lift-curve slope.

The magnitude of section lift-curve slope and the position of local aerodynamic center are, of course, not arbitrarily variable on a physical wing. Indeed, these parameters are uniquely determined by wing geometry and flow conditions. The two sets of calculations mentioned previously, therefore, do not necessarily represent physically attainable conditions. They do, however, give some indication of the reliability of linear-theory results and may also be used to obtain an indication of possible effects on flutter characteristics of finite-thickness airfoil shapes or other factors which might change aerodynamic parameters from the linear-theory values.

Subsonic and transonic flutter experiments (refs. 3 to 5) have indicated that flow density affects wing flutter characteristics in such a way that for a given wing at a given Mach number flutter generally occurs at approximately constant dynamic pressure, at least over a range of mass ratio (ratio of fluid mass to wing mass) normally encountered in flight and wind-tunnel testing. However, because of the number of variables involved, it is difficult to determine accurately by experiment the variation of flutter characteristics with density. The effects of density variation on flutter characteristics have previously been calculated by using two-dimensional incompressible-flow aerodynamic parameters. (See refs. 3 to 5, for example.) As indicated in the discussion of reference 5, these calculations may be expected to indicate flutter at approximately constant dynamic pressure only for high-aspect-ratio swept wings or for unswept wings. Inasmuch as the two-dimensional incompressible-flow type of flutter calculation used in reference 5 can be considered as a special case of the flutter calculation method of reference 1, it is considered desirable to examine the effect of density variations on flutter characteristics calculated by the method of reference 1 for several finite-span swept and unswept wings at subsonic and supersonic Mach numbers. Accordingly, flutter characteristics calculated by the method of reference 1 are presented herein as a function of flow density (or mass ratio) for 12 wings with sweep angles from 0° to 52.5°, aspect ratios from 2.4 to 7.4, taper ratios of 0.6 and 1.0, and center-of-gravity positions between 34 percent chord and 59 percent chord. The results of these

calculations are examined to determine whether and under what conditions flutter at constant dynamic pressure is indicated.

In order to correlate data obtained under varying test conditions, the results of many recent flutter investigations (refs. 6 to 10, for example) have been presented as the ratio of experimental flutter speed to that calculated by using two-dimensional incompressible-flow aerodynamic parameters. As indicated in references 1 and 2, it has been previously assumed that the resulting flutter-speed ratio was only slightly dependent on density. This supposition presupposes that density changes will affect experimental flutter speeds and those calculated from two-dimensional incompressible-flow aerodynamics in approximately the same way. Reference 5 indicated that this supposition was not valid for low-aspect-ratio swept wings at transonic Mach numbers. In the present report the dependence of the flutter-speed ratio on flow density at subsonic and supersonic Mach numbers is examined by using the flutter calculation procedure of reference 1 for the 12 wings mentioned previously.

This report also considers a slight modification to the method of reference 1 with respect to the location of the local aerodynamic center at subsonic speeds. Specifically, it is suggested that when calculated subsonic distributions of section lift-curve slope are used, the local aerodynamic centers be taken at the quarter chord of streamwise sections rather than at the quarter chord of sections normal to the elastic axis.

The noncirculatory aerodynamic terms appearing in the flutter calculation procedures of references 1, 11, and 12 have been thought to have only a small effect on the calculated flutter speed. The importance of these terms is examined herein by comparing experimental flutter data and flutter calculations made by the complete method of reference 1 with flutter calculations for several wings made by omitting the noncirculatory aerodynamic terms from the method of reference 1.

SYMBOLS

A   aspect ratio of full wing including fuselage intercept

a   nondimensional distance from midchord to elastic axis measured perpendicular to elastic axis, positive rearward, fraction of semichord b

ac   nondimensional distance from leading edge to local aerodynamic center (for steady flow) measured streamwise, fraction of streamwise chord

ac_n nondimensional distance from midchord to local aerodynamic center (for steady flow) measured perpendicular to elastic axis, positive rearward, fraction of semichord b

$ac_{n,l}$ values of ac_n obtained from linearized aerodynamic theory

Δac_n change of ac_n

b semichord of wing measured perpendicular to elastic axis

b_r semichord of wing measured perpendicular to elastic axis at spanwise reference station $\eta = 0.75$

C complex circulation function, $F + iG$

C_{l_α} local lift-curve slope for a streamwise section in steady flow

$C_{l_\alpha,n}$ local lift-curve slope for a section perpendicular to elastic axis in steady flow

$C_{l_\alpha,n,l}$ values of $C_{l_\alpha,n}$ obtained from linearized aerodynamic theory

e multiplier used to obtain variations in magnitude (but not in distribution) of $C_{l_\alpha,n}$

F circulation function which modifies in-phase load components

G circulation function which introduces out-of-phase load components

h local vertical translational displacement of wing at elastic axis

k_{nr} reduced frequency based on spanwise reference station $(\eta = 0.75)$ and on velocity component normal to elastic axis, $b_r\omega/v_n$

M Mach number

M_n Mach number component perpendicular to leading edge

M_α oscillatory moment about elastic axis per unit length of wing, positive leading edge up

m_r	mass of wing per unit length along elastic axis evaluated at spanwise reference station ($\eta = 0.75$)
P	oscillatory lift per unit length of wing along elastic axis, positive downward
V	flutter speed, measured parallel to free stream (experimental values or values calculated by method of ref. 1)
V_R	calculated reference flutter speed obtained by using $C_{l_{\alpha,n}} = 2\pi$, $ac_n = -\frac{1}{2}$, and $C = F_I + iG_I$
v_n	component of free-stream velocity perpendicular to elastic axis
x_α	nondimensional distance from elastic axis to local center of gravity measured perpendicular to elastic axis, positive rearward, fraction of semichord b
κ_r	wing section mass ratio evaluated at spanwise reference station ($\eta = 0.75$), $\dfrac{\pi \rho b_r^2}{m_r}$
$\Lambda_{c/4}$	sweep angle of wing quarter chord, positive for sweepback
Λ_{ea}	sweep angle of wing elastic axis, positive for sweepback
λ	taper ratio of full wing including fuselage intercept
η	nondimensional coordinate (either spanwise or along elastic axis) measured from wing root, fraction of exposed panel span or fraction of panel length along elastic axis
θ	local torsional displacement of wing measured about elastic axis
ρ	air density
σ	local bending slope of elastic axis
τ	local rate of change of twist angle with distance along the elastic axis
ω	circular frequency of vibration at flutter
ω_α	circular frequency of first uncoupled torsional vibration mode of wing measured about elastic axis

ω_h circular frequency of uncoupled bending vibration mode of wing (subscripts 1 and 2 denote first and second bending modes)

ω_R circular frequency of vibration at flutter calculated by using $C_{l_{\alpha,n}} = 2\pi$, $ac_n = -\frac{1}{2}$, and $C = F_I + iG_I$

Subscripts:

C   circulation functions for compressible flow obtained in reference 1 from loading coefficients for two-dimensional wings oscillating in compressible flow

I   circulation functions for incompressible flow obtained in reference 11 for two-dimensional wings oscillating in incompressible flow

PROCEDURE FOLLOWED IN THE FLUTTER ANALYSIS

Wing Designation

The three-digit system used to identify the wings with taper ratio of 0.6 is the same as that used in reference 1. The first digit in this system is the aspect ratio of the full wing to the nearest integer. The second and third digits give the quarter-chord sweep angle to the nearest degree. For example, wing 445 has an aspect ratio of 4, a sweep angle of 45°, and a full-wing taper ratio of 0.6. Since some of the wings discussed in this report have identical plan forms but different center-of-gravity positions (see, for example, ref. 7), a single letter is appended to the plan-form designation to signify a forward or rearward shift in center of gravity. For example, wing 445 has a center of gravity at approximately 46 percent chord, whereas the center of gravity of wing 445F is at about 34 percent chord, and that of wing 445R is at about 58 percent chord. Wing 400 has a center of gravity at approximately 45 percent chord, but wing 400R has a center of gravity at about 59 percent chord.

For the wings with taper ratio of 1.0, the same system is used, except that a fourth digit 1 is added to distinguish the taper ratio. For example, wing 4451 has a full-wing aspect ratio of 4, a sweep angle of 45°, and a taper ratio of 1.0.

All of the wing plan forms treated in this report are shown in figure 1.

Determination of the Local Aerodynamic Center

for Subsonic Speeds

The flutter calculation procedure of reference 1 utilizes geometric, structural, and aerodynamic quantities associated with wing sections normal to the elastic axis. In particular, for computational convenience, values of the section lift-curve slope C_{l_α} and the local aerodynamic center ac, which are usually available for streamwise sections, are converted to $C_{l_{\alpha,n}}$ and ac_n for sections normal to the elastic axis by means of the geometrical relations

$$C_{l_{\alpha,n}} = \frac{C_{l_\alpha}}{\cos \Lambda_{ea}} \tag{1}$$

and

$$ac_n = \left(2ac \left\{ \cos \Lambda_{ea} + \left[\tan \Lambda_{c/4} - \frac{1}{A} \frac{1 - \lambda}{1 + \lambda}(1 - 2a) \right] \sin \Lambda_{ea} \right\} \right.$$
$$\left. - (1 + a) \left[\cos \Lambda_{ea} + \left(\tan \Lambda_{c/4} + \frac{1}{A} \frac{1 - \lambda}{1 + \lambda} \right) \sin \Lambda_{ea} \right] \right) \cos \Lambda_{ea} + a \tag{2}$$

in the notation of the present report.

For subsonic speeds below critical Mach number, it is reasonable to take the local aerodynamic centers at the local quarter-chord positions. However, the question immediately arises whether the aerodynamic center should be assumed to be at the quarter chord of a streamwise section $\left(ac = \frac{1}{4} \right)$ or of a section normal to the elastic axis $\left(ac_n = -\frac{1}{2} \right)$. It may be noted that these two locations normally coincide for wings which are either unswept or untapered. The strip-theory flutter calculation method of reference 12 takes the aerodynamic center at the quarter chord of a section normal to the elastic axis. This location arose from the application of aerodynamic expressions for two-dimensional incompressible flow (from ref. 11) to strips normal to the elastic axis. In the present method, however, the local aerodynamic centers at subsonic speeds are taken at the quarter chord of streamwise sections for the following reasons: first, for subsonic speeds the spanwise distributions of C_{l_α} are calculated by the lifting-line method of reference 13 as adapted for calculation in reference 14. The method of references 13 and 14 locates the lifting line and hence the aerodynamic center at the local streamwise

quarter chord $\left(\text{ac} = \frac{1}{4}\right)$. Second, the use of the streamwise quarter chord is consistent with the procedure employed for supersonic speeds; that is, C_{l_α} and ac are determined for streamwise sections and then converted to $C_{l_\alpha,n}$ and ac_n by means of equations (1) and (2). Thus the use of ac $= \frac{1}{4}$ at subsonic speeds is consistent both with the method of calculating C_{l_α} at subsonic speeds and with the method for calculating C_{l_α} and ac at supersonic speeds.

It should be observed that for subsonic Mach numbers higher than critical it may become necessary to employ experimentally determined steady-flow aerodynamic parameters in order to account for the variation of aerodynamic center with Mach number. (See ref. 2.)

For normally tapered $(\lambda < 1)$ swept wings, the use of ac $= \frac{1}{4}$ in equation (2) will yield ac_n values of slightly greater magnitude (aerodynamic center nearer the leading edge) than $\text{ac}_n = -\frac{1}{2}$. The use of $\text{ac}_n = -\frac{1}{2}$ would thus result in slightly higher flutter speeds than the use of ac $= \frac{1}{4}$. As shown in reference 2, the use of incompressible-flow circulation functions $\left(C = F_I + iG_I\right)$ for nonzero subsonic Mach numbers results in flutter speeds slightly lower than those obtained by using $C = \frac{F_C}{F_I}\left(F_I + iG_I\right)$, the form of circulation function appearing in the flutter calculation method of reference 1. For purposes of comparison some subsonic flutter calculations made by using $\text{ac}_n = -\frac{1}{2}$ and $C = F_I + iG_I$ are shown herein for the wings of figure 1 in addition to the calculations made by using ac $= \frac{1}{4}$ and $C = \frac{F_C}{F_I}\left(F_I + iG_I\right)$. The magnitude of the factor F_C/F_I is indicated in figure 2.

Systematic Variation of Aerodynamic Parameters and Density

Variation of local aerodynamic center and local lift-curve slope.- As mentioned previously, the variations of $C_{l_\alpha,n}$ and ac_n used herein were employed in two sets of subsonic and supersonic flutter calculations for three swept wings and four unswept wings (wings 445, 445F, 445R, 400, 400R, 4001, and 7001). In the first set of calculations

$$C_{l_{\alpha,n}} = C_{l_{\alpha,n,l}} \tag{3}$$

and

$$ac_n = ac_{n,l} + \Delta ac_n \tag{4}$$

where Δac_n is constant in any one flutter calculation but is systematically varied for each wing at each Mach number. This set of calculations thus indicates the effect on calculated flutter speed of arbitrary constant-percent-chord variations in local aerodynamic center. In the second set of calculations

$$C_{l_{\alpha,n}} = eC_{l_{\alpha,n,l}} \tag{5}$$

and

$$ac_n = ac_{n,l} \tag{6}$$

where e is constant in any one flutter calculation but is systematically varied for each wing at each Mach number. This set of calculations thus indicates the effect on calculated flutter speed of arbitrary variations in the magnitude (but not the distribution) of local lift-curve slope. Throughout these calculations flow density is maintained constant for each wing.

Variation of flow density.- As indicated previously, subsonic and supersonic flutter calculations have been made using various flow densities for the 12 swept and unswept wings of figure 1. These calculations employed $C_{l_{\alpha,n}}$ and ac_n values obtained from linearized steady-flow aerodynamic theory. The density range covered for each wing generally encompasses the densities associated with all experimental flutter points given for the particular wing in references 6 to 10.

Omission of noncirculatory aerodynamic terms.- In the flutter calculation procedure of reference 1 the section lift P and pitching moment M_α are given by

$$P = -\pi\rho b^2\left[\ddot{h} + v_n\dot{\theta} + v_n\dot{\alpha}\tan\Lambda_{ea} - ba\left(\ddot{\theta} + v_n\ddot{\tau}\tan\Lambda_{ea}\right)\right] \Big\} \quad \text{Noncirculatory}$$

$$- C_{l_{\alpha,n}}\rho v_n bCQ \qquad\qquad\qquad\qquad \Big\} \quad \text{Circulatory}$$

$$\tag{7}$$

and

$$M_\alpha = -\pi\rho b^4\left(\frac{1}{8} + a^2\right)\left(\ddot{\theta} + v_n\dot{\tau}\,\tan\Lambda_{ea}\right)$$

$$+ \pi\rho b^2 v_n\left(\dot{h} + v_n\sigma\,\tan\Lambda_{ea}\right) + \pi\rho b^3 a\left(\ddot{h} + v_n\dot{\sigma}\,\tan\Lambda_{ea}\right)$$ Noncirculatory

$$+ \pi\rho b^2 v_n{}^2\left(\theta - ab\tau\,\tan\Lambda_{ea}\right)$$

$$- 2\pi\rho v_n b^2\left[\frac{1}{2} - \left(a - ac_n\right)C\,\frac{C_{l_{\alpha,n}}}{2\pi}\right]Q$$ Circulatory

(8)

where

$$Q = \dot{h} + v_n\theta + v_n\sigma\,\tan\Lambda_{ea} + b\left(\frac{C_{l_{\alpha,n}}}{2\pi} + ac_n - a\right)\left(\dot{\theta} + v_n\tau\,\tan\Lambda_{ea}\right)$$

Since the noncirculatory terms of equations (7) and (8) essentially represent virtual-mass type effects, and since the method of reference 1 is considered to be applicable only to cases involving low to moderate reduced frequencies, it has been thought that these noncirculatory terms have only a small effect on the calculated flutter speed. (See discussion of noncirculatory flow in refs. 1, 15, and 16.) In order to investigate the importance of the noncirculatory terms, several subsonic and supersonic flutter calculations have been made for five swept wings (wings 445, 445R, 645, 452, and 430) by omitting the noncirculatory terms from the method of reference 1. These calculations are compared with calculations made by using the complete expressions for P and M_α (eqs. (7) and (8)) and with experimental flutter data.

Vibration modes employed in the flutter calculations.- Since calculated flutter characteristics appear not to be very sensitive to slight changes in mode shapes, and since the wings of this study are not highly tapered, flutter calculations for all of the wings presented herein were made by using the uncoupled mode shapes of a uniform cantilever beam. For all wings, the first torsion mode and the first and second bending modes were used. However, for wing 445, subsonic and supersonic flutter calculations have also been made by using only the first torsion mode and the first bending mode. Comparison of the results of these two-mode calculations with the results of the three-mode calculations and with the experimental flutter data should give some indication of the importance of including higher modes in the analysis for both subsonic and supersonic Mach numbers, at least for this particular wing.

RESULTS AND DISCUSSION

Presentation of Results

Subsonic and supersonic flutter calculations have been made by the method of reference 1 for 12 swept and unswept wings in order to evaluate the effects on calculated flutter characteristics of variations in aerodynamic parameters and flow density. The plan forms of these 12 wings are shown in figure 1. Spanwise distributions of $C_{l_{\alpha},n} = C_{l_{\alpha},n,l}$ and $ac_n = ac_{n,l}$ as obtained from linearized steady-flow aerodynamic theory for each wing are shown in figures 27 to 35 of reference 1. These values of $C_{l_{\alpha},n,l}$ and $ac_{n,l}$ formed the aerodynamic basis for the present study. (See eqs. (3) to (6).)

Structural data as well as experimental flutter data for all of these wings were obtained from references 1 and 6 to 10. The experimental flutter points shown herein were obtained at various values of density ρ; whereas, for a particular wing, all of the points calculated in this investigation were obtained at a constant value of ρ (unless otherwise indicated) which represented approximately an average of the experimental densities. For each experimental point, however, the normalizing V_R was calculated by using the appropriate experimental density. The reference flutter speeds used in references 6, 9, and 10 for wings 245, 430, 400, 4001, and 7001 were calculated by employing only two degrees of freedom (first bending mode and first torsion mode). Since calculations employing three degrees of freedom (first and second bending modes and first torsion mode), as used herein, yield values of V_R which are slightly different from the two-degree-of-freedom values, the experimental V/V_R values for the wings listed above have been multiplied by the ratio

$$\frac{V_R \text{ (for two degrees of freedom)}}{V_R \text{ (for three degrees of freedom)}}$$ so that both calculated and experimental flutter-speed ratios as presented herein are normalized by V_R for three degrees of freedom.

Variation of aerodynamic parameters.- The effects on calculated flutter characteristics (flutter speed and frequency) of constant-percent-chord shifts in local aerodynamic center (eqs. (3) and (4)) are shown in figures 3 to 16 and are compared with experimental flutter data in figures 17 to 24. Figures 3 to 16 also show the effects on calculated flutter characteristics of changes in the magnitude (but not in the distribution) of local lift-curve slope (eqs. (5) and (6)).

An empirical flutter-speed formula given in reference 17 indicates that, if the ratio of first bending-mode frequency to first torsion-mode

frequency is small, then for a given wing at a given density the following proportionality applies

$$\frac{V}{V_R} \propto \sqrt{\frac{1}{C_{L_\alpha}}} \sqrt{\frac{1}{\left(\frac{x}{c}\right)_{cg} - \left(\frac{x}{c}\right)_{ac}}} \qquad (9)$$

where C_{L_α} is the wing lift-curve slope and $\left(\frac{x}{c}\right)_{cg} - \left(\frac{x}{c}\right)_{ac}$ is the chordwise distance between the section center of gravity and the section aerodynamic center. If $\left(\frac{x}{c}\right)_{cg} - \left(\frac{x}{c}\right)_{ac}$ is evaluated at the reference station $\eta = 0.75$, then the proportionality relation (9) may be written in the notation of the present report as

$$\frac{V}{V_R} \propto \frac{1}{\sqrt{e}} \frac{1}{\left(\sqrt{a + x_\alpha - ac_n - \Delta ac_n}\right)_{\eta=0.75}} \qquad (10)$$

From the relation (10) it appears that the principal effects of variations in lift-curve slope factor e might be accounted for by plotting $\sqrt{e} \frac{V}{V_R}$ instead of $\frac{V}{V_R}$. The relation (10) also indicates that the principal effects of constant-percent-chord variations in aerodynamic center Δac_n might be accounted for by plotting $\left(\sqrt{a + x_\alpha - ac_n - \Delta ac_n}\right)_{\eta=0.75} \frac{V}{V_R}$ instead of $\frac{V}{V_R}$. In order to examine the possibilities of such correlations the curves of figures 3 to 9 have been replotted in figures 25 to 31 as $\sqrt{e} \frac{V}{V_R}$ against e and $\left(\sqrt{a + x_\alpha - ac_n - \Delta ac_n}\right)_{\eta=0.75} \frac{V}{V_R}$ against Δac_n.

Figures 32 to 47 contain both experimental flutter data and subsonic flutter characteristics calculated by using $ac = \frac{1}{4}$ and $C = \frac{F_C}{F_I}\left(F_I + iG_I\right)$ and by using $ac_n = -\frac{1}{2}$ and $C = F_I + iG_I$. Figures 32, 34, 36, 37, 38, 40, 42, 44, 45, and 46 also contain some flutter results obtained by omitting the noncirculatory aerodynamic terms from the flutter calculation method of reference 1.

Variation of flow density.- The variation of flutter-speed coefficient $V/b_r\omega_\alpha$ with flow density ρ and mass ratio κ_r is shown in

figures 48 to 58. In these figures $V/b_r\omega_\alpha$ (for constant Mach number) and ρ are plotted on logarithmic scales to facilitate determination of whether flutter at constant dynamic pressure is indicated. The influence of density changes on flutter-speed ratio V/V_R and flutter-frequency ratio ω/ω_α is illustrated in figures 59 to 80. From these calculations the amount of scatter to be expected in the experimental flutter data of references 6 to 10 based solely on density changes has been determined. The results are compared with the actual experimental scatter in figures 81 to 104.

Finally, in figures 105 and 106 flutter characteristics calculated by using two degrees of freedom (first torsion mode and first bending mode) are compared with flutter characteristics calculated by using three degrees of freedom (first torsion mode and first and second bending mode) and with experimental flutter data for wing 445.

An index to the above-mentioned figures is provided in table I.

Influence on Calculated Flutter Characteristics

of Variations in Aerodynamic Parameters

Local aerodynamic center.- As expected, figures 3 to 16 illustrate the following qualitative results: The variations of calculated flutter speed with systematic constant-percent-chord variations in local aerodynamic center indicate that for all wings and Mach numbers calculated the flutter speed increases as the aerodynamic center moves rearward. As Mach number increases through the transonic range, causing the aerodynamic center to move rearward, the flutter speed becomes increasingly sensitive to changes in aerodynamic center. Further, comparison of results for wings 445, 445F, and 445R (figs. 3 to 5) and for wings 400 and 400R (figs. 6 and 7) indicate that the farther rearward the local center of gravity, and hence the greater the distance between center of gravity and aerodynamic center, the less the sensitivity to aerodynamic-center changes. This statement applies both to the systematic variations of aerodynamic center Δac_n and to changes in ac_n resulting from changes in Mach number. It may be observed from figures 6 and 9 that in comparison with results for the other wings, the calculated flutter speeds for wings 400 and 7001 are extremely sensitive to aerodynamic-center changes at supersonic Mach numbers. This great sensitivity arises because for these two wings at supersonic speeds the local aerodynamic centers are very close to the local centers of gravity.

The calculated flutter frequencies shown in figures 10 to 16 show that with one exception the flutter frequencies increase as aerodynamic center moves rearward and that as Mach number increases, the frequency

as well as the flutter speed becomes increasingly sensitive to aerodynamic center changes. The exception to this statement is wing 7001 at supersonic speeds. Figure 16 shows that flutter frequencies for wing 7001 at supersonic speeds actually decrease slightly as aerodynamic center is moved rearward.

The effects of systematic changes of aerodynamic center on the variation of flutter speed and frequency with Mach number are shown in the crossplots in figures 17 to 24. Figures 17, 18, 21, and 22 show again that the rearward center of gravity of wing 400R results in variations (with ac_n) of flutter speed and frequency which are much smaller than those associated with wing 400. Inasmuch as linearized aerodynamic theory characteristically predicts aerodynamic centers which are farther rearward than those obtained experimentally, it would appear that flutter calculations using linearized-theory aerodynamics should be more reliable for wing 400R than for wing 400 especially at supersonic speeds. The solid curves of figures 17, 18, 21, and 22 show this to be true. Figure 20 shows that for wing 7001 good agreement between calculated and experimental supersonic flutter speeds is obtained with local aerodynamic center only one percent chord forward of the linearized-theory position ($\Delta ac_n = -0.02$).

Quantitatively, for wings 400 and 400R results obtained by using linearized-theory aerodynamic parameters may be compared with results obtained by using $C_{l_{\alpha,n}}$ and ac_n from flight tests of the X-1E airplane since the wing geometry of the X-1E was closely similar to wings 400 and 400R. Figure 5 of reference 2 shows that over the middle and outboard portions of the wing panel $C_{l_{\alpha,n}}$ at $M = 1.41$ for the X-1E airplane is very close to $C_{l_{\alpha,n}}$ at $M = \sqrt{2}$ obtained from linear theory. However, the local aerodynamic centers for the X-1E are about 6.3 percent chord forward of those given by linear theory. Use of $C_{l_{\alpha,n}}$ and ac_n for the X-1E in flutter calculations for wings 400 and 400R at $M = \sqrt{2}$ results in a 51-percent reduction of flutter speed for wing 400 but only a 9-percent reduction for wing 400R compared with linear-theory results. (See figs. 6, 7, 17, and 18.) Similarly use of $C_{l_{\alpha,n}}$ and ac_n for the X-1E results in a 54-percent reduction of calculated flutter frequency for wing 400 but only a 2-percent reduction for wing 400R. (See figs. 13, 14, 21, and 22.) These comparisons give some indication of the magnitude of error which can occur when linear-theory aerodynamic parameters are used in flutter calculations for finite-thickness wings in a real fluid, particularly when the local aerodynamic centers are close to the local centers of gravity.

In figures 32 to 47 subsonic flutter characteristics calculated by using $ac_n = -\frac{1}{2}$ and $C = F_I + iG_I$ are compared with results obtained

by using $ac = \frac{1}{4}$ and $C = \frac{F_C}{F_I}(F_I + iG_I)$. As expected, the flutter speeds

and frequencies calculated by these two procedures generally differ by
only a very small amount. For the swept, tapered wings the maximum
difference between flutter speeds calculated by these two procedures

occurs at $M = 0$ where $\frac{F_C}{F_I} = 1.0$, and $ac_n = -\frac{1}{2}$ yields higher flutter

speeds than $ac = \frac{1}{4}$. The largest difference (about 4 percent) occurs for

wing 445F because the forward local centers of gravity of that wing are
comparatively close to the local aerodynamic centers, and that condition
yields increased sensitivity to ac_n changes. (Compare figs. 3, 4,
and 5.) As Mach number increases from 0, F_C/F_I decreases from 1.0,
and subsonic flutter speeds calculated by the two above-mentioned proce-
dures come closer together. For all of the swept, tapered wings except
wings 245 and 445F the difference is insignificant at $M = 0.75$. For
the three untapered wings (wings 4451, 4001, and 7001) substitution of
$ac = \frac{1}{4}$ into equation (2) yields $ac_n = -\frac{1}{2}$ so that the two above-

mentioned procedures give identical results at $M = 0$. (See figs. 19,
20, 23, 24, 39, and 47.) At higher subsonic Mach numbers the two proce-
dures reflect only the difference between using $C = \frac{F_C}{F_I}(F_I + iG_I)$ and

$C = F_I + iG_I$. As indicated in references 1 and 2 this difference should
be small as long as the Mach number component normal to the leading edge
is not large. This statement is supported here by figures 19, 20, 23,
24, 39, and 47. For swept wing 4451 at $M = 0.75$ (fig. 39) the two
procedures yield flutter speeds which differ by only 2 percent. For
unswept wing 7001 (fig. 20), however, the component of Mach number normal
to the leading edge is the same as stream Mach number, and at $M = 0.75$
the two procedures yield flutter speeds which differ by about 8 percent.
The corresponding differences in flutter frequency, however, are insig-
nificant for all of the wings.

Figures 25 to 31 show attempted correlations of the effects of ac_n
changes based on the relation given by equation (10). Most of the curves
of figures 25 to 31 indicate little variation of the quantity
$\left(\sqrt{a + x_\alpha - ac_n - \Delta ac_n}\right)_{\eta=0.75} \frac{V}{V_R}$ with changes in ac_n. The exceptions
to this statement are the curves for the highest Mach numbers and for the
wings with the more forward local centers of gravity. Thus it appears
that equations (9) and (10) should predict with reasonable accuracy the
effects of ac_n changes as long as the changes Δac_n are not too large
and as long as the local aerodynamic centers are not close to the local
centers of gravity.

Local lift-curve slope.- As expected (see eq. (10)), figures 3 to 9 indicate that calculated flutter speed generally decreases as local lift-curve slope increases. The one exception to this statement is the curve shown in figure 9 for wing 7001 at $M = 1.30$. This curve shows an unexpected increase of flutter speed as lift-curve slope increases. An examination of the structural and aerodynamic quantities for wing 7001 revealed that the increase of flutter speed with increasing lift-curve slope is associated with the location of local aerodynamic centers rearward of the elastic axis. For wing 7001 at $M = 1.30$, this condition existed over the major portion of the wing and resulted in a change of sign for the circulatory component of the section pitching moment M_α. (See eq. (8).) For wing 7001 at $M = 1.15470$ and for wing 400 at $M = 1.15470$ and $M = \sqrt{2}$, the condition existed over a smaller portion of the wing and resulted in comparatively small decreases of flutter speed with increasing lift-curve slope. (See figs. 6 and 9.)

Figures 25 to 31 show attempted correlations of the effects of $C_{l_{\alpha,n}}$ changes based on the relation given by equation (10). Most of the curves of $\sqrt{e}\,\dfrac{V}{V_R}$ show a tendency to rise with increasing e, indicating that calculated flutter speed generally does not decrease quite as rapidly as the inverse square root of lift-curve slope. The deviations previously described for wings 400 and 7001 at supersonic speeds are clearly brought out in figures 28 and 31. Figures 25 to 31 seem to indicate that equations (9) and (10) should predict with reasonable accuracy the effects of $C_{l_{\alpha,n}}$ changes as long as the local aerodynamic centers are not close to the local centers of gravity and as long as the local aerodynamic centers are forward of the elastic axis.

Influence on Calculated Flutter Characteristics

of Variations in Flow Density

In figures 48 to 58 the calculated flutter-speed coefficient $\dfrac{V}{b_r \omega_\alpha}$ for 11 wings has been plotted logarithmically as a function of flow density and as a function of the mass ratio $\kappa_r = \dfrac{\pi \rho b_r^2}{m_r}$. On these plots flutter at constant dynamic pressure would be indicated by a straight line of slope $-\dfrac{1}{2}$. These figures show that for most of the wings calculated the variation of flutter-speed coefficient $\dfrac{V}{b_r \omega_\alpha}$ with flow density for nonzero Mach numbers has the same general character as the variation of $\dfrac{V_R}{b_r \omega_\alpha}$. Also, for all of the swept wings the curves of figures 48 to 58

have slopes of magnitude significantly less than $\left|-\frac{1}{2}\right|$. However, for unswept wings 400 and 7001 the curves of $\frac{V_R}{b_r\omega_\alpha}$ and of $\frac{V}{b_r\omega_\alpha}$ for M = 0.75 closely follow a slope of $-\frac{1}{2}$ indicating flutter at approximately constant dynamic pressure. For unswept wings 400R and 4001 all of the curves shown indicate flutter at approximately constant dynamic pressure. The approximate slope of $-\frac{1}{2}$ for $\frac{V_R}{b_r\omega_\alpha}$ for all of the unswept wings supports the statement in reference 5 that for the V_R calculation, flutter at constant dynamic pressure is indicated only for unswept wings or for swept wings of high aspect ratio. Figures 54 and 58 show, however, that even though $\frac{V_R}{b_r\omega_\alpha}$ values for the unswept wings indicate flutter at constant dynamic pressure, constant-dynamic-pressure flutter may not occur for supersonic Mach numbers, particularly when local aerodynamic centers lie close to local centers of gravity as occurs for wings 400 and 7001.

The influence of density changes on calculated flutter-speed ratio V/V_R and flutter-frequency ratio ω/ω_α is illustrated in figures 59 to 80. In figures 59 to 69 the small variations of calculated subsonic V/V_R with density changes seem to indicate that the presentation of subsonic flutter speeds in the form V/V_R is probably acceptable if the density range covered is no greater than those shown. Use of the V/V_R form for supersonic flutter speeds, however, may result in unacceptable scatter if the density range covered is large.

Figures 70 to 80 generally show appreciable increases of flutter frequency with increasing density and thus indicate significant increases in the aerodynamic contribution to the apparent wing stiffness. The exceptions to this statement are wing 400 at $M = \sqrt{2}$ (fig. 76) and wing 7001 at M = 1.15470 and M = 1.30 (fig. 80). These are again the conditions for which the local aerodynamic centers lie rearward of the elastic axis over a large portion of the wing.

From figures 59 to 80 the amount of scatter to be expected in the experimental flutter data of references 6 to 10 based solely on density changes has been determined. Figures 81 to 104 show comparisons of these estimates and the actual scatter of the data. These figures show that for some of the wings density changes may be responsible for an appreciable portion of the scatter. It should also be noted that the experimental scatter shown in these figures tends to be systematic, and the experimental flutter-speed ratios tend to vary with density in the same manner as the calculated values, particularly at supersonic Mach numbers.

Omission of Noncirculatory Aerodynamic Terms

As indicated earlier, some flutter calculations have been made with the noncirculatory components of section lift P (eq. (7)) and pitching moment M_α (eq. (8)) omitted. The results of these calculations (figs. 32, 34, 36, 37, 38, 40, 42, 44, 45, and 46) indicate that the effects of the noncirculatory terms on subsonic and supersonic flutter speeds are small (of the order of 15 percent or less) but not negligible. The effects on flutter frequencies of omitting the noncirculatory terms are appreciably greater than the effects on the flutter speeds. Thus the importance of the noncirculatory terms is not insignificant, and they should not be deleted from subsequent flutter calculations.

Effect of the Higher Modes on Calculated

Flutter Characteristics

As mentioned earlier, all of the flutter calculations previously presented were made by using the first torsion mode and the first and second bending modes of a uniform cantilever beam. In order to obtain a preliminary estimate of the importance in the flutter analysis of the second and higher modes, subsonic and supersonic flutter calculations have been made for wing 445 by using only the first torsion mode and the first bending mode. These calculations are compared with the three-mode results in figures 105 and 106. It is evident that the second bending mode contributes significantly to the flutter-speed ratio V/V_R only at the higher supersonic Mach numbers shown. The effect of the second bending mode on the actual speed, however, is indicated by the fact that

$$\frac{V_R \text{ (two modes)}}{V_R \text{ (three modes)}} = 1.038$$

so that at $M = 0.75$,

$$\frac{V \text{ (two modes)}}{V \text{ (three modes)}} = 1.051$$

but at $M = 1.75$,

$$\frac{V \text{ (two modes)}}{V \text{ (three modes)}} = 1.184$$

Flutter frequencies calculated with two modes and with three modes differ by only a small amount through the Mach number range calculated. Thus,

as might be expected, when flutter frequencies increase (as Mach number increases, for example) the higher modes become more important in the flutter calculation.

CONCLUSIONS

Subsonic and supersonic flutter calculations have been made by the method of NACA Research Memorandum L57L10 for 12 swept and unswept wings in order to evaluate the effects on calculated flutter characteristics of variations in aerodynamic parameters and flow density. For all of these wings the ratio of first bending-mode frequency to first torsion-mode frequency was of the order of 0.3 or less. With section lift-curve slopes and local aerodynamic centers obtained from linearized aerodynamic theory used as the basis, systematic constant-percent-chord shifts of local aerodynamic center and systematic changes in the magnitude (but not in the distribution) of section lift-curve slope indicate the following:

1. If the local aerodynamic centers are sufficiently forward of the local centers of gravity, the calculated flutter speed appears to vary approximately as the inverse square root of the distance between local aerodynamic center and local center of gravity.

2. When local aerodynamic centers are close to the local centers of gravity, calculated flutter speed is extremely sensitive to small changes in aerodynamic-center position, and the above empirical rule is no longer valid. When this latter condition exists, flutter calculations based on linear-theory aerodynamics are likely to be considerably in error because linearized theory characteristically predicts aerodynamic centers that are farther rearward than those observed on finite-thickness wings in a real fluid.

3. If the local aerodynamic centers are forward of the elastic axis and are not close to the local centers of gravity, the calculated flutter speed appears to vary approximately as the inverse square root of lift-curve slope.

4. If local aerodynamic center moves rearward of the elastic axis, a change of sign occurs in the circulatory component of section pitching moment, and calculated flutter speeds may actually increase with increasing lift-curve slope.

Some variations of flow density employed in flutter calculations based on steady-flow linearized-theory aerodynamics indicate the following:

5. Flutter at constant dynamic pressure (flutter speed varying as the $-\frac{1}{2}$ power of density) was indicated only for unswept wings for which the local aerodynamic centers were sufficiently forward of the local centers of gravity.

6. For unswept wings with aerodynamic centers close to the centers of gravity and for all of the swept wings, calculated flutter speed varied approximately as a power of density of magnitude smaller than $\left|-\frac{1}{2}\right|$.

7. Presentation of flutter speeds in the form of a flutter-speed ratio, flutter speed divided by flutter speed calculated from two-dimensional incompressible-flow aerodynamics, is probably acceptable for most wings at subsonic Mach numbers. For supersonic Mach numbers, however, the increased variation of this ratio with density changes may introduce unacceptable scatter if the density range covered is large.

Langley Research Center,
National Aeronautics and Space Administration,
Langley Field, Va., August 25, 1959.

L
4
6
4

REFERENCES

1. Yates, E. Carson, Jr.: Calculation of Flutter Characteristics for Finite-Span Swept or Unswept Wings at Subsonic and Supersonic Speeds by a Modified Strip Analysis. NACA RM L57L10, 1958.

2. Yates, E. Carson, Jr.: Use of Experimental Steady-Flow Aerodynamic Parameters in the Calculation of Flutter Characteristics for Finite-Span Swept or Unswept Wings at Subsonic, Transonic, and Supersonic Speeds. NASA TM X-183, 1959.

3. Theodorsen, Theodore, and Garrick, I. E.: Machanism of Flutter - A Theoretical and Experimental Investigation of the Flutter Problem. NACA Rep. 685, 1940.

4. Woolston, Donald S., and Castile, George E.: Some Effects of Variations in Several Parameters Including Fluid Density on the Flutter Speed of Light Uniform Cantilever Wings. NACA TN 2558, 1951.

5. Kelly, H. Neale: Some Effects of Mass Ratio on the Transonic Flutter Characteristics of Untapered 45° Sweptback Wings of Aspect Ratios 2 and 3.5. NACA RM L58D17, 1958.

6. Unangst, John R., and Jones, George W., Jr.: Some Effects of Sweep and Aspect Ratio on the Transonic Flutter Characteristics of a Series of Thin Cantilever Wings Having a Taper Ratio of 0.6. NACA RM L55I13a, 1956.

7. Jones, George W, Jr., and Unangst, John R.: Investigation To Determine Effects of Center-of-Gravity Location on Transonic Flutter Characteristics of a 45° Sweptback Wing. NACA RM L55K30, 1956.

8. Ruhlin, Charles L.: Experimental Transonic Flutter Characteristics of an Untapered, 45° Sweptback, Aspect-Ratio-4 Wing. NACA RM L55L22, 1956.

9. Pratt, George L.: Experimental Flutter Investigation of a Thin Unswept Wing at Transonic Speeds. NACA RM L55A18, 1955.

10. Bursnall, William J.: Initial Flutter Tests in the Langley Transonic Blowdown Tunnel and Comparison With Free-Flight Flutter Results. NACA RM L52K14, 1953.

11. Theodorsen, Theodore: General Theory of Aerodynamic Instability and the Mechanism of Flutter. NACA Rep. 496, 1935.

12. Barmby, J. G., Cunningham, H. J., and Garrick, I. E.: Study of Effects of Sweep on the Flutter of Cantilever Wings. NACA Rep. 1014, 1951. (Supersedes NACA TN 2121.)

13. Weissinger, J.: The Lift Distribution of Swept-Back Wings. NACA TM 1120, 1947.

14. DeYoung, John, and Harper, Charles W.: Theoretical Symmetric Span Loading at Subsonic Speeds for Wings Having Arbitrary Plan Form. NACA Rep. 921, 1948.

15. Miles, John W.: On Virtual Mass and Transient Motion in Subsonic Compressible Flow. Quarterly Jour. Mech. and Appl. Math., vol. IV, pt. 4, Dec. 1951, pp. 388-400.

16. Mazelsky, Bernard: On the Noncirculatory Flow About a Two-Dimensional Airfoil at Subsonic Speeds. Jour. Aero. Sci. (Readers' Forum), vol. 19, no. 12, Dec. 1952, pp. 848-849.

17. Loftin, Laurence K., Jr.: Flutter Characteristics of Swept Wings at Transonic Speeds. NACA RM L55E19a, 1955.

L
4
6
4

TABLE I

FIGURE INDEX

			Wings — Figure number												
Ordinate	Abscissa	Parameter	445	445F	445R	245	645	452	430	400	400R	4451	4001	7001
$\frac{V}{V_R}$	$e,\ \Delta ac_n$	M	3	4	5					6	7		8	9
$\frac{\omega}{\omega_\alpha}$	$e,\ \Delta ac_n$	M	10	11	12					13	14		15	16
$\frac{V}{V_R}$	M	Δac_n								17	18		19	20
$\frac{\omega}{\omega_\alpha}$	M	Δac_n								21	22		23	24
$\sqrt{e}\,\dfrac{V}{V_R}$	e	M	25	26	27					28	29		30	31
$\left(\sqrt{e + x_\alpha - ac_n - \Delta ac_n}\,\right)_{\eta=0.75}\dfrac{V}{V_R}$	Δac_n	M	25	26	27					28	29		30	31
$\frac{V}{V_R}$	M		32	33	34	35	36	37	38			39		
$\frac{\omega}{\omega_\alpha}$	M		40	41	42	43	44	45	46			47		
$\frac{V}{b_r\omega_\alpha},\ \frac{V}{V_R}$	$\rho,\ \kappa_r$	M	48	49	50		51	52	53	54	55	56	57	58
$\frac{\omega}{\omega_\alpha},\ \frac{V}{V_R}$	$\rho,\ \kappa_r$	M	59	60	61		62	63	64	65	66	67	68	69
$\frac{\omega}{\omega_\alpha},\ \frac{V}{V_R}$	$\rho,\ \kappa_r$	M	70	71	72		73	74	75	76	77	78	79	80
$\frac{\omega}{\omega_\alpha}$	M	ρ	81	82	83	84	85	86	87	88	89	90	91	92
$\frac{V}{V_R}$	M	ρ	93	94	95	96	97	98	99	100	101	102	103	104
$\frac{\omega}{\omega_\alpha}$	M	Number of modes	105											
$\frac{V}{V_R}$	M	Number of modes	106											

(a) Wings with $\lambda = 0.6$.

(b) Wings with $\lambda = 1.0$.

Figure 1.- Plan forms of wings for which flutter characteristics were calculated.
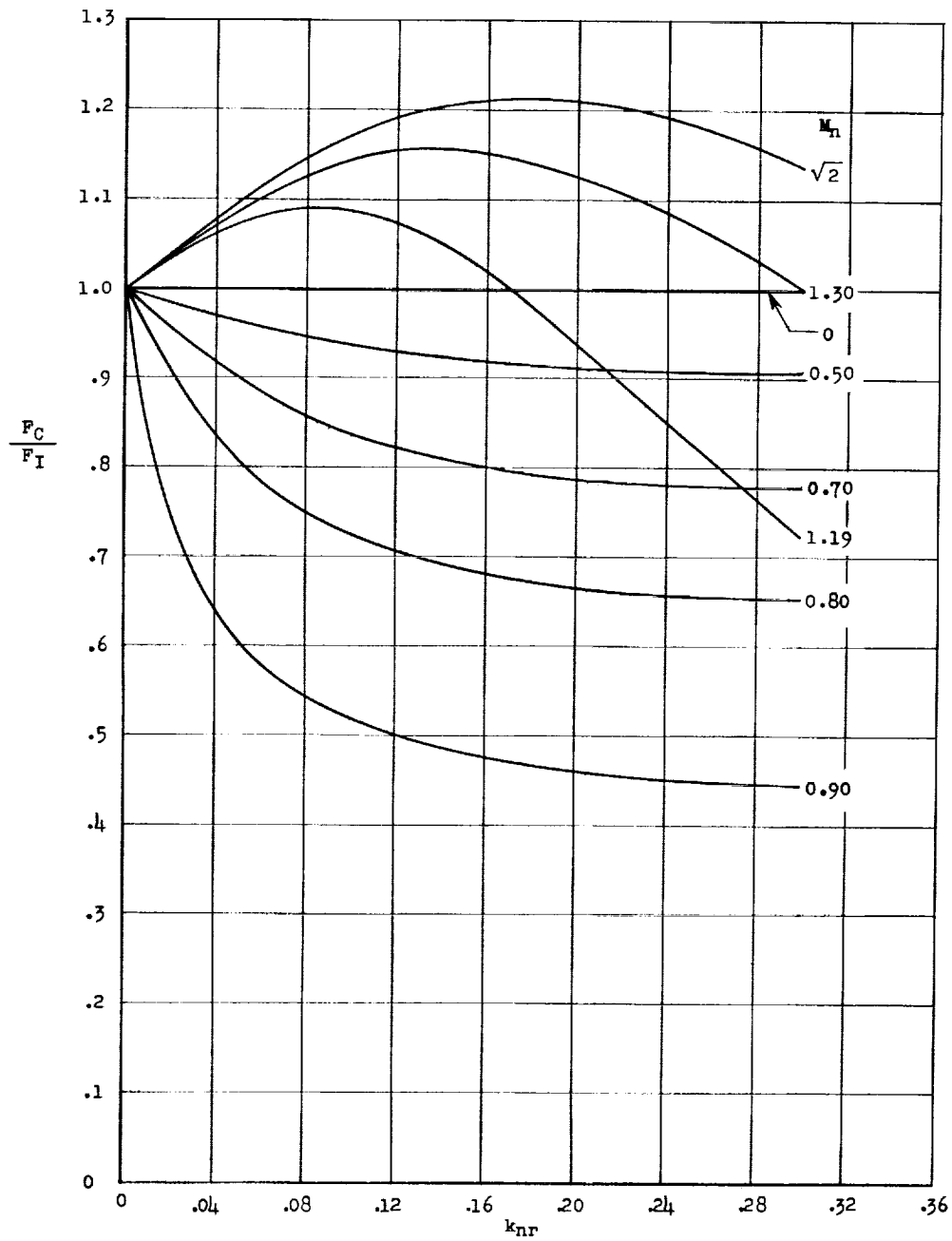
Figure 2.- Variation with reduced frequency k_{nr} of the factor F_C/F_I which accounts for the effect of compressibility in the circulation function $C = \dfrac{F_C}{F_I}\left(F_I + iG_I\right)$.

L-464
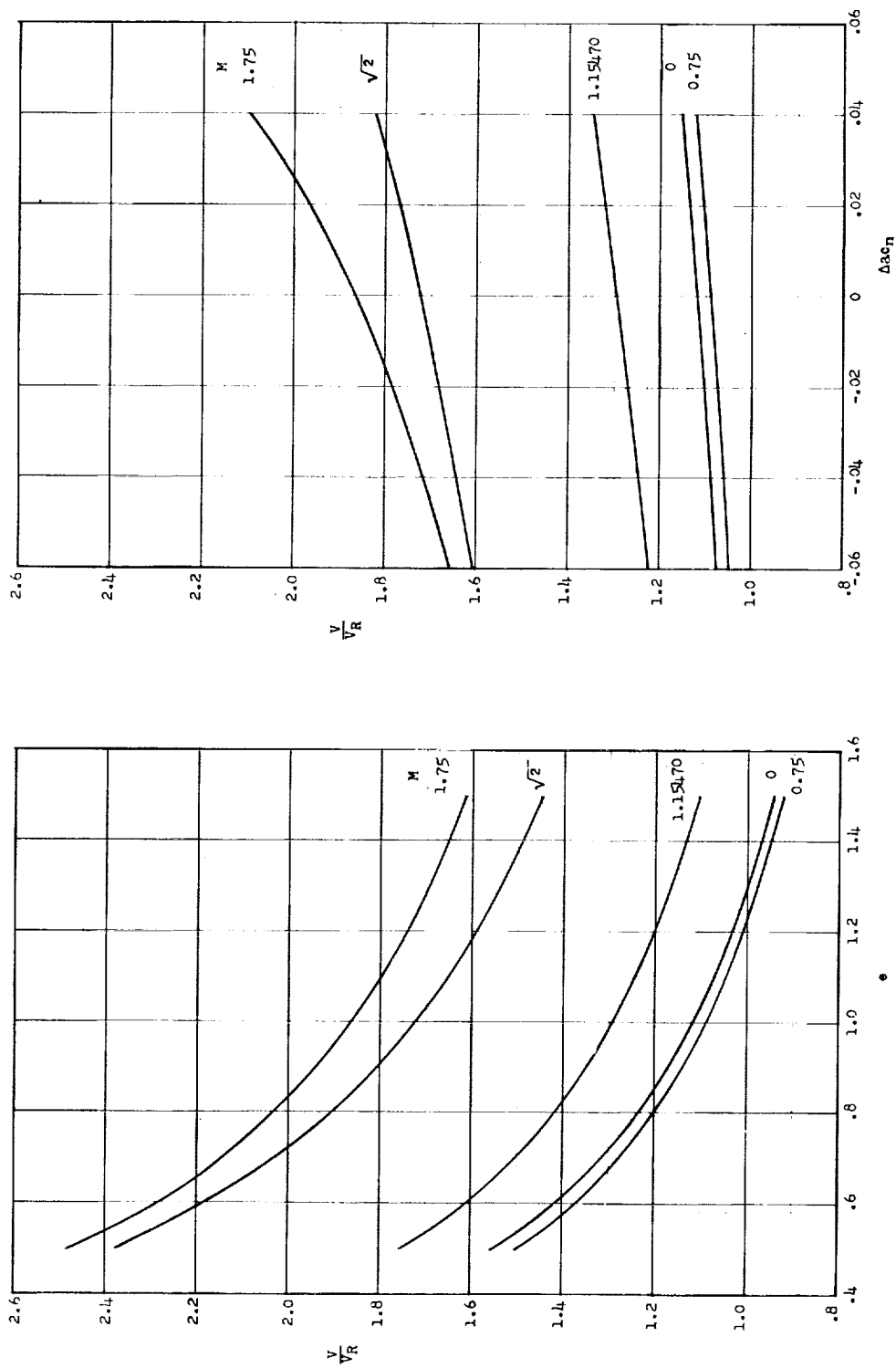
Figure 3.- Variation of flutter speed with lift factor e and with aerodynamic-center shift Δac_n for wing 445. V_R is calculated for $e = 1$ and $\Delta ac_n = 0$. $\rho = 0.003800$ slug/cu ft; $V_R = 735.0$ ft/sec.
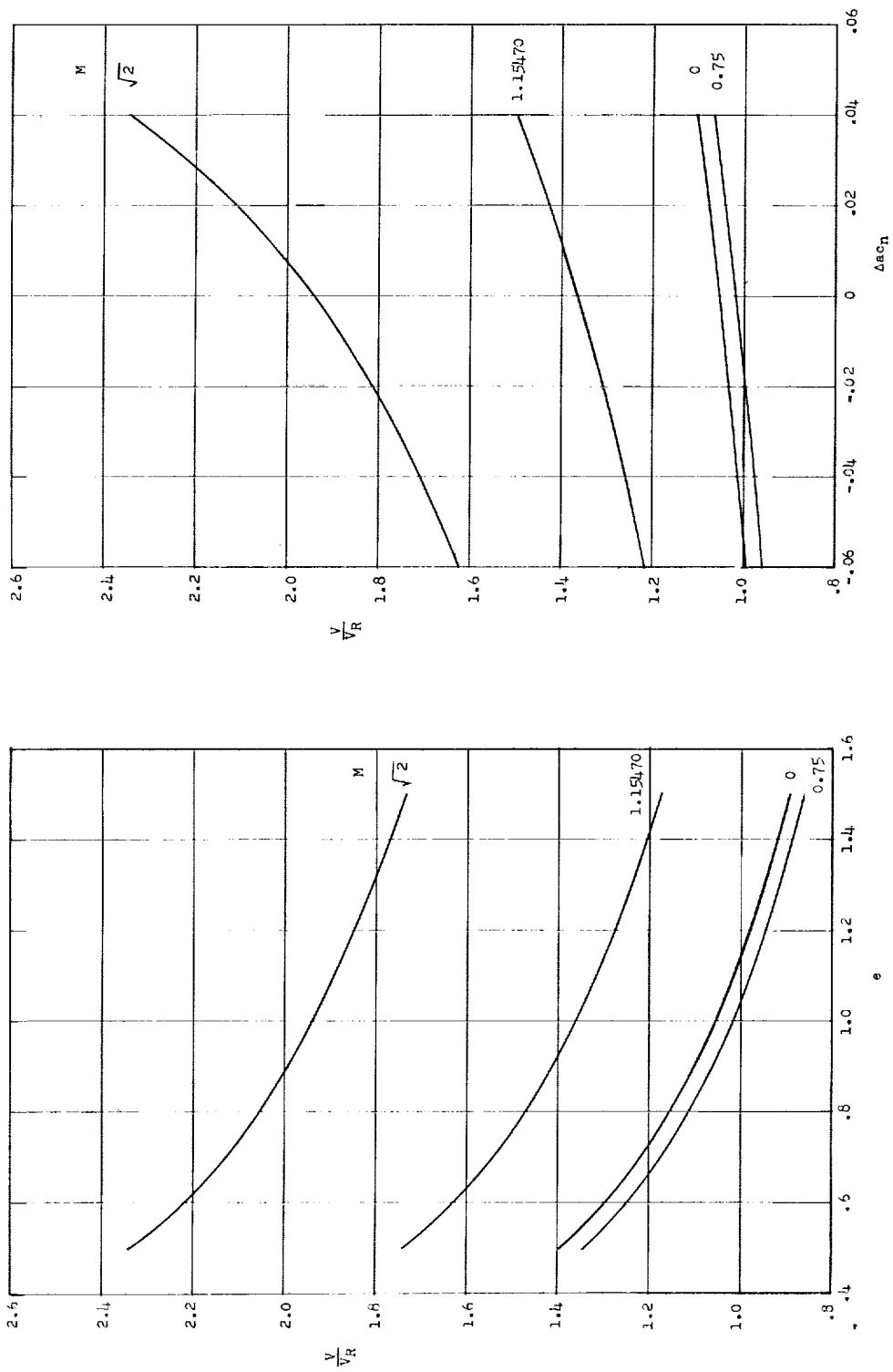
Figure 4.- Variation of flutter speed with lift factor e and with aerodynamic-center shift Δac_n for wing 445F. V_R is calculated for e = 1 and Δac_n = 0. ρ = 0.003000 slug/cu ft; V_R = 840.0 ft/sec.

L-464

L-464
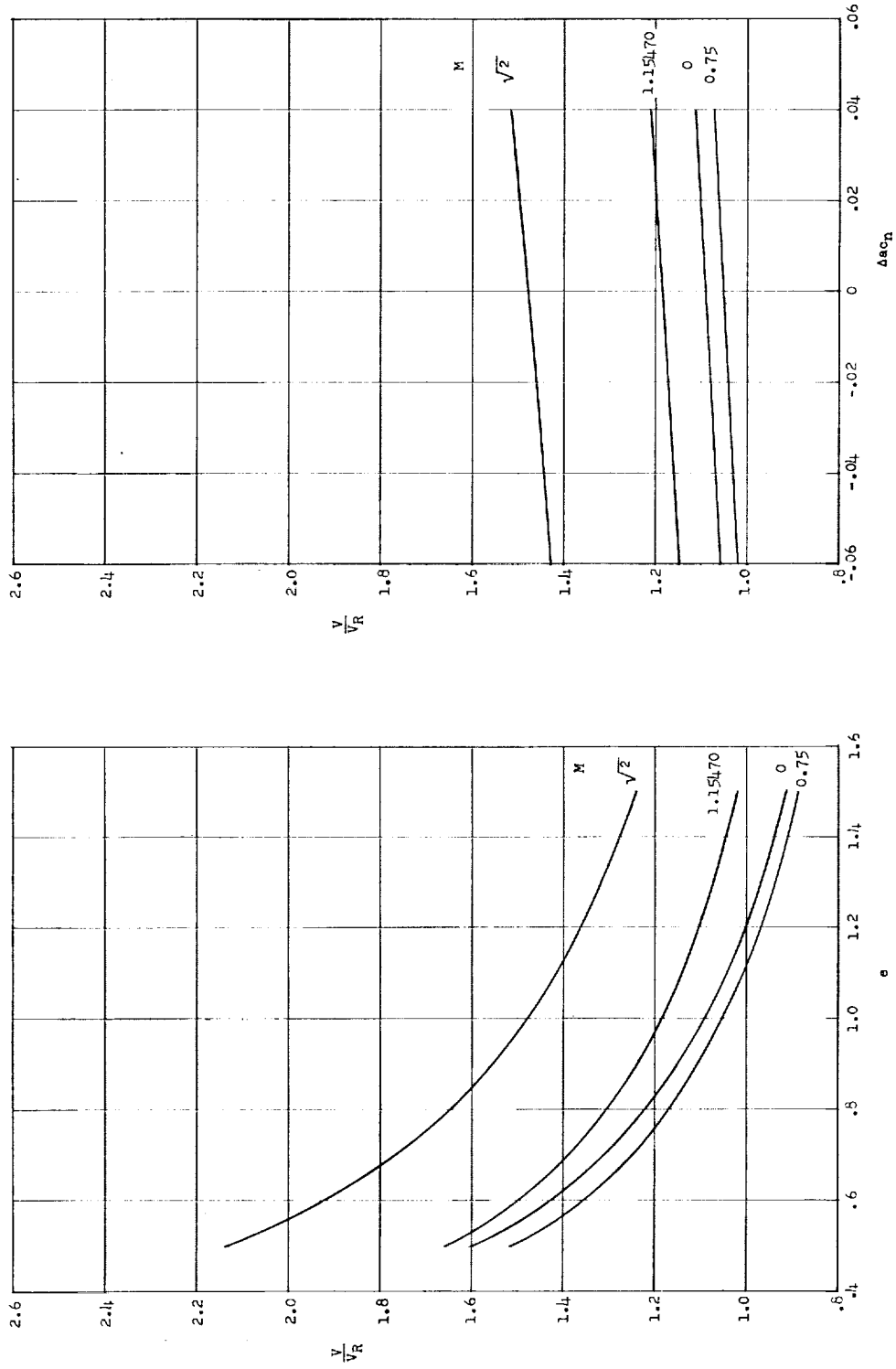
Figure 5.- Variation of flutter speed with lift factor e and with aerodynamic-center shift Δac_n for wing 445R. V_R is calculated for $e = 1$ and $\Delta ac_n = 0$. $\rho = 0.002378$ slug/cu ft; $V_R = 928.7$ ft/sec.
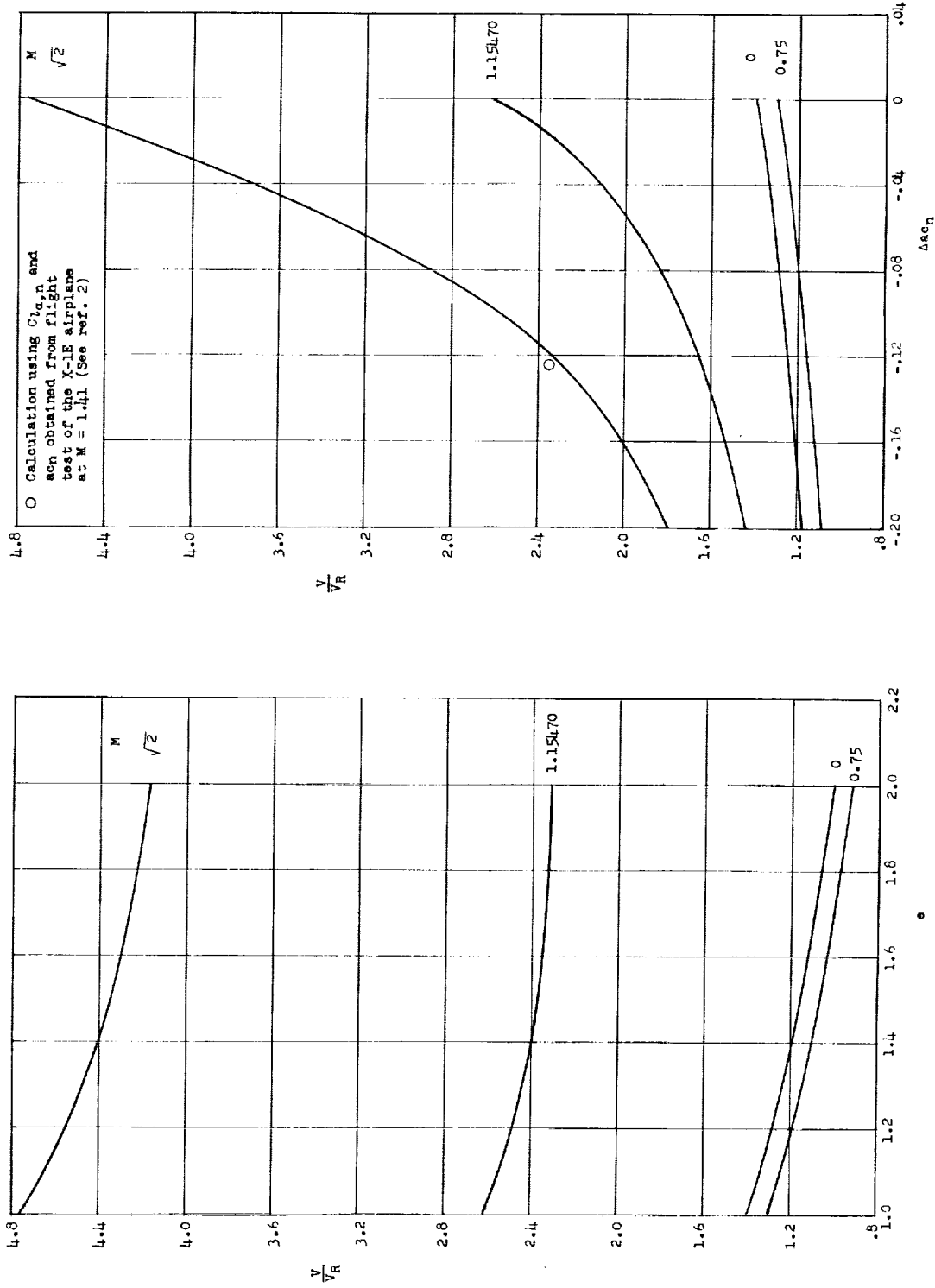
Figure 6.- Variation of flutter speed with lift factor e and with aerodynamic-center shift Δac_n for wing 400. V_R is calculated for $e = 1$ and $\Delta ac_n = 0$. $\rho = 0.002378$ slug/cu ft; $V_R = 976.5$ ft/sec.

L-464
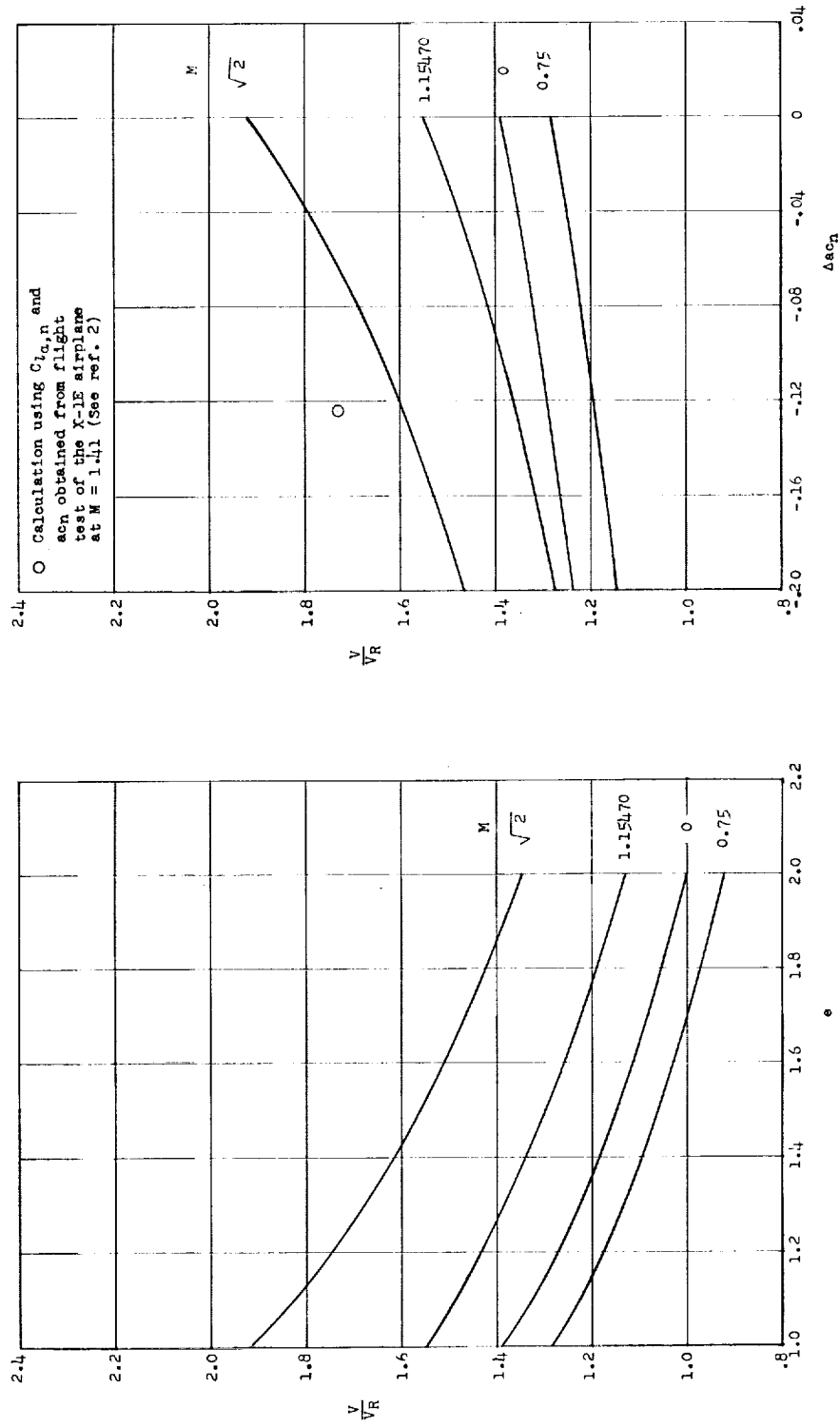
Figure 7.- Variation of flutter speed with lift factor e and with aerodynamic-center shift Δac_n for wing 400R. V_R is calculated for $e = 1$ and $\Delta ac_n = 0$. $\rho = 0.003100$ slug/cu ft; $V_R = 852.5$ ft/sec.
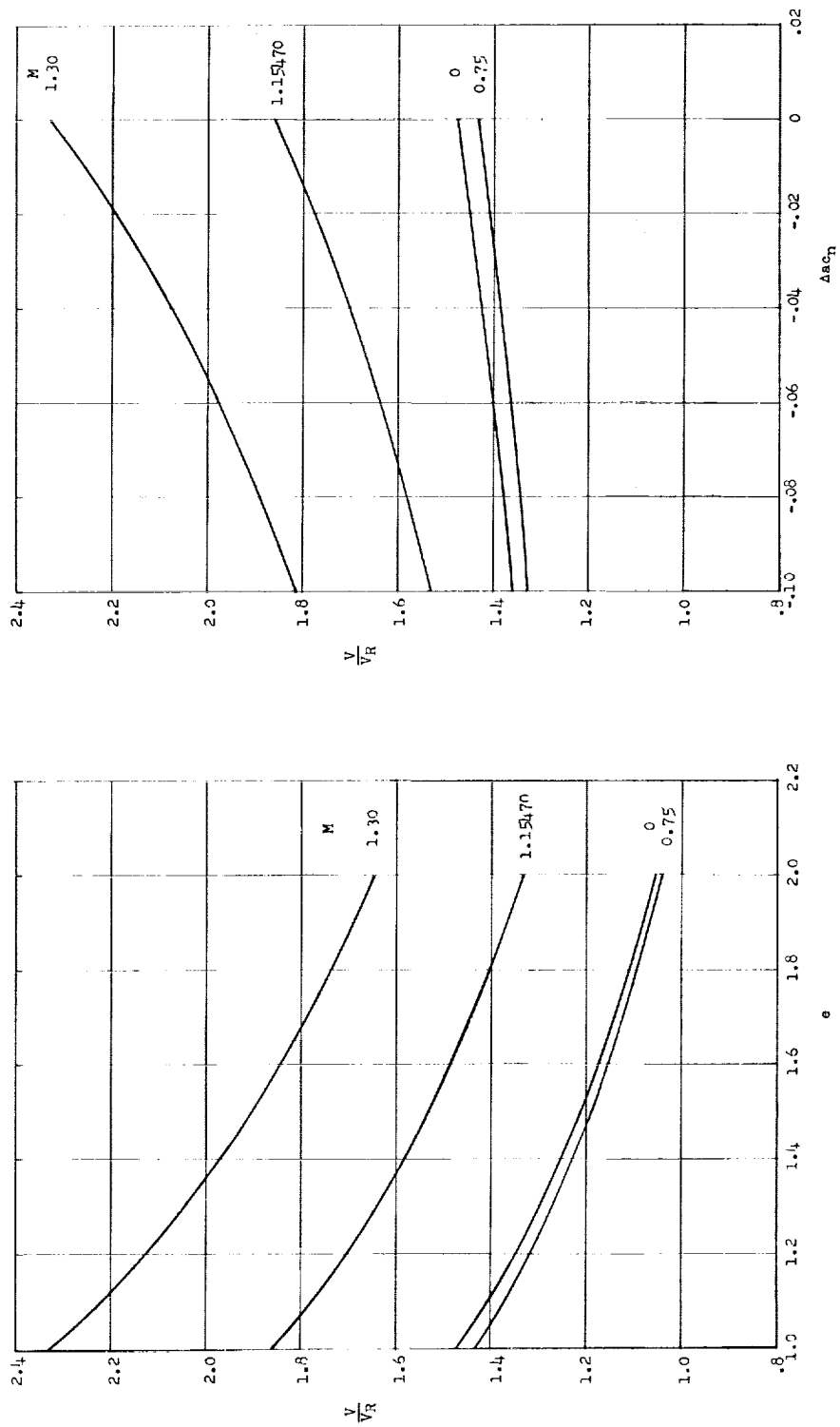
Figure 8.- Variation of flutter speed with lift factor e and with aerodynamic-center shift Δac_n for wing 4001. V_R is calculated for $e = 1$ and $\Delta ac_n = 0$. $\rho = 0.002378$ slug/cu ft; $V_R = 828.5$ ft/sec.

L-464
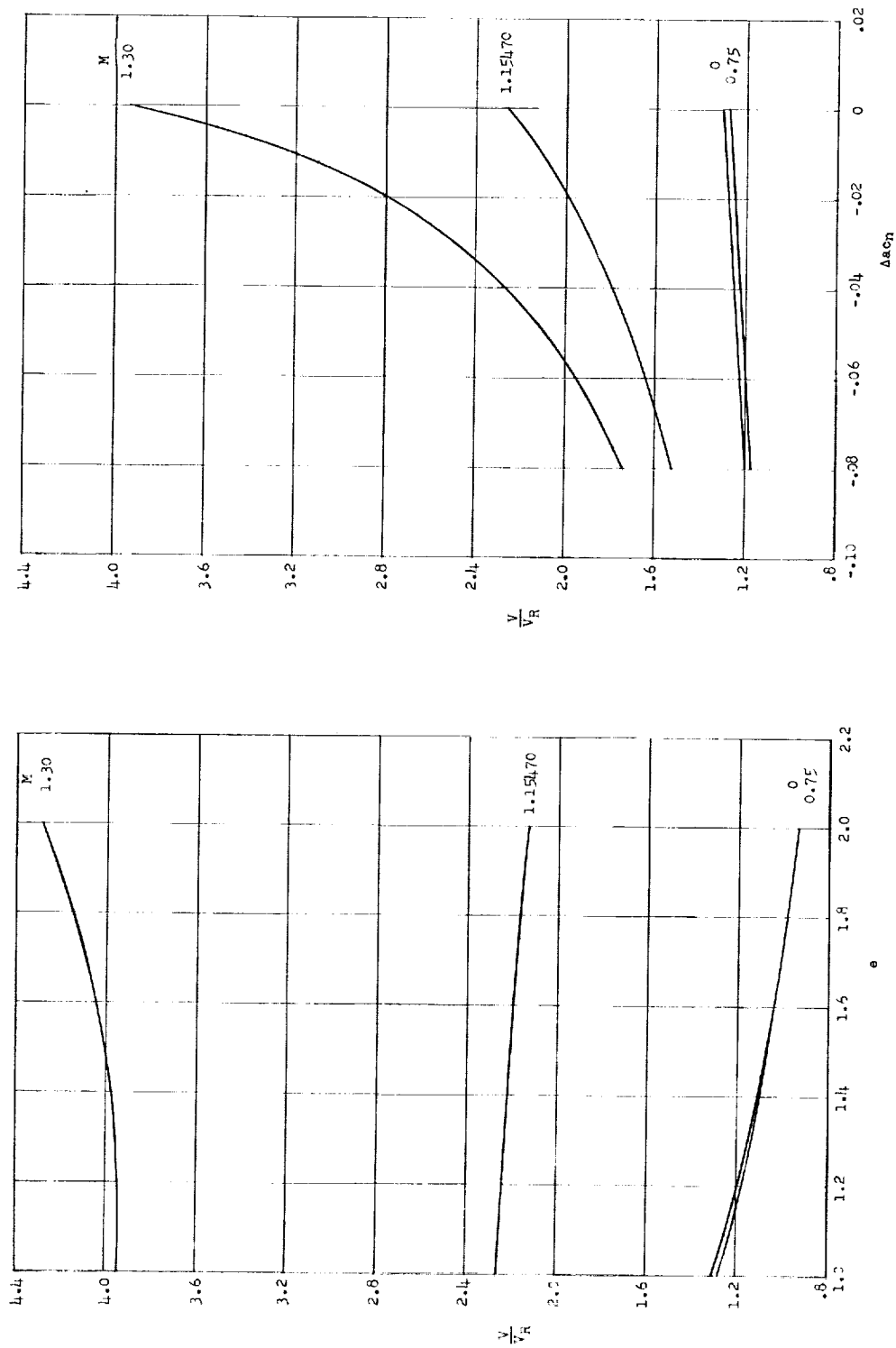
Figure 9.- Variation of flutter speed with lift factor e and with aerodynamic-center shift Δac_n for wing 7001. V_R is calculated for e = 1 and $\Delta ac_n = 0$. $\rho = 0.005500$ slug/cu ft; $V_R = 844.8$ ft/sec.

34
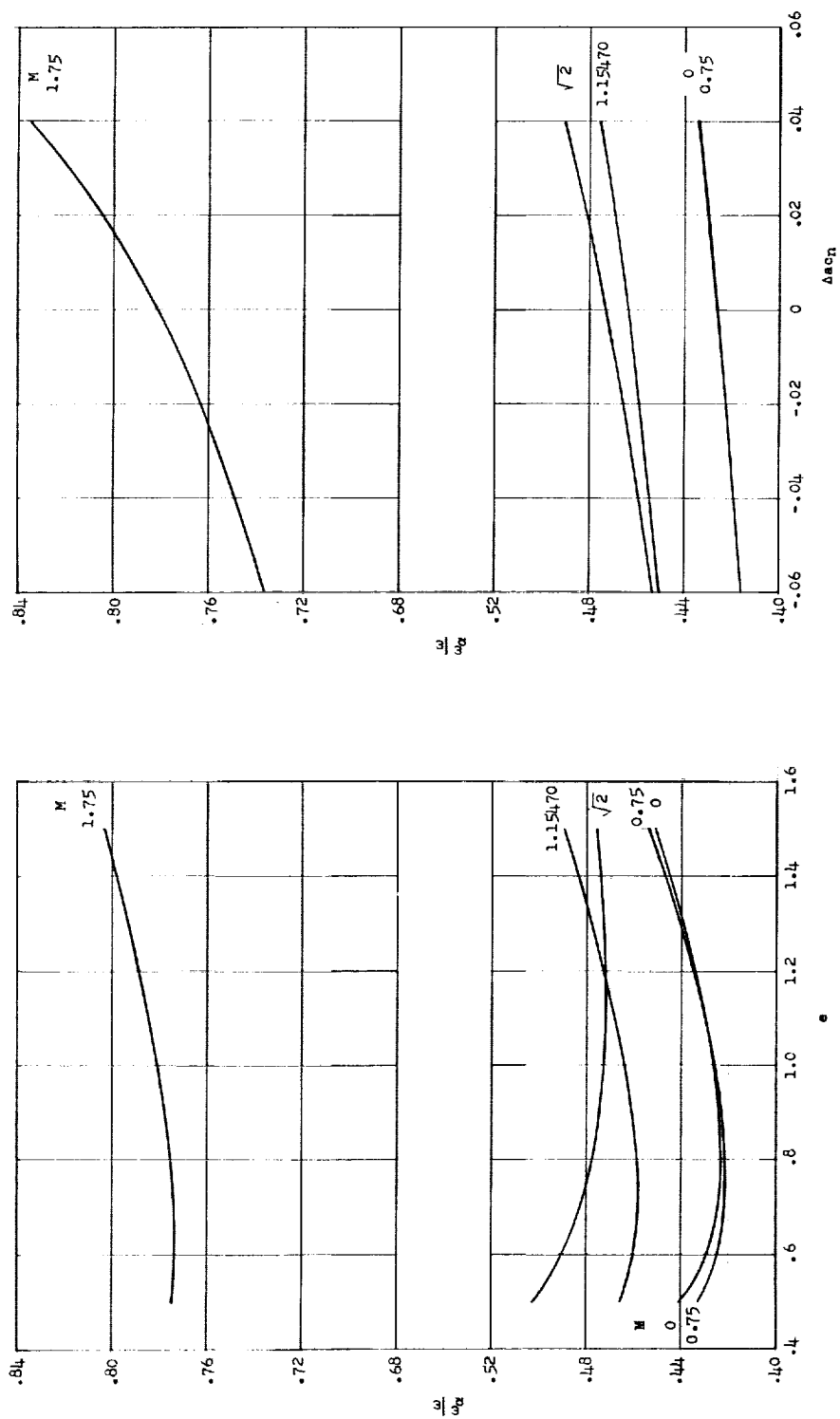
Figure 10.- Variation of flutter frequency with lift factor e and with aerodynamic-center shift Δac_n for wing 445. $\rho = 0.003800$ slug/cu ft; $\omega_\alpha = 2,192$ radians/sec.

L-464
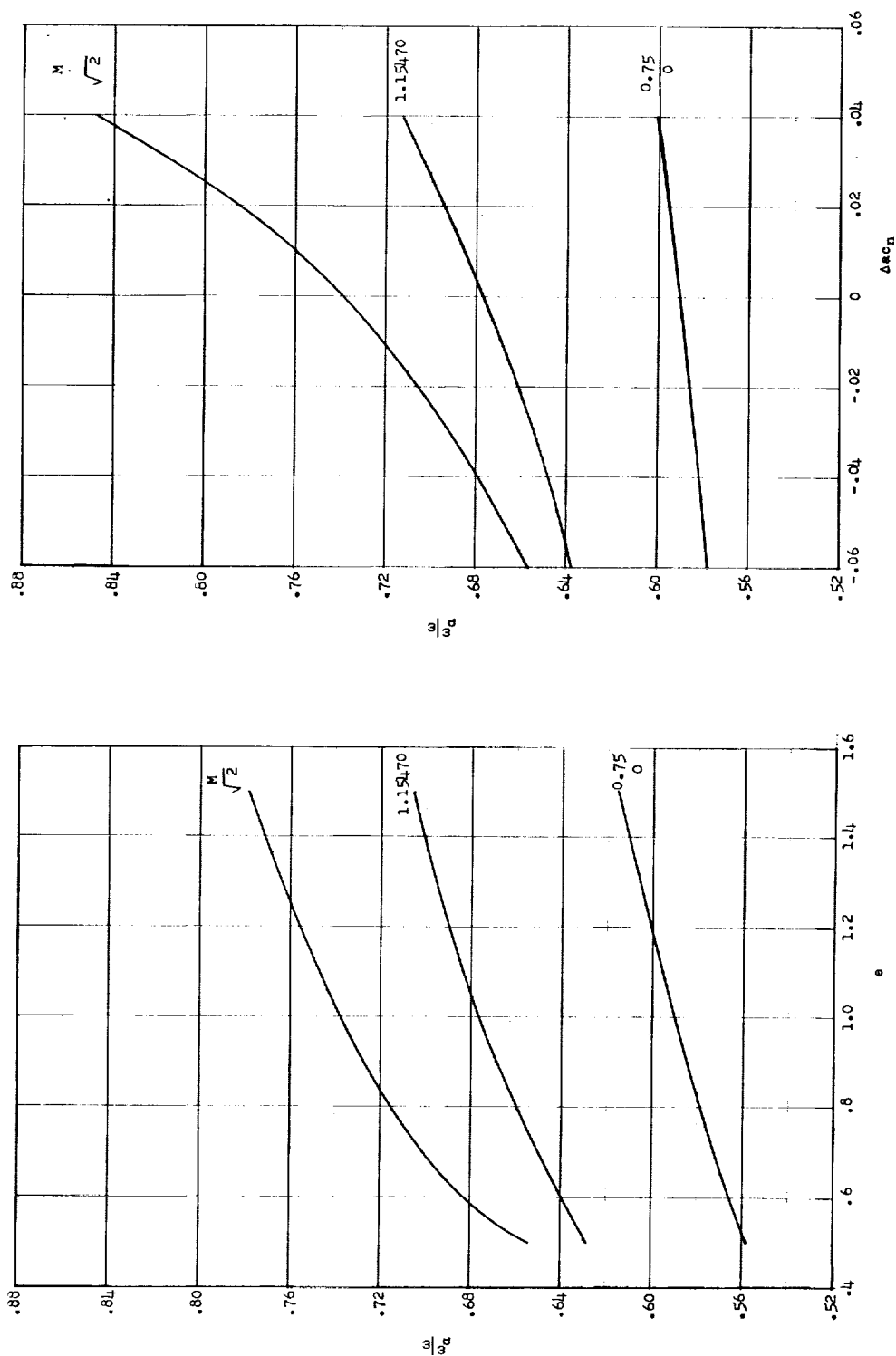
Figure 11.- Variation of flutter frequency with lift factor e and with aerodynamic-center shift
Δac_n for wing 445F. $\rho = 0.003000$ slug/cu ft; $\omega_\alpha = 1,144$ radians/sec.
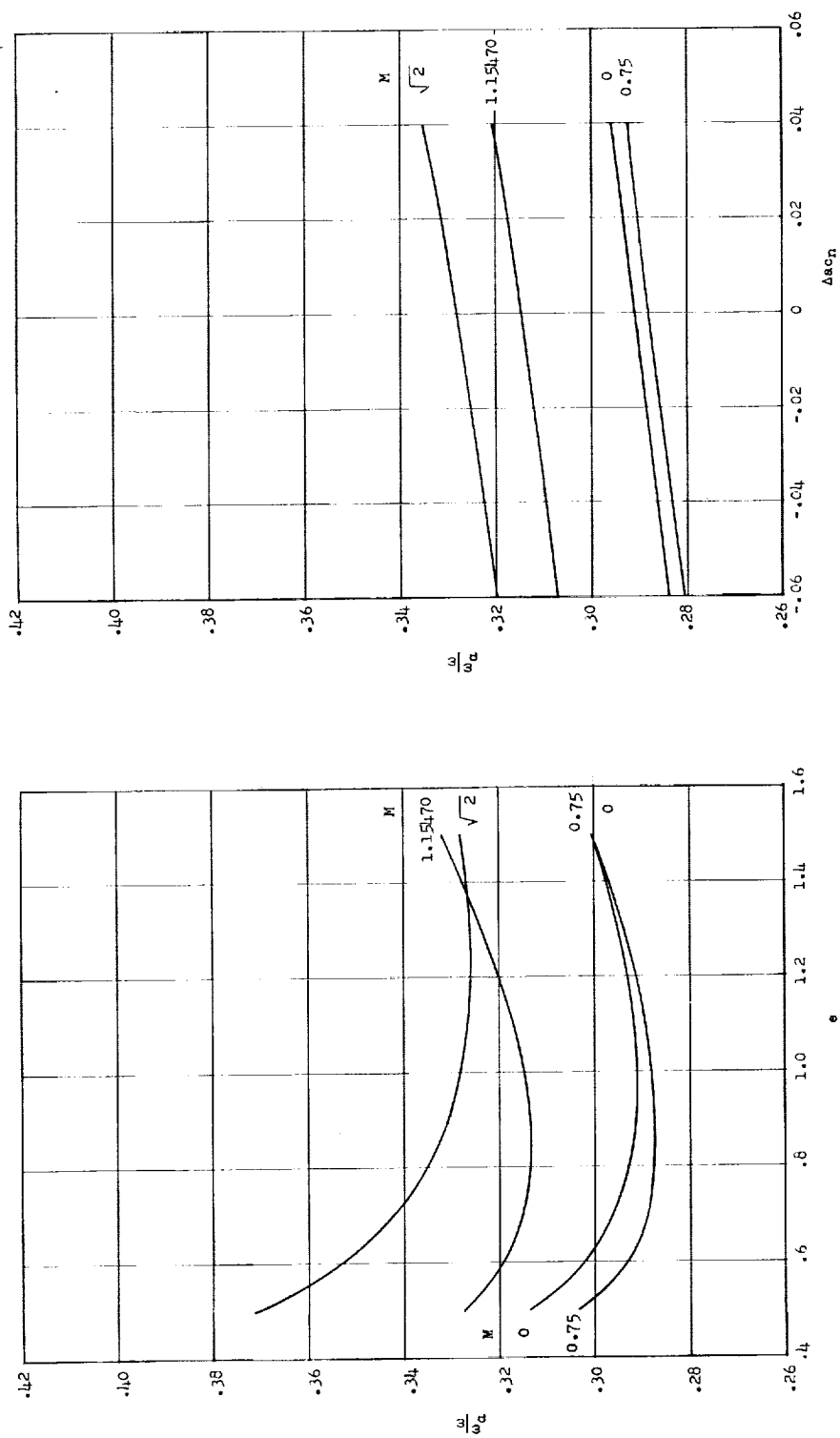
Figure 12.- Variation of flutter frequency with lift factor e and with aerodynamic-center shift Δac_n for wing 445R. $\rho = 0.002378$ slug/cu ft; $\omega_\alpha = 2,306$ radians/sec.

L-464
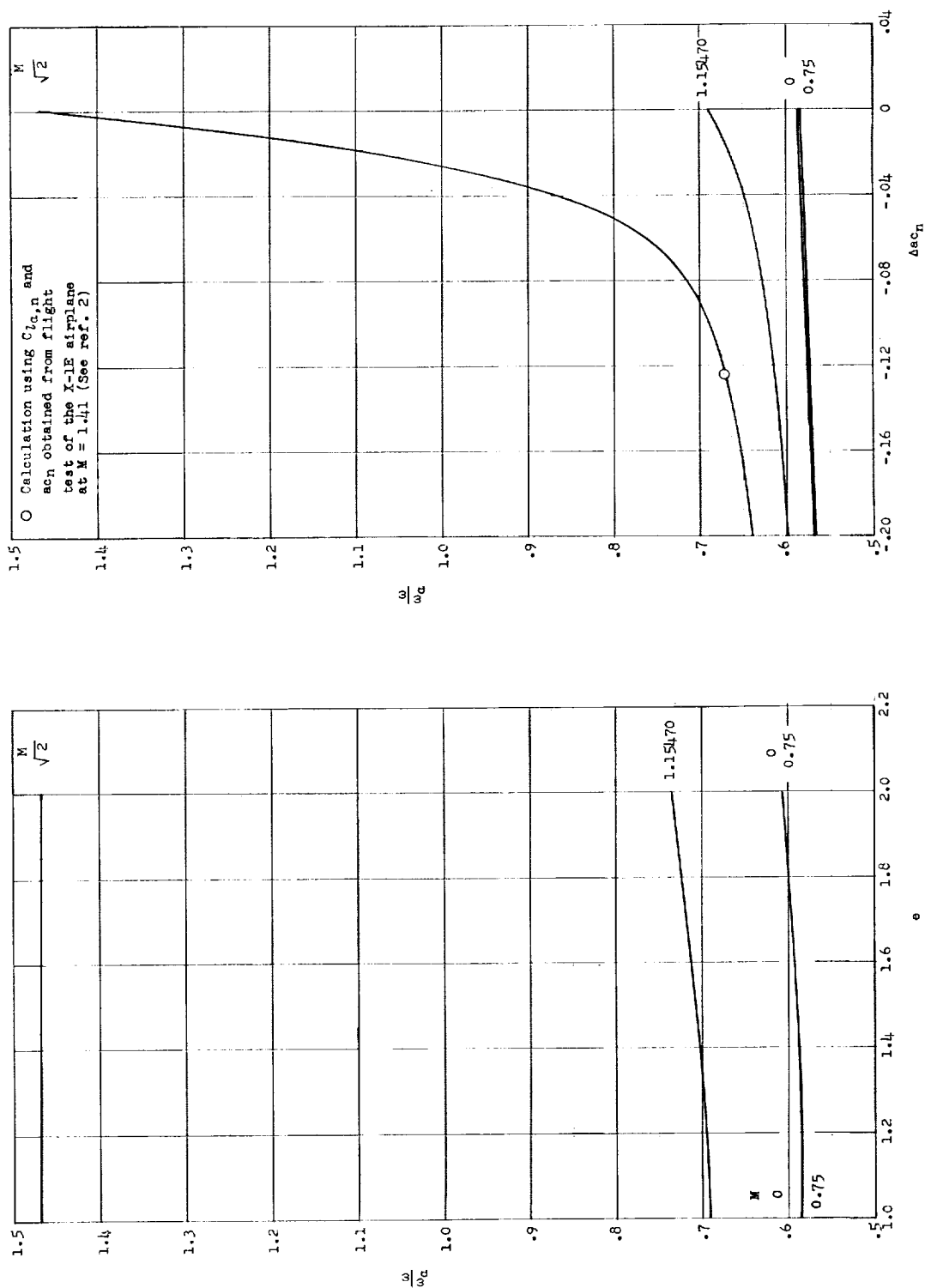
Figure 13.- Variation of flutter frequency with lift factor e and with aerodynamic-center shift Δac_n for wing 400. $\rho = 0.002378$ slug/cu ft; $\omega_\alpha = 2,463$ radians/sec.

38
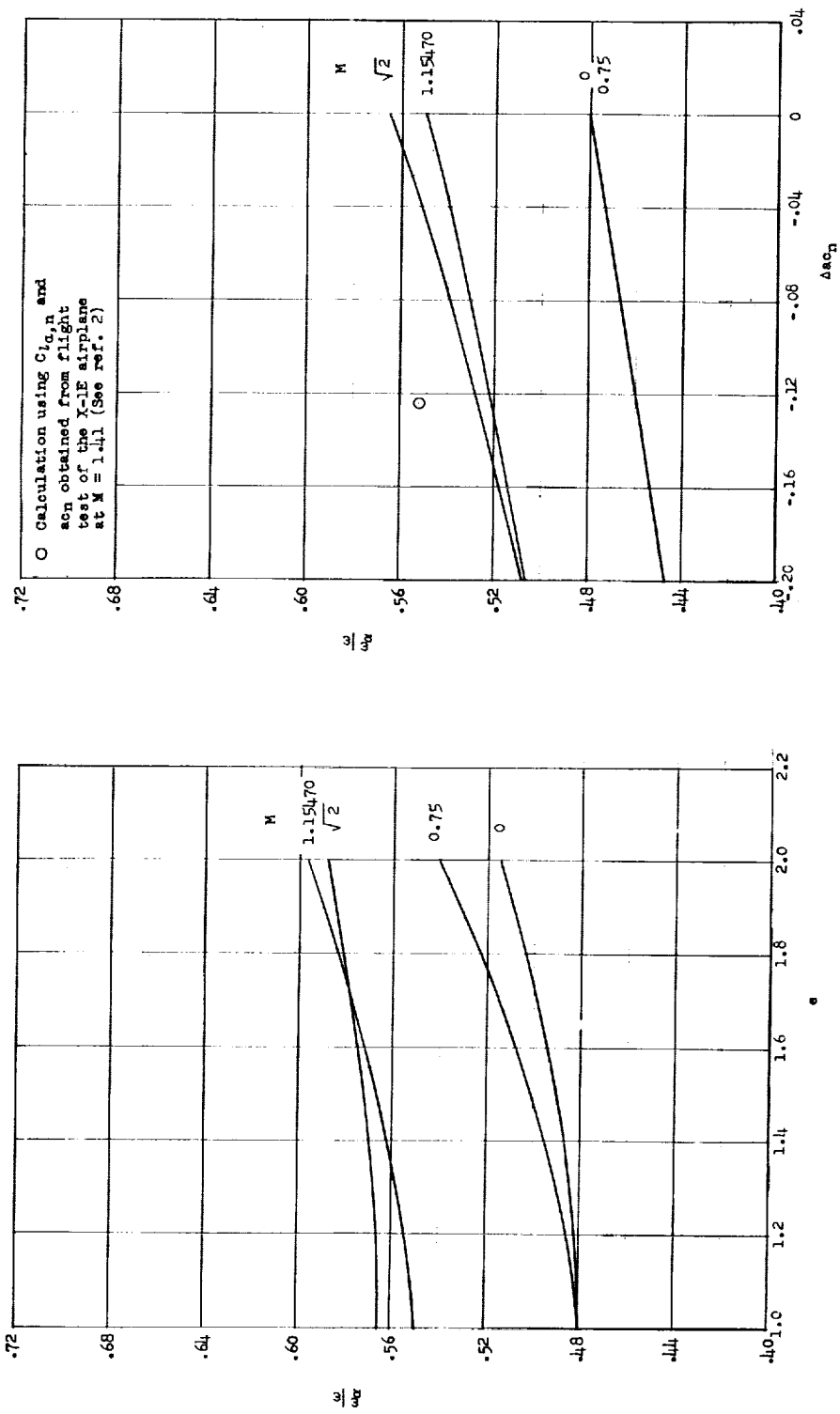
Figure 14.- Variation of flutter frequency with lift factor e and with aerodynamic-center shift Δac_n for wing 400R. $\rho = 0.003100$ slug/cu ft; $\omega_\alpha = 1,982$ radians/sec.
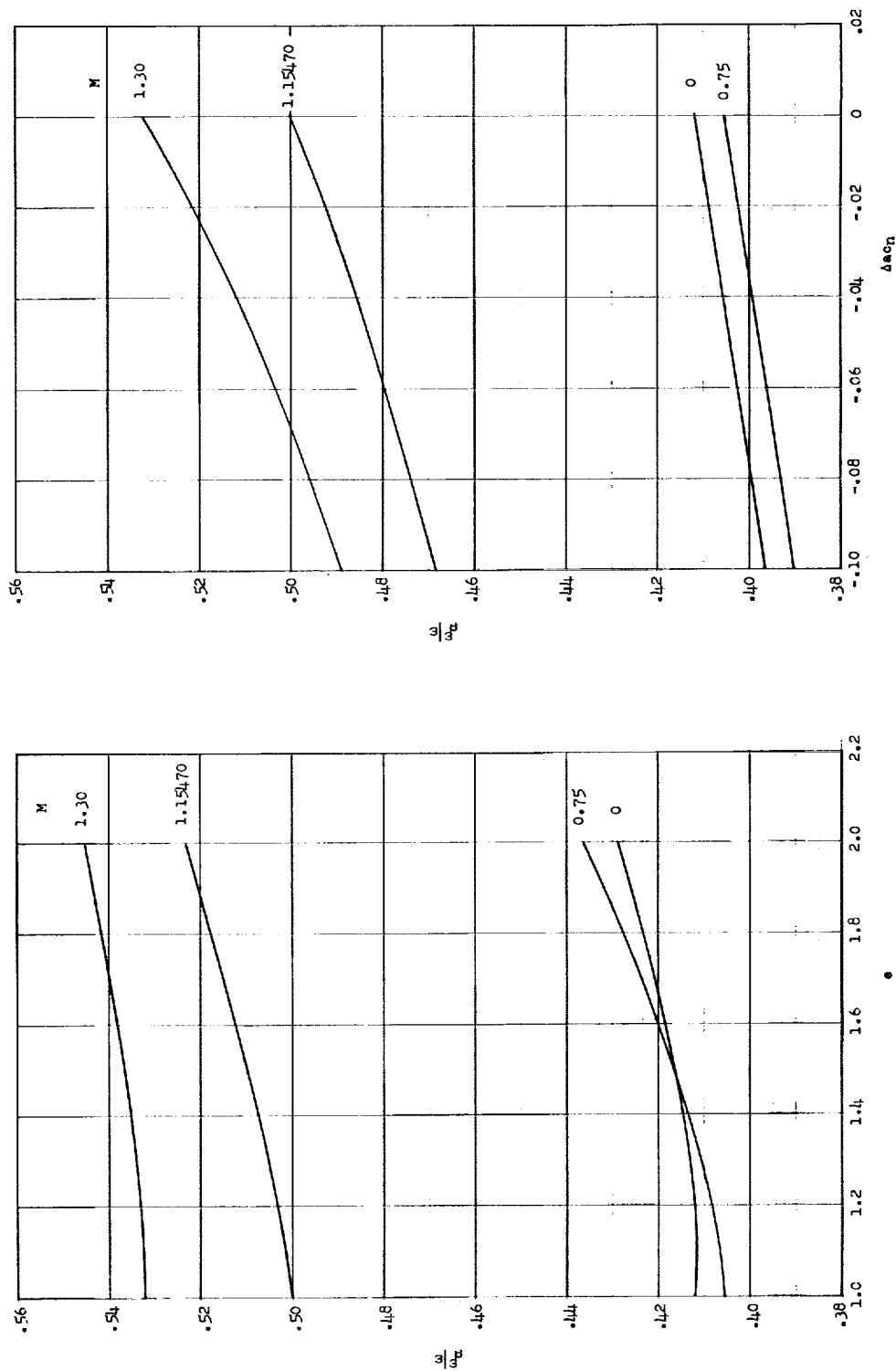
Figure 15.- Variation of flutter frequency with lift factor e and with aerodynamic-center shift Δac_n for wing 4001. $\rho = 0.002378$ slug/cu ft; $\omega_\alpha = 2,048$ radians/sec.
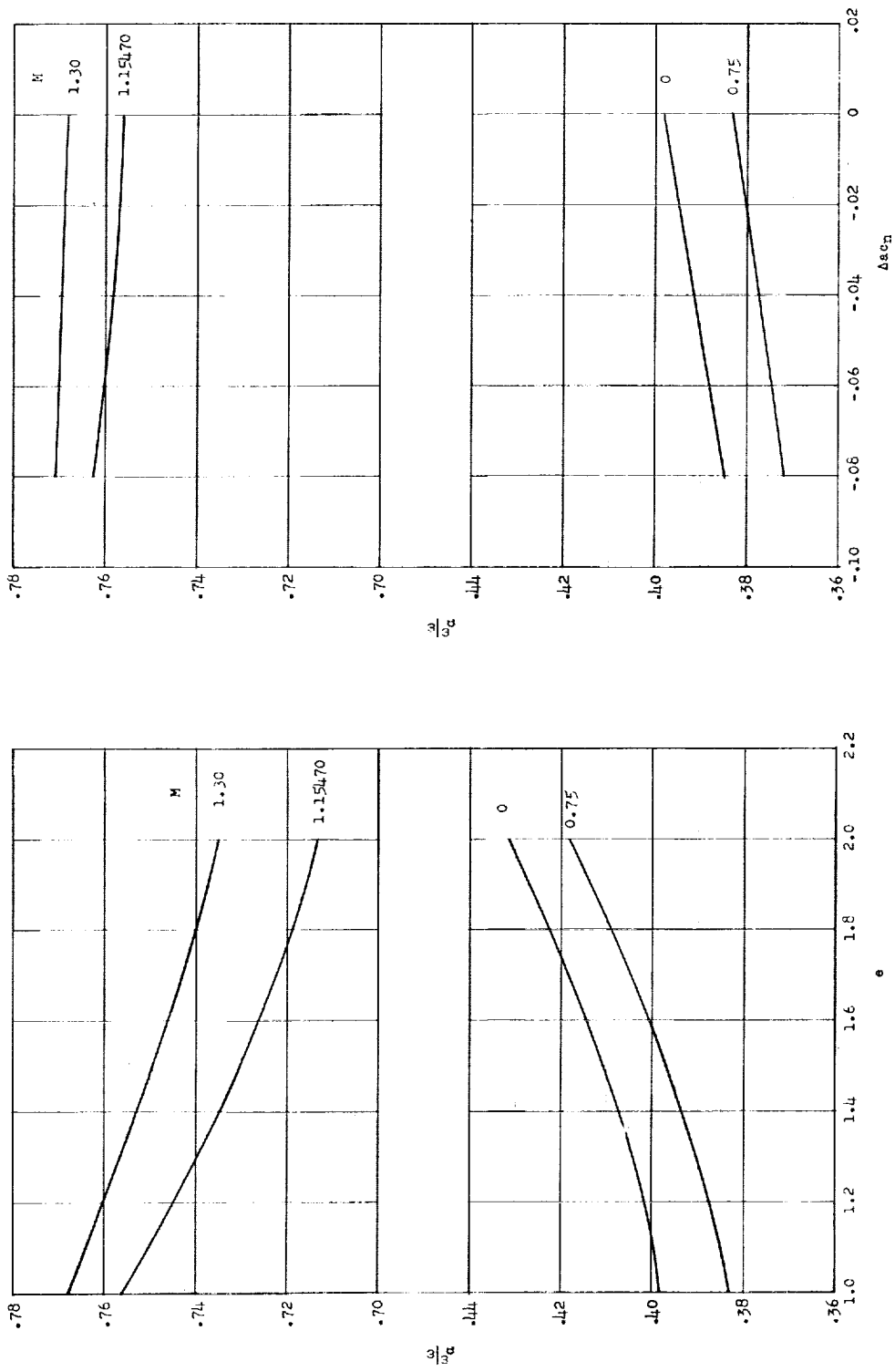
Figure 16.- Variation of flutter frequency with lift factor e and with aerodynamic-center shift
Δac_n for wing 7001. $\rho = 0.005500$ slug/cu ft; $\omega_\alpha = 2,271$ radians/sec.

L-404
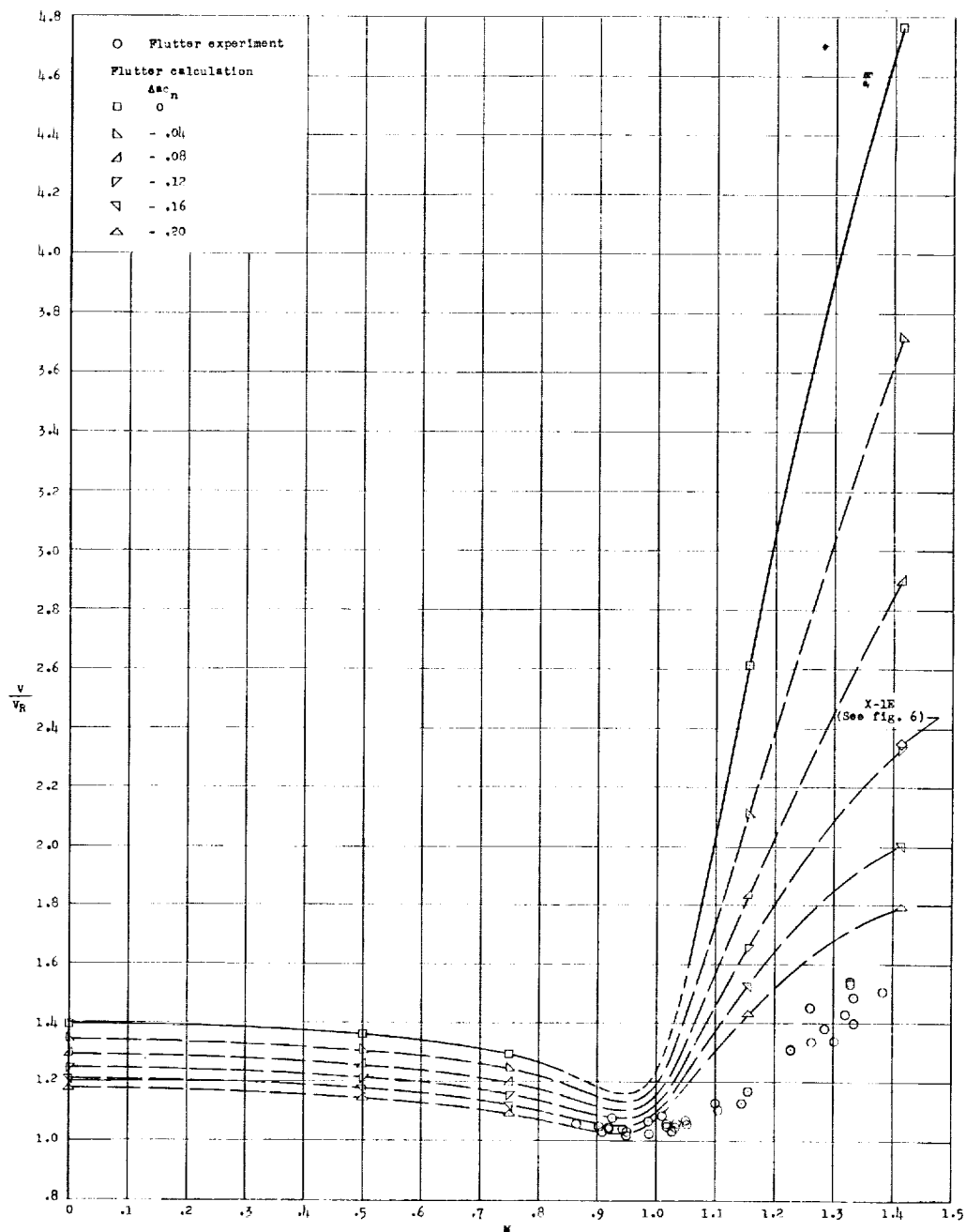
Figure 17.- Effect of ac_n changes on the variation of flutter speed with Mach number for wing 400. For calculated points $\rho = 0.002378$ slug/cu ft and $V_R = 976.5$ ft/sec.
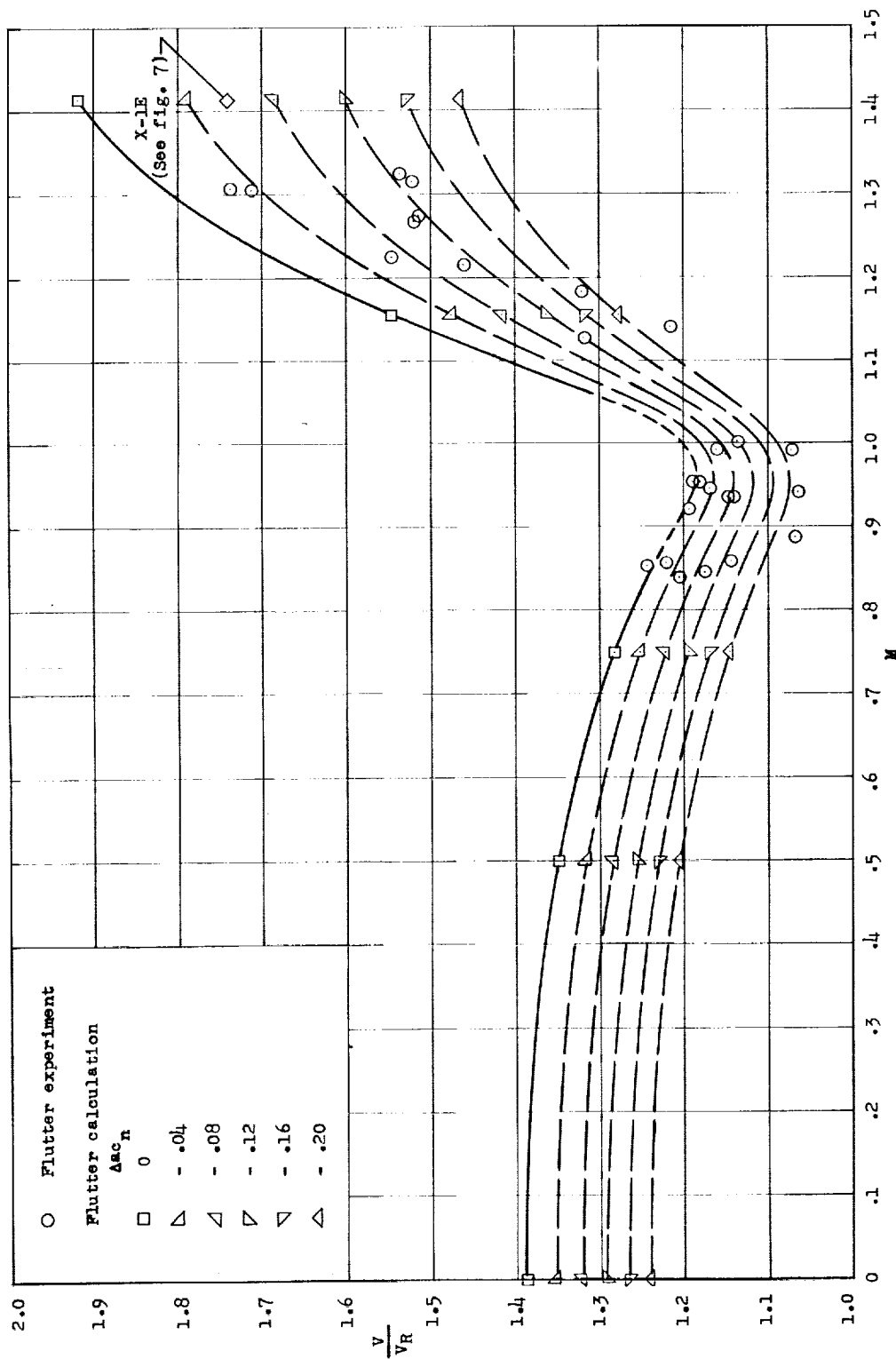
Figure 18.- Effect of ac_n changes on the variation of flutter speed with Mach number for wing 400R. For calculated points $\rho = 0.003100$ slug/cu ft and $V_R = 852.5$ ft/sec.
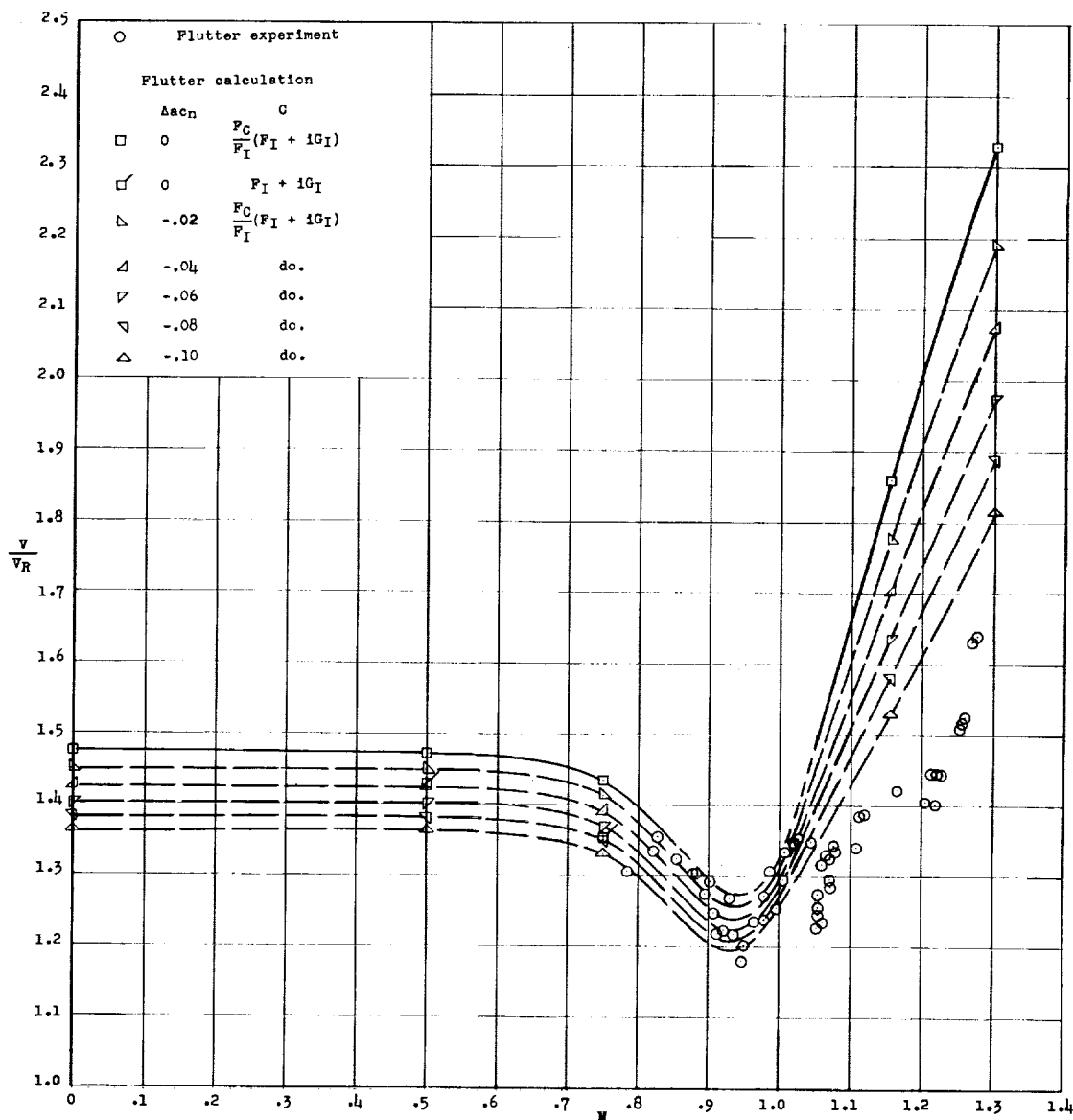
Figure 19.- Effect of ac_n changes on the variation of flutter speed with Mach number for wing 4001. For calculated points $\rho = 0.002378$ slug/cu ft and $V_R = 828.5$ ft/sec.
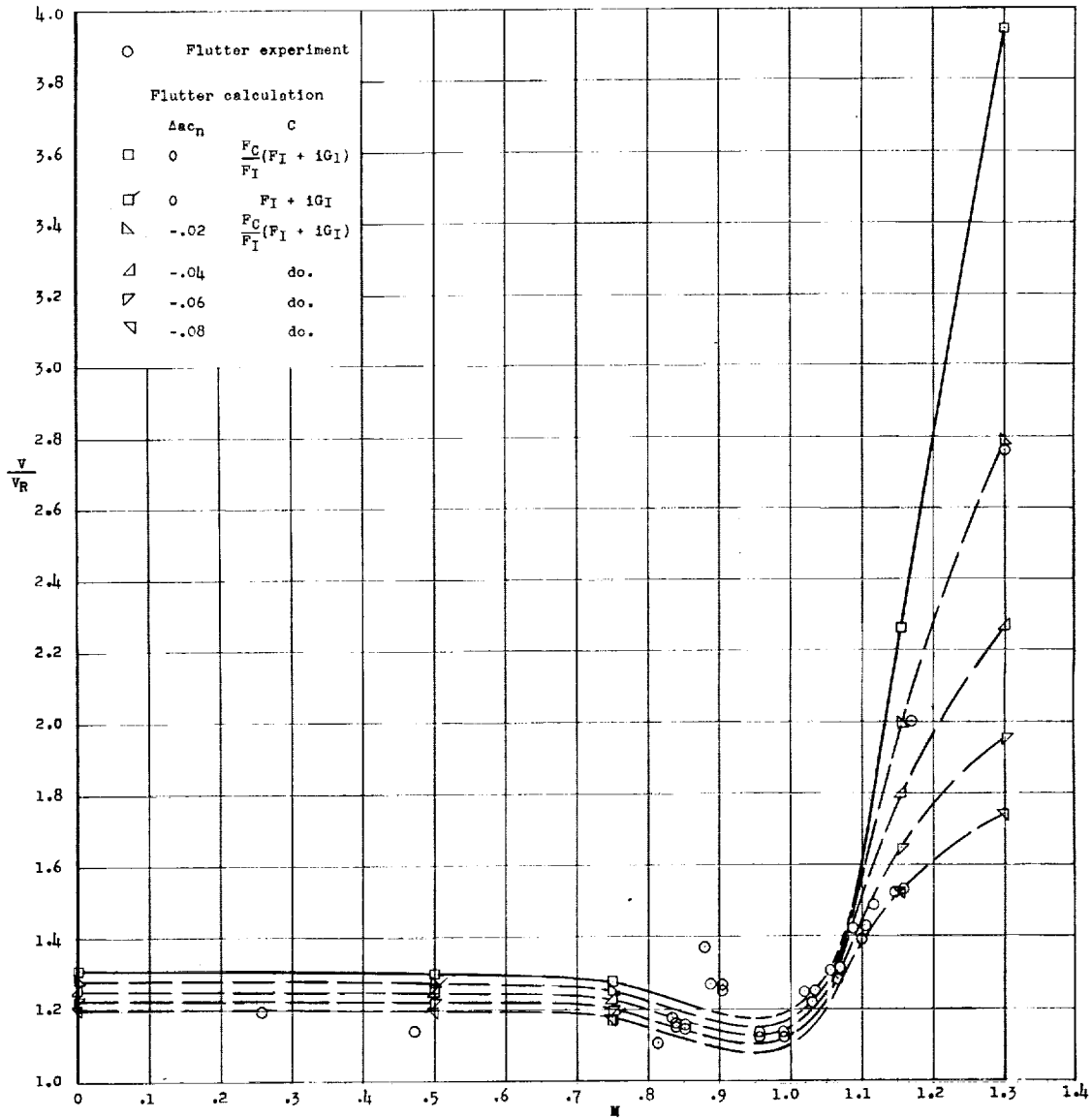
Figure 20.- Effect of ac_n changes on the variation of flutter
speed with Mach number for wing 7001. For calculated points
$\rho = 0.005500$ slug/cu ft and $V_R = 844.8$ ft/sec.

L-464
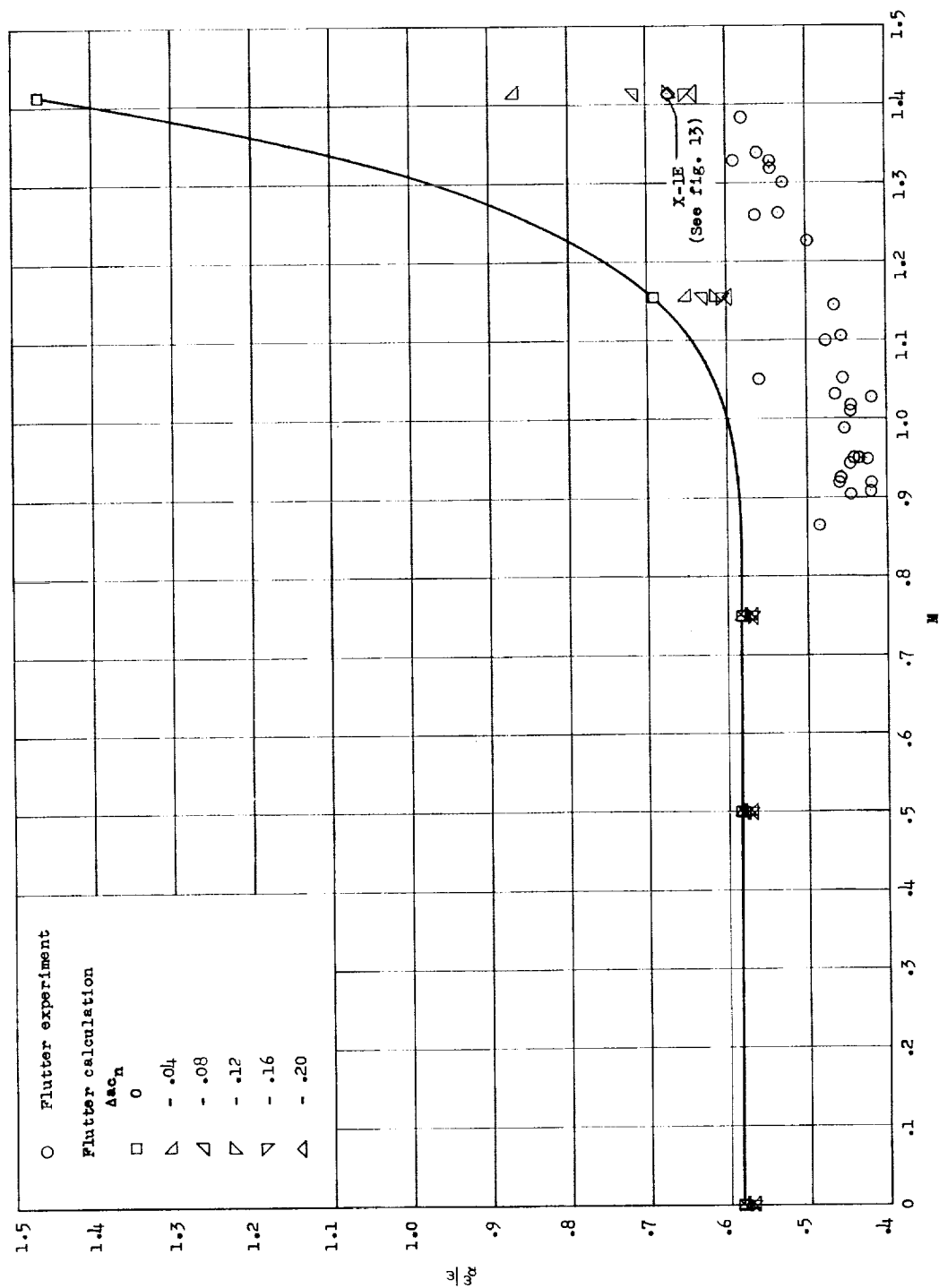
Figure 21.- Effect of ac_n changes on the variation of flutter frequency with Mach number for wing 400. For calculated points $\rho = 0.002378$ slug/cu ft and $\omega_\alpha = 2,463$ radians/sec.
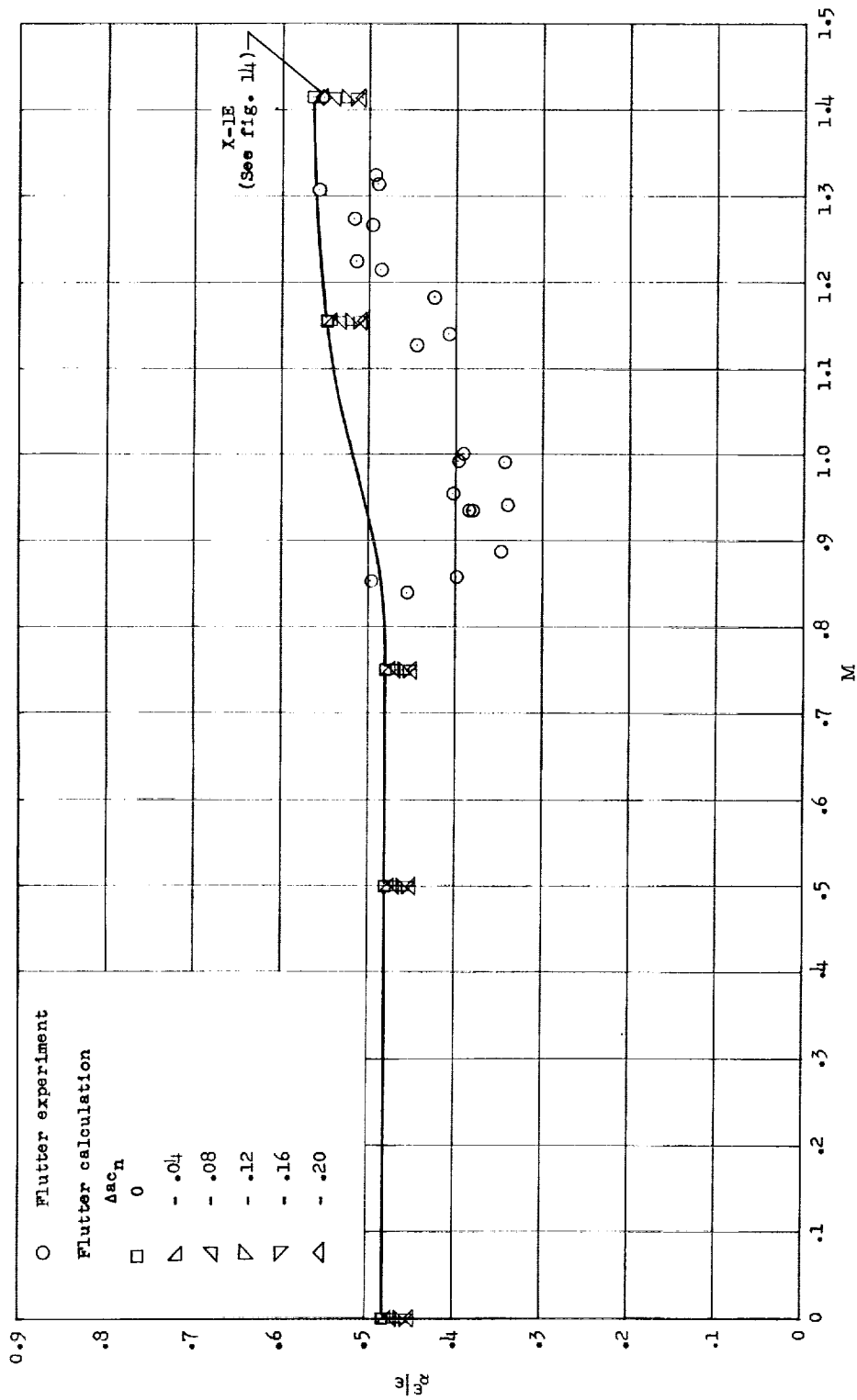
Figure 22.- Effect of ac_n changes on the variation of flutter frequency with Mach number for wing 400R. For calculated points $\rho = 0.003100$ slug/cu ft and $\omega_\alpha = 1,982$ radians/sec.
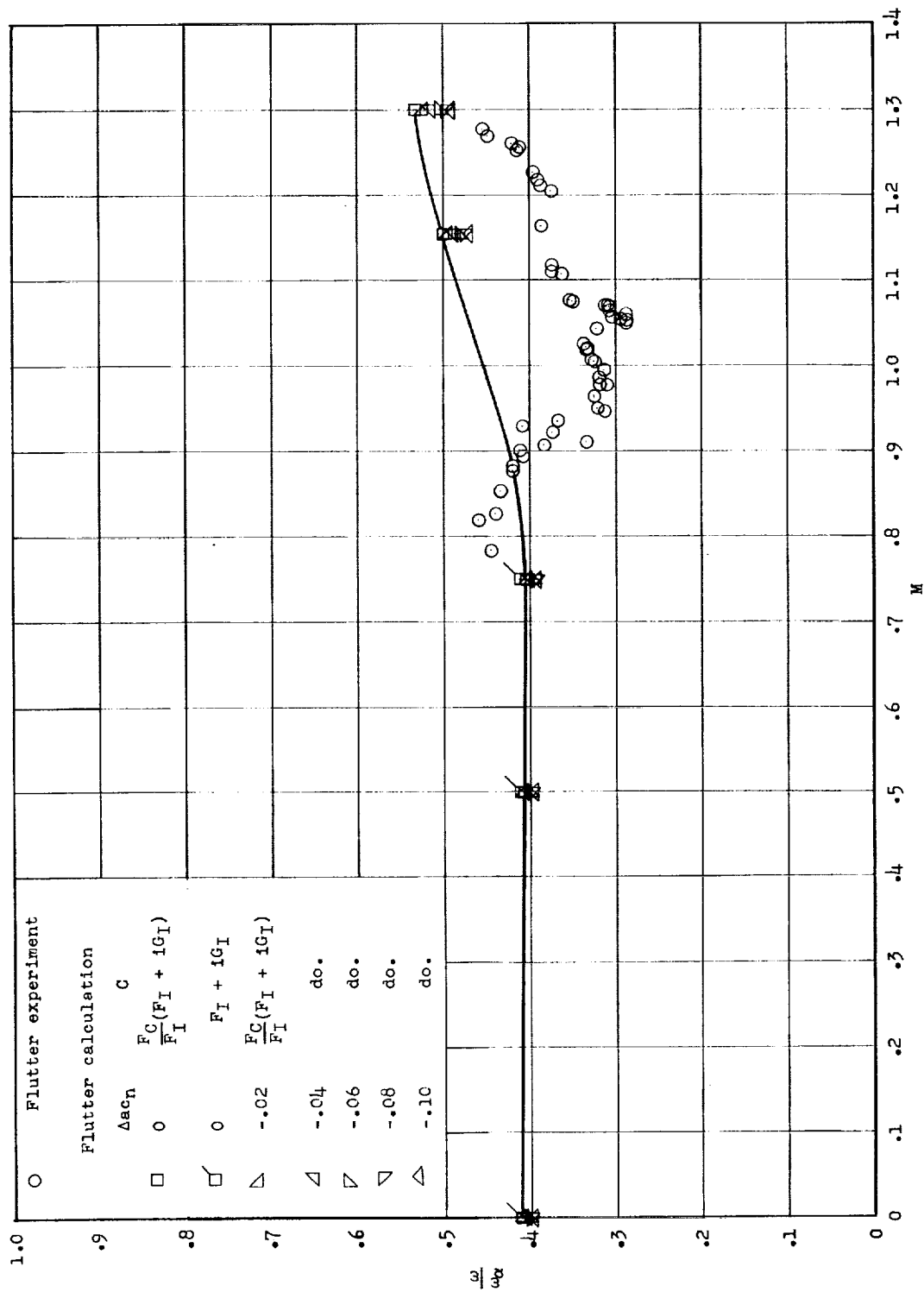
Figure 23.- Effect of ac_n changes on the variation of flutter frequency with Mach number for wing 4001. For calculated points $\rho = 0.002378$ slug/cu ft and $\omega_\alpha = 2,048$ radians/sec.
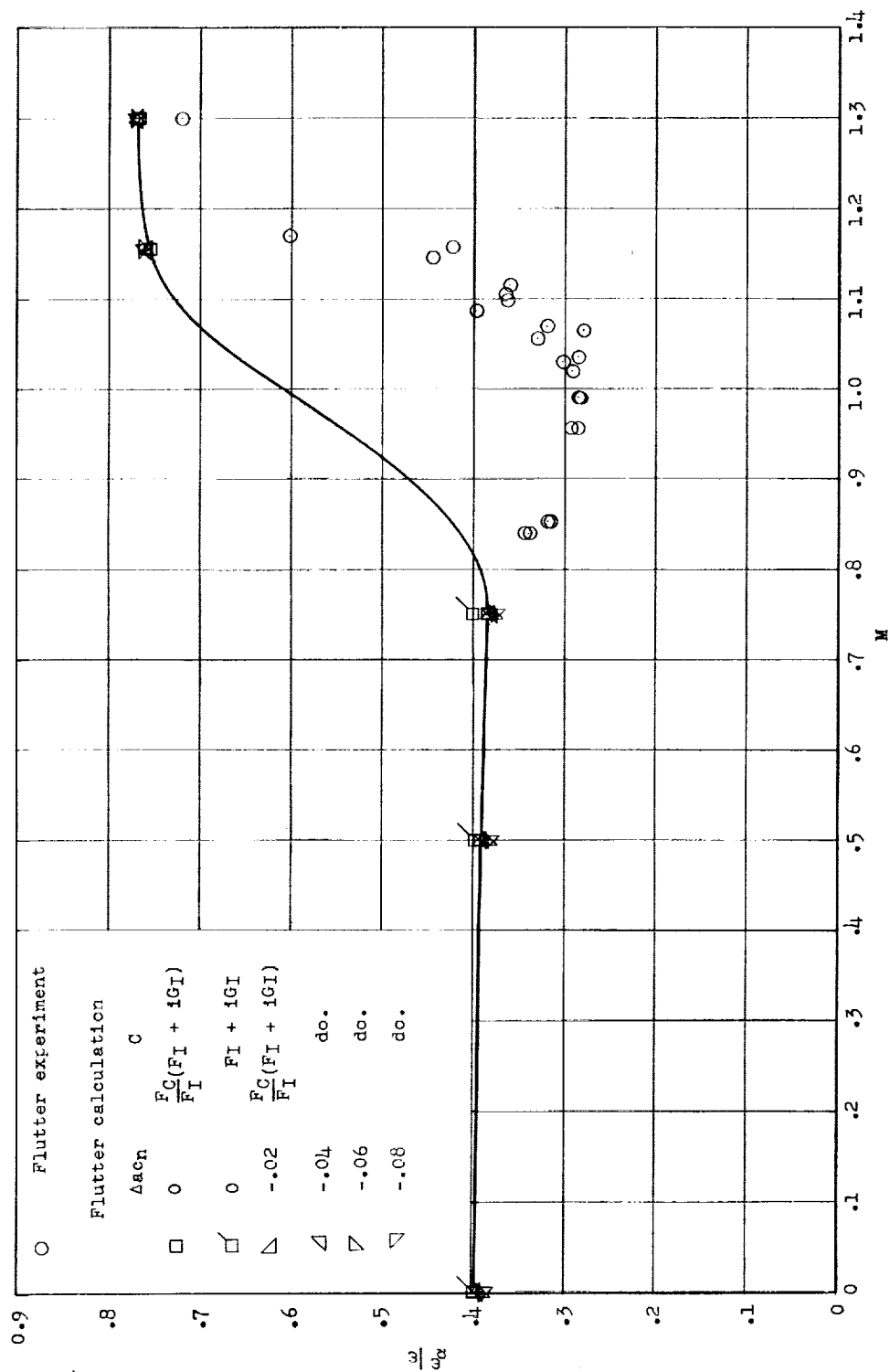
Figure 24.- Effect of Δa_{cn} changes on the variation of flutter frequency with Mach number for wing 7001. For calculated points $\rho = 0.005500$ slug/cu ft and $\omega_\alpha = 2,271$ radians/sec.
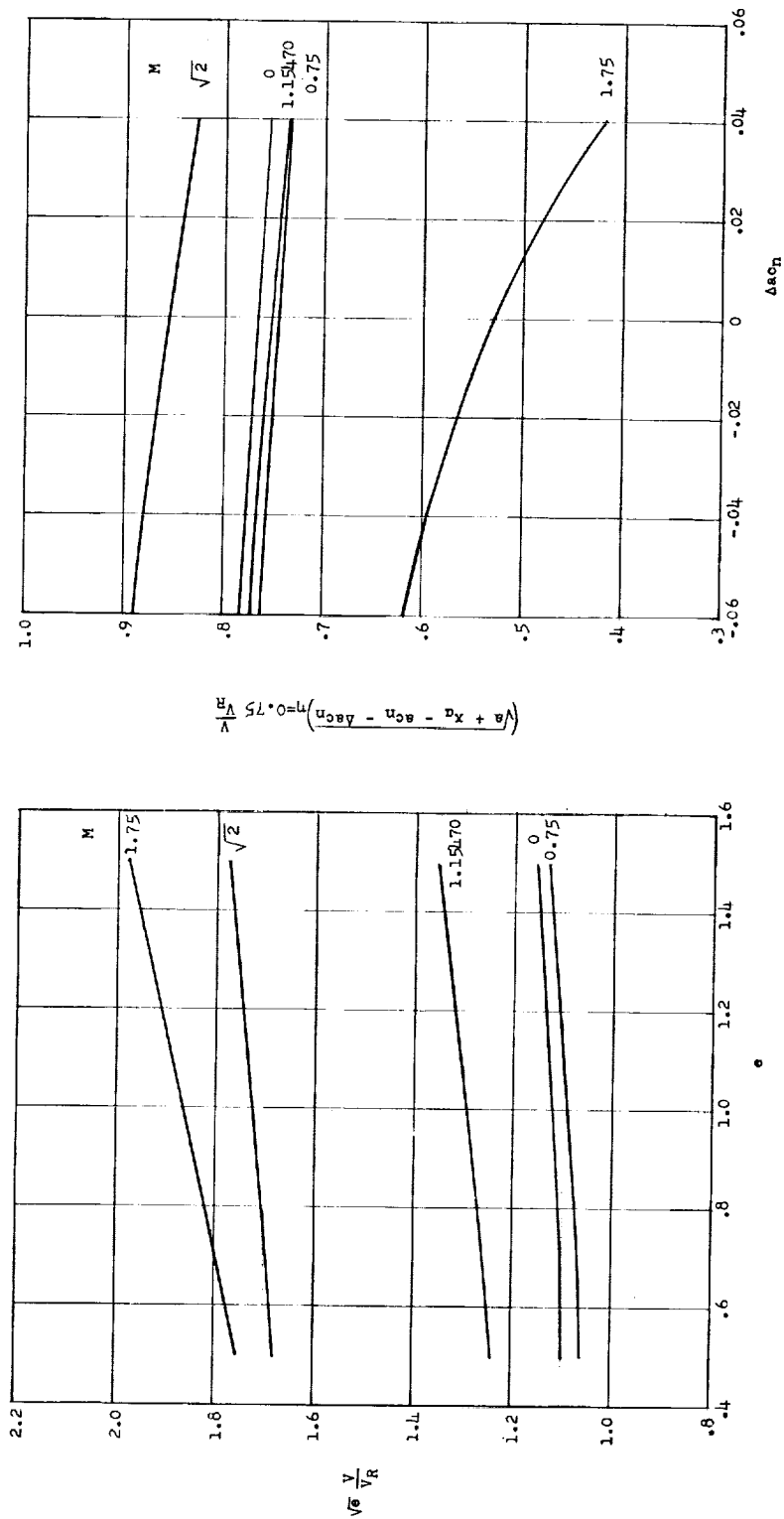
Figure 25.- Variation of $\sqrt{e}\ \dfrac{V}{V_R}$ with lift factor e and of $\left(\sqrt{a + x_\alpha - ac_n - \Delta ac_n}\right)_{\eta=0.75}\dfrac{V}{V_R}$ with aerodynamic-center shift Δac_n for wing 445. V_R is calculated for $e = 1$ and $\Delta ac_n = 0$. $\rho = 0.003800$ slug/cu ft; $V_R = 735.0$ ft/sec.
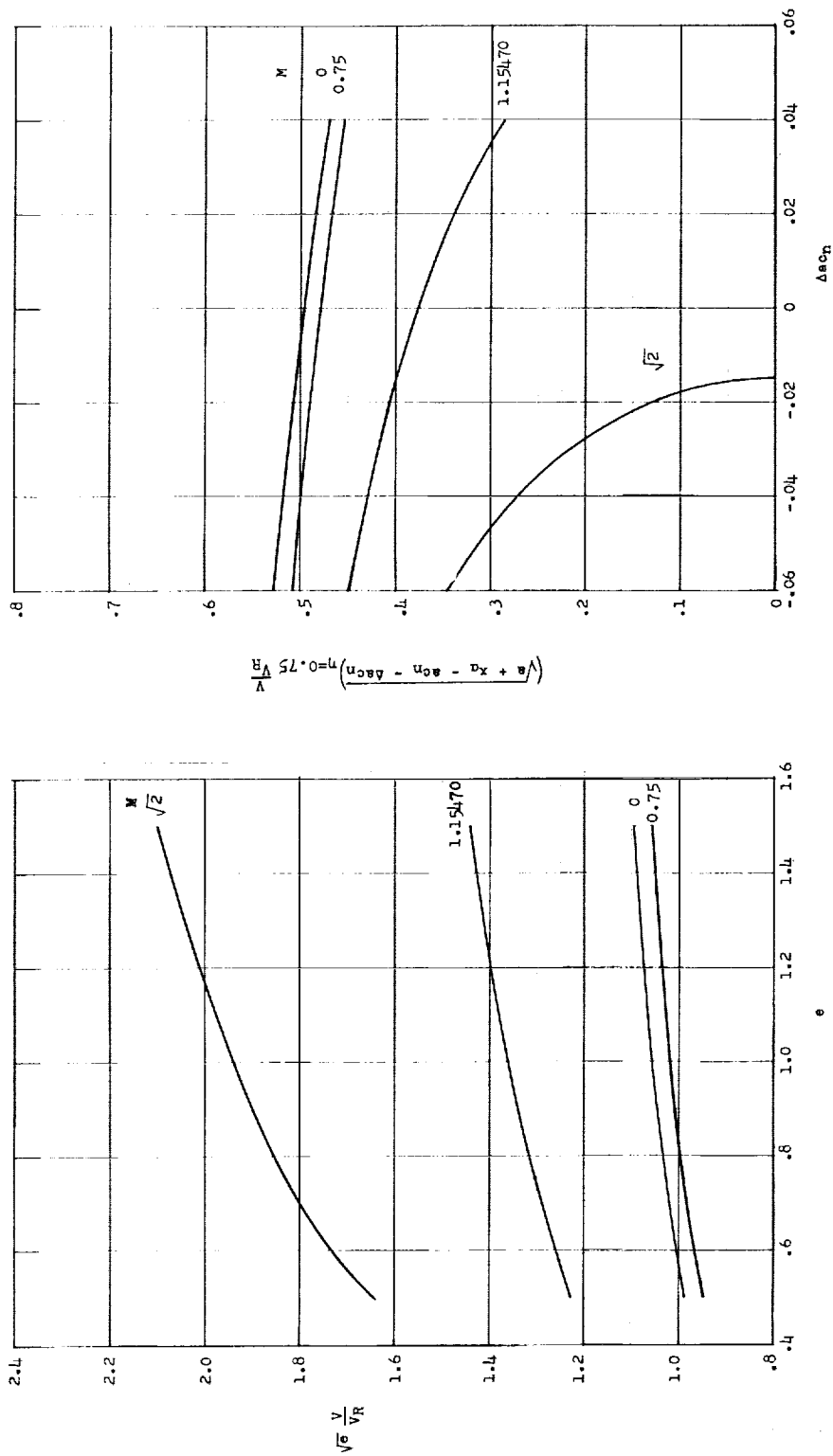
Figure 26.- Variation of $\sqrt{e}\ \dfrac{V}{V_R}$ with lift factor e and of $\left(\sqrt{a + x_\alpha - ac_n - \Delta ac_n}\right)_{\eta=0.75} \dfrac{V}{V_R}$ with aerodynamic-center shift Δac_n for wing 445F. V_R is calculated for $e = 1$ and $\Delta ac_n = 0.$ $\rho = 0.003000$ slug/cu ft; $V_R = 840.0$ ft/sec.

L-464
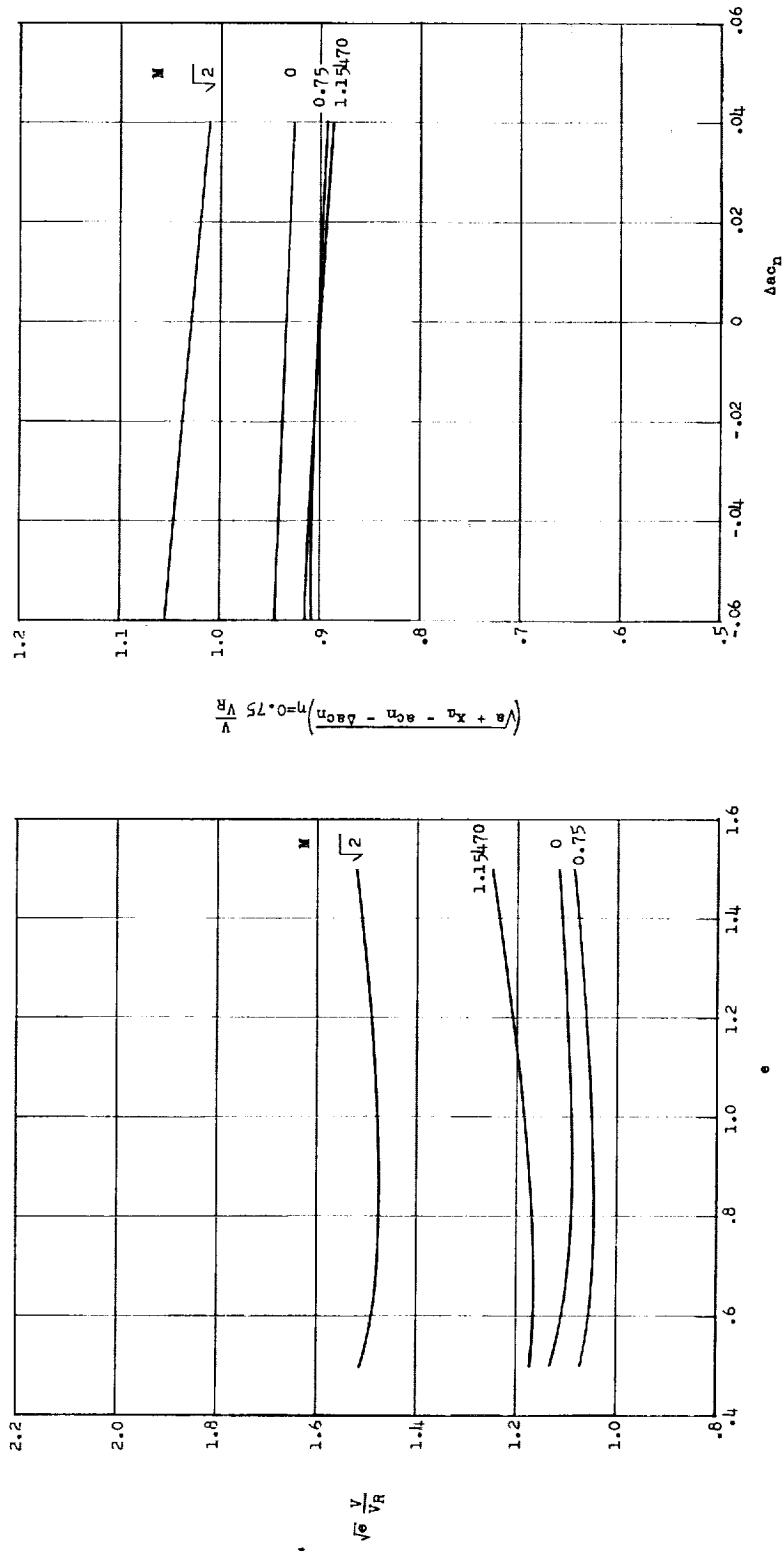
Figure 27.- Variation of $\sqrt{e} \dfrac{V}{V_R}$ with lift factor e and of $\left(\sqrt{a + x_\alpha - ac_n - \overline{\Delta ac_n}}\right)_{\eta=0.75} \dfrac{V}{V_R}$ with aerodynamic-center shift Δac_n for wing 445R. V_R is calculated for $e = 1$ and $\Delta ac_n = 0$. $\rho = 0.002378$ slug/cu ft; $V_R = 928.7$ ft/sec.
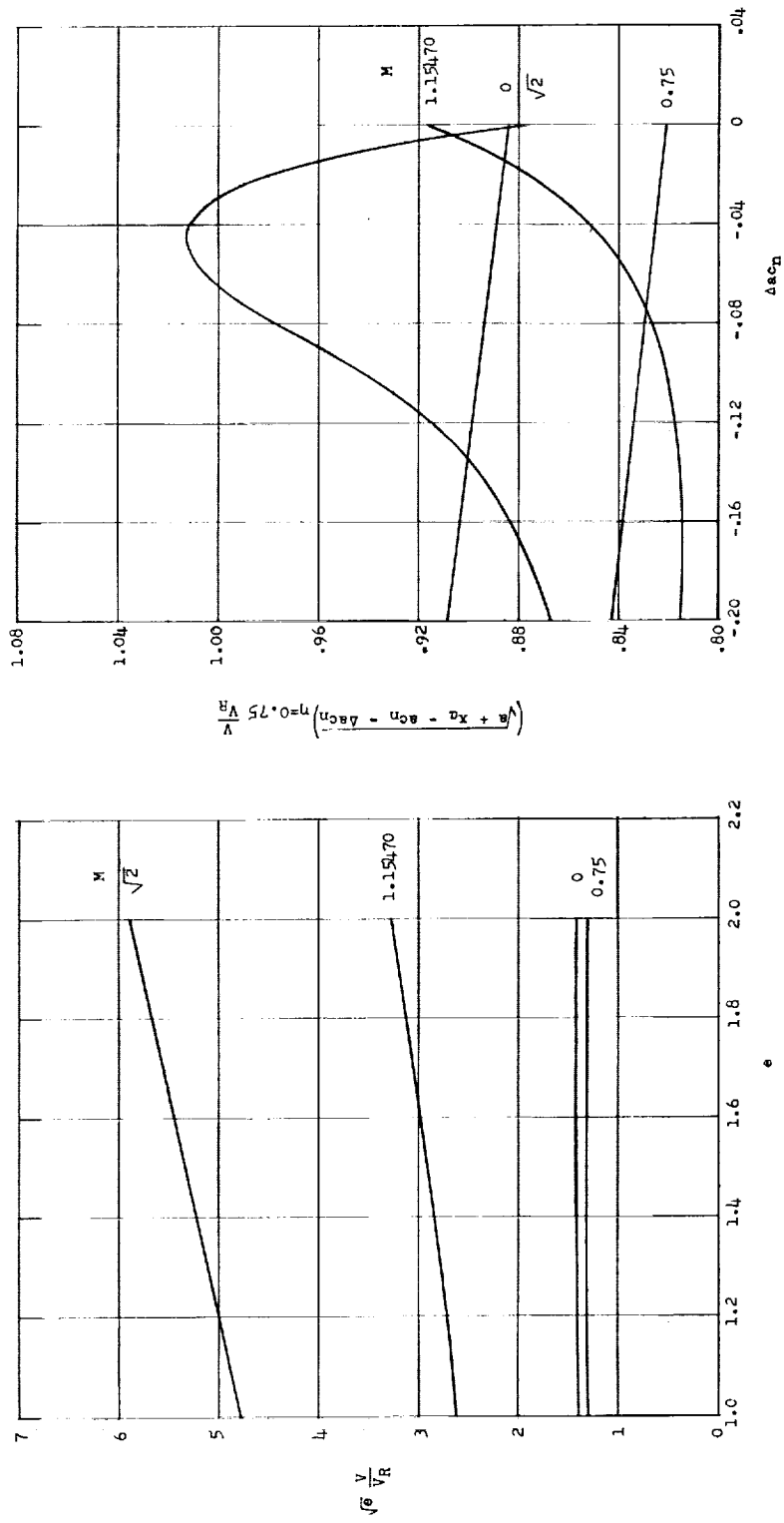
Figure 28.- Variation of $\sqrt{e}\,\dfrac{V}{V_R}$ with lift factor e and of $\left(\sqrt{a + x_\alpha - ac_n - \Delta ac_n}\right)_{\eta=0.75}\dfrac{V}{V_R}$ with aerodynamic-center shift Δac_n for wing 400. V_R is calculated for $e = 1$ and $\Delta ac_n = 0$. $\rho = 0.002378$ slug/cu ft; $V_R = 976.5$ ft/sec.
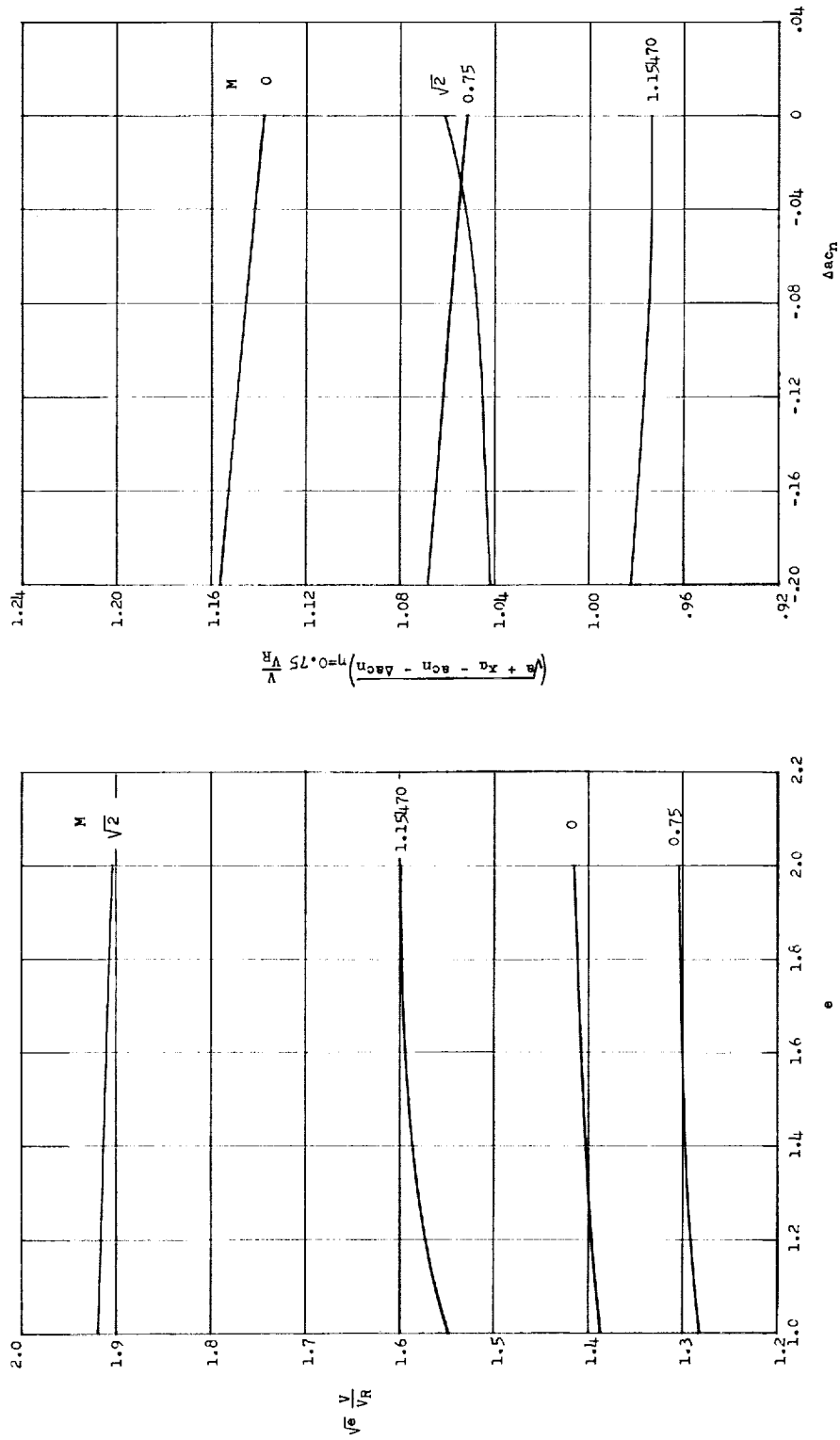
Figure 29.- Variation of $\sqrt{e}\,\dfrac{V}{V_R}$ with lift factor e and of $\left(\sqrt{a + x_\alpha - ac_n - \Delta ac_n}\right)_{\eta=0.75}\dfrac{V}{V_R}$ with aerodynamic-center shift Δac_n for wing 400R. V_R is calculated for $e = 1$ and $\Delta ac_n = 0$. $\rho = 0.003100$ slug/cu ft; $V_R = 852.5$ ft/sec.
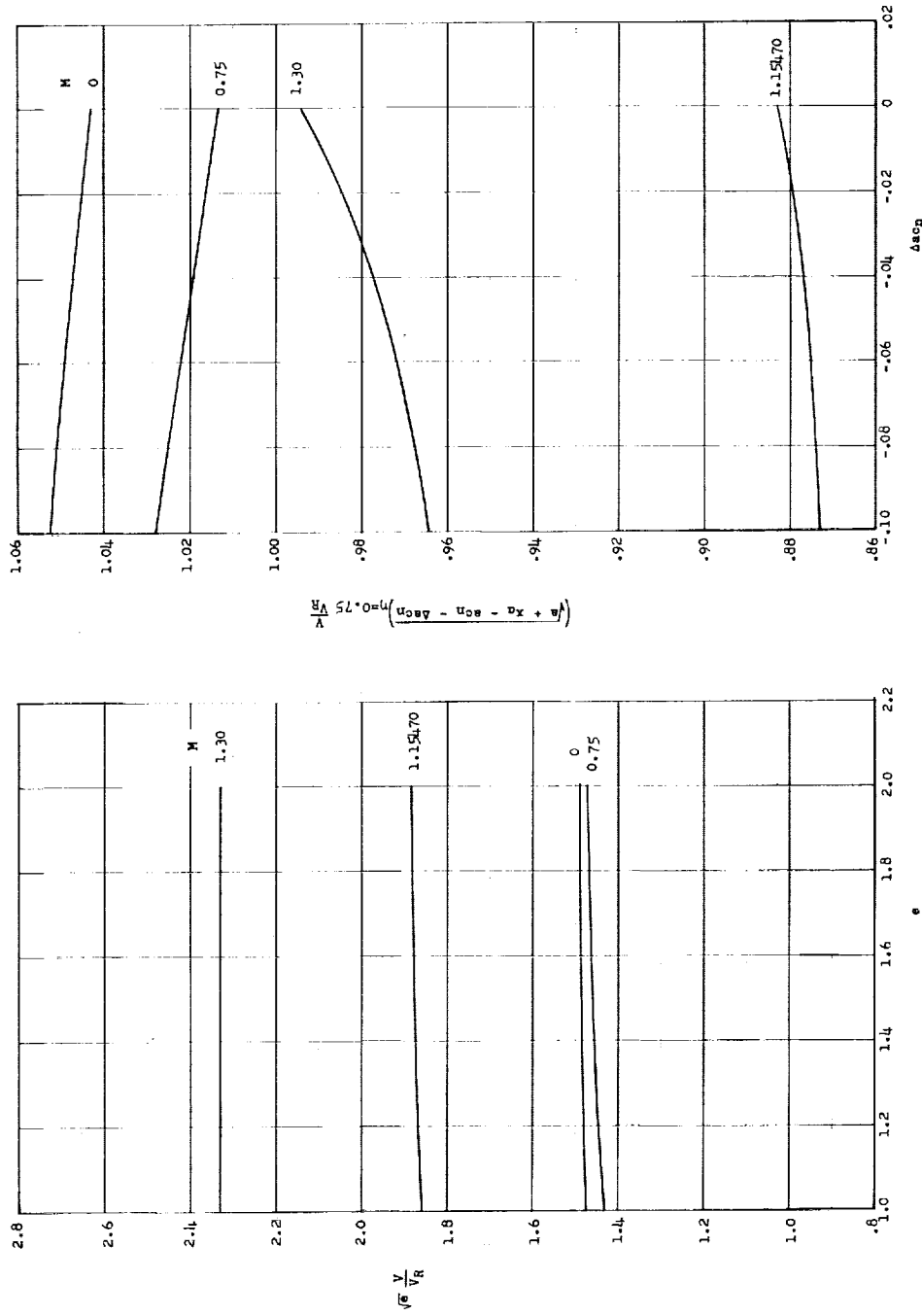
Figure 30.- Variation of $\sqrt{e} \, \dfrac{V}{V_R}$ with lift factor e and of $\left(\sqrt{a + x_\alpha - ac_n - \Delta ac_n}\right)_{\eta=0.75} \dfrac{V}{V_R}$ with aerodynamic-center shift Δac_n for wing 4001. V_R is calculated for $e = 1$ and $\Delta ac_n = 0$. $\rho = 0.002378$ slug/cu ft; $V_R = 828.5$ ft/sec.
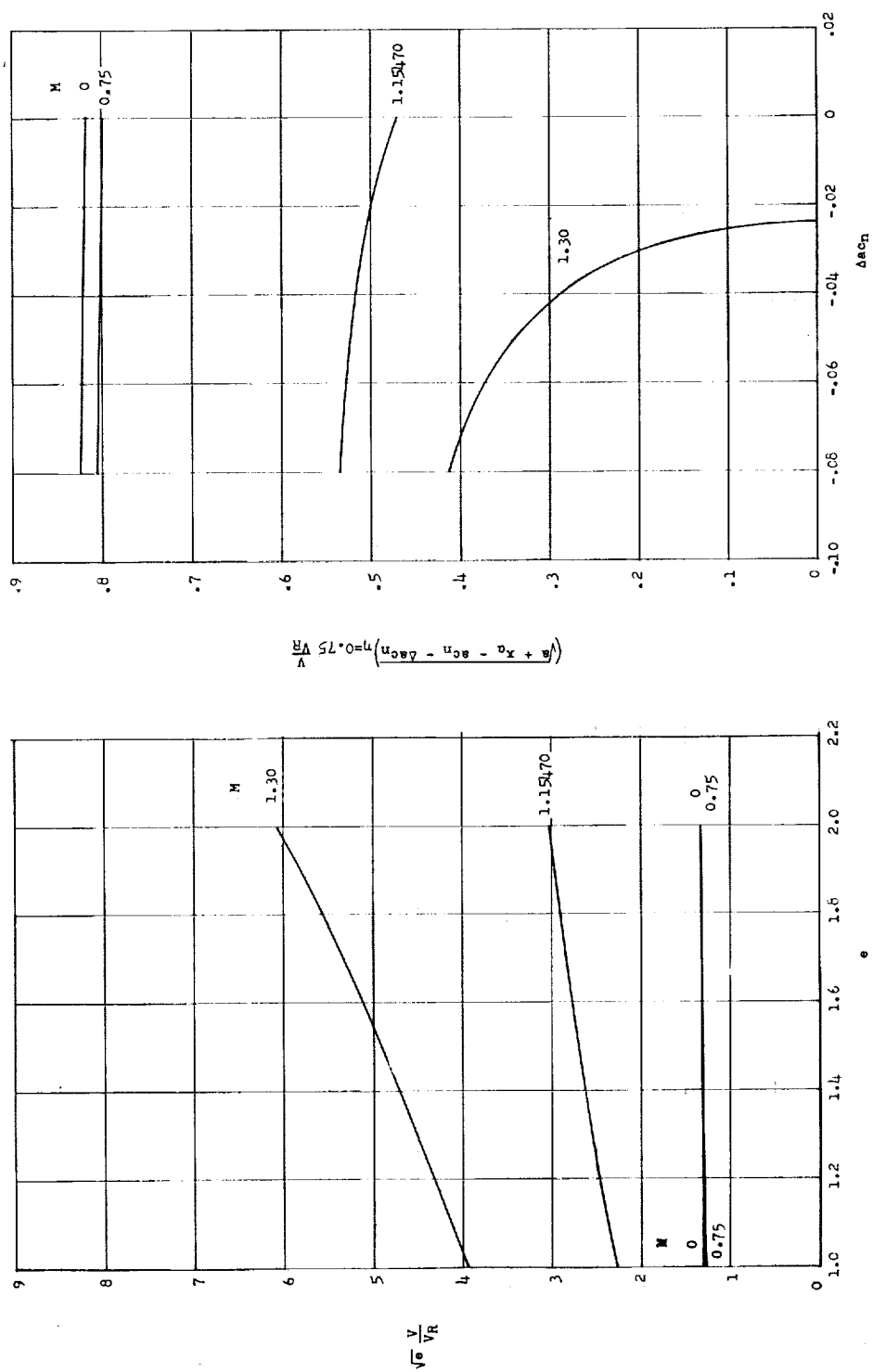
Figure 31.- Variation of $\sqrt{e}\,\dfrac{V}{V_R}$ with lift factor e and of $\left(\sqrt{a + x_\alpha - ac_n - \Delta ac_n}\right)_{\eta=0.75}\dfrac{V}{V_R}$ with aerodynamic-center shift Δac_n for wing 7001. V_R is calculated for $e = 1$ and $\Delta ac_n = 0.$ $\rho = 0.005500$ slug/cu ft; $V_R = 844.8$ ft/sec.
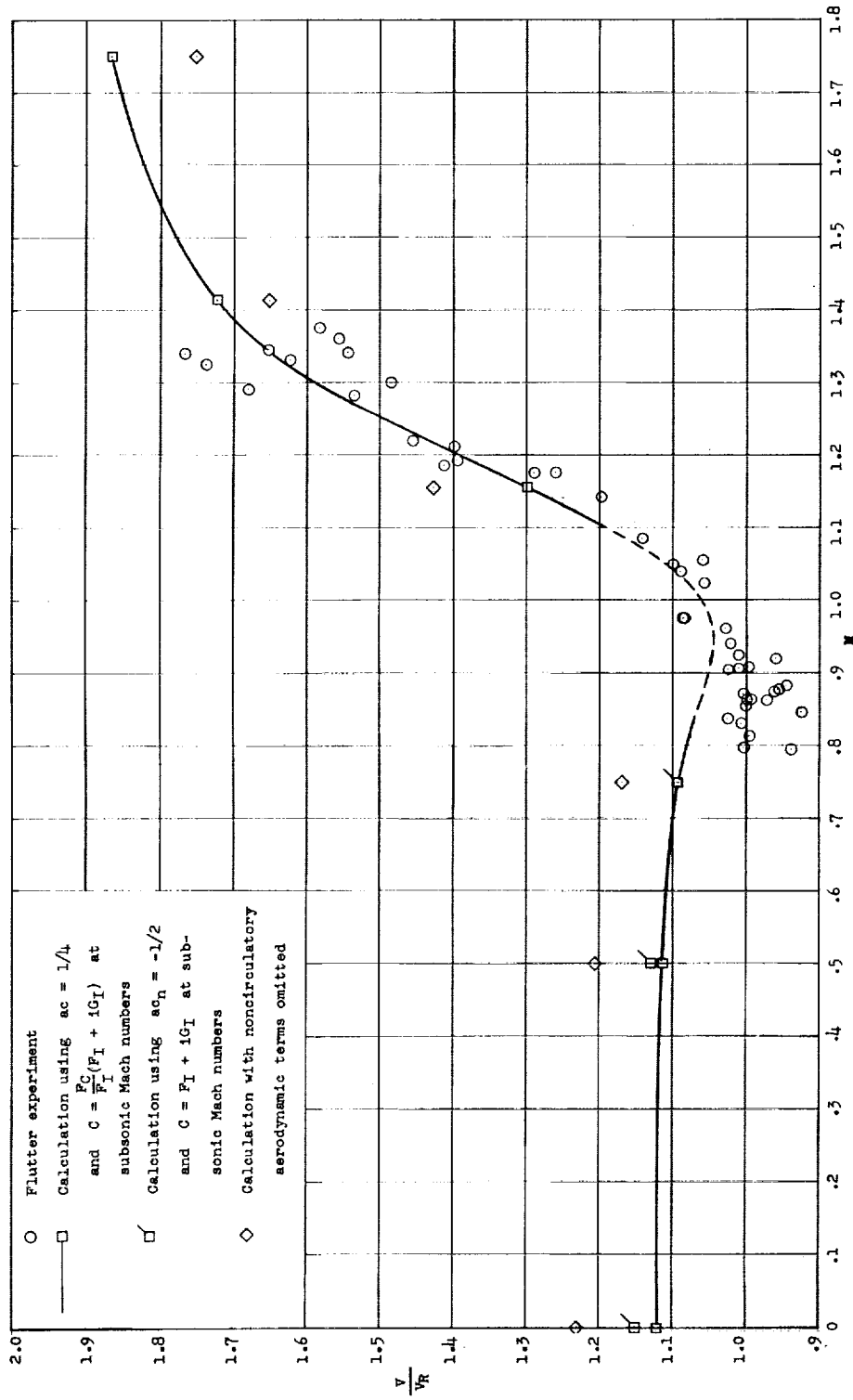
Figure 32.- Variation of flutter speed with Mach number for wing 445. For calculated points $\rho = 0.003800$ slug/cu ft and $V_R = 735.0$ ft/sec.

L-464
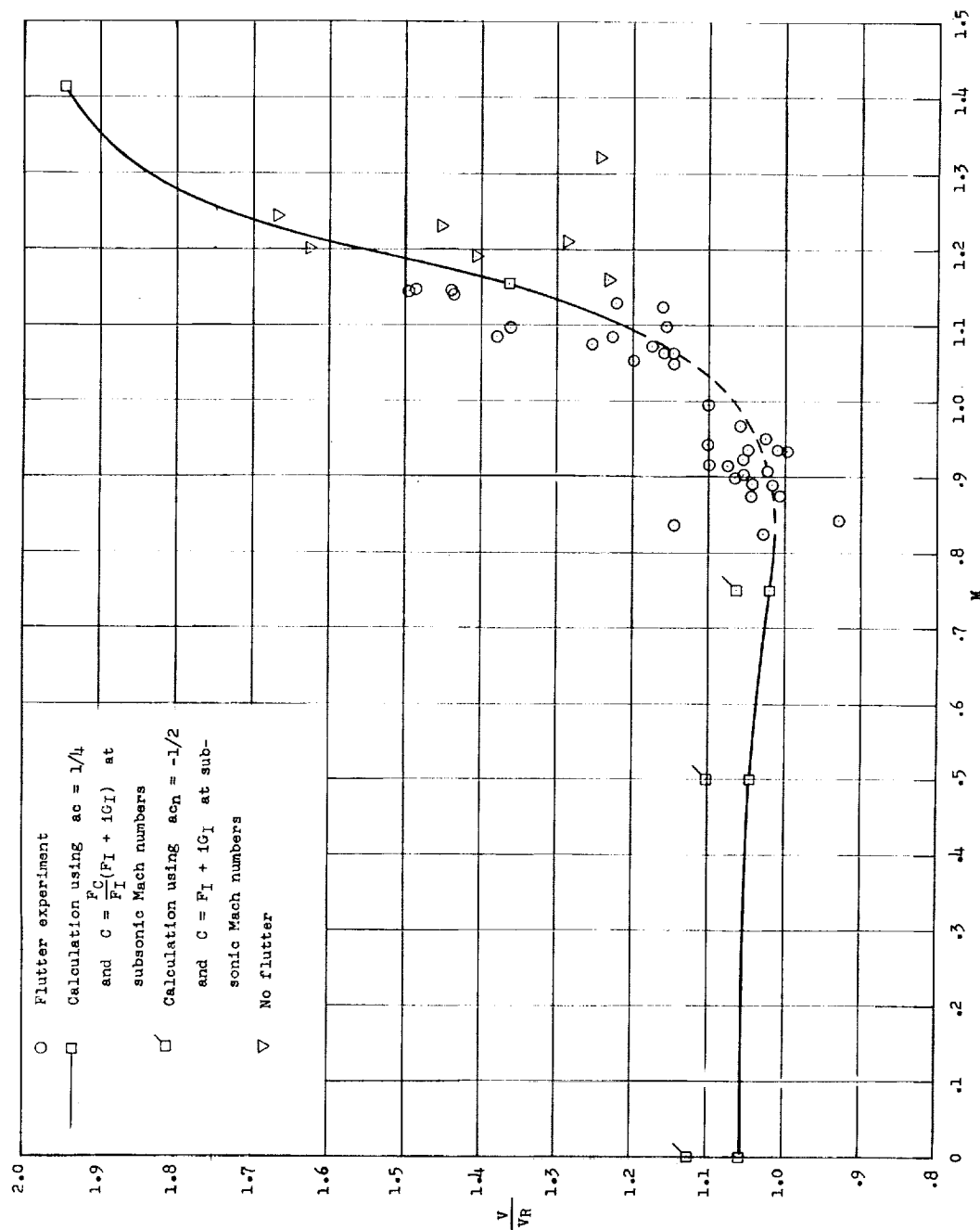
Figure 33.- Variation of flutter speed with Mach number for wing 445F. For calculated points $\rho = 0.003000$ slug/cu ft and $V_R = 840.0$ ft/sec.

58
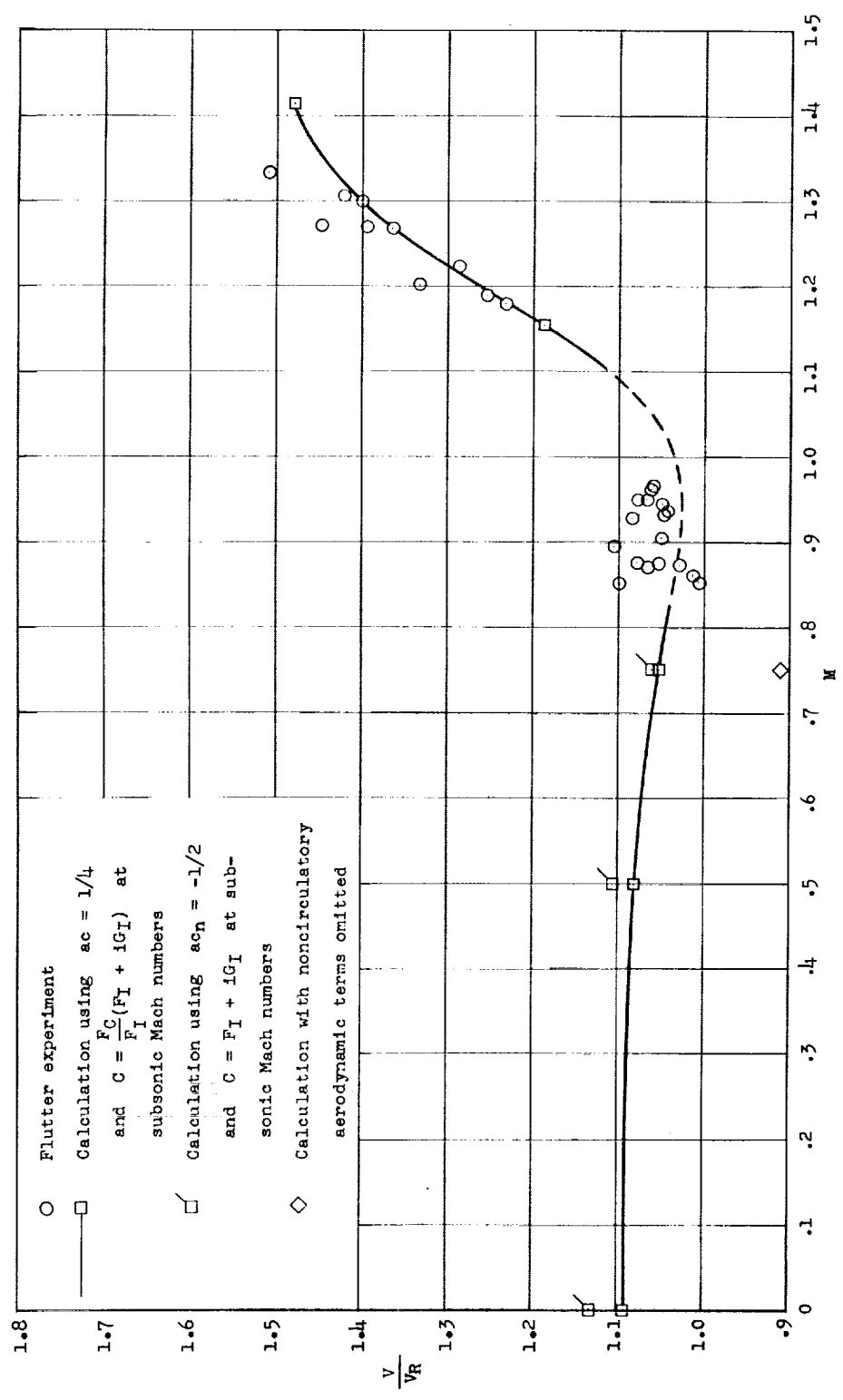
Figure 34.- Variation of flutter speed with Mach number for wing 445R. For calculated points ρ = 0.002378 slug/cu ft and V_R = 928.7 ft/sec.

L-464

2.4

O   Flutter experiment

□   Calculation using ac = 1/4

and $C = \dfrac{F_C}{F_I}(F_I + iG_I)$ at

subsonic Mach numbers

Calculation using $ac_n = -1/2$

and $C = F_I + iG_I$ at sub-

sonic Mach numbers

2.3

2.2

2.1

2.0

1.9

1.8

$\dfrac{V}{V_R}$

1.7

1.6

1.5

1.4

1.3

1.2

1.1

1.0

.7   .8   .9   1.0   1.1   1.2   1.3   1.4   1.5

M
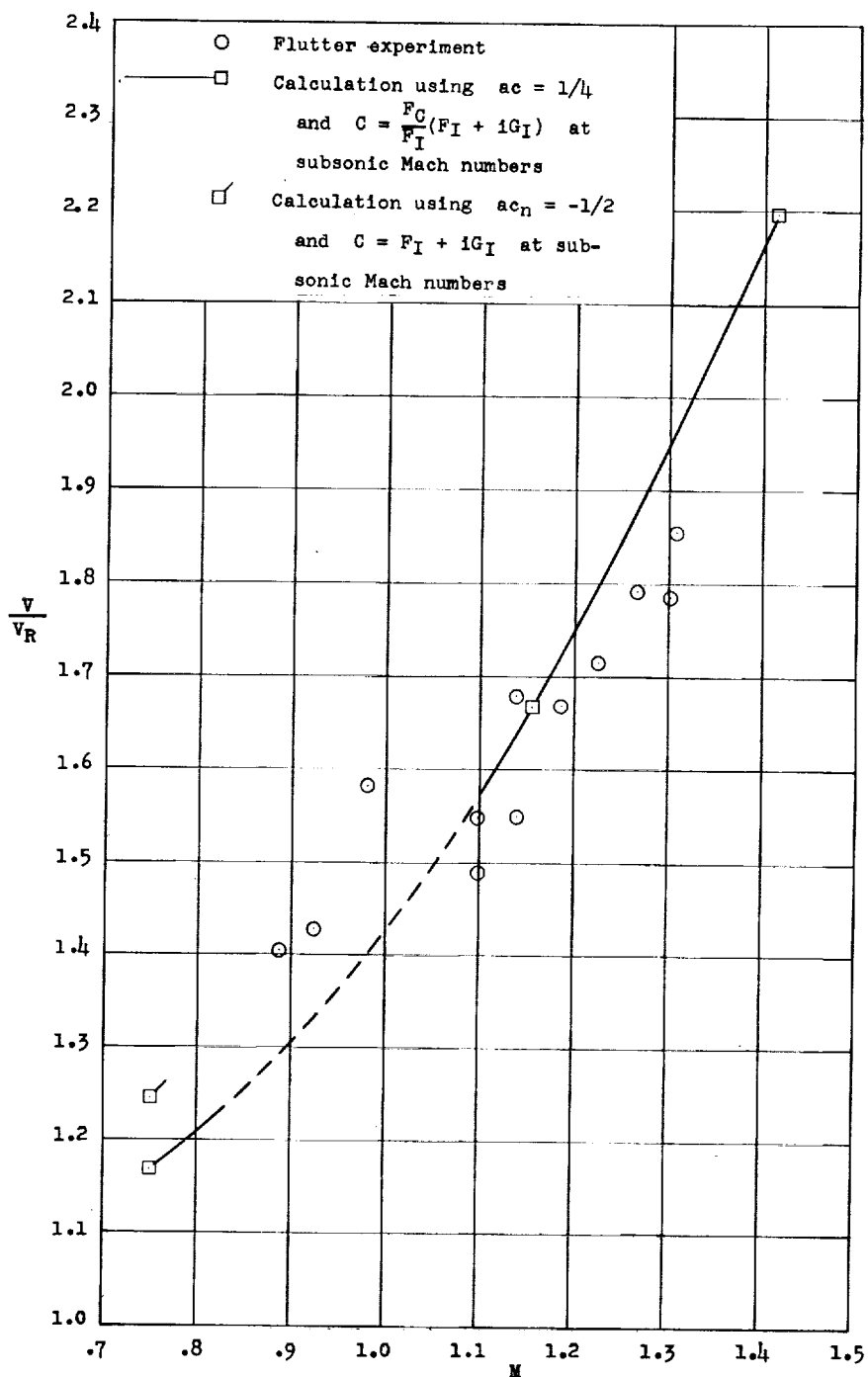
Figure 35.- Variation of flutter speed with Mach number for
wing 245. For calculated points ρ = 0.003900 slug/cu ft
and V_R = 650.4 ft/sec.
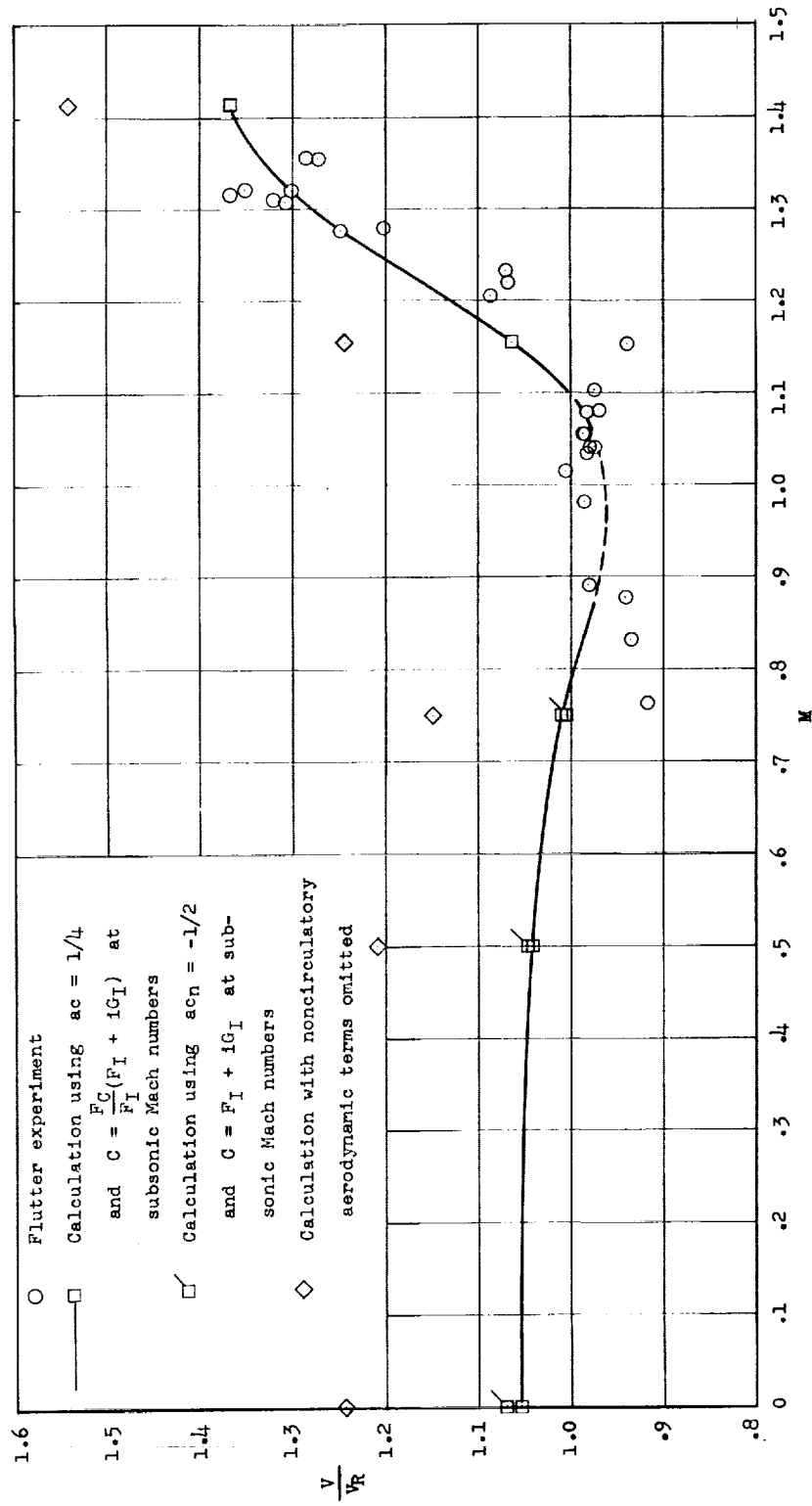
Figure 36.- Variation of flutter speed with Mach number for wing 645. For calculated points
$\rho = 0.003500$ slug/cu ft and $V_R = 901.1$ ft/sec.
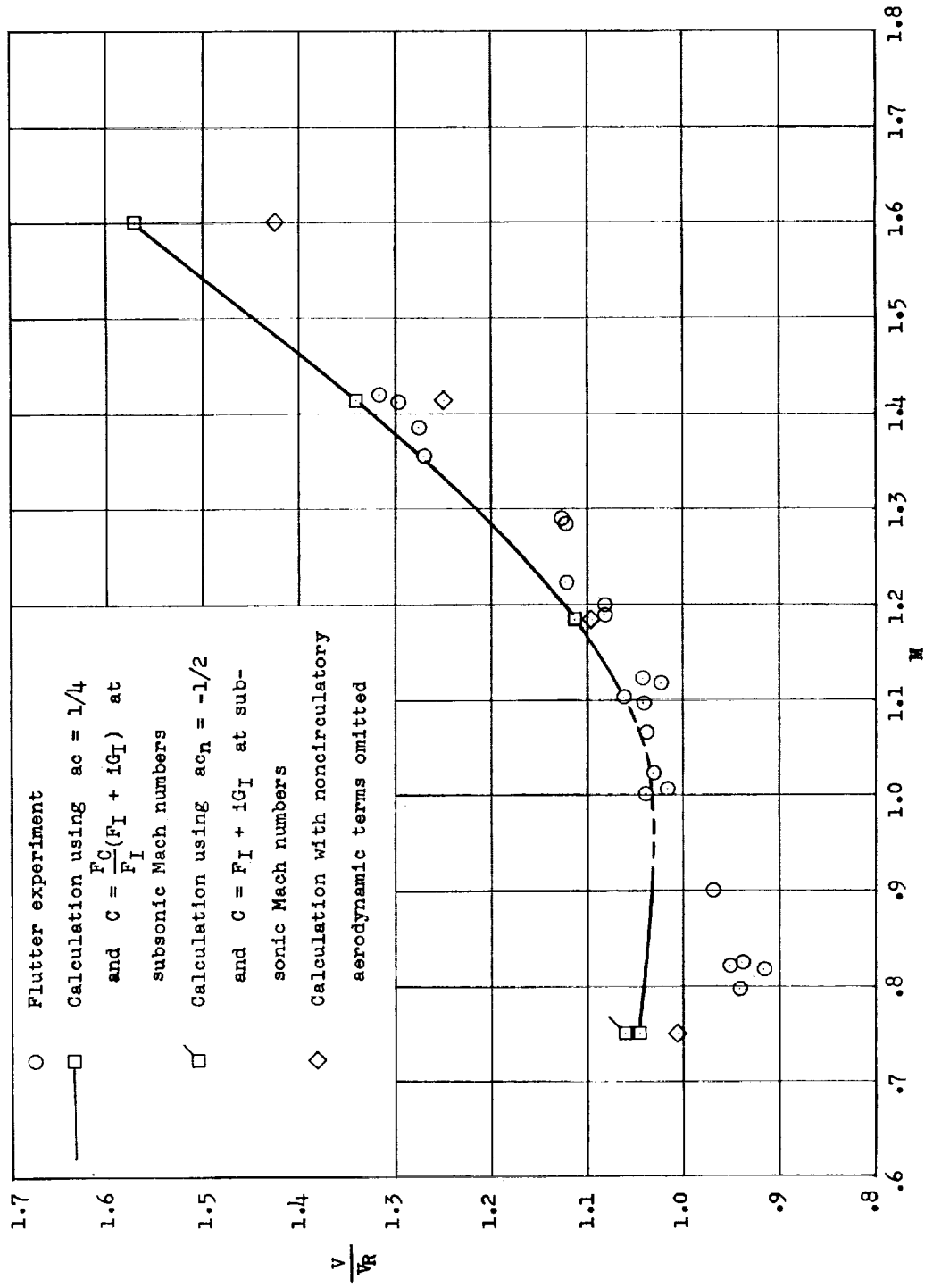
Figure 37.- Variation of flutter speed with Mach number for wing 452. For calculated points
$\rho = 0.002700$ slug/cu ft and $V_R = 988.7$ ft/sec.

62
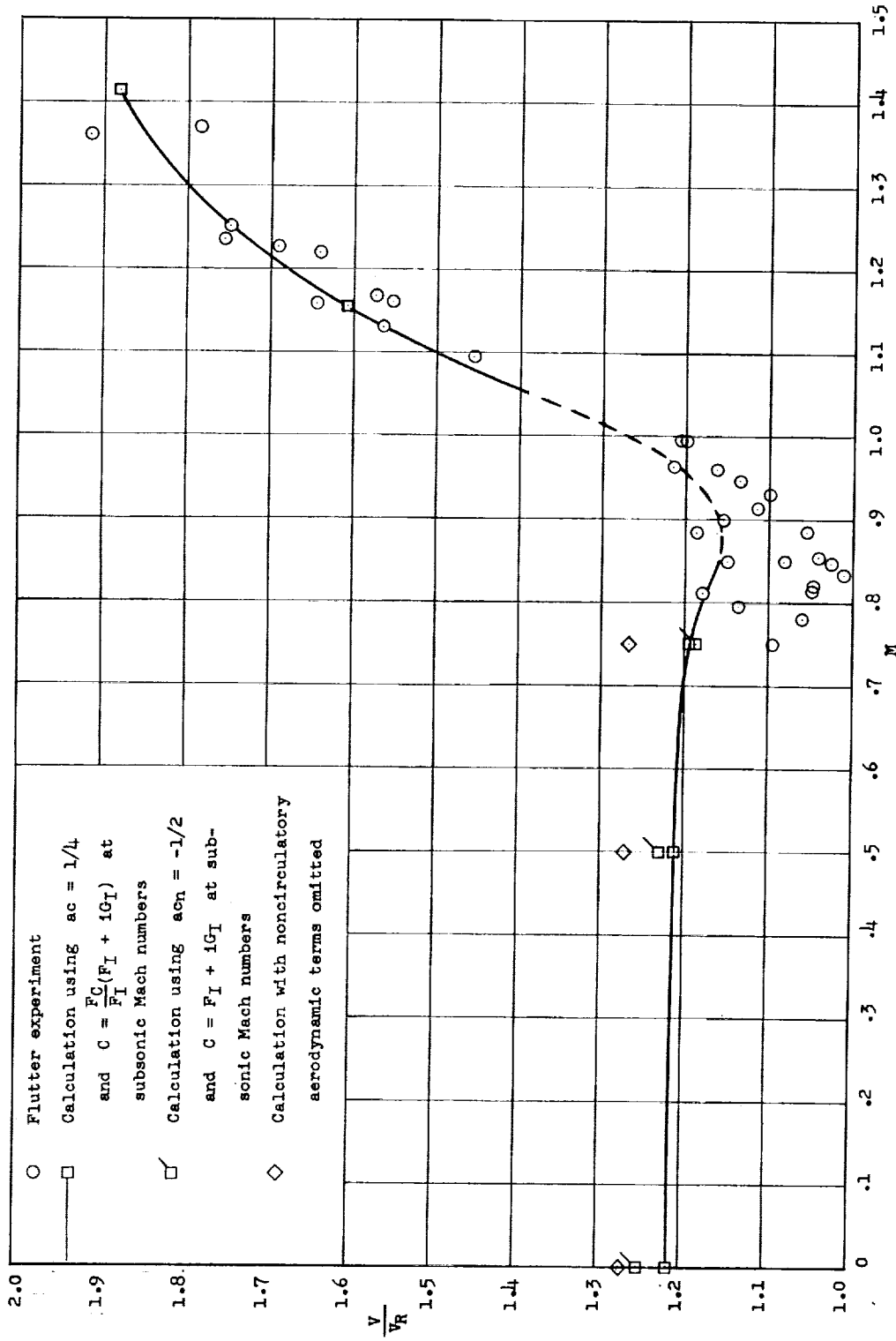
Figure 38.- Variation of flutter speed with Mach number for wing 430. For calculated points $\rho = 0.003700$ slug/cu ft and $V_R = 694.7$ ft/sec.

L-464
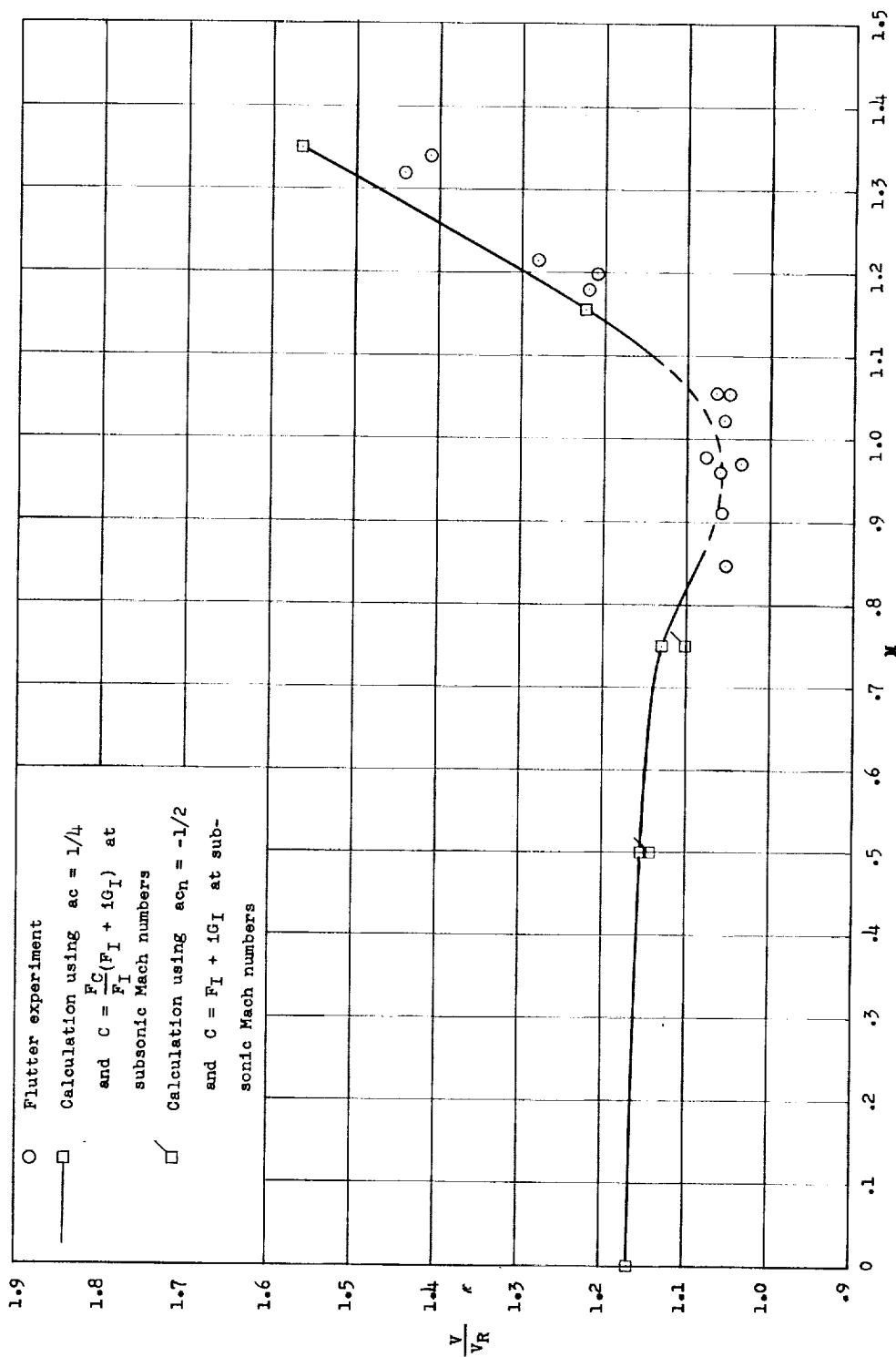
Figure 39.- Variation of flutter speed with Mach number for wing 4451. For calculated points $\rho = 0.003200$ slug/cu ft and $V_R = 944.7$ ft/sec.
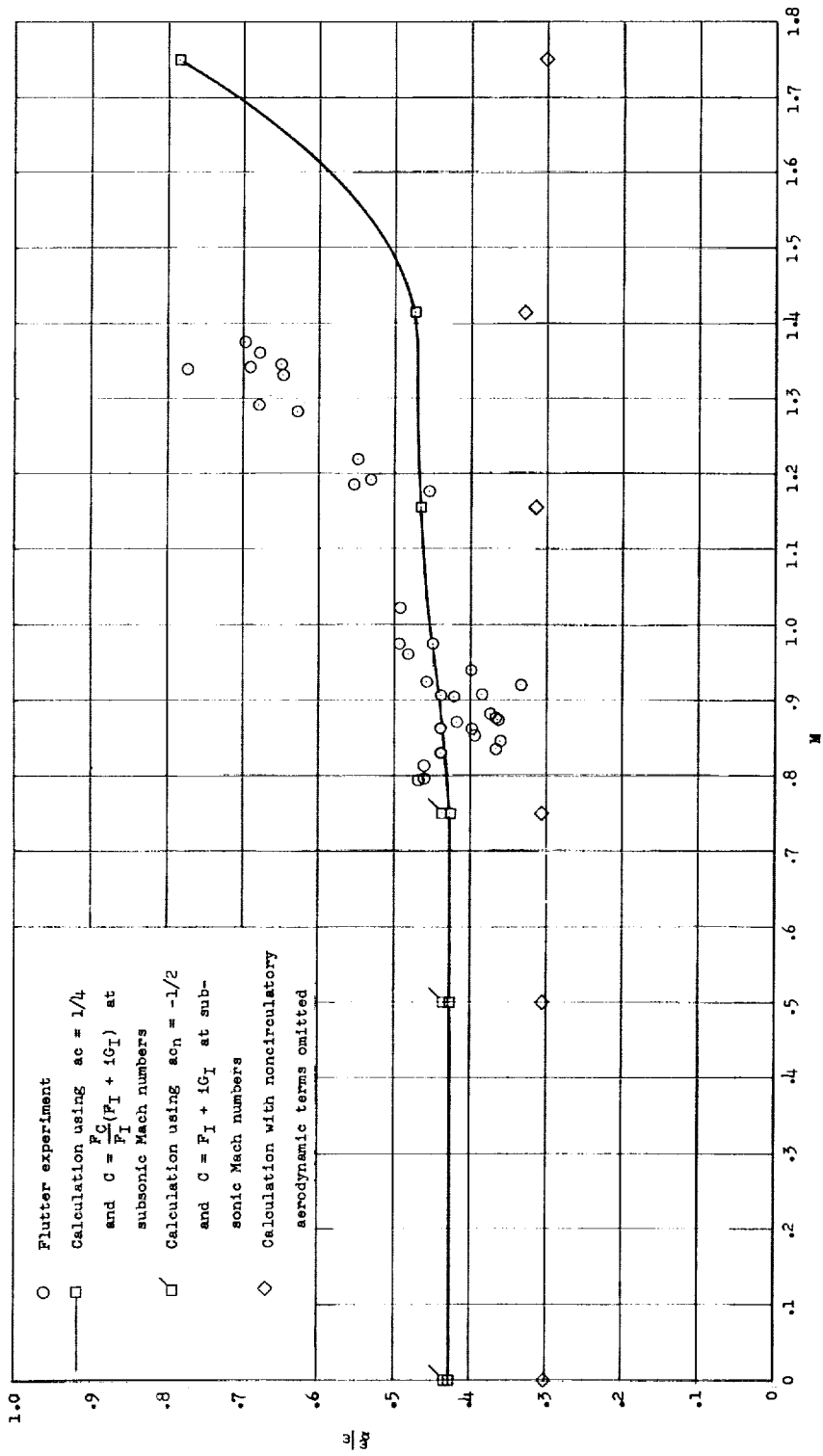
Figure 40.- Variation of flutter frequency with Mach number for wing 445. For calculated points $\rho = 0.003800$ slug/cu ft and $\omega_\alpha = 2{,}192$ radians/sec.
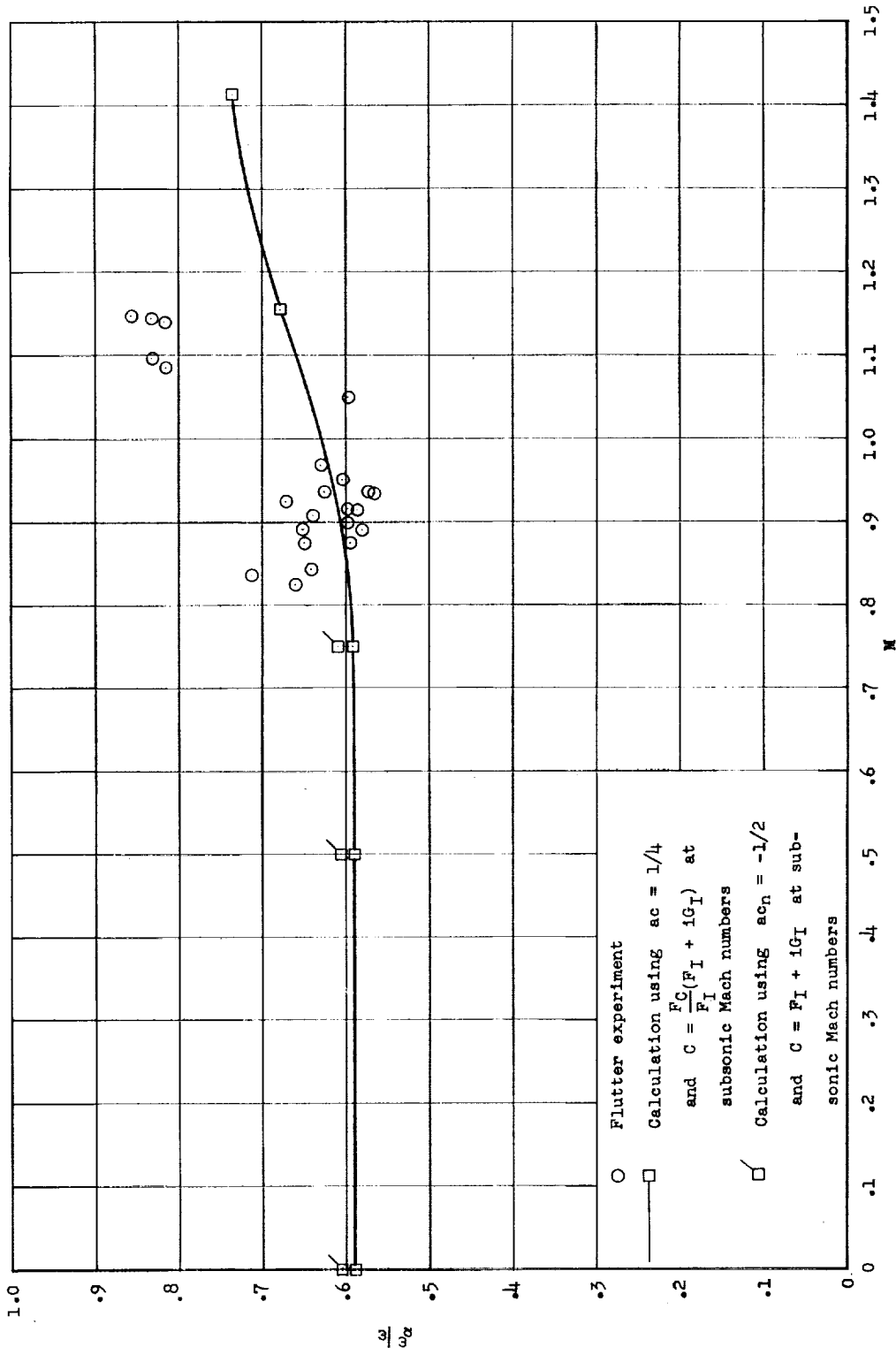
Figure 41.- Variation of flutter frequency with Mach number for wing 445F. For calculated points $\rho = 0.003000$ slug/cu ft and $\omega_\alpha = 1,144$ radians/sec.
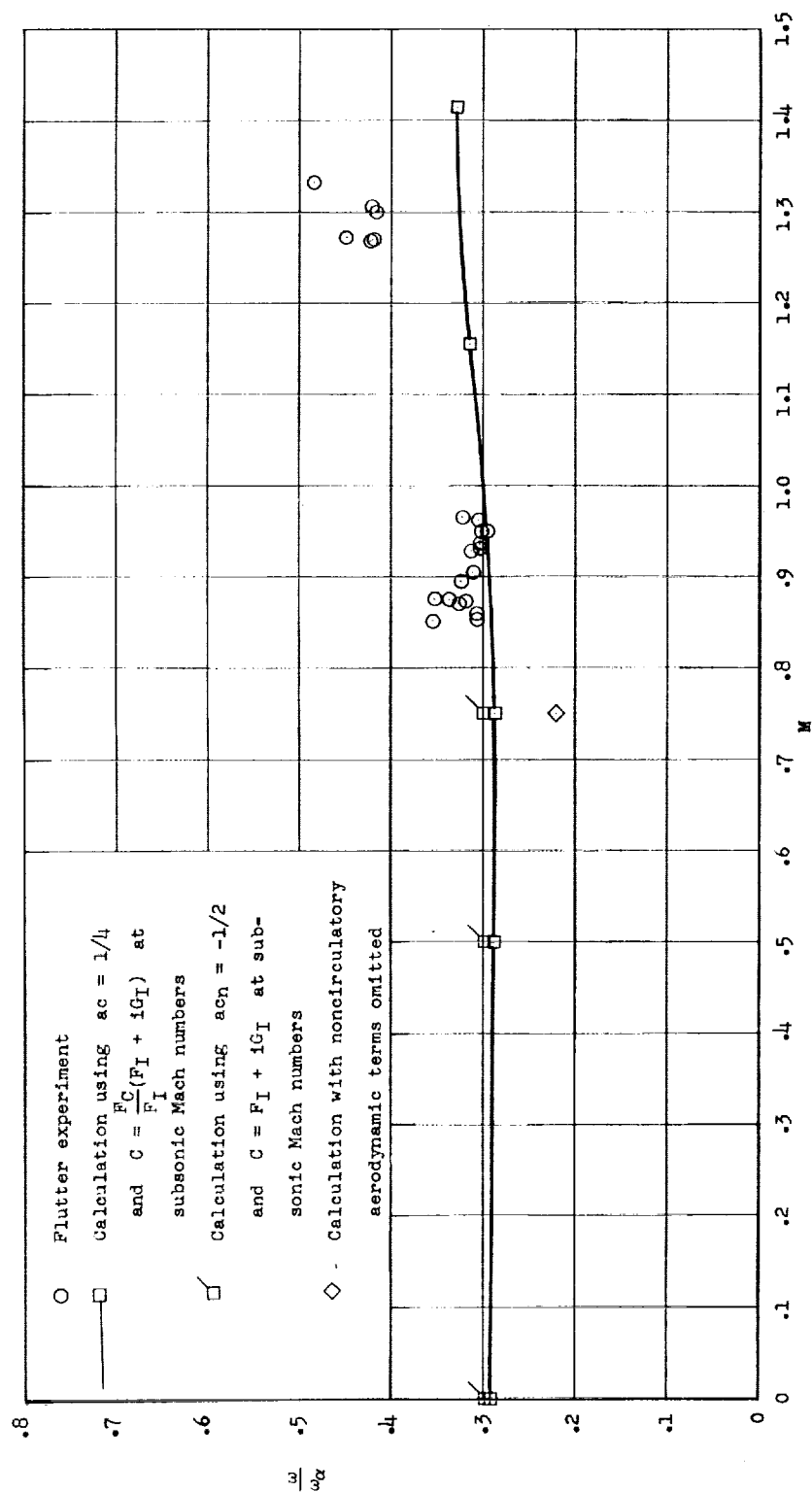
Figure 42.- Variation of flutter frequency with Mach number for wing 445R. For calculated points
ρ = 0.002378 slug/cu ft and ω_α = 2,306 radians/sec.
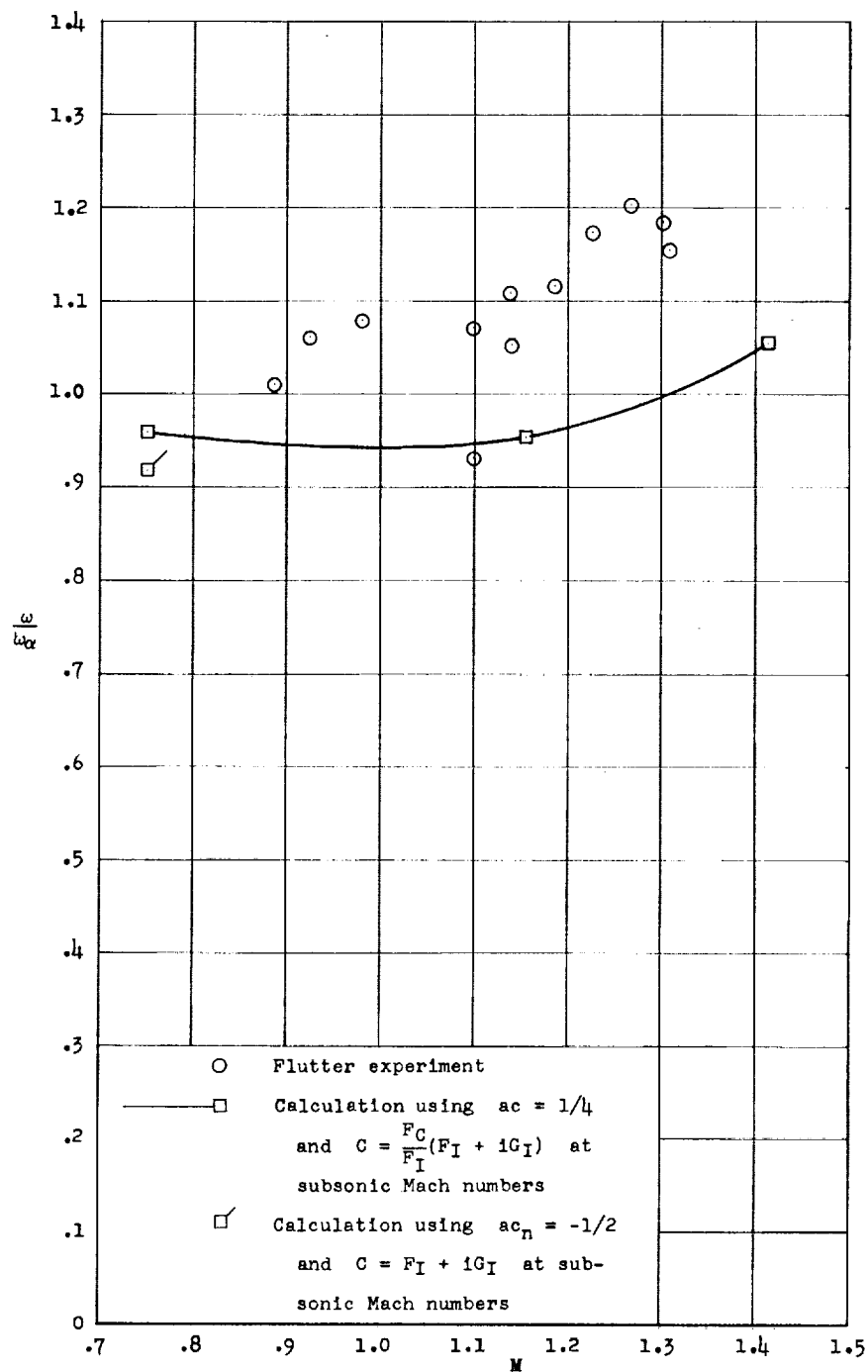
Figure 43.- Variation of flutter frequency with Mach number for wing 245. For calculated points $\rho = 0.003900$ slug/cu ft and $\omega_\alpha = 1,665$ radians/sec.
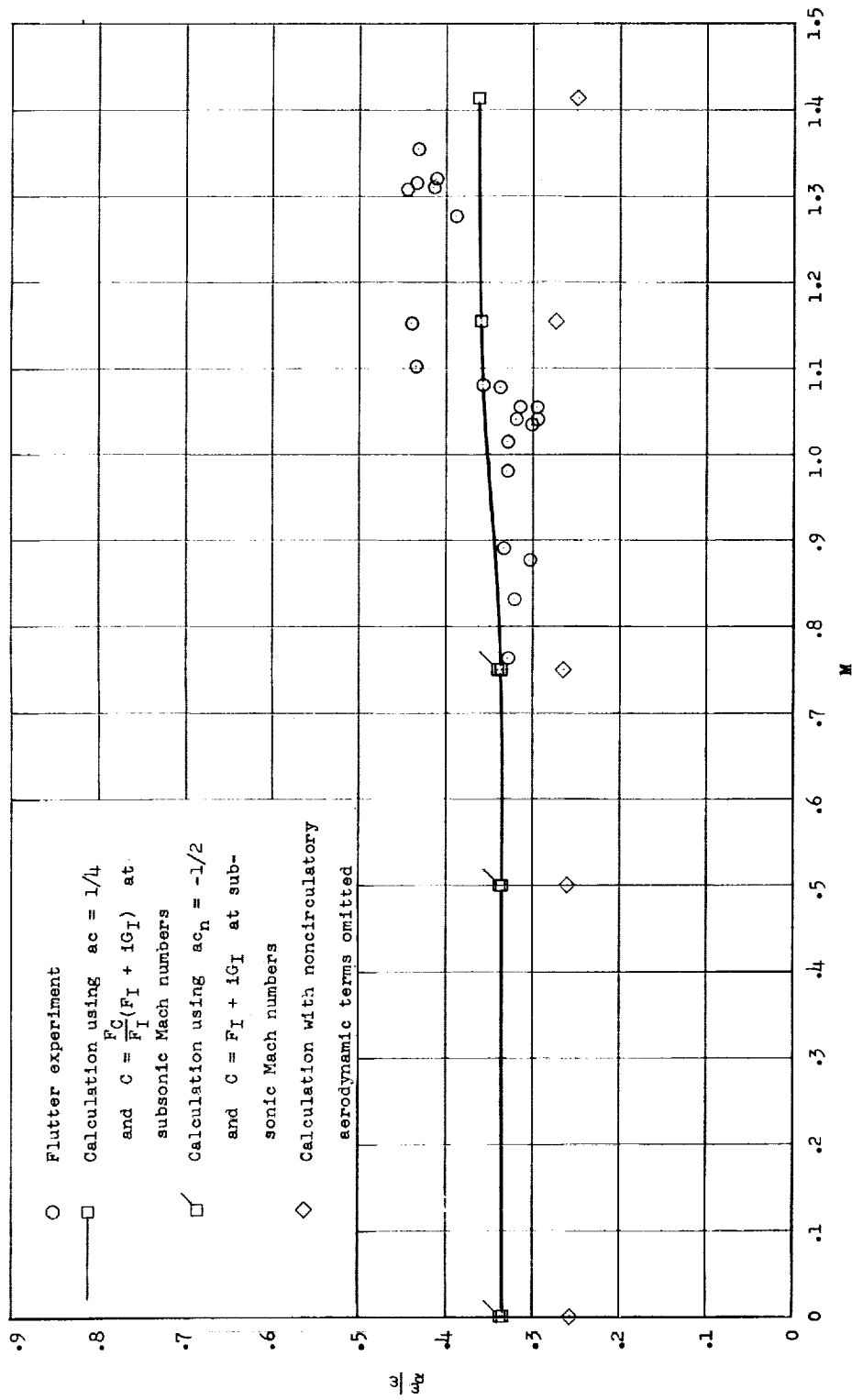
Figure 44.- Variation of flutter frequency with Mach number for wing 645. For calculated points $\rho = 0.003500$ slug/cu ft and $\omega_\alpha = 3,173$ radians/sec.

L-464

L-464
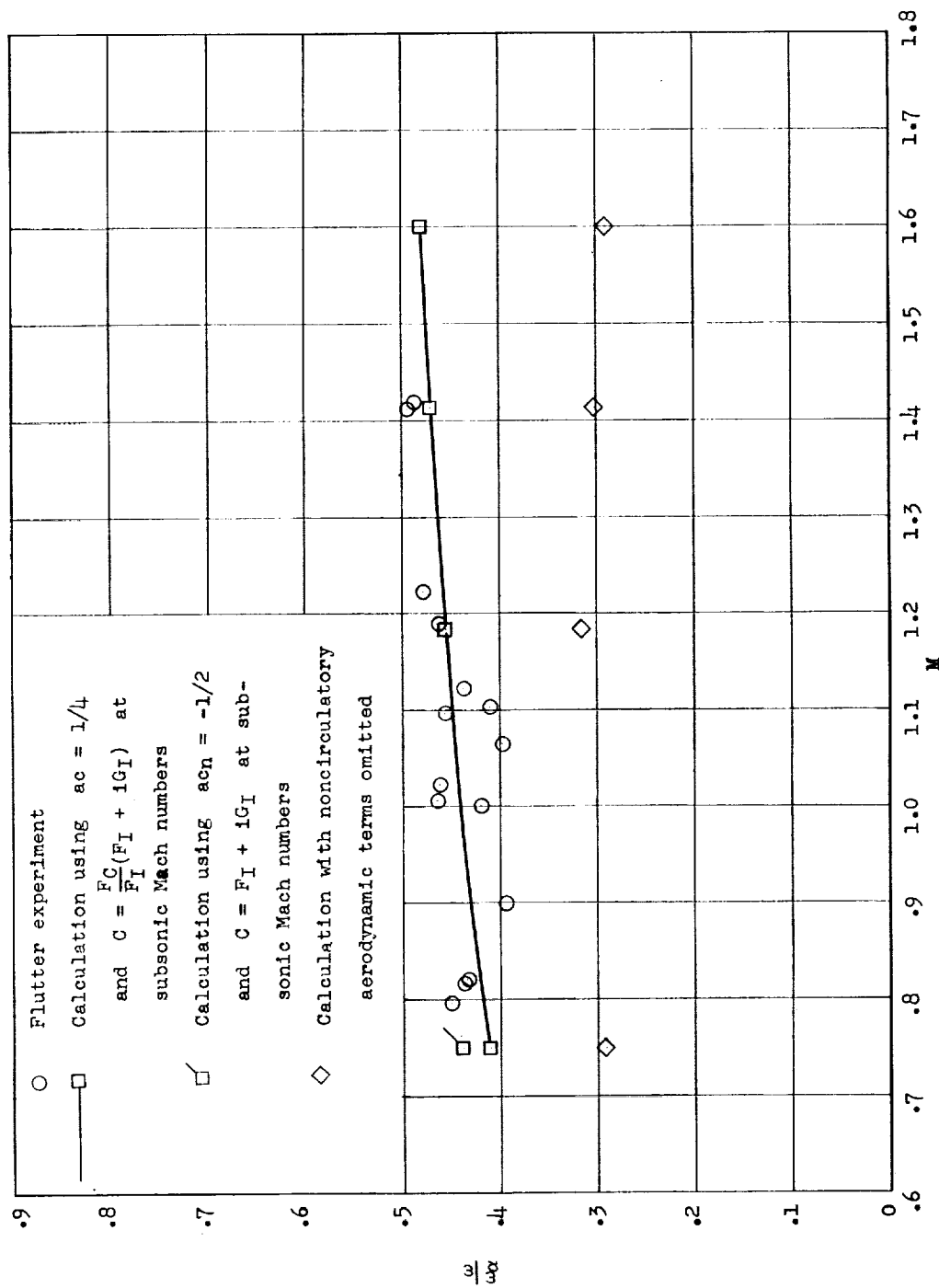
Figure 45.- Variation of flutter frequency with Mach number for wing 452. For calculated points
$\rho = 0.002700$ slug/cu ft and $\omega_\alpha = 2,300$ radians/sec.
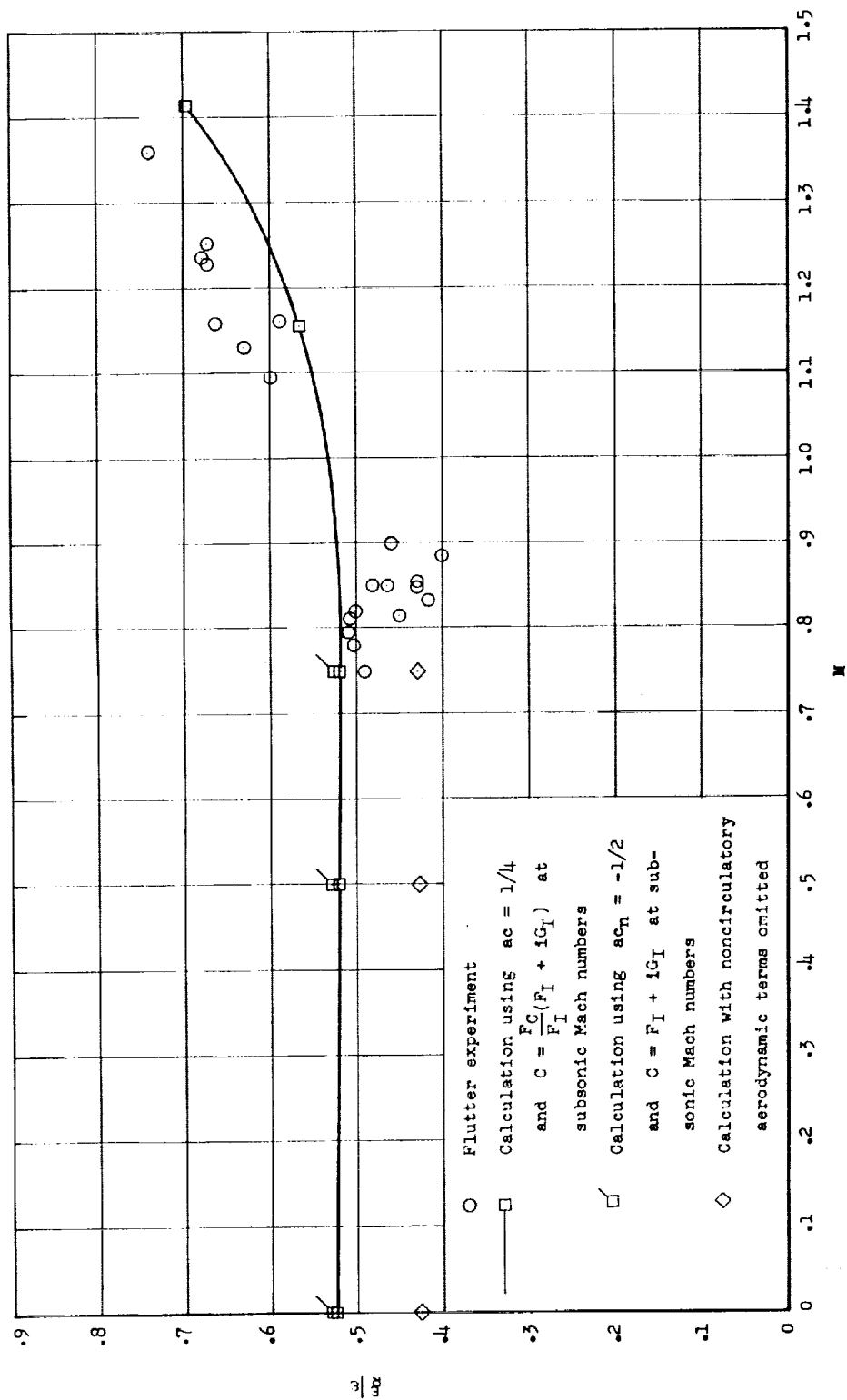
Figure 46.- Variation of flutter frequency with Mach number for wing 430. For calculated points $\rho = 0.003700$ slug/cu ft and $\omega_\alpha = 2,158$ radians/sec.
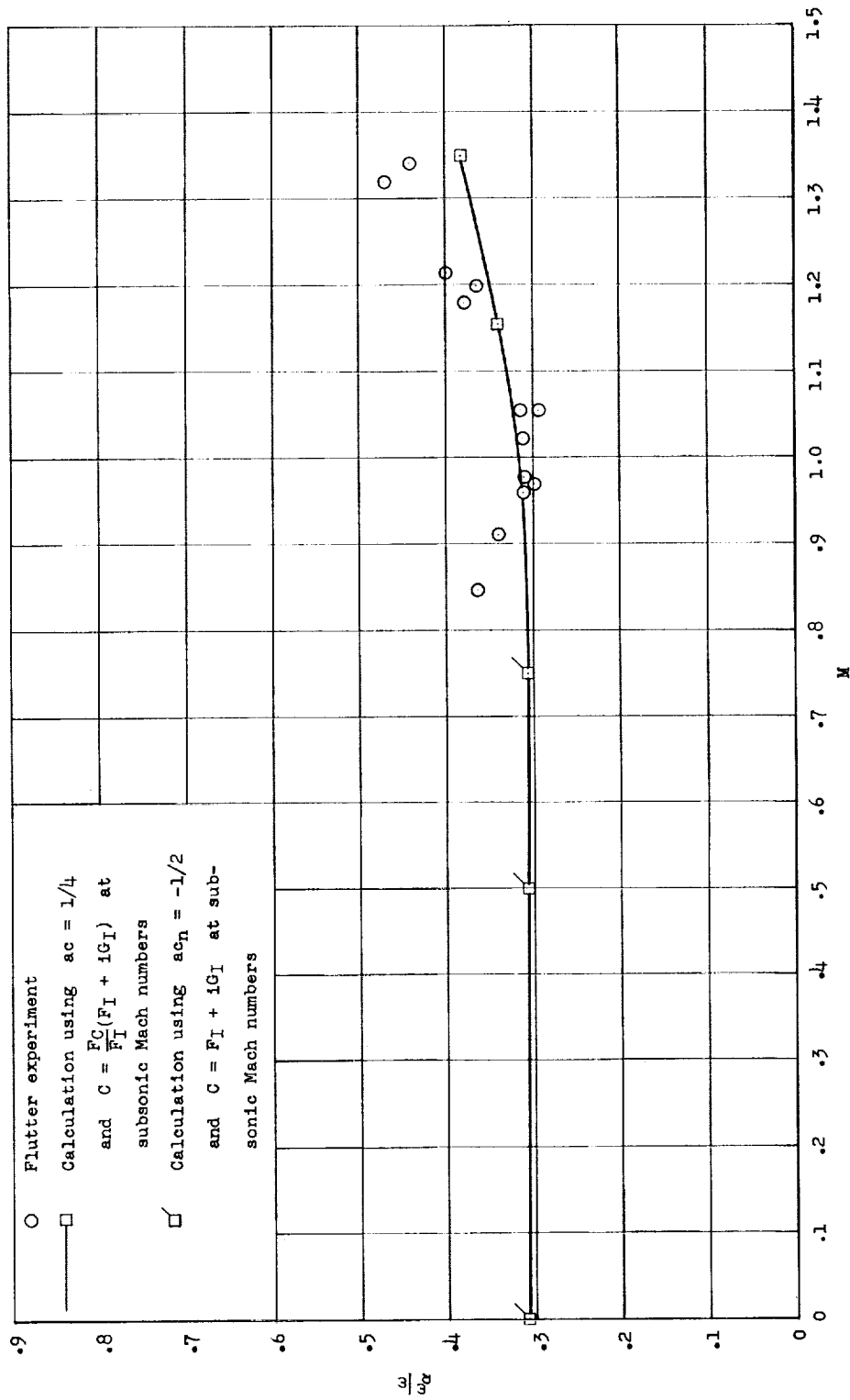
Figure 47.- Variation of flutter frequency with Mach number for wing 4451. For calculated points $\rho = 0.003200$ slug/cu ft and $\omega_\alpha = 2,352$ radians/sec.
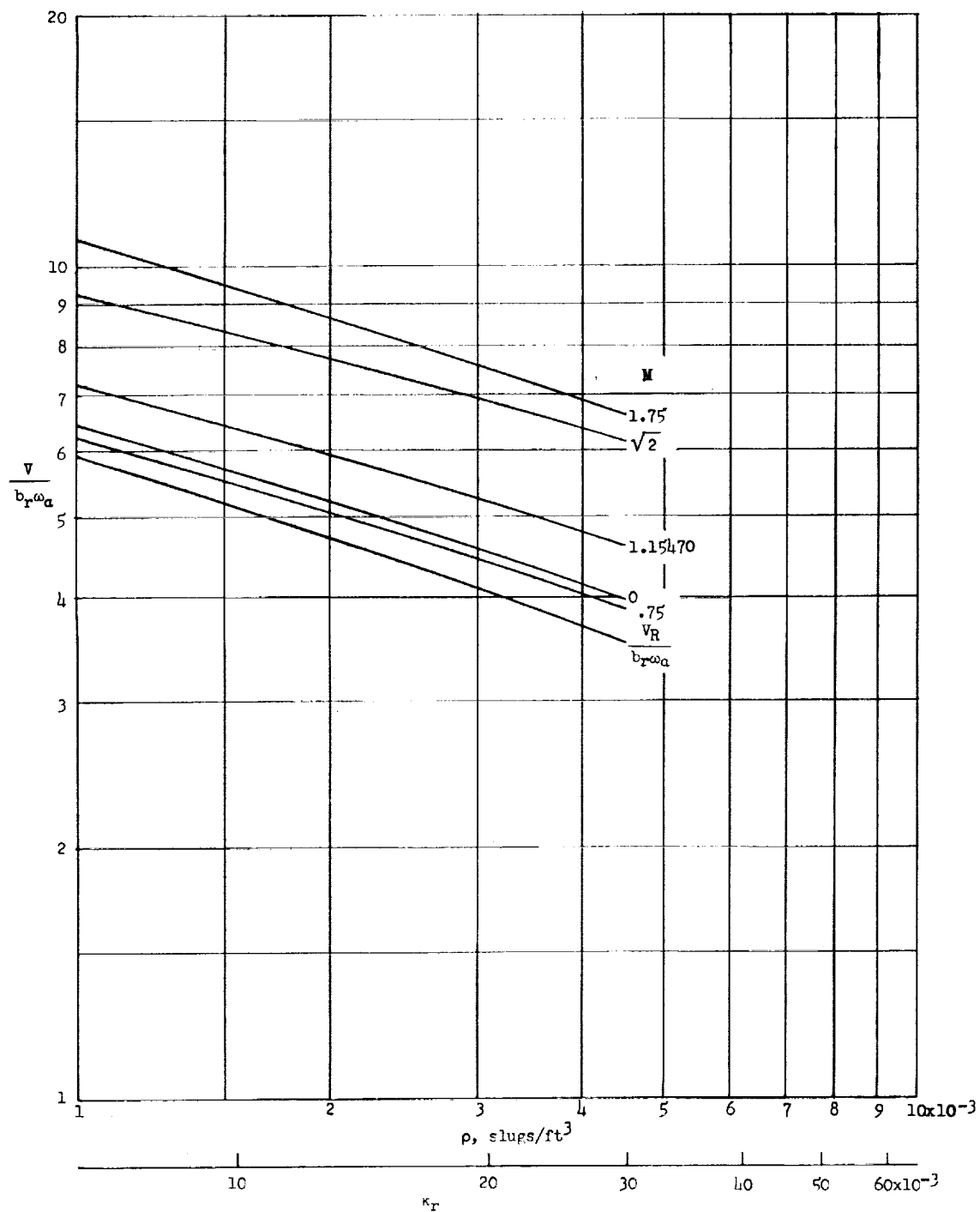
Figure 48.- Variation of flutter-speed coefficient with density for wing 445.

L-464
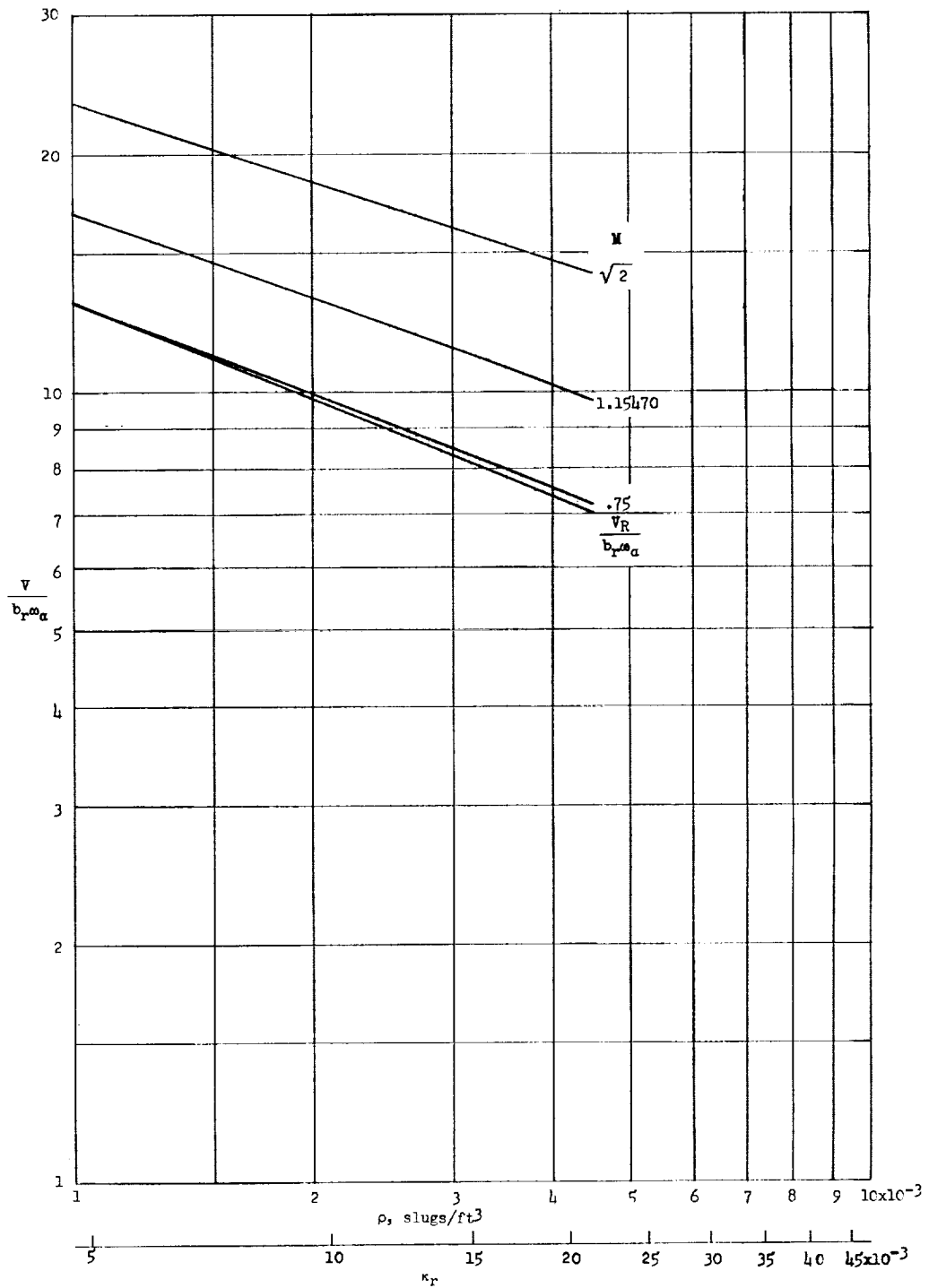
Figure 49.- Variation of flutter-speed coefficient with density for
wing 445F.
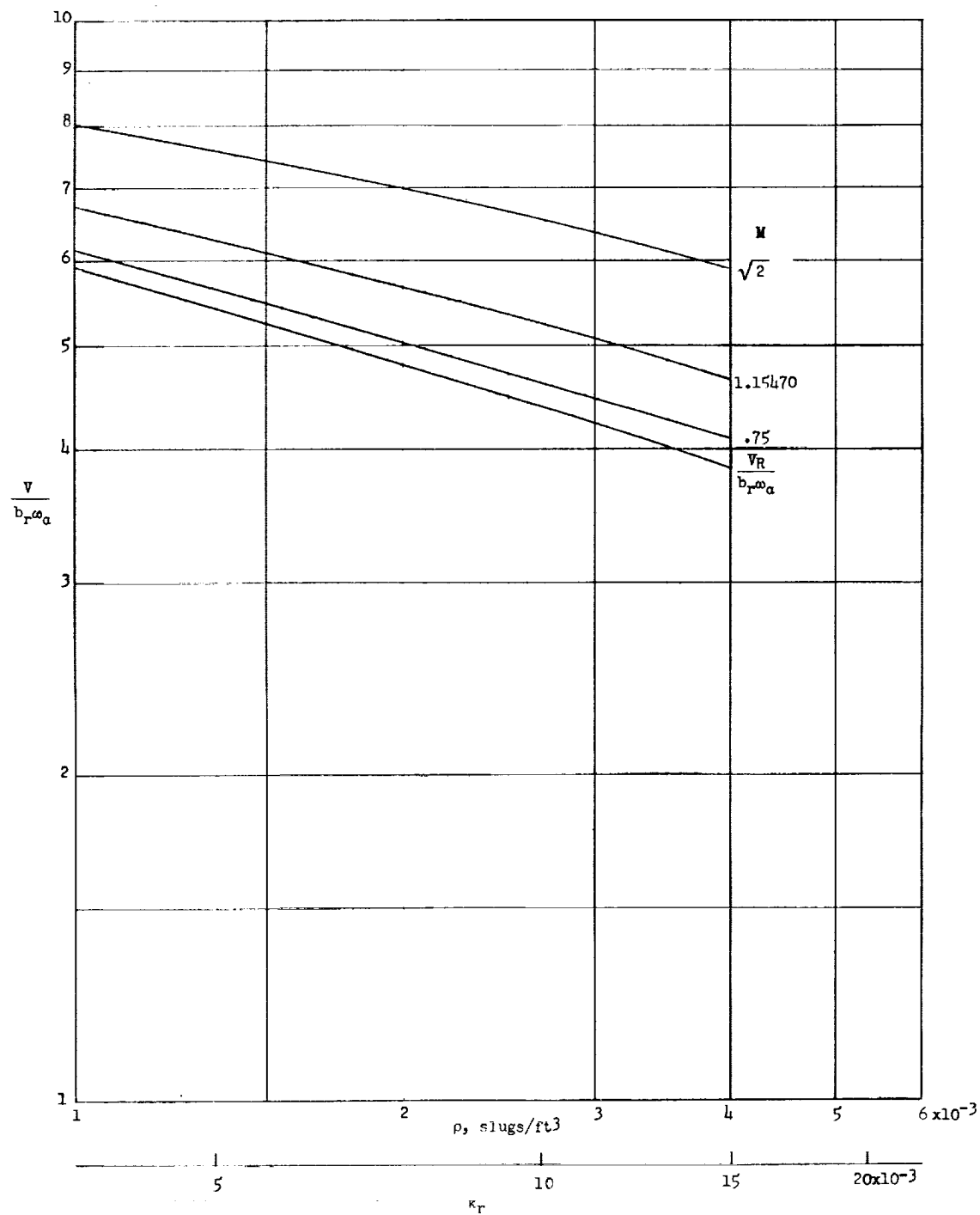
Figure 50.- Variation of flutter-speed coefficient with density for wing 445R.
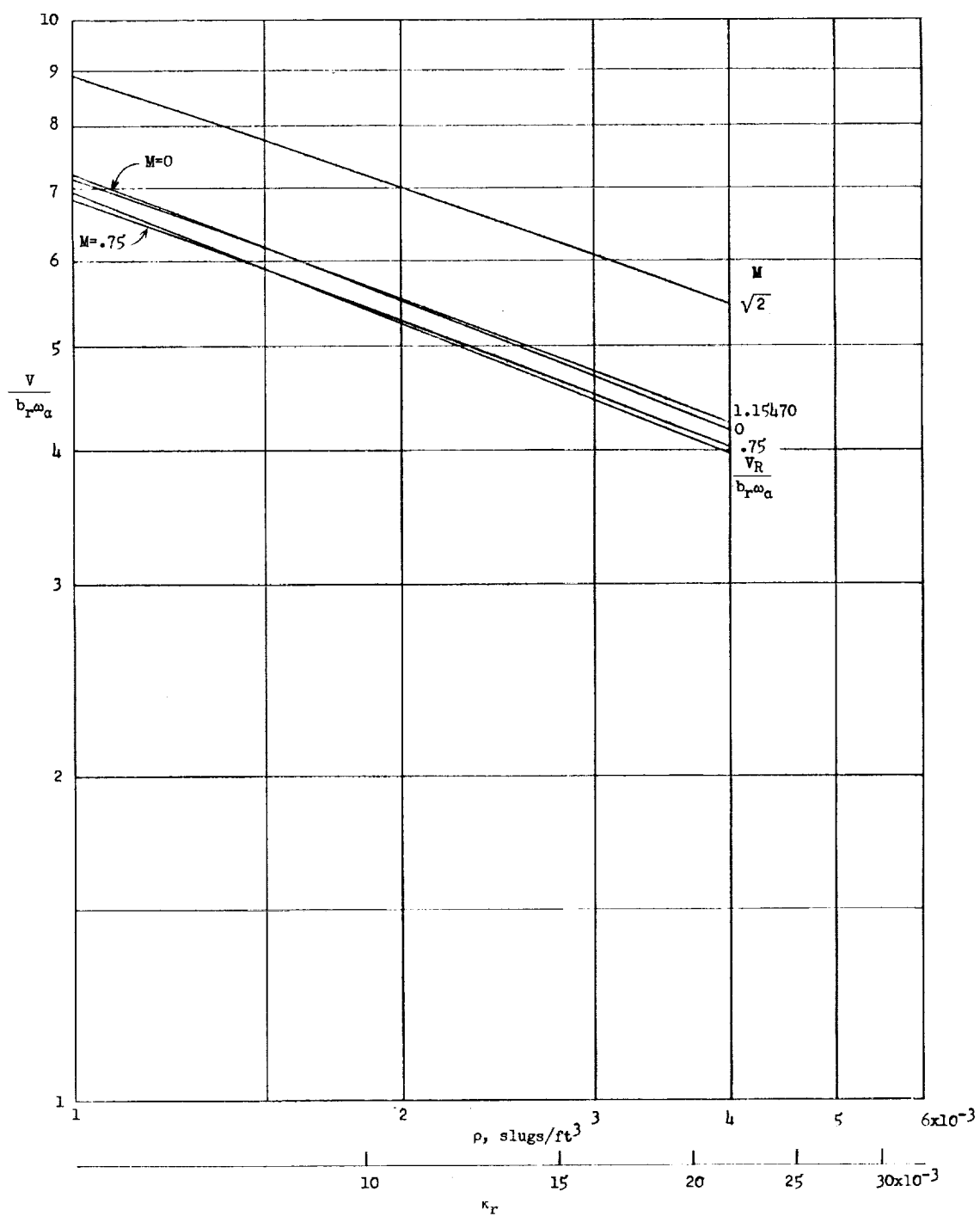
Figure 51.- Variation of flutter-speed coefficient with density for wing 645.
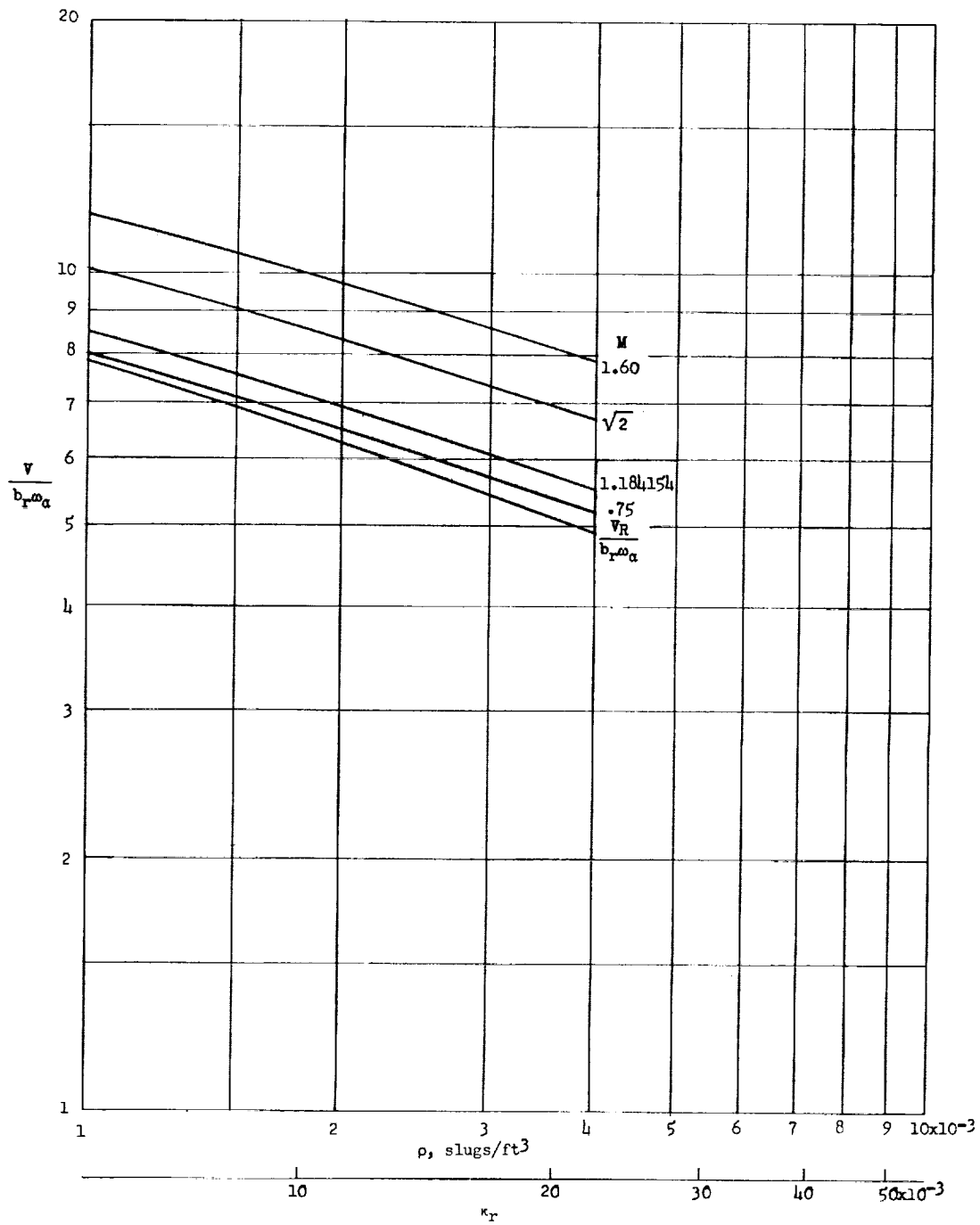
Figure 52.- Variation of flutter-speed coefficient with density for wing 452.

L-464
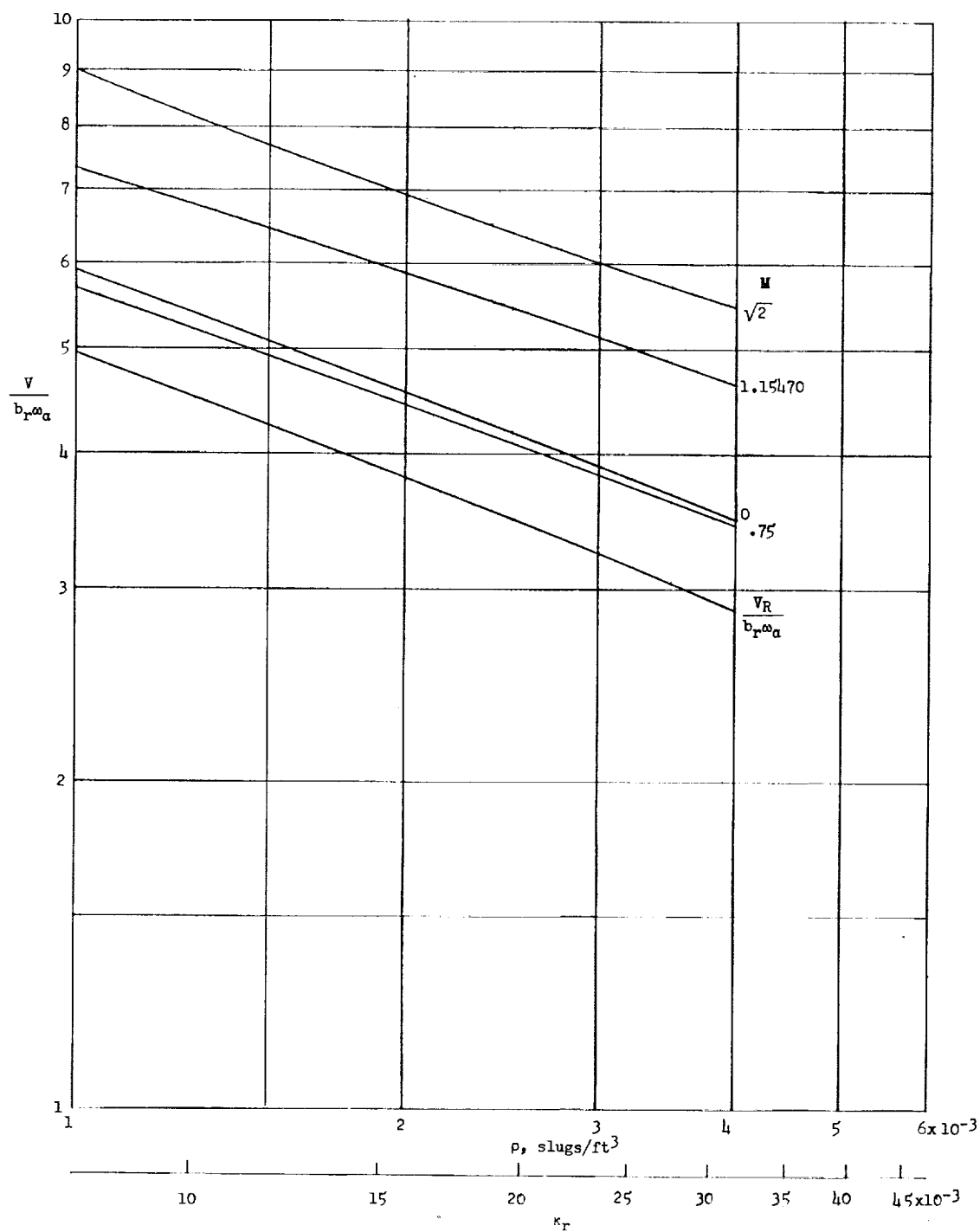
Figure 53.- Variation of flutter-speed coefficient with density for wing 430.
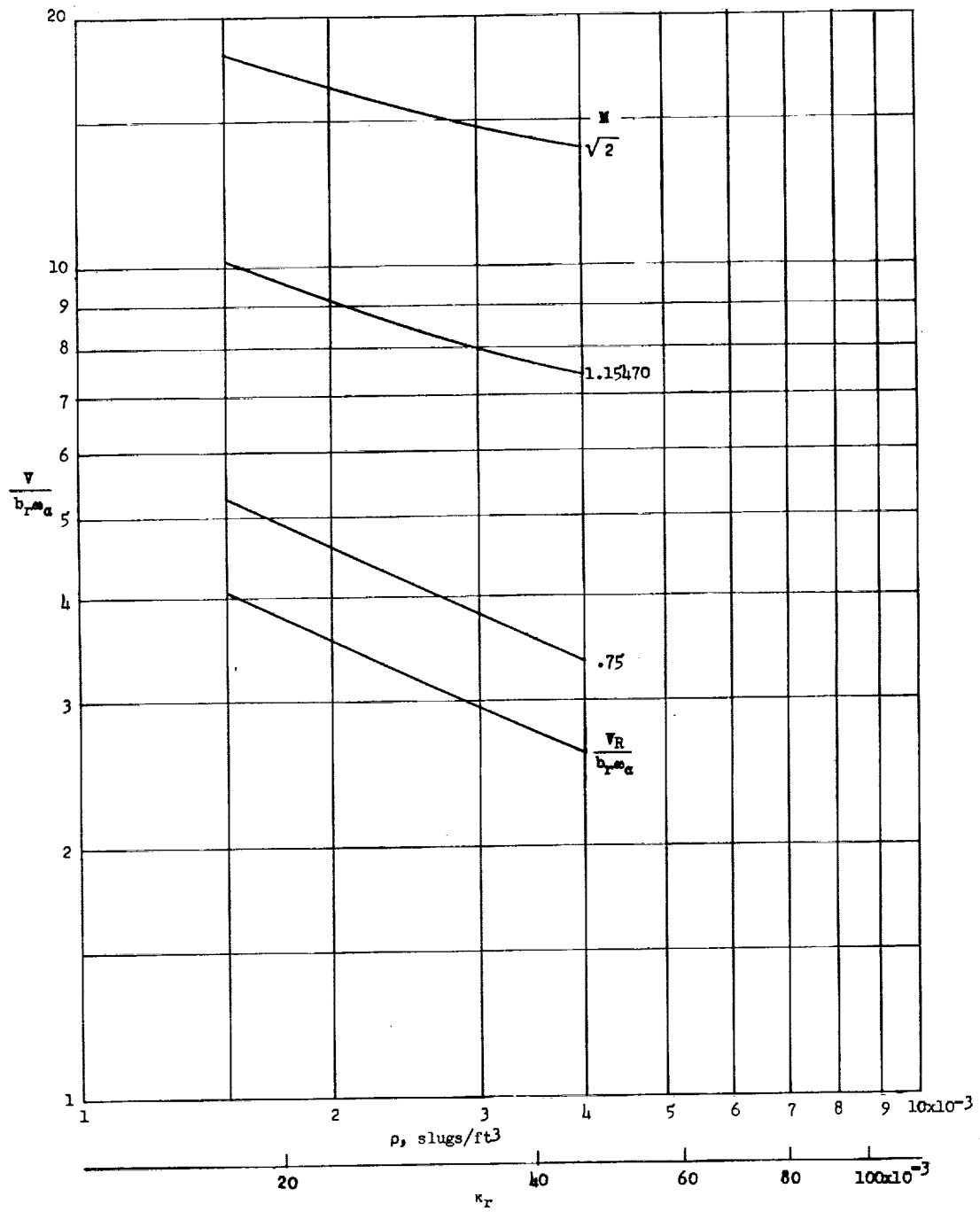
Figure 54.- Variation of flutter-speed coefficient with density for wing 400.
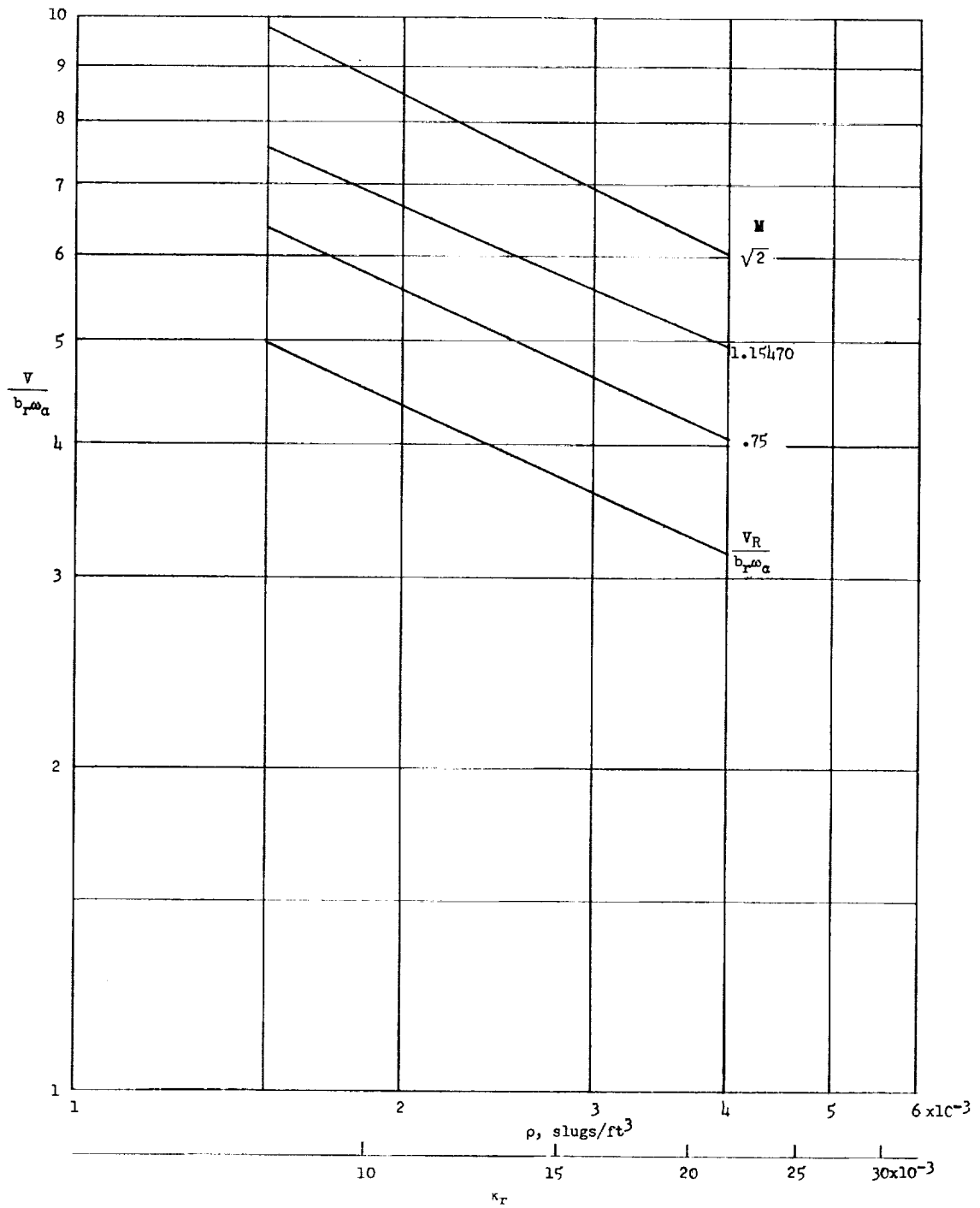
L-464

Figure 55.- Variation of flutter-speed coefficient with density for wing 400R.
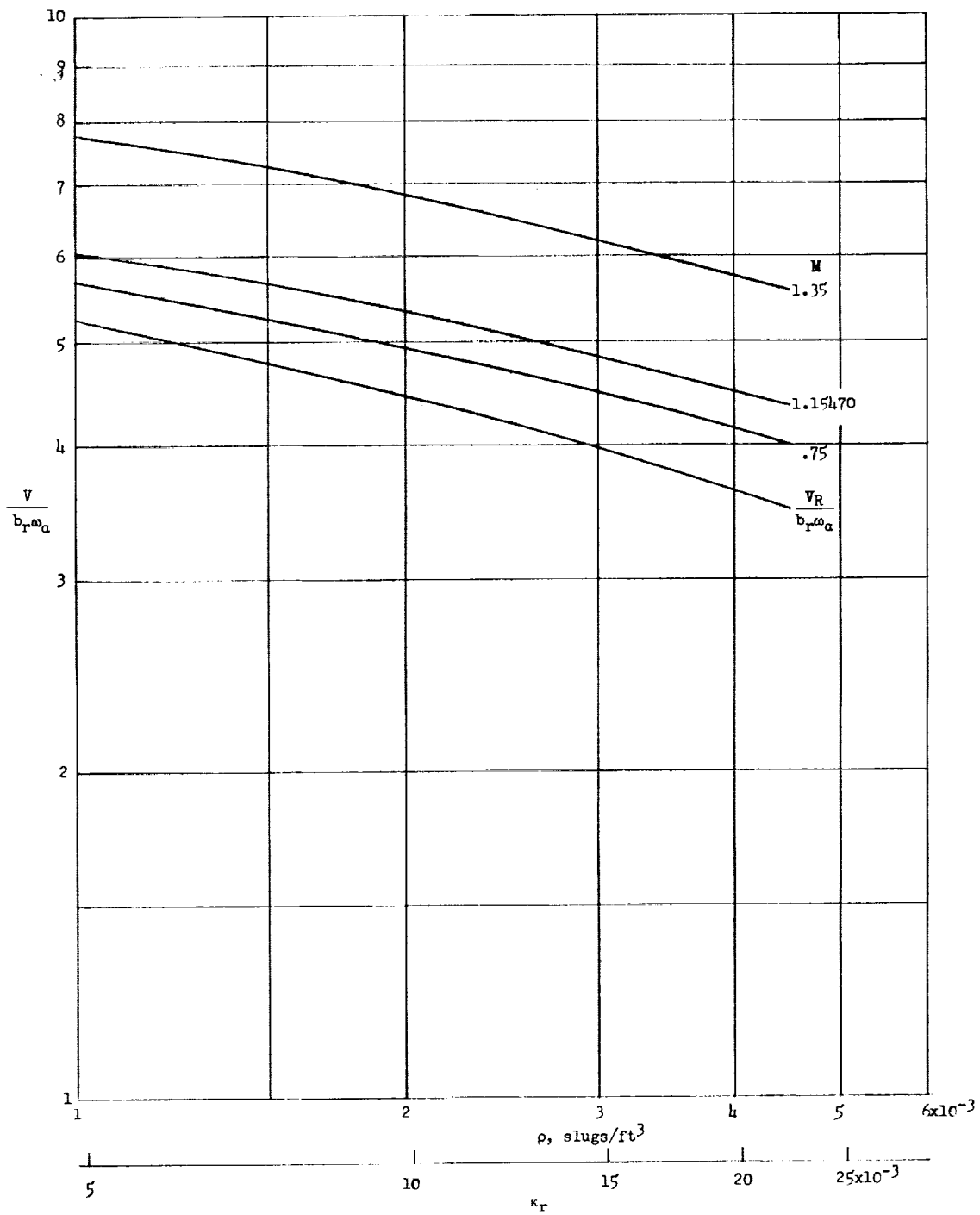
Figure 56.- Variation of flutter-speed coefficient with density for wing 4451.
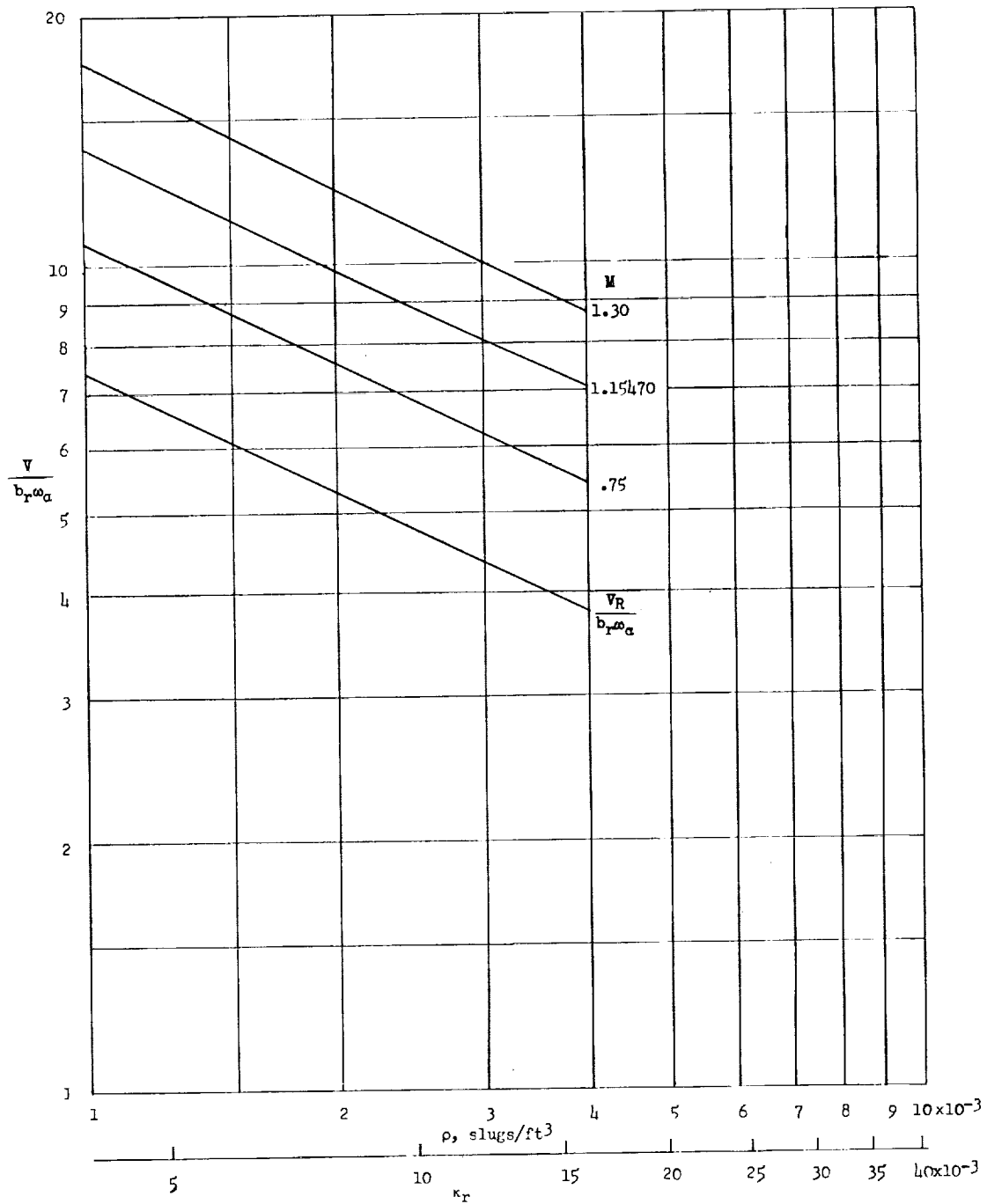
Figure 57.- Variation of flutter-speed coefficient with density for wing 4001.
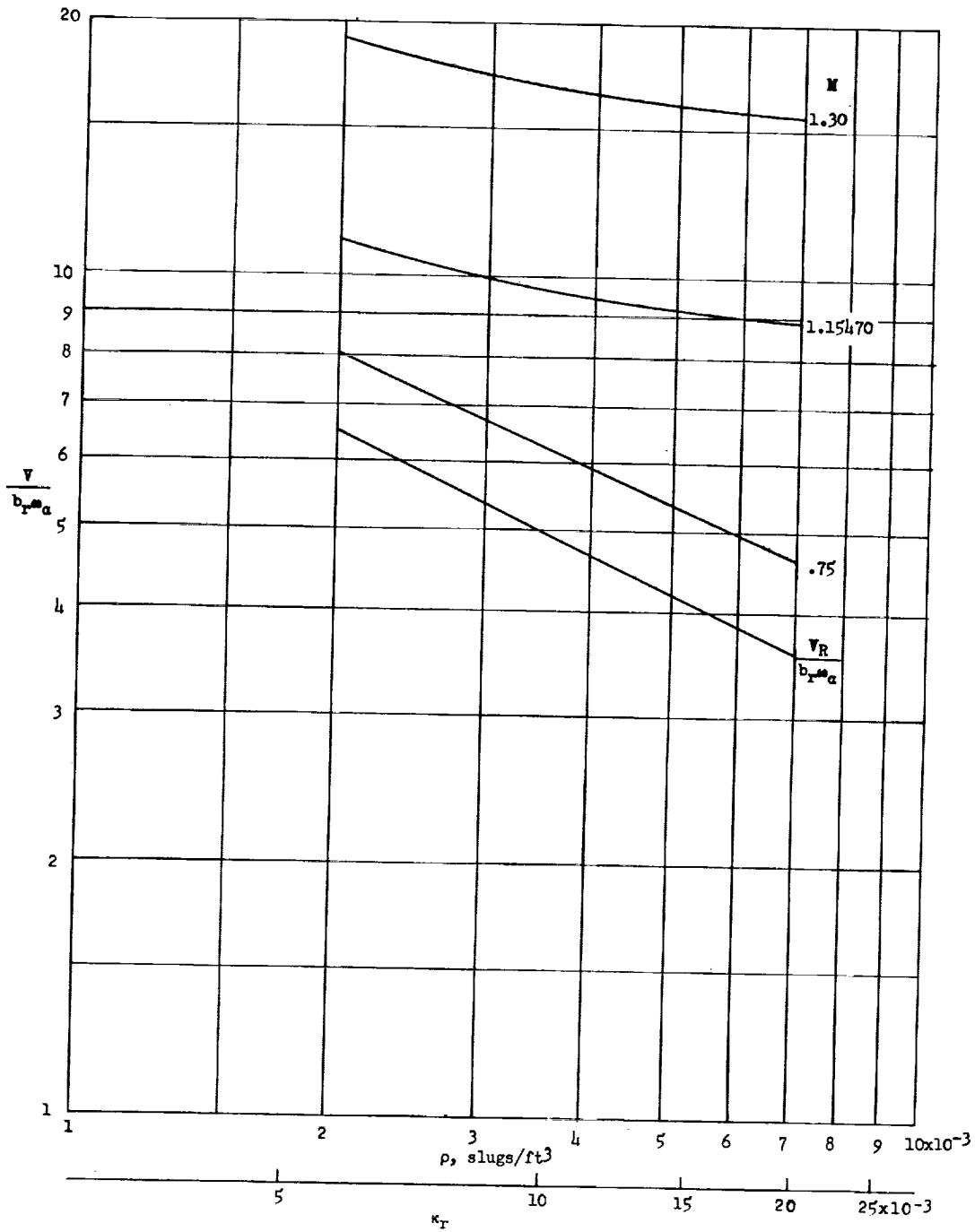
Figure 58.- Variation of flutter-speed coefficient with density for wing 7001.
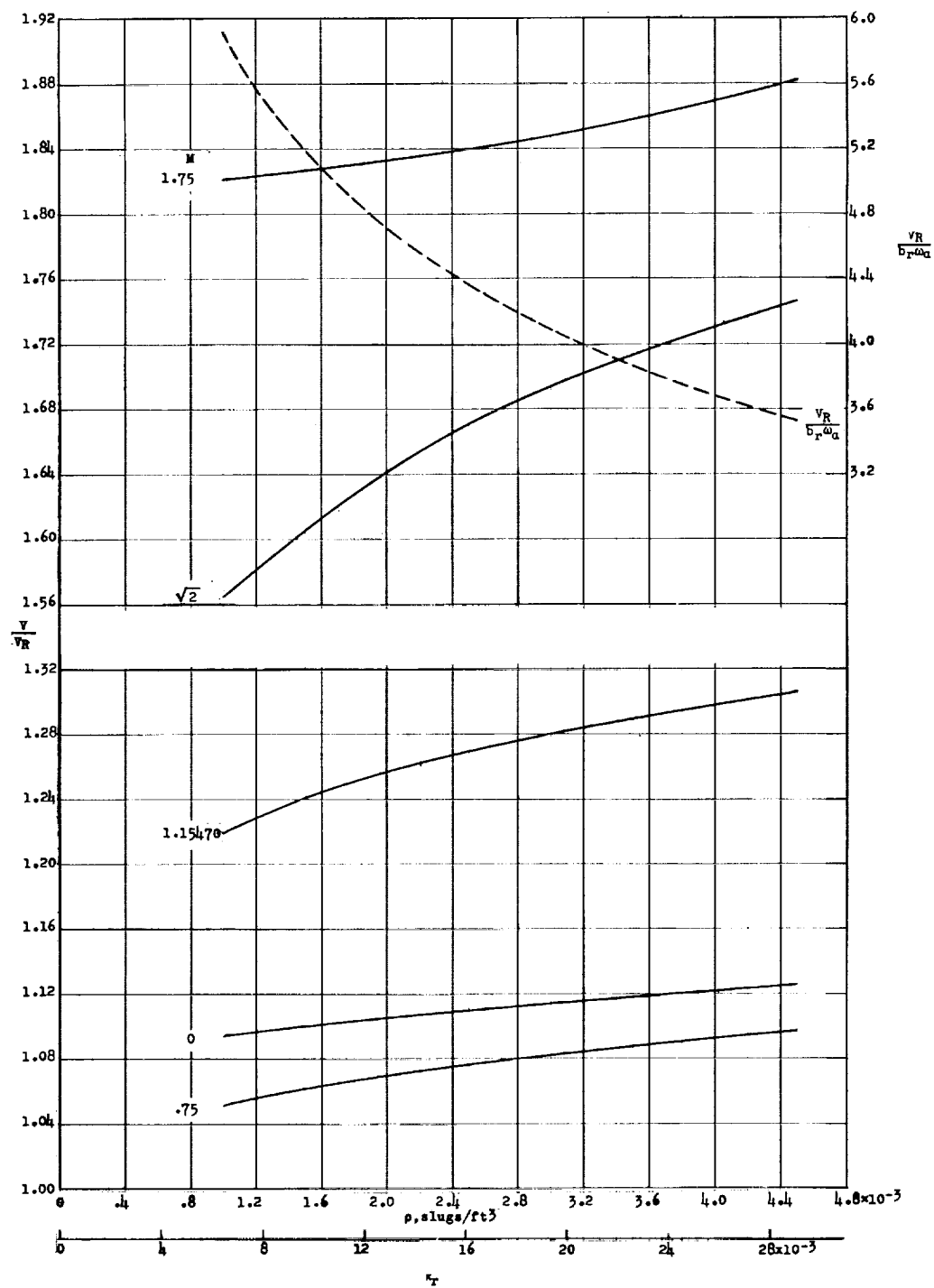
Figure 59.- Variation of flutter-speed ratio with flow density for wing 445.
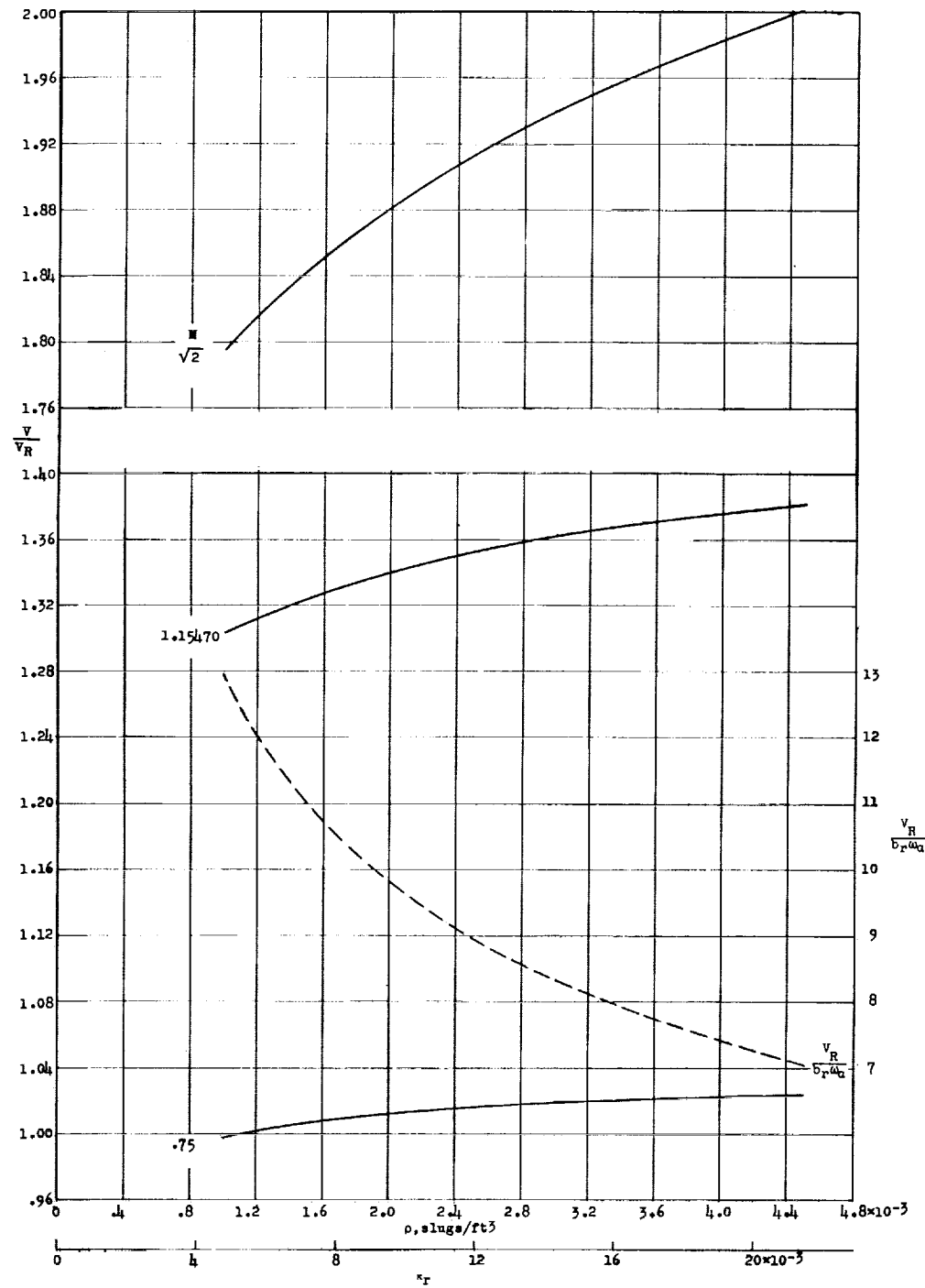
Figure 60.- Variation of flutter-speed ratio with flow density for wing 445F.
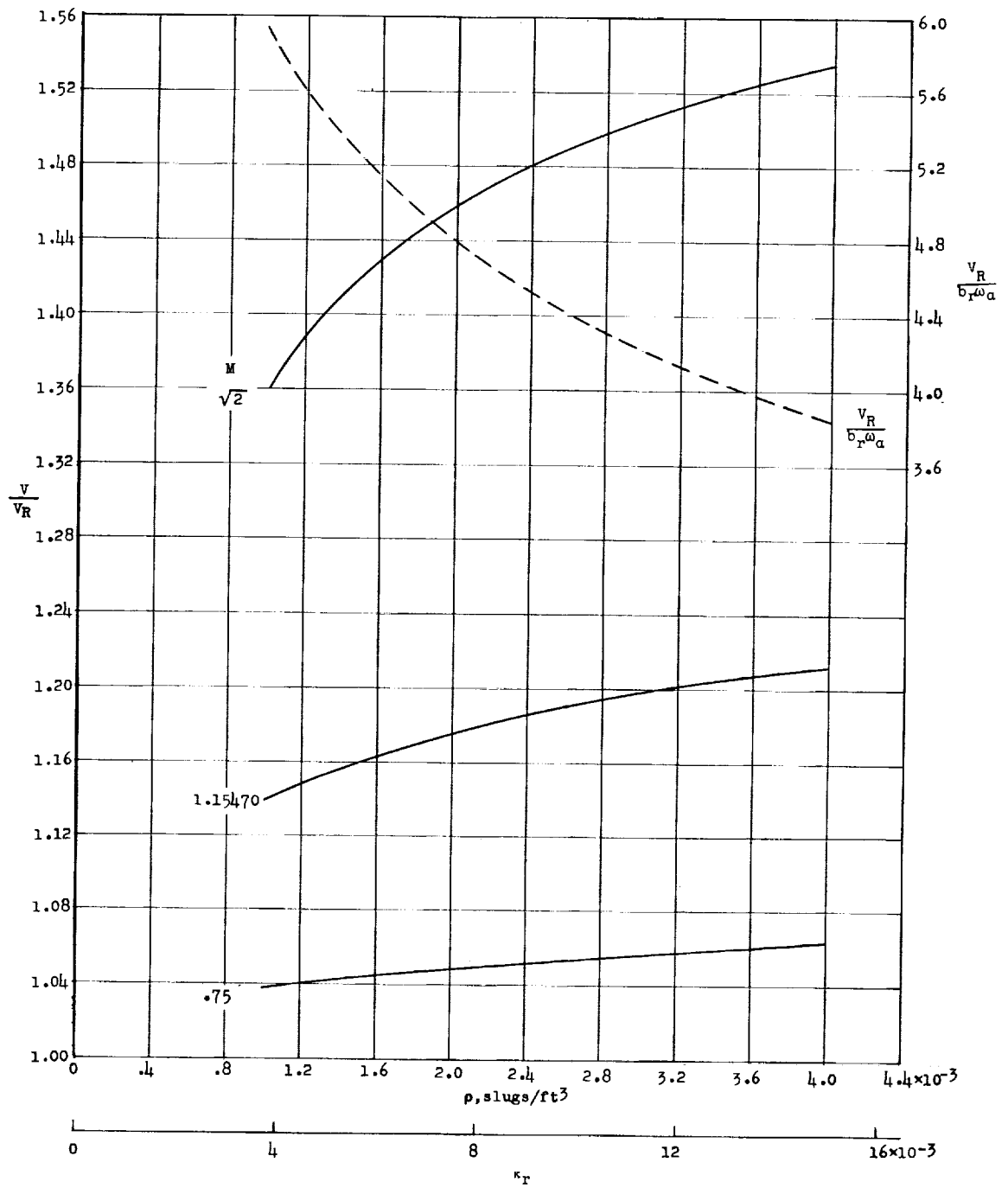
Figure 61.- Variation of flutter-speed ratio with flow density for
wing 445R.
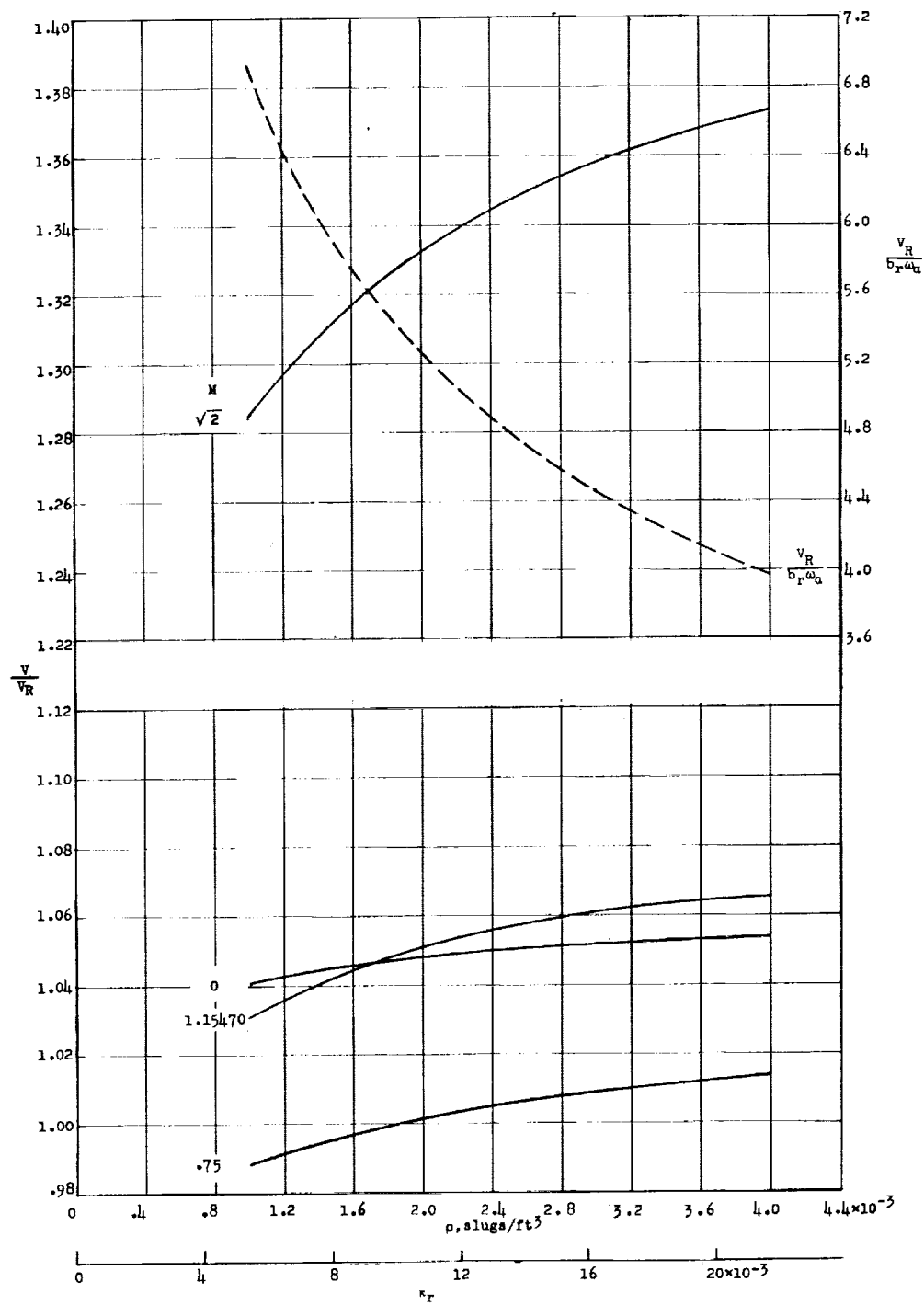
Figure 62.- Variation of flutter-speed ratio with flow density for wing 645.
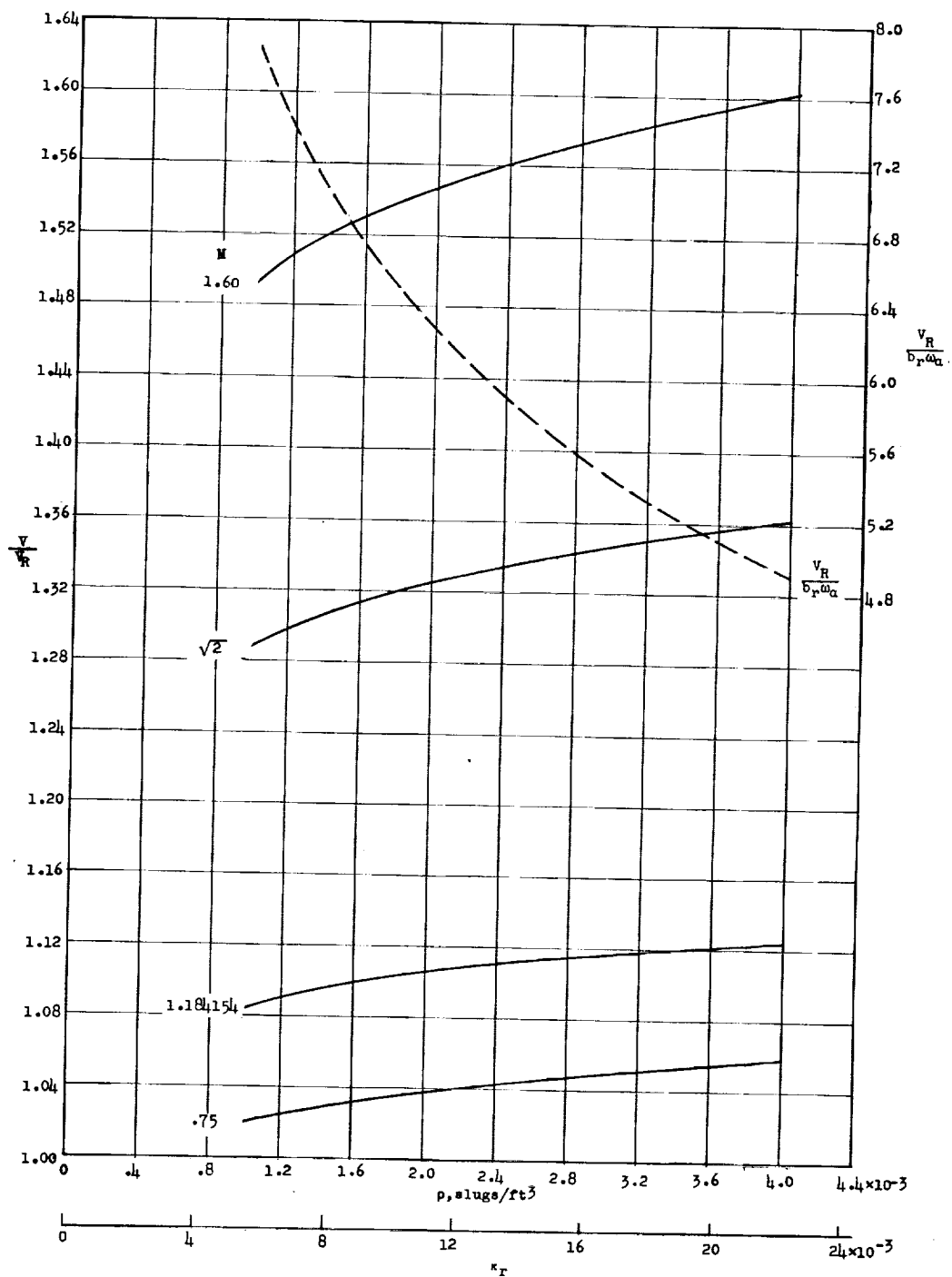
L-464

Figure 63.- Variation of flutter-speed ratio with flow density for wing 452.
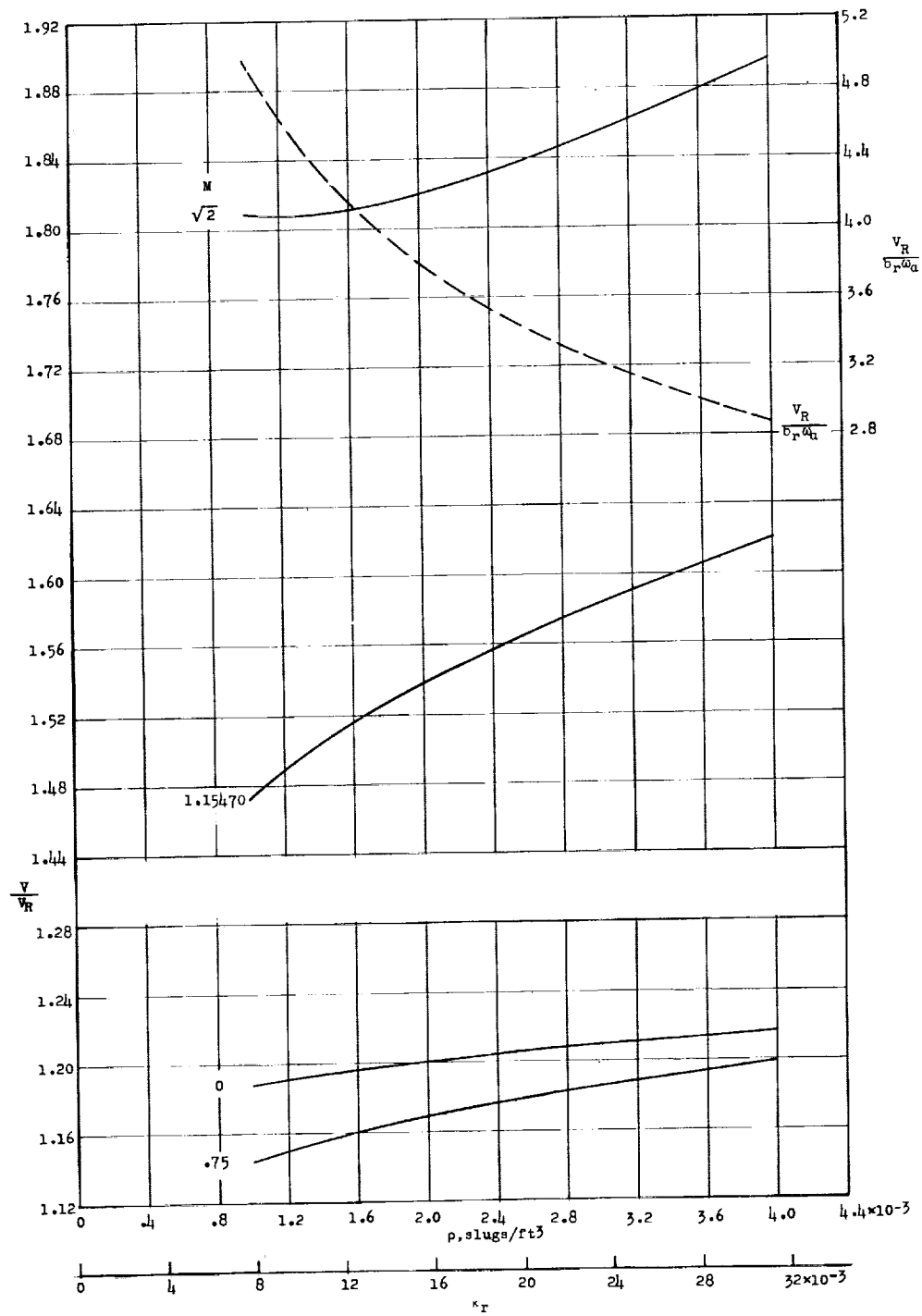
Figure 64.- Variation of flutter-speed ratio with flow density for wing 430.
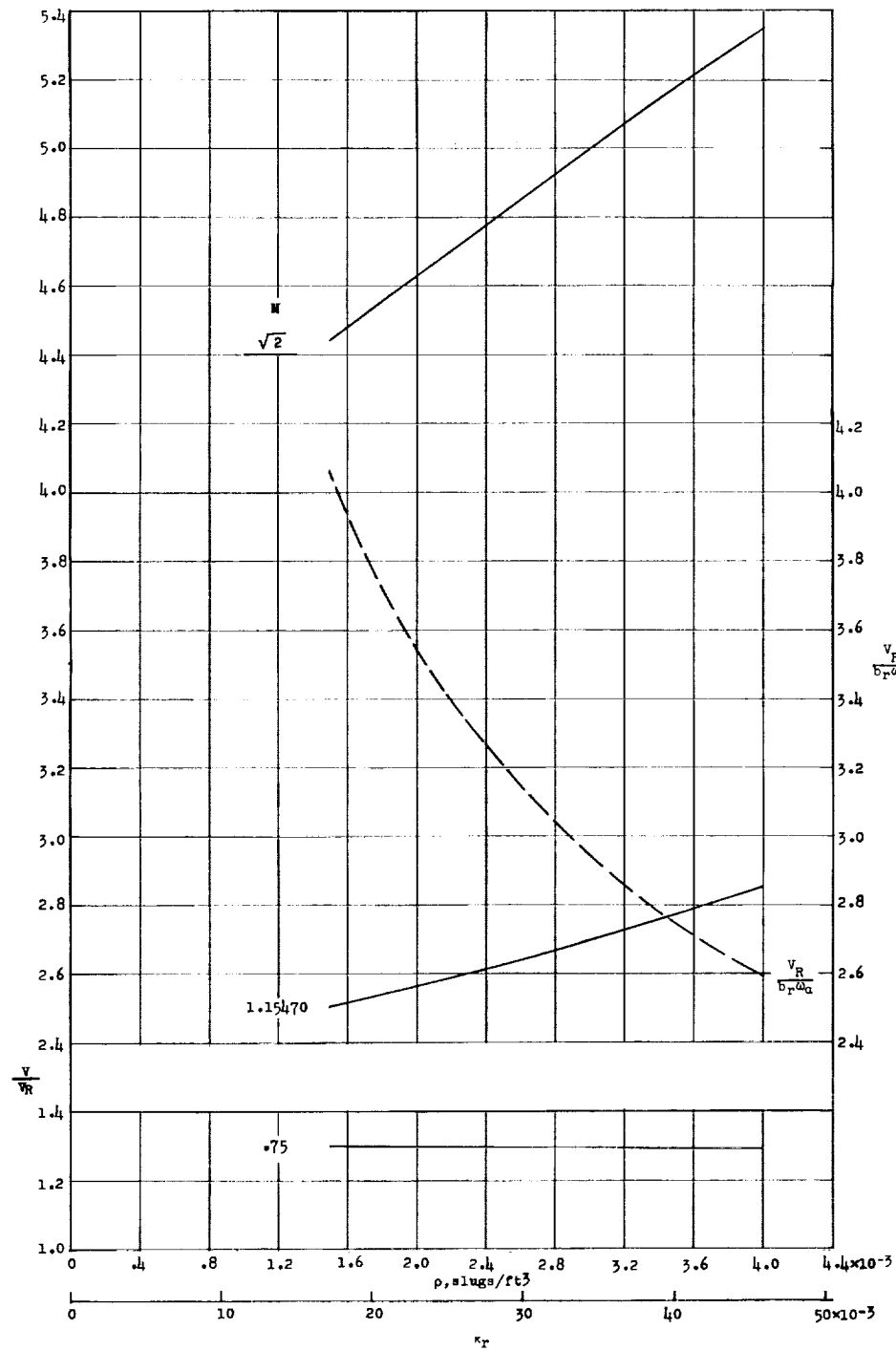
Figure 65.- Variation of flutter-speed ratio with flow density for wing 400.
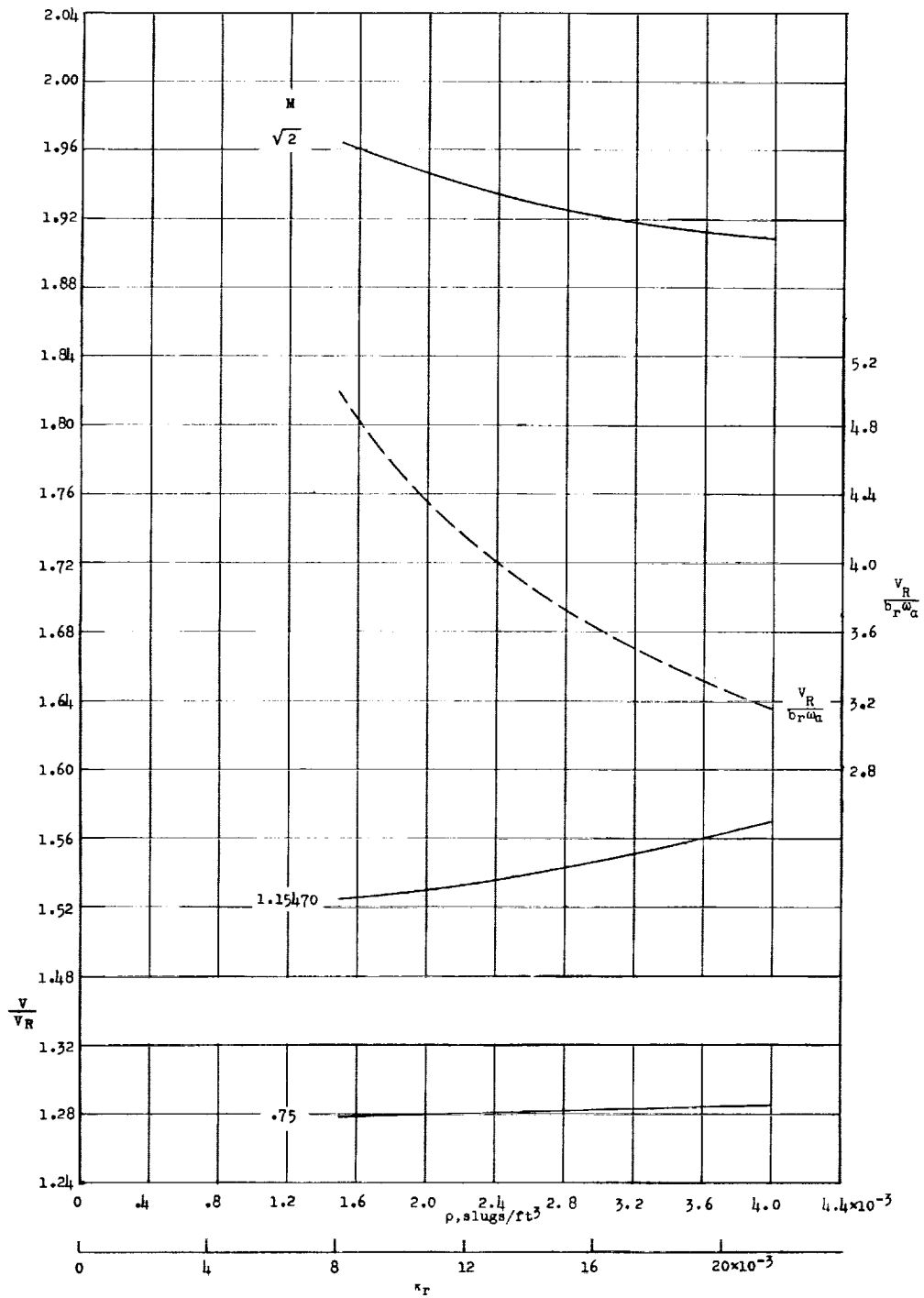
Figure 66.- Variation of flutter-speed ratio with flow density for wing 400R.

L-464
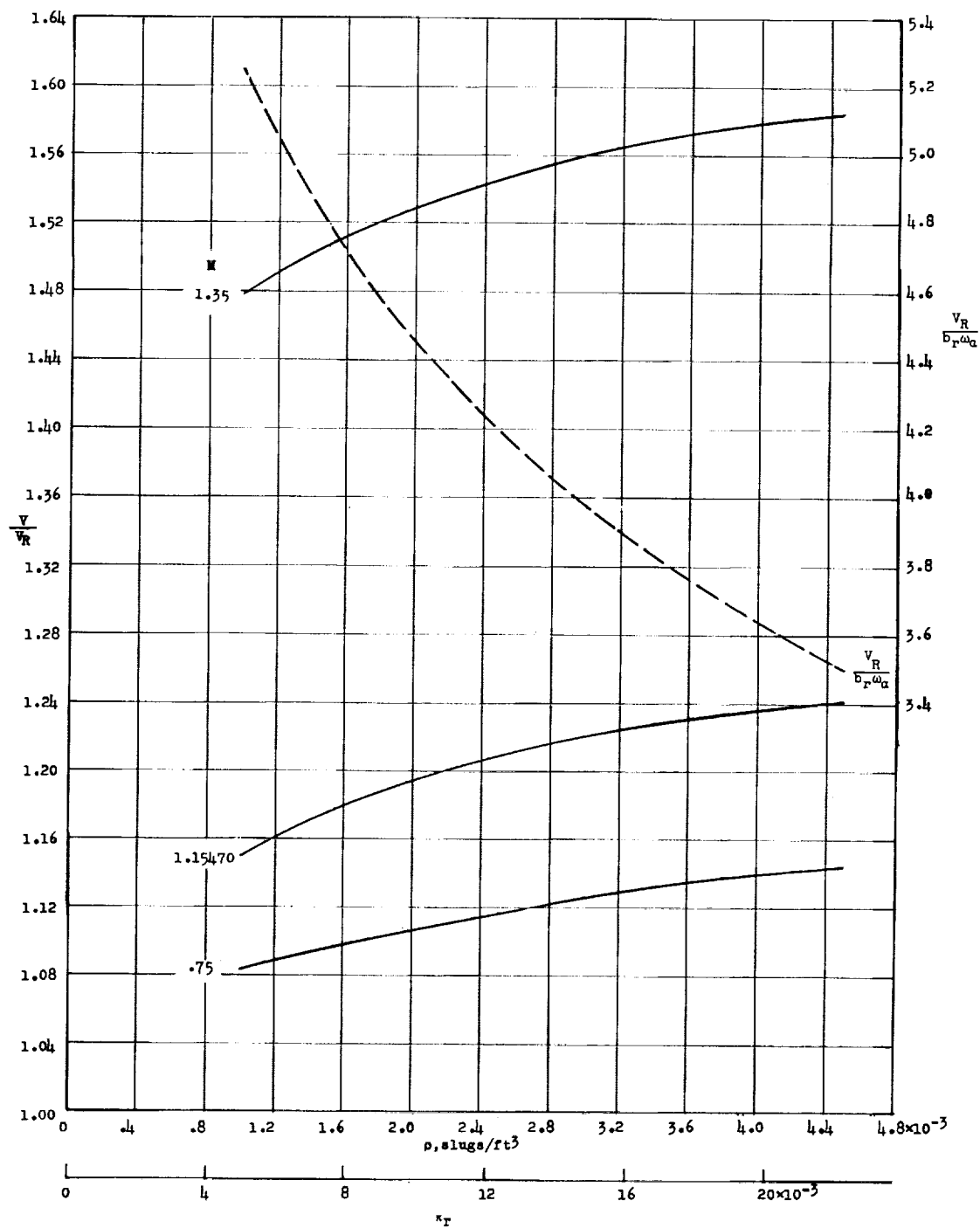
Figure 67.- Variation of flutter-speed ratio with flow density for wing 4451.
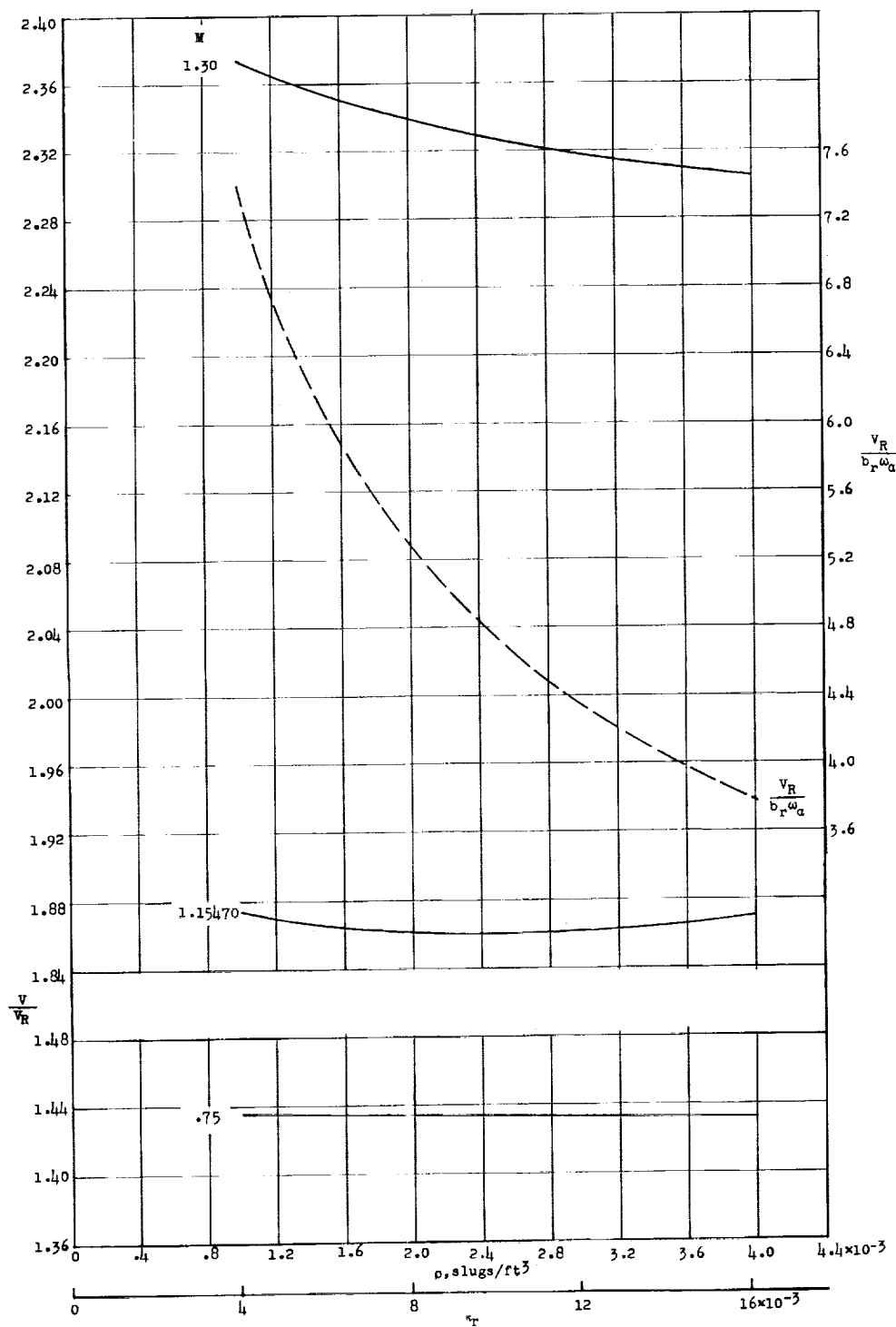
Figure 68.- Variation of flutter-speed ratio with flow density for wing 4001.
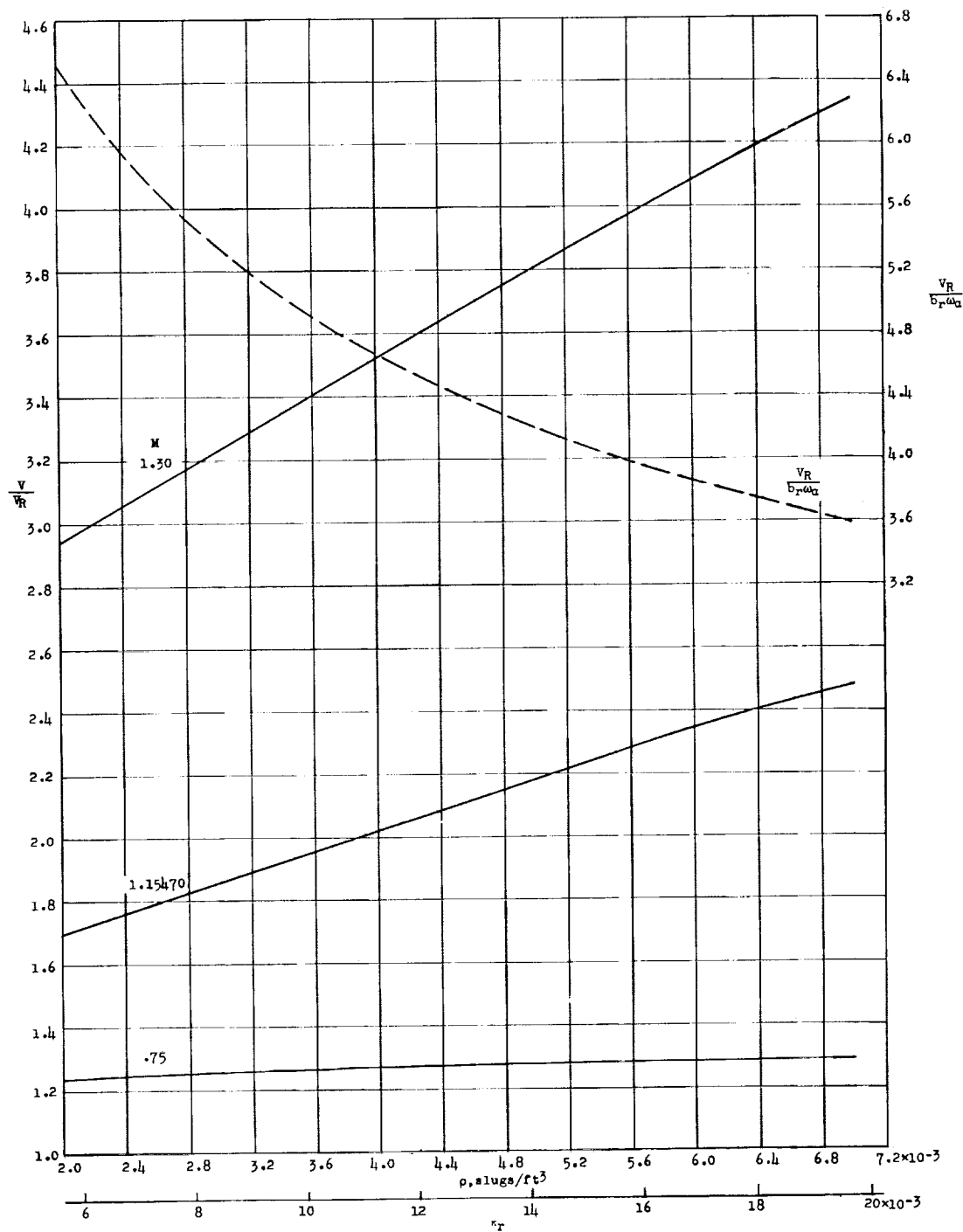
Figure 69.- Variation of flutter-speed ratio with flow density for wing 7001.
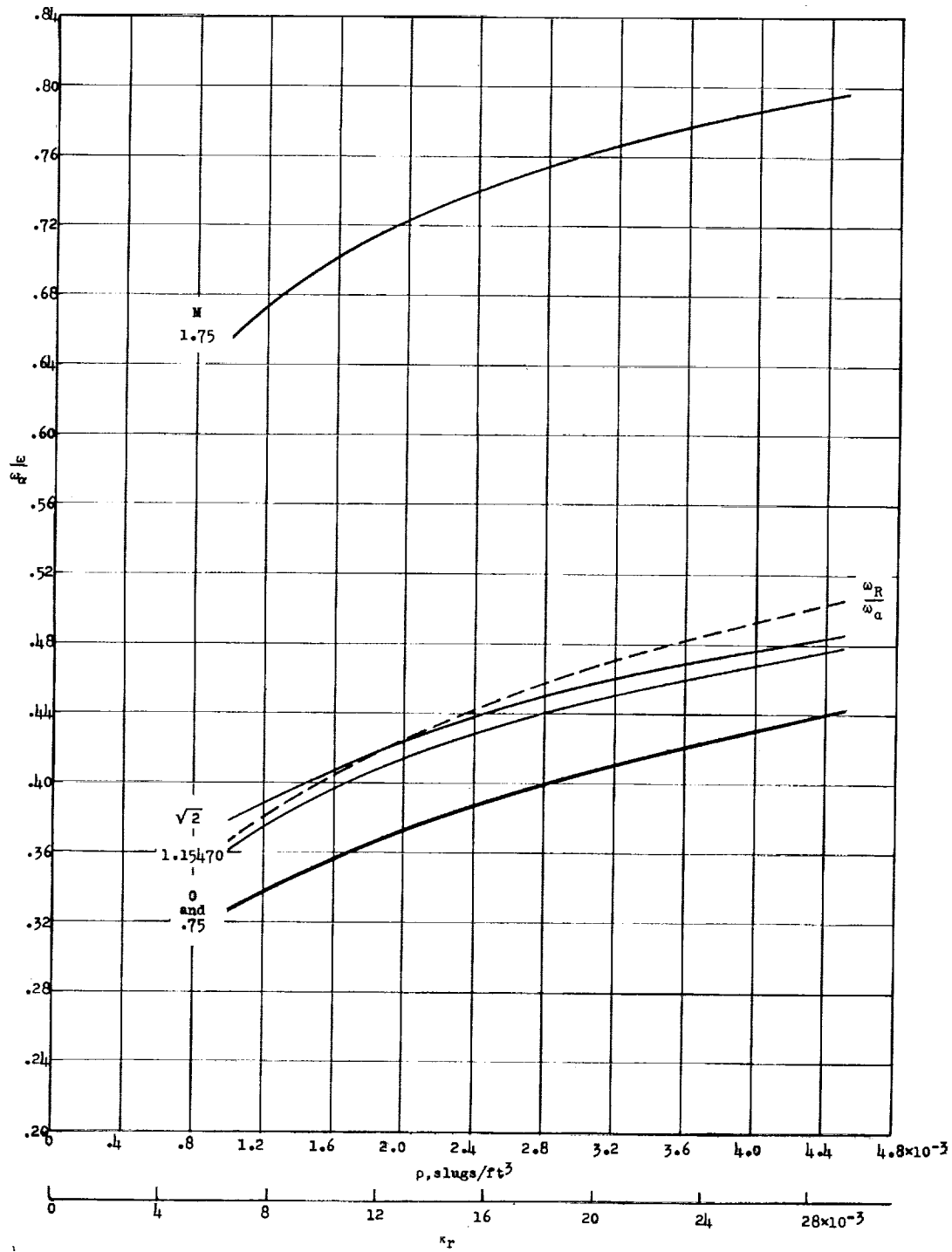
Figure 70.- Variation of flutter frequency with flow density for
wing 445. ω_α = 2,192 radians/sec.

L-464
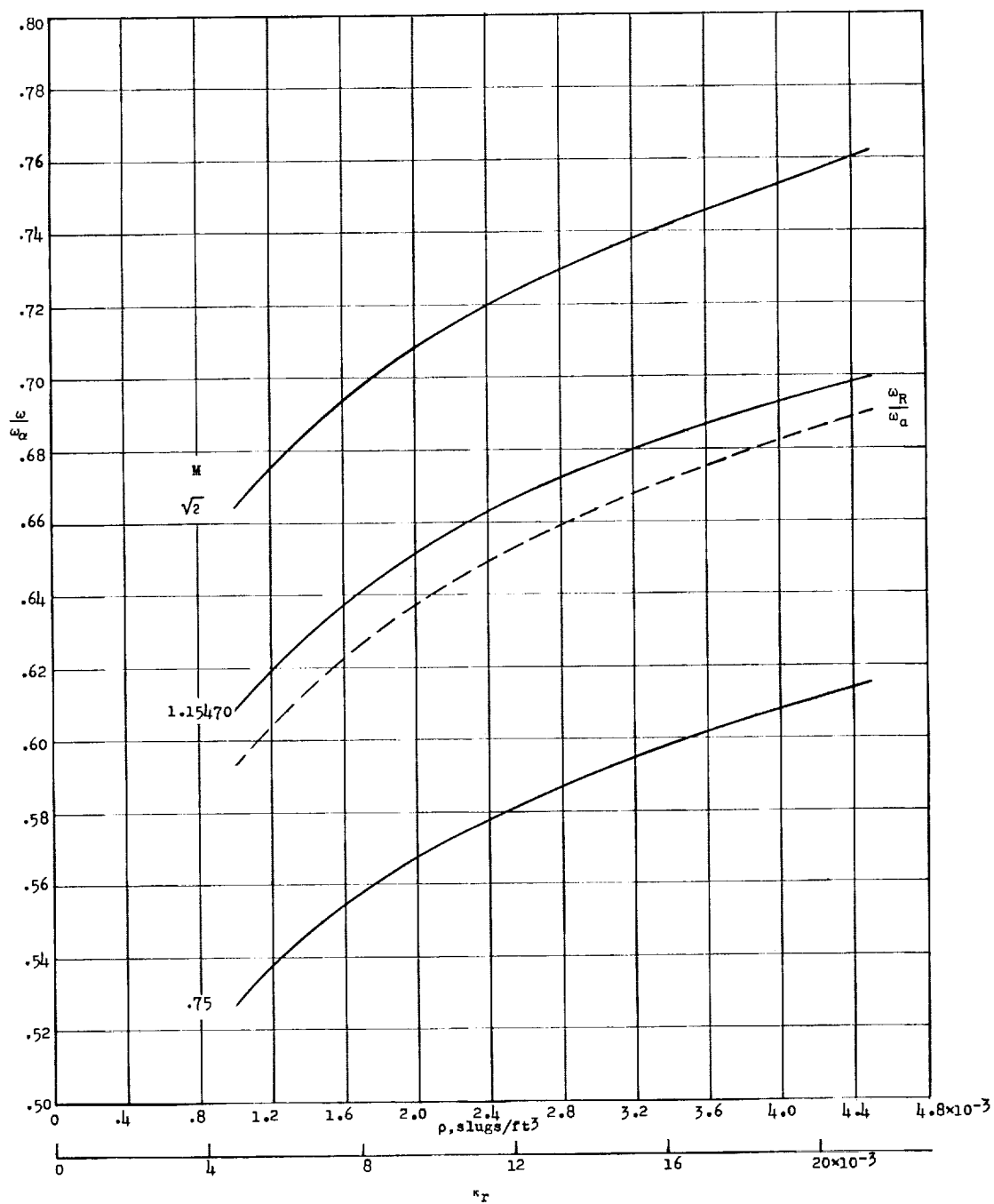
Figure 71.- Variation of flutter frequency with flow density for wing 445F. $\omega_\alpha = 1,144$ radians/sec.
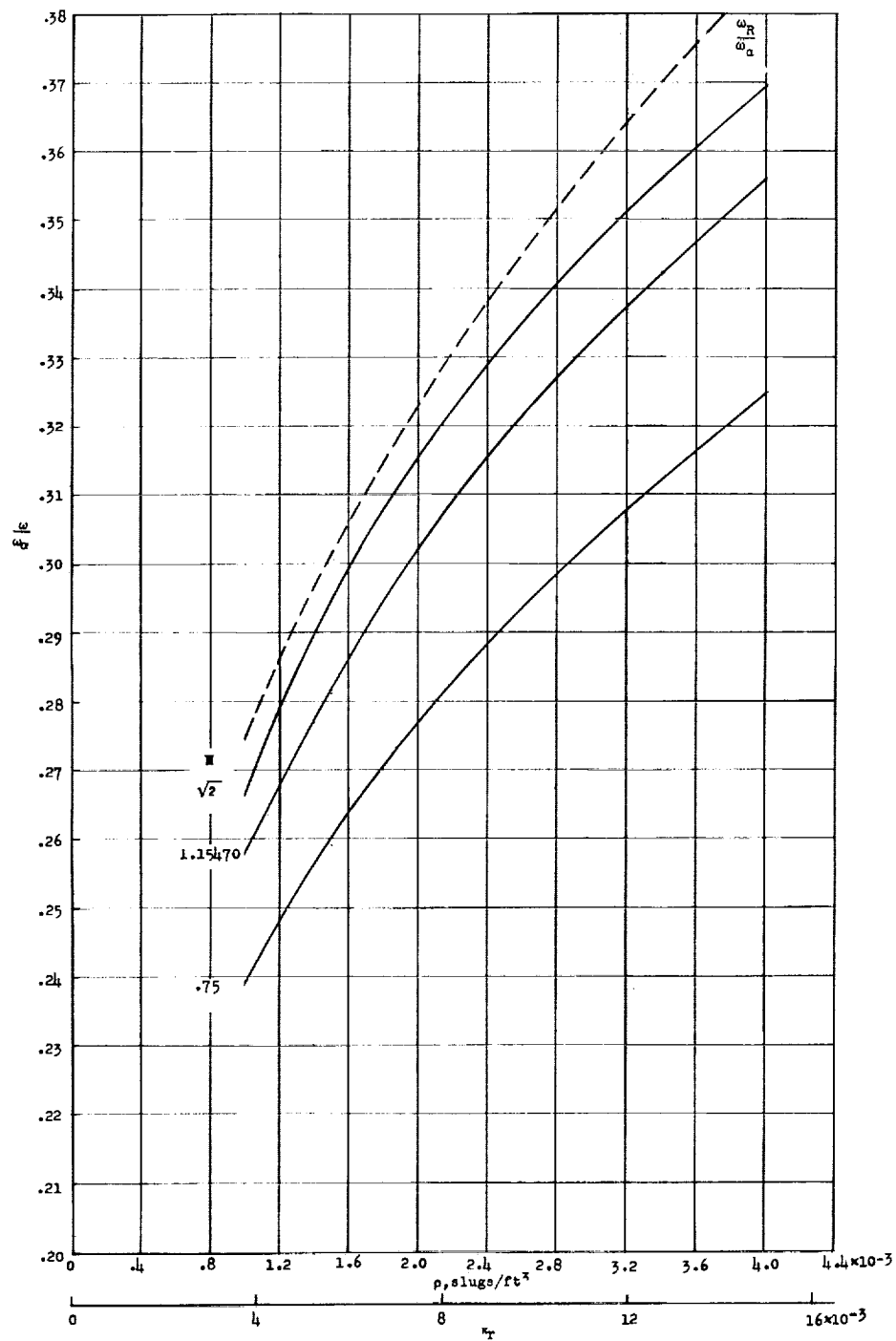
Figure 72.- Variation of flutter frequency with flow density for
wing 445R. ω_α = 2,306 radians/sec.
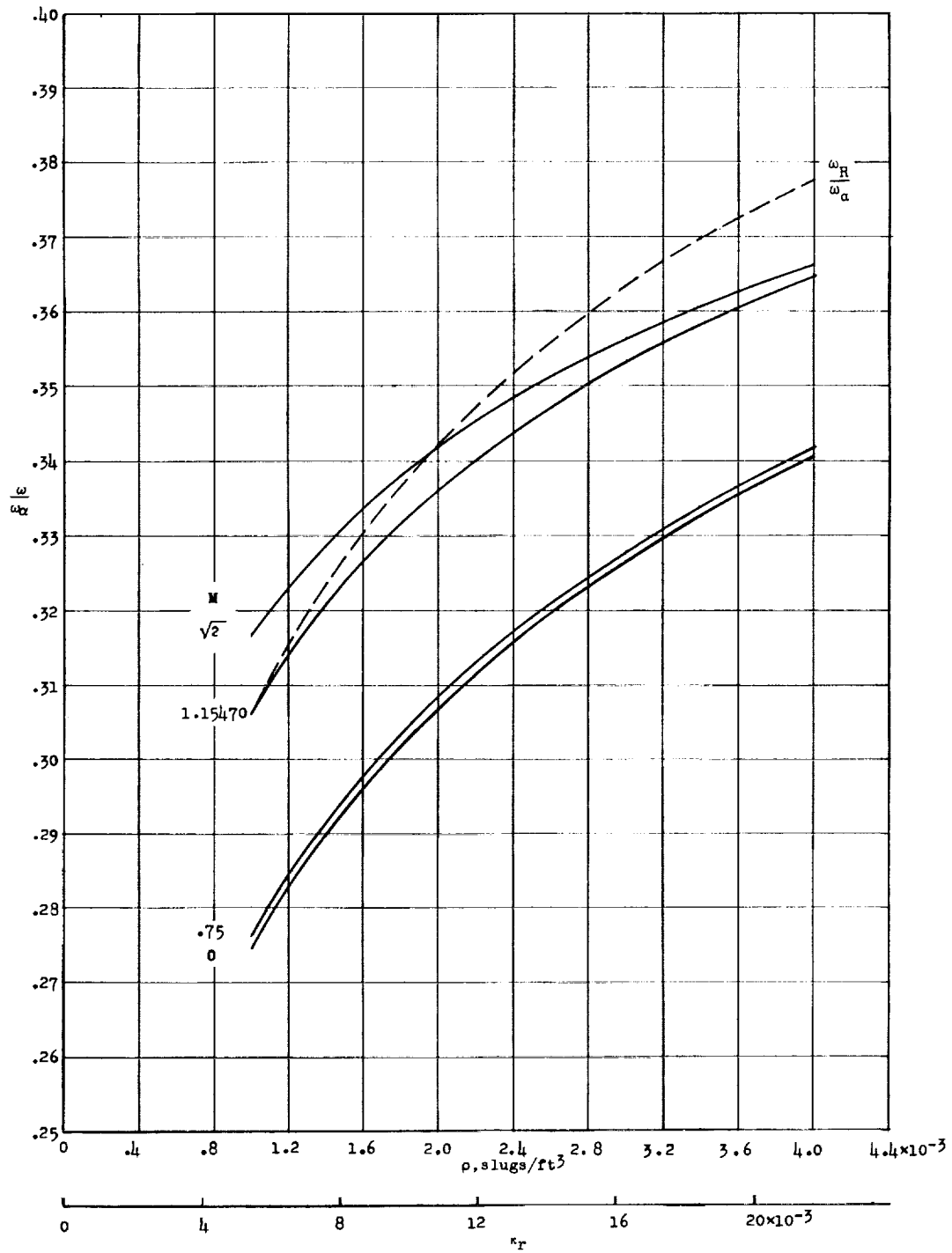
Figure 73.- Variation of flutter frequency with flow density for wing 645. $\omega_\alpha = 3{,}173$ radians/sec.
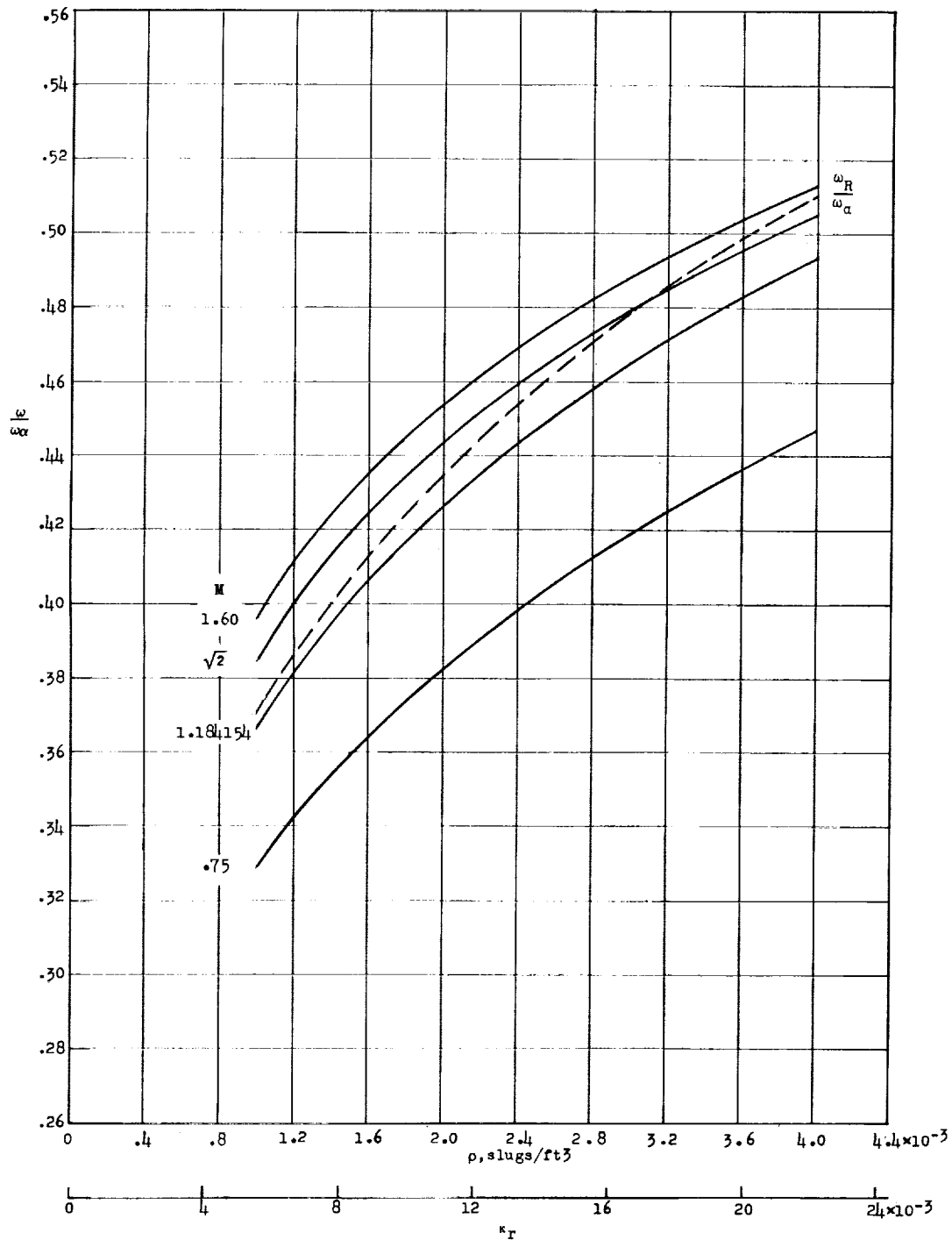
Figure 74.- Variation of flutter frequency with flow density for wing 452. ω_α = 2,300 radians/sec.
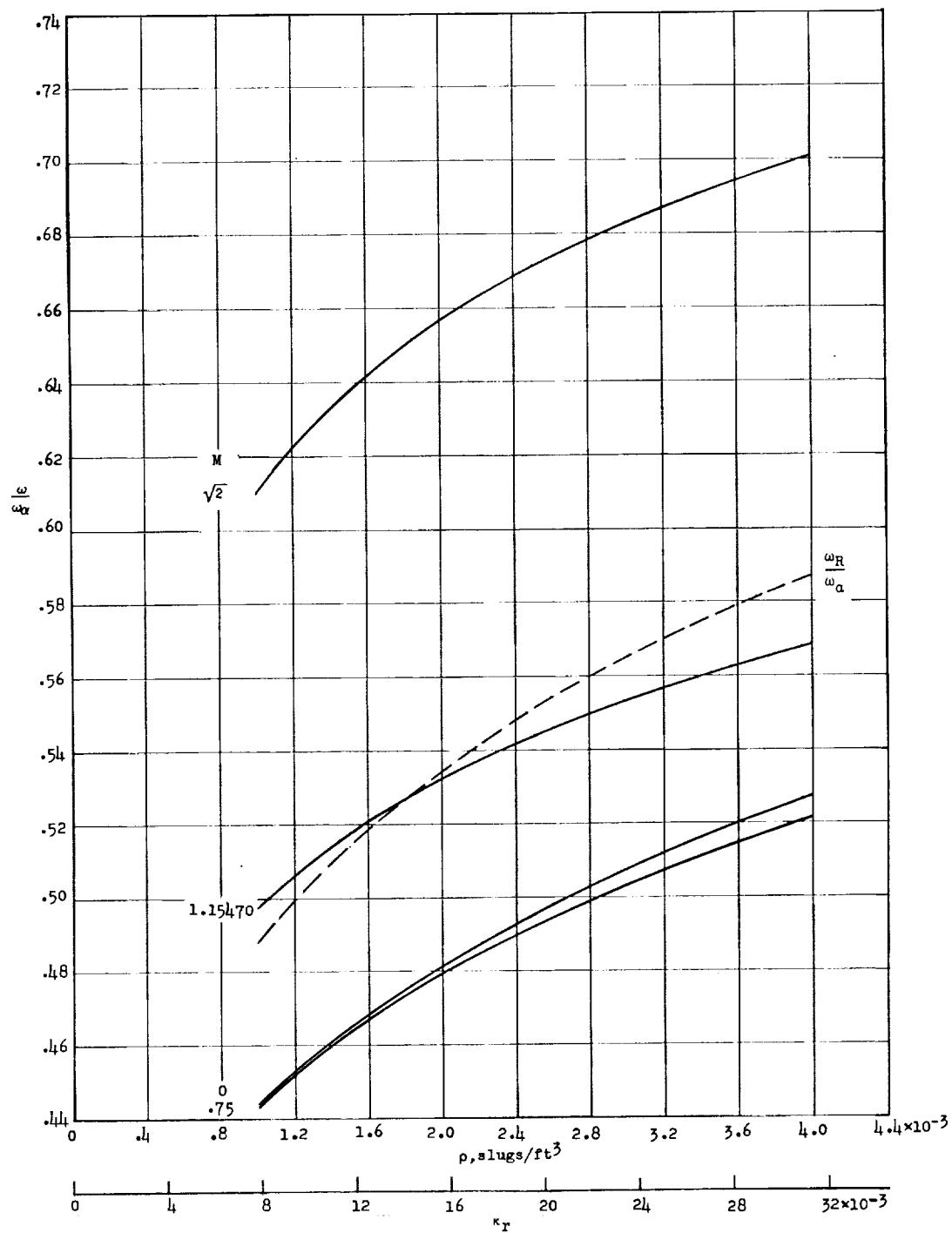
Figure 75.- Variation of flutter frequency with flow density for wing 430. ω_α = 2,158 radians/sec.
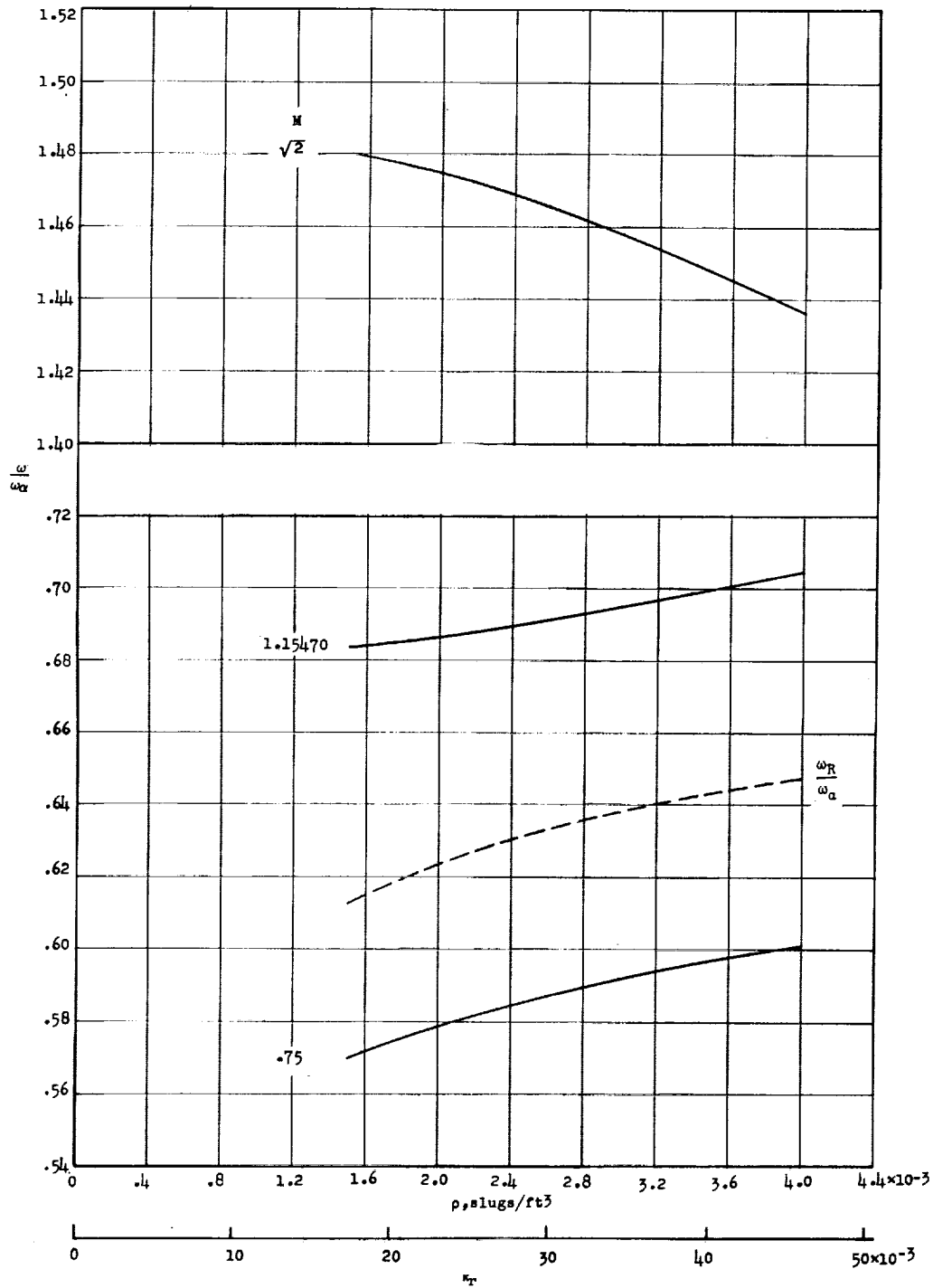
Figure 76.- Variation of flutter frequency with flow density for wing 400. $\omega_\alpha = 2{,}463$ radians/sec.
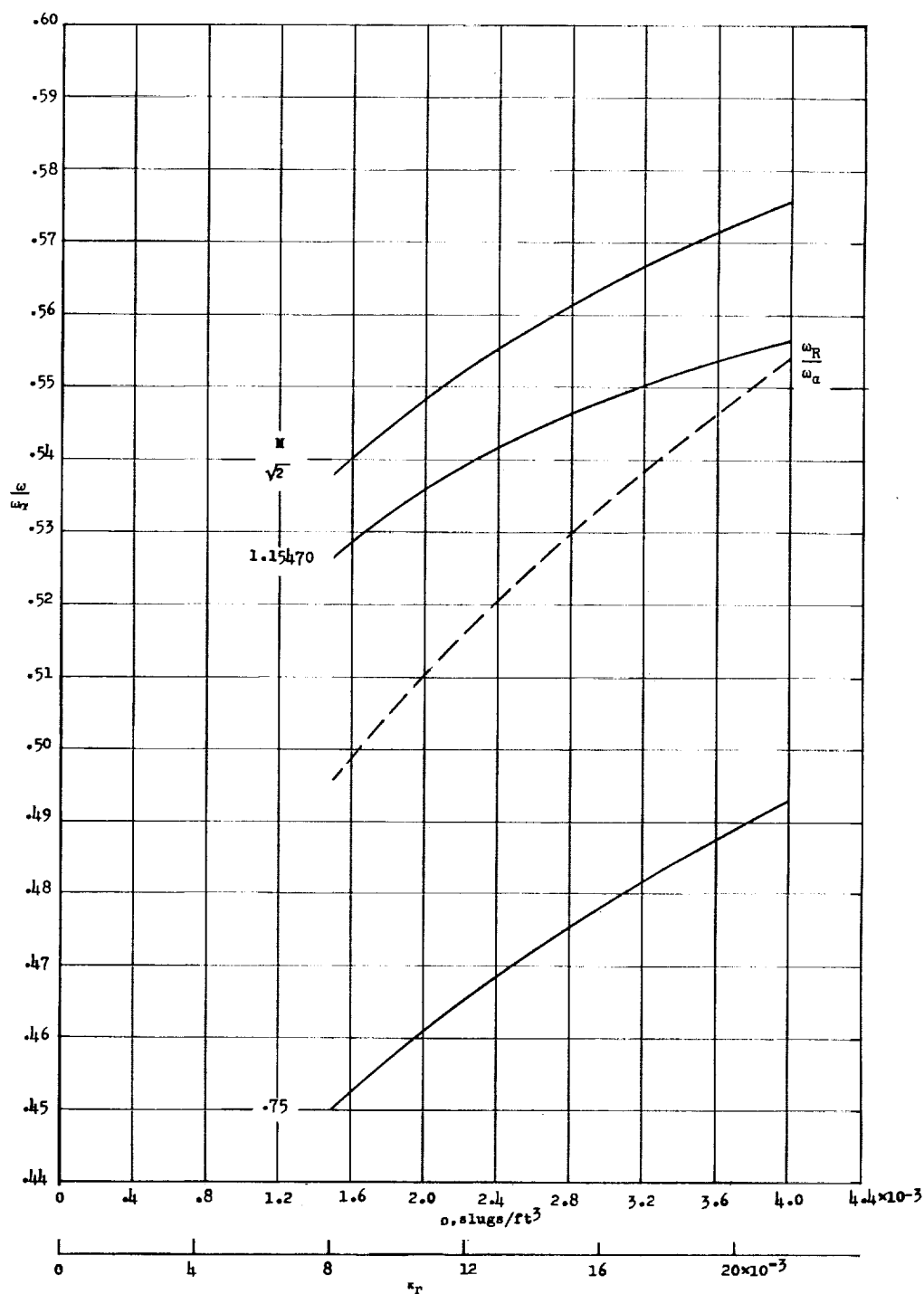
Figure 77.- Variation of flutter frequency with flow density for wing 400R. $\omega_\alpha = 1,982$ radians/sec.

L-464
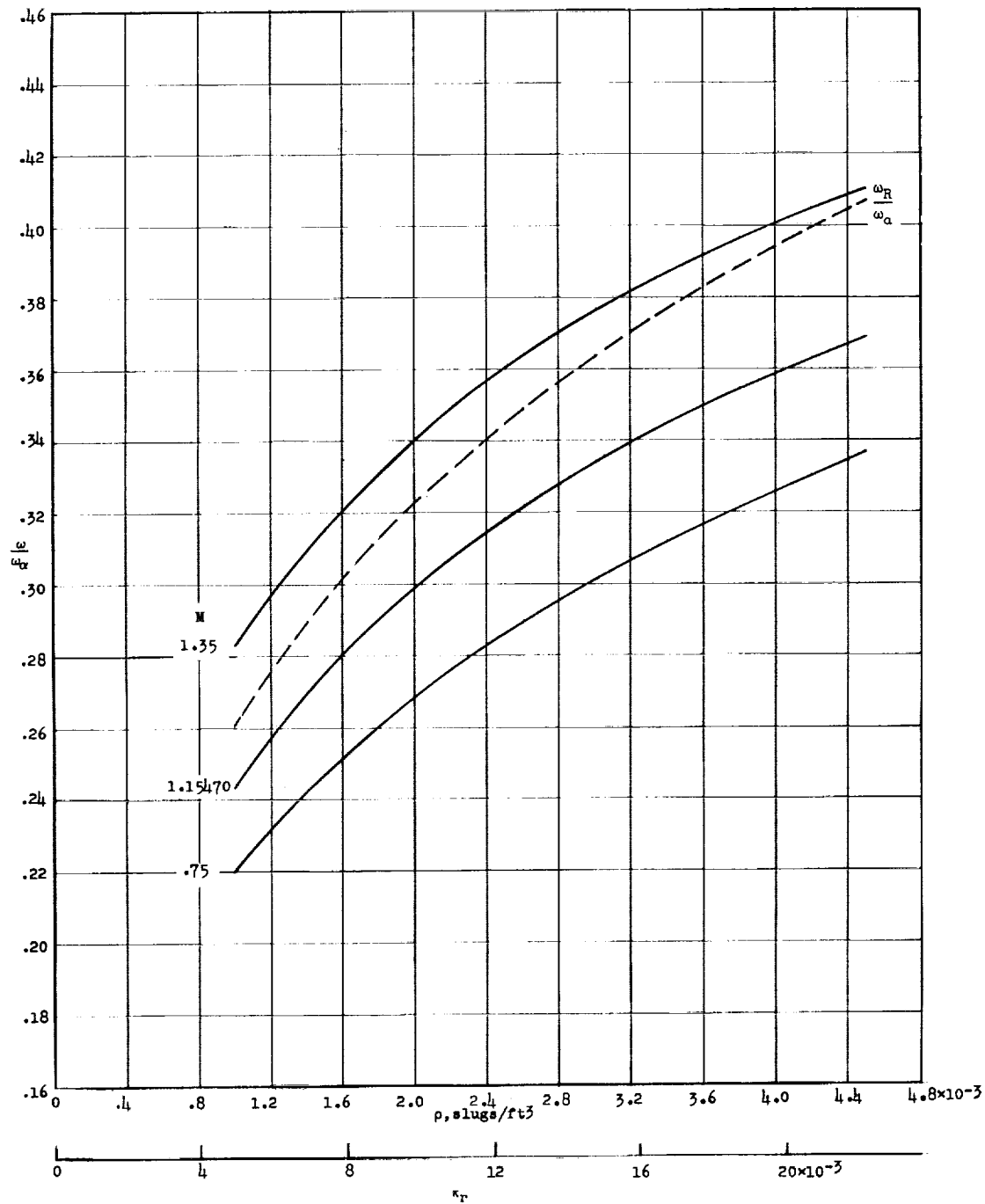
Figure 78.- Variation of flutter frequency with flow density for wing 4451. ω_α = 2,352 radians/sec.

L-464
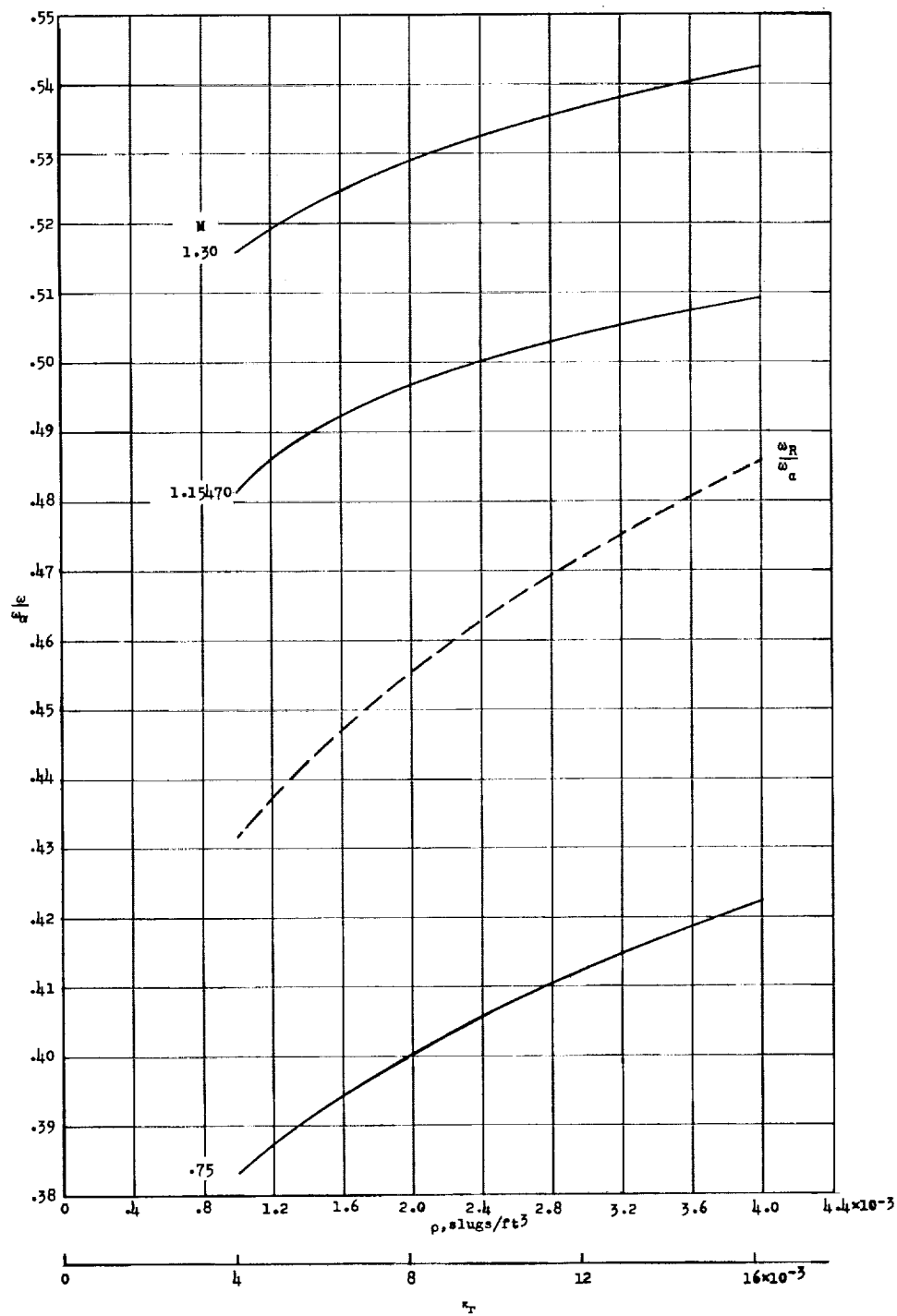
Figure 79.- Variation of flutter frequency with flow density for wing 4001. ω_α = 2,048 radians/sec.

104
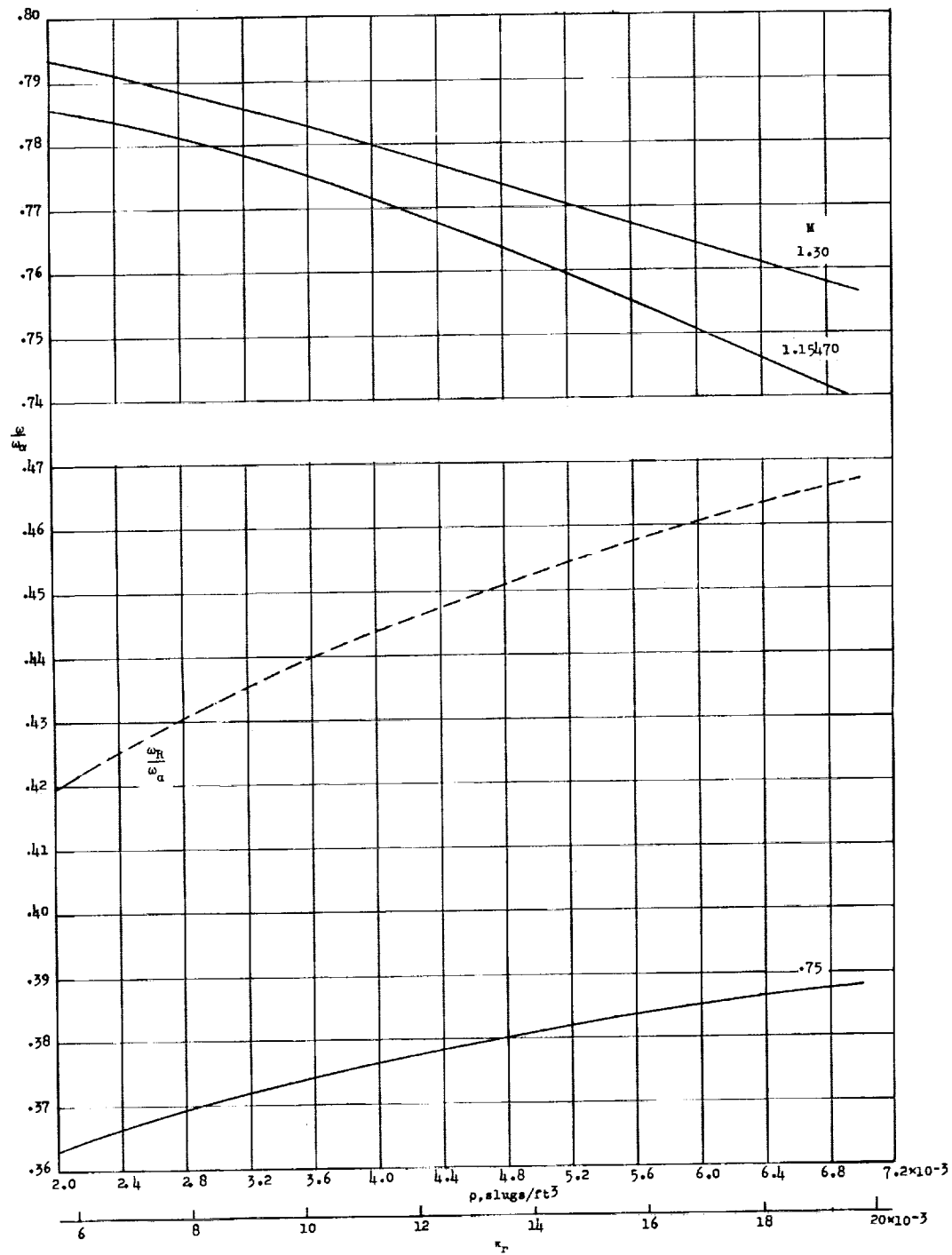
Figure 80.- Variation of flutter frequency with flow density for
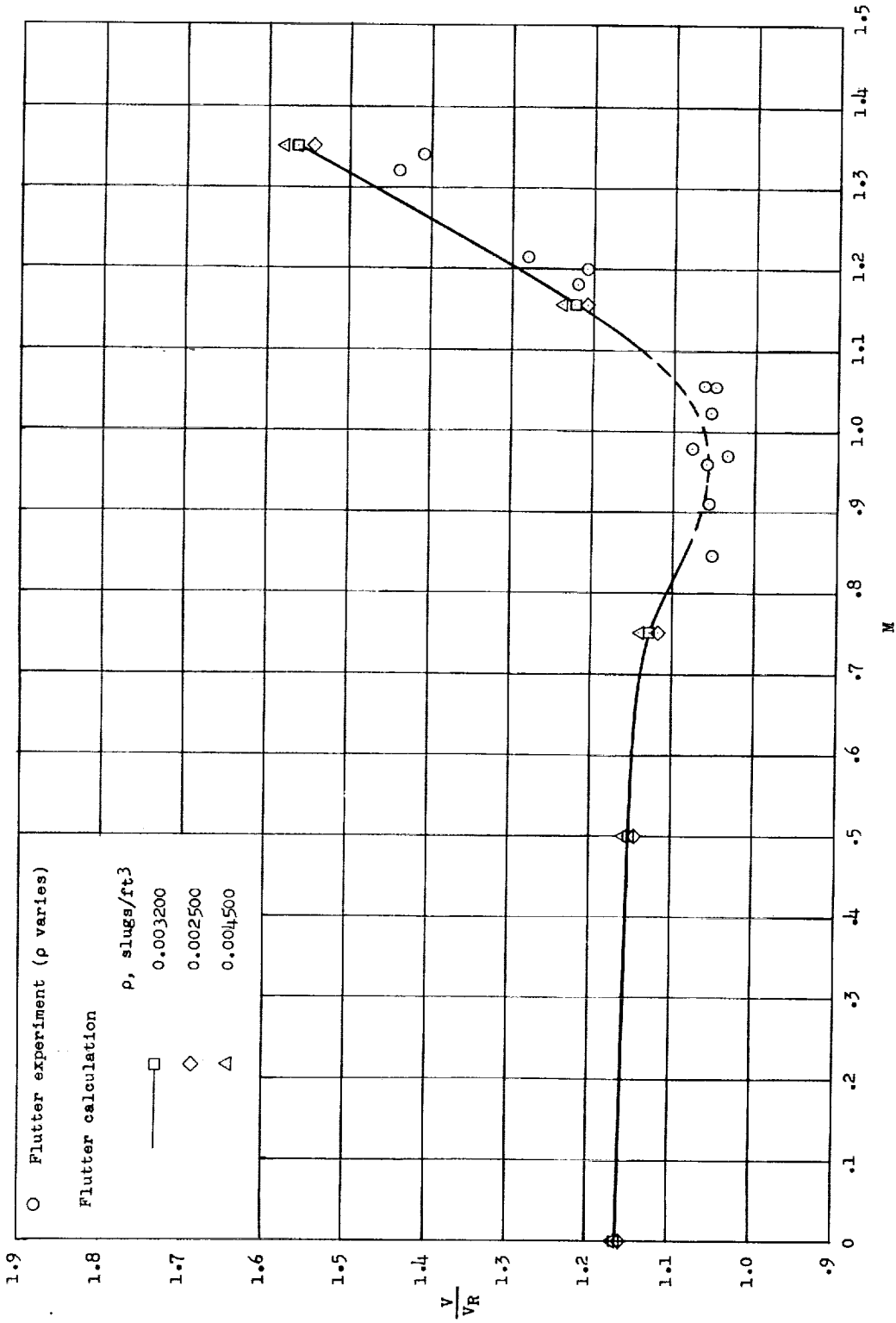wing 7001. ω_α = 2,271 radians/sec.
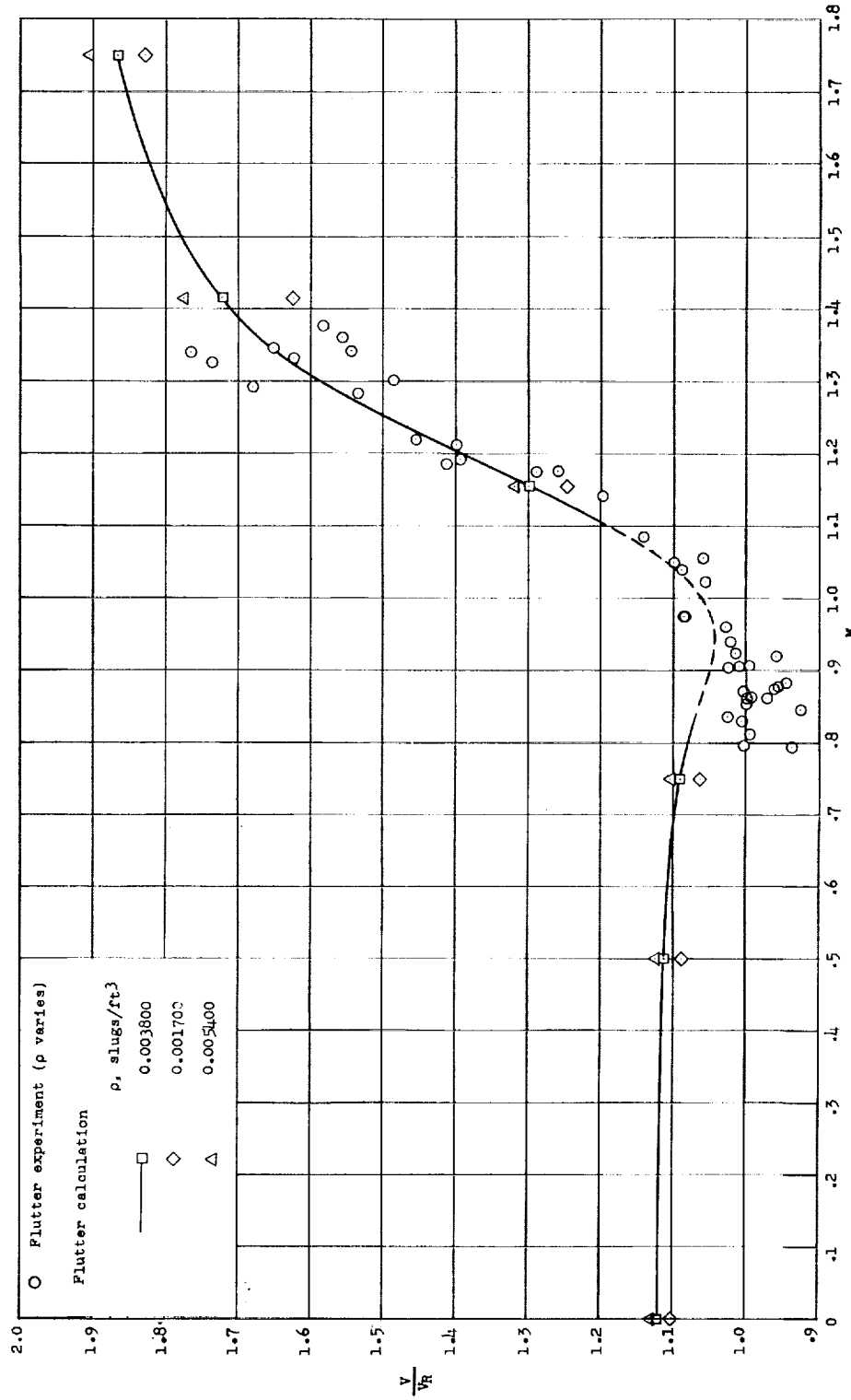
Figure 81.- Effect of density changes on the variation of flutter-speed ratio with Mach number for wing 445). V and V_R are both calculated for the density indicated.
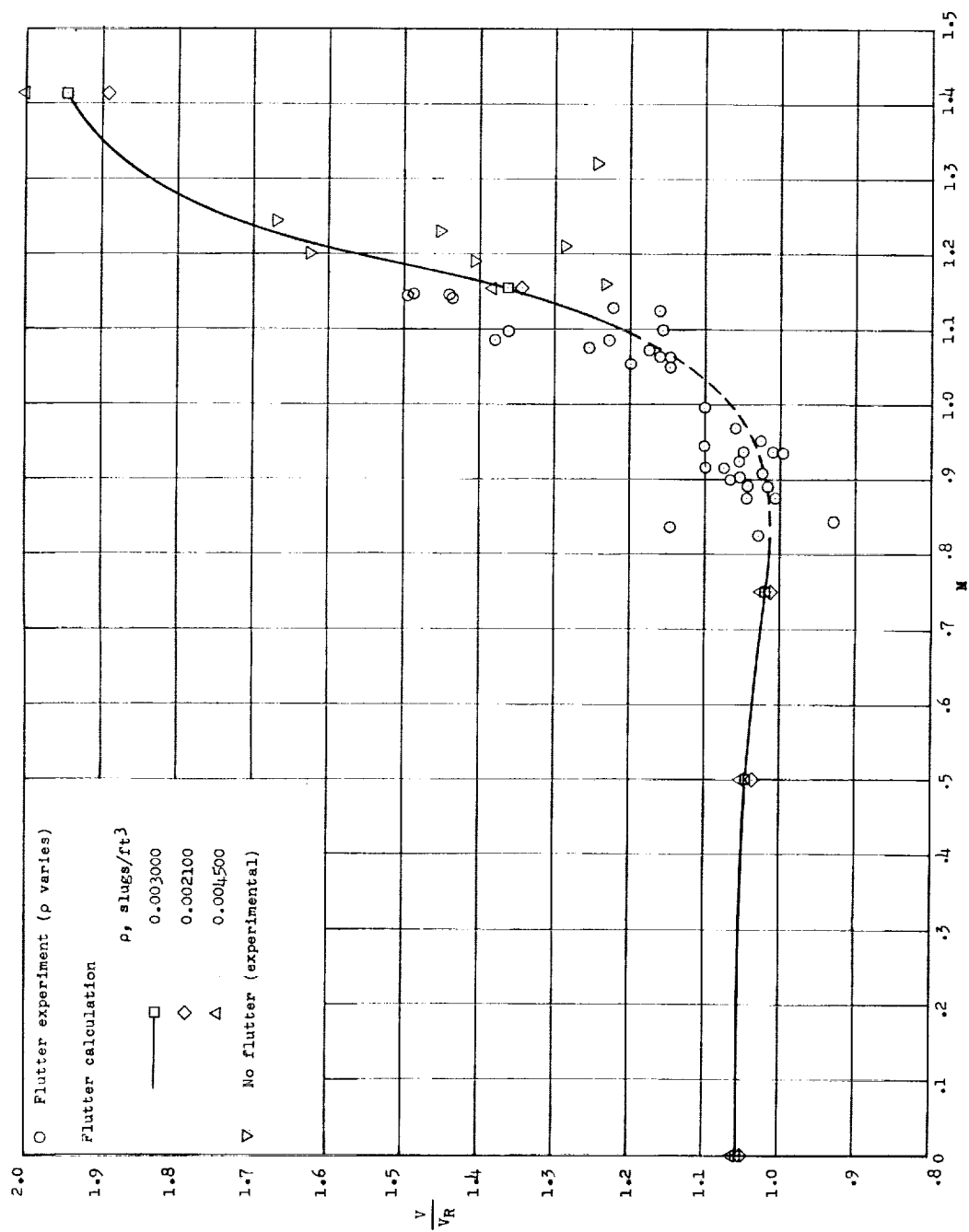
Figure 82.- Effect of density changes on the variation of flutter-speed ratio with Mach number for wing 445F. V and V_R are both calculated for the density indicated.
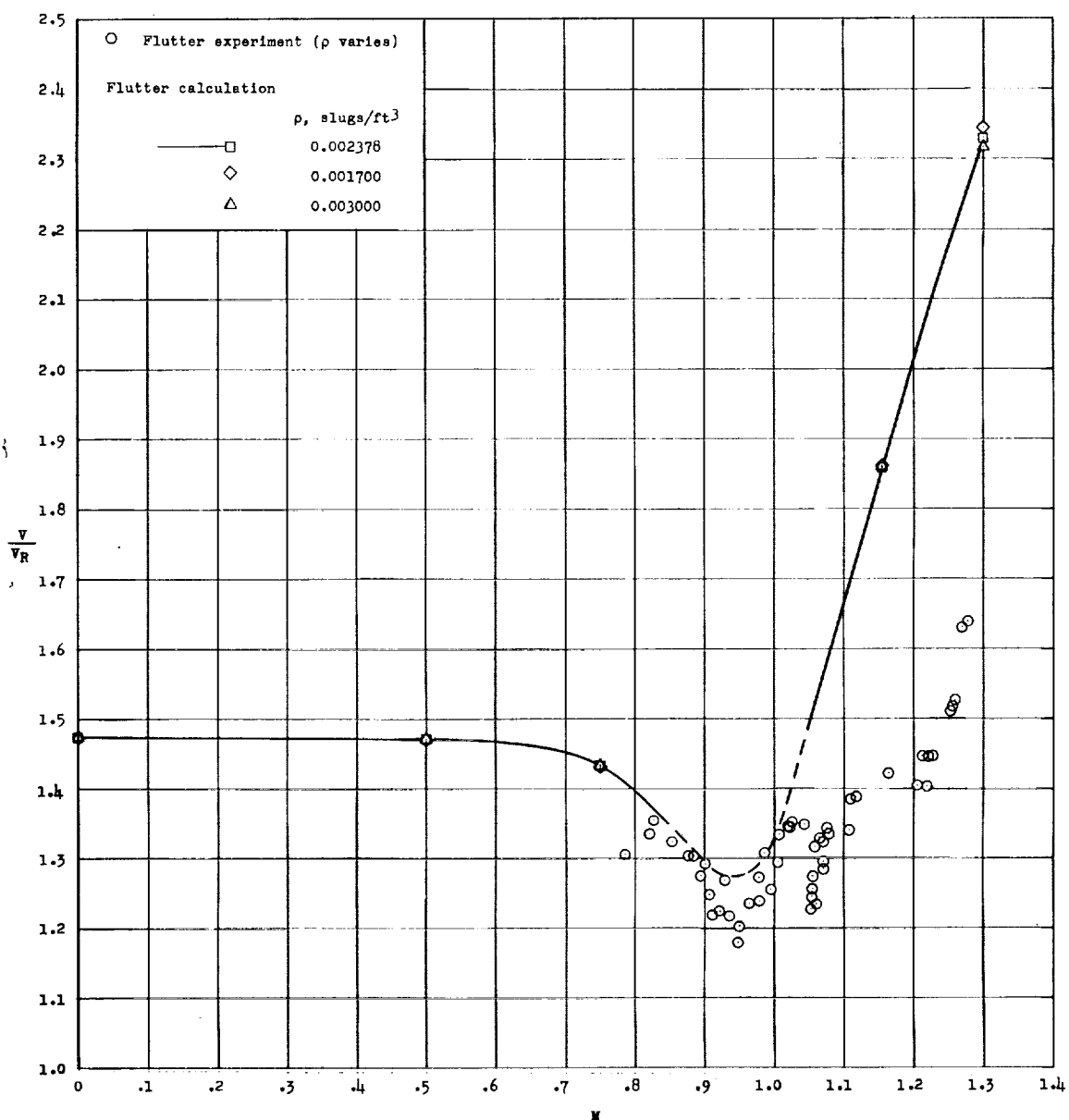
L-464
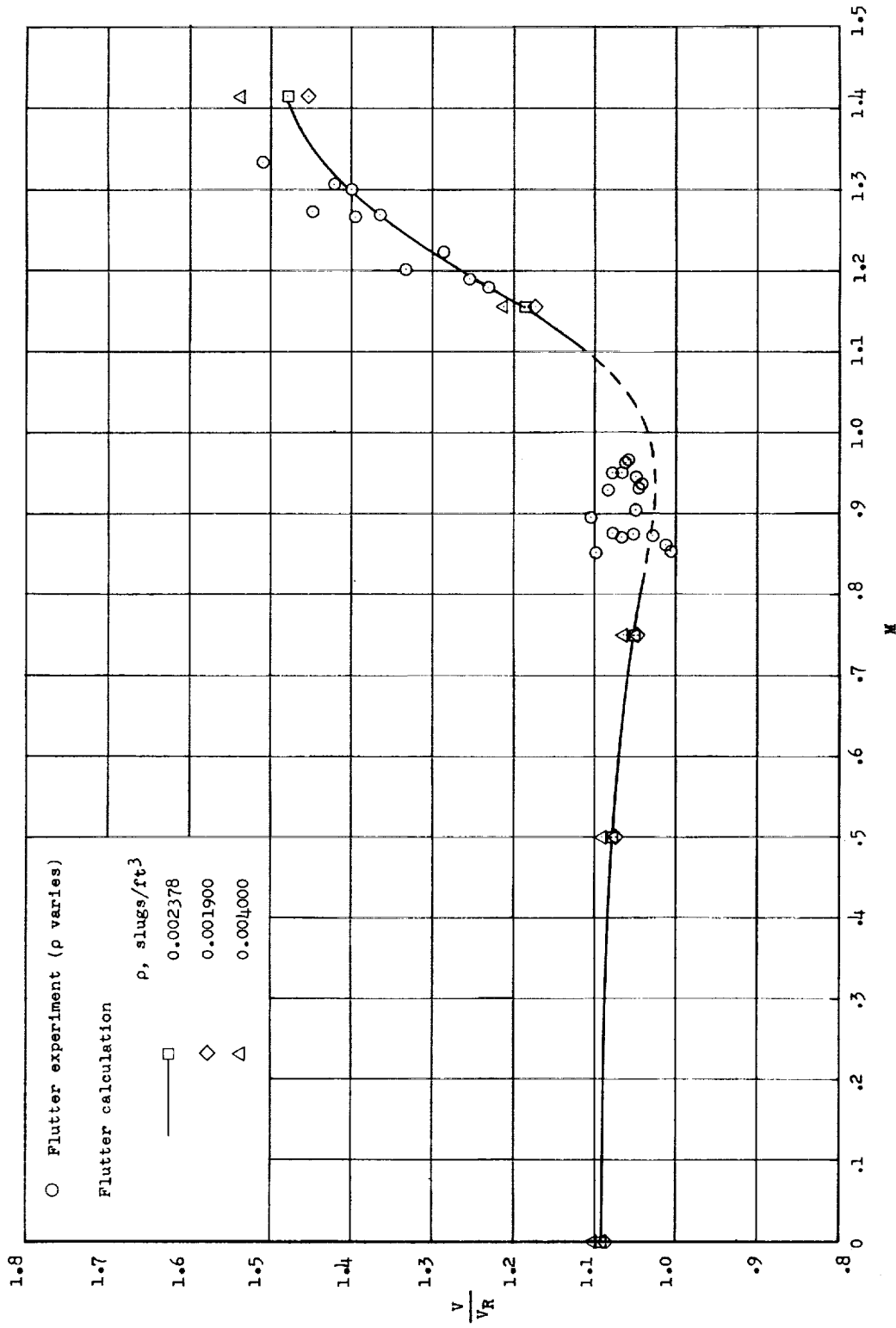
Figure 83.- Effect of density changes on the variation of flutter-speed ratio with Mach number for wing 445R. V and V_R are both calculated for the density indicated.
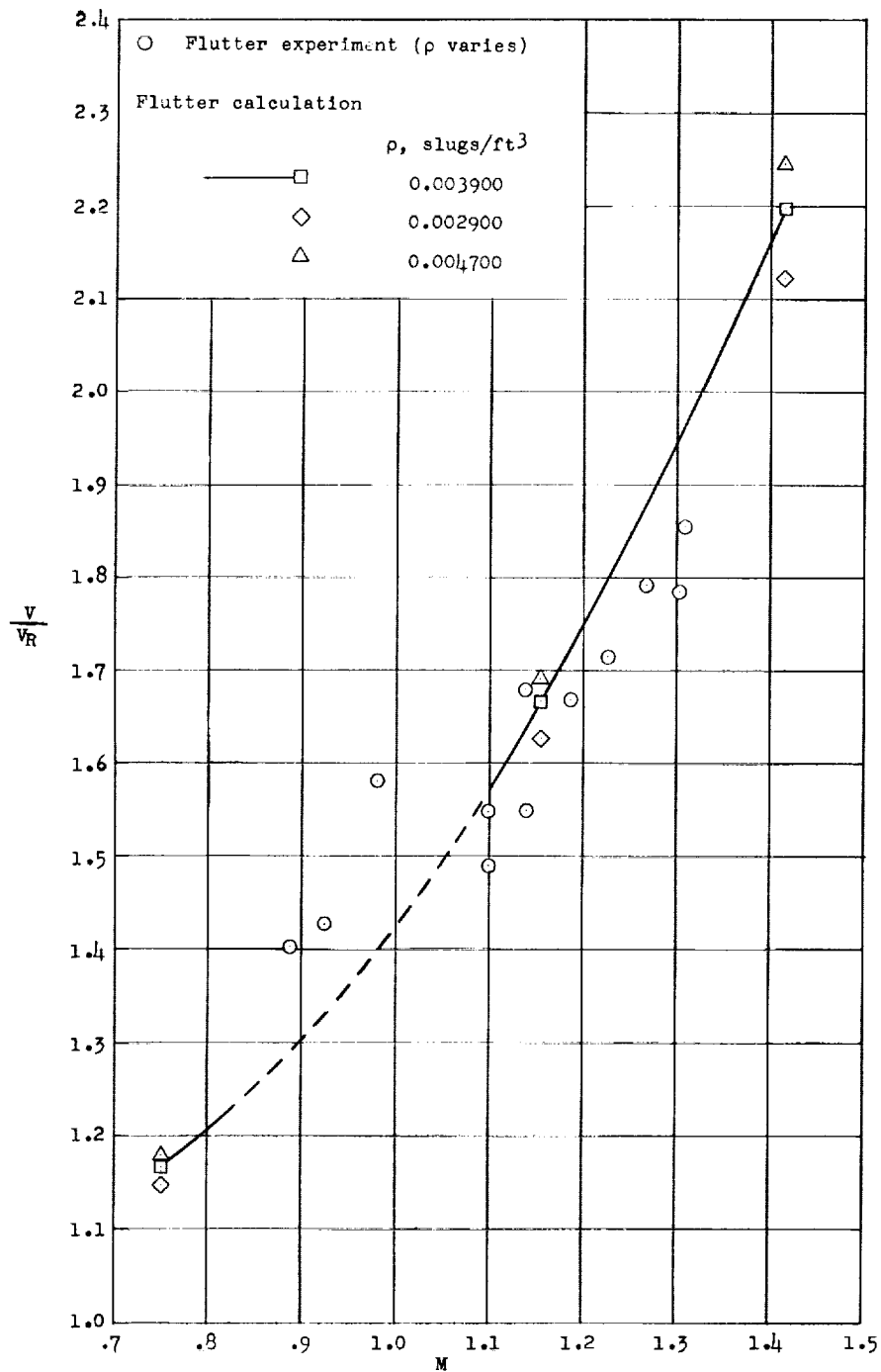
Figure 84.- Effect of density changes on the variation of flutter-speed
ratio with Mach number for wing 245. V and V_R are both calculated
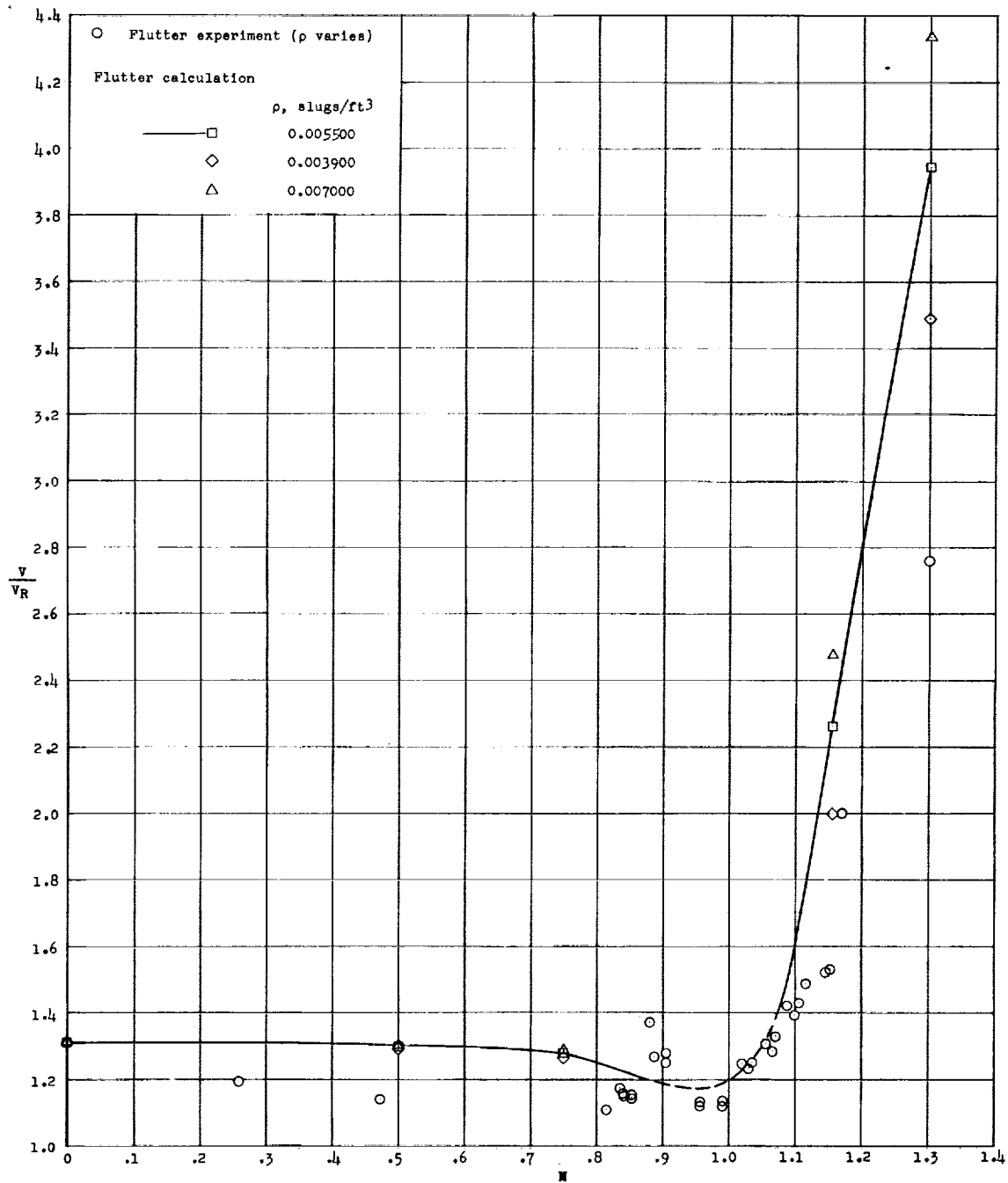for the density indicated.

L-464
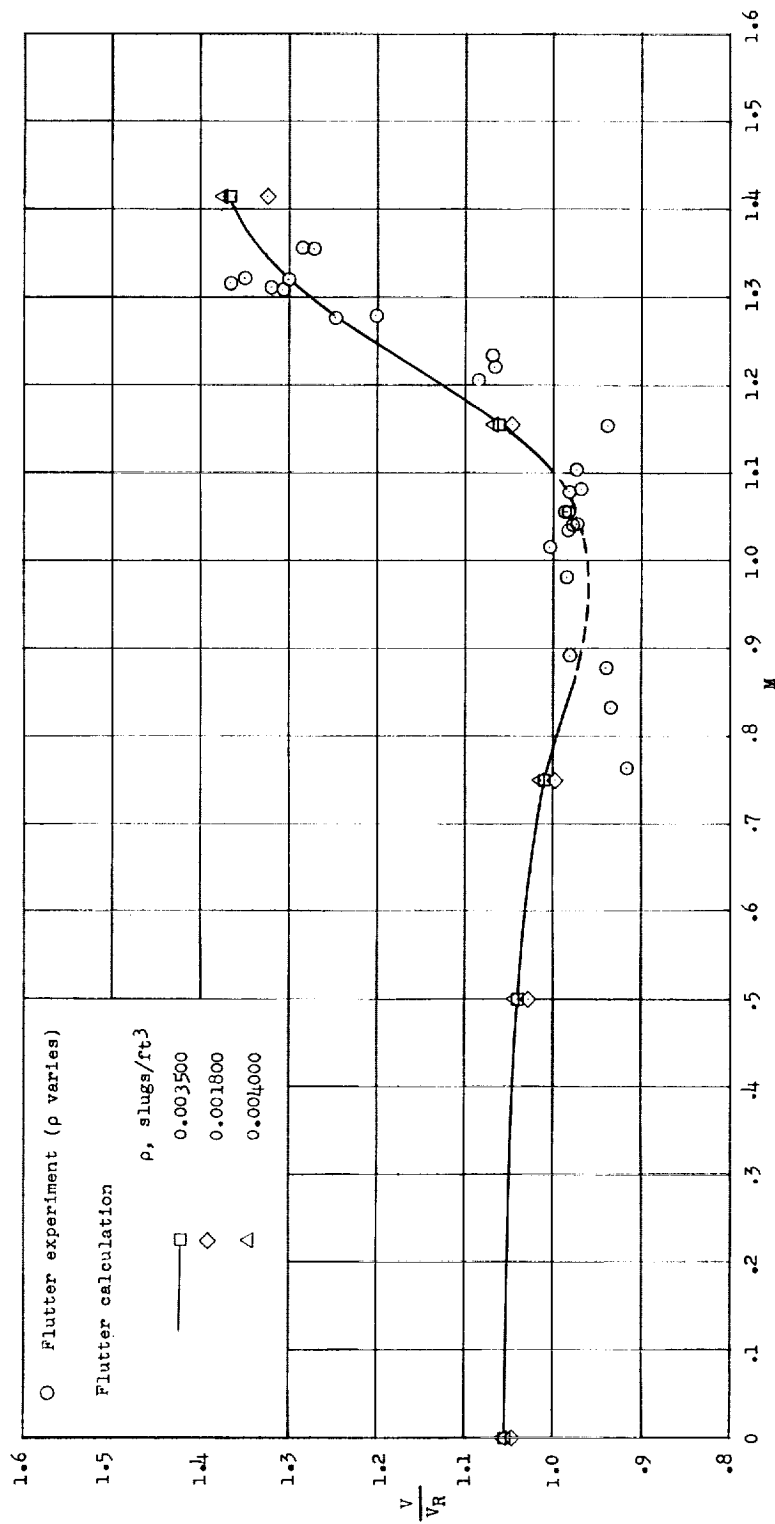
Figure 85.- Effect of density changes on the variation of flutter-speed ratio with Mach number for wing 645. V and V_R are both calculated for the density indicated.
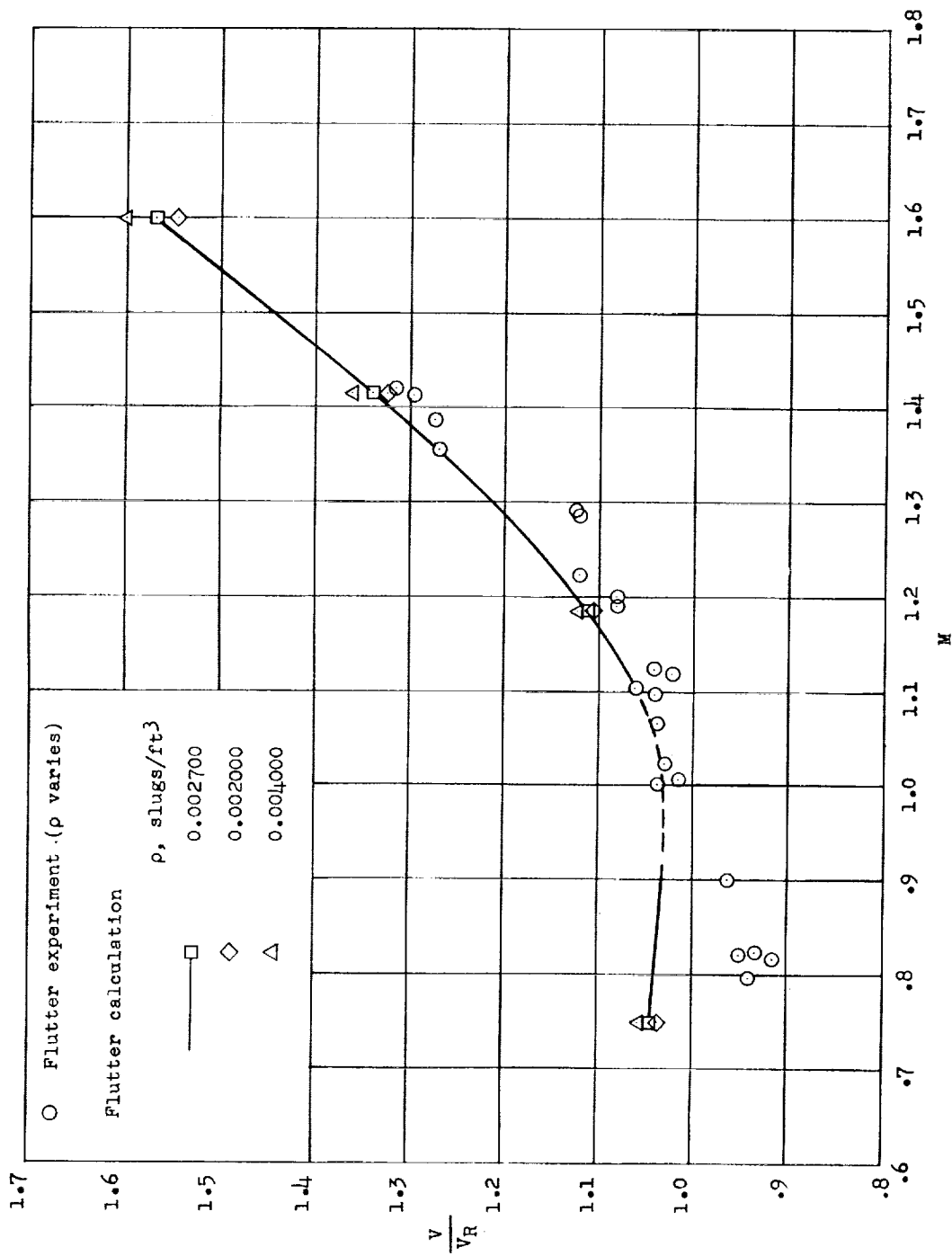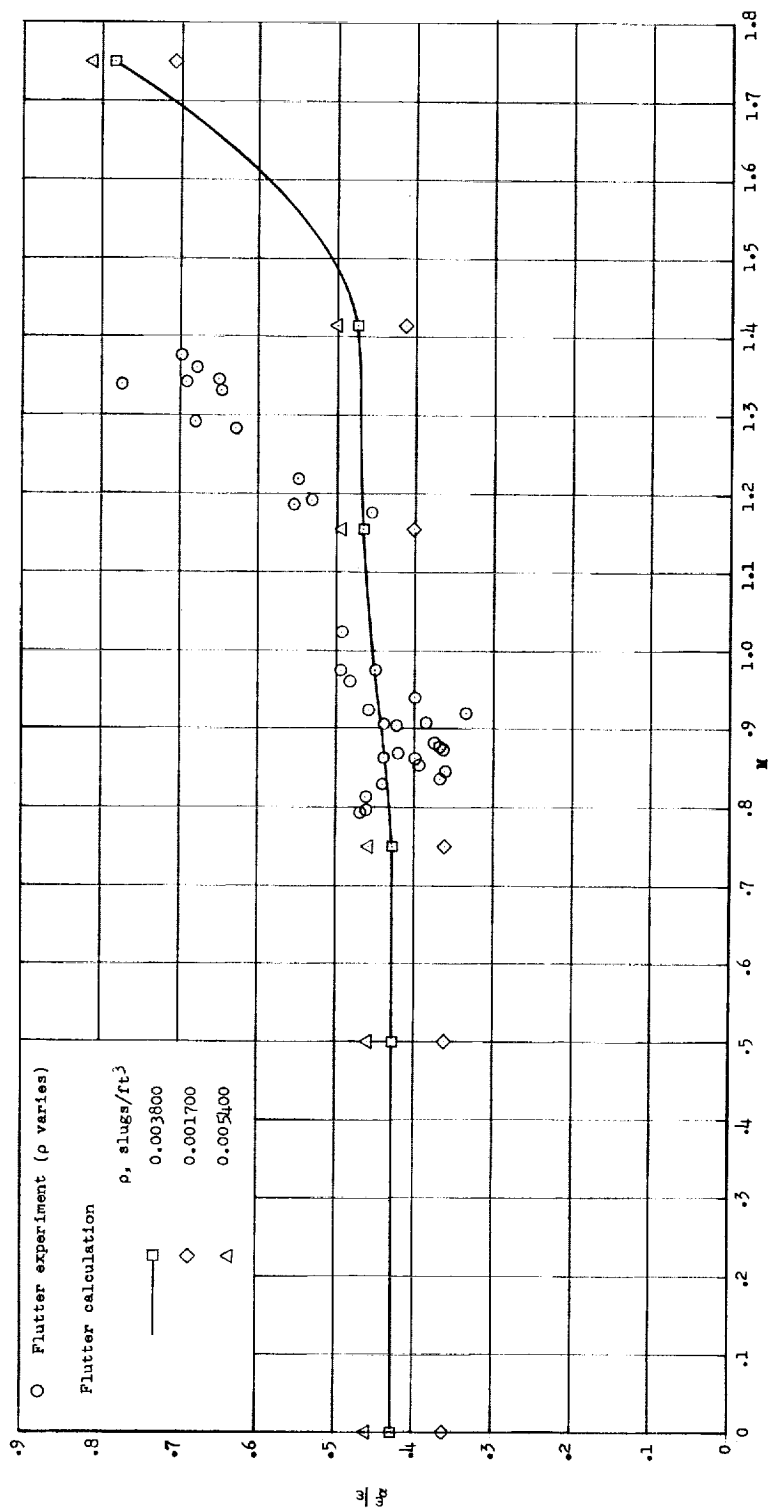
Figure 86.- Effect of density changes on the variation of flutter-speed ratio with Mach number for wing 452. V and V_R are both calculated for the density indicated.

L-464
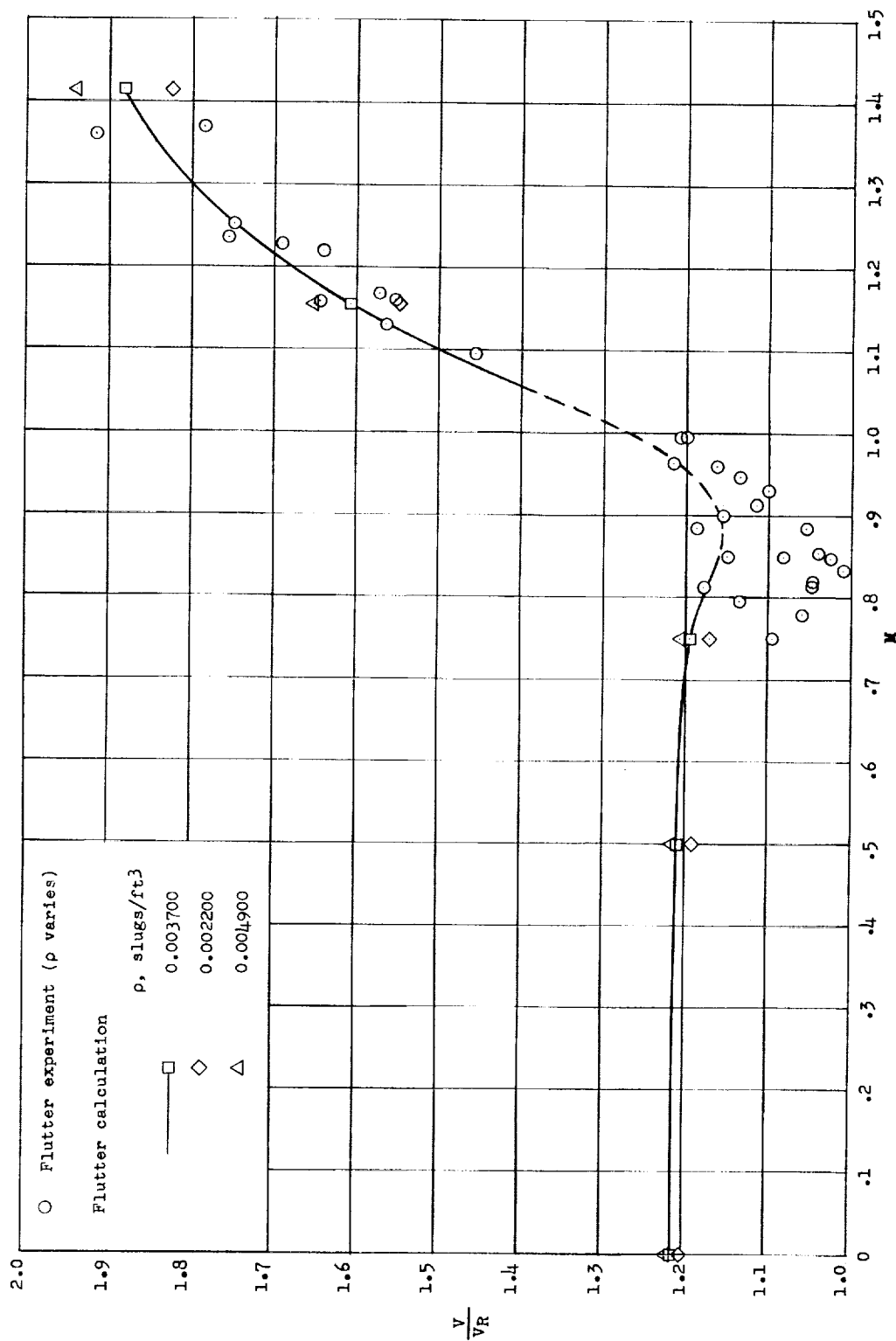
Figure 87.- Effect of density changes on the variation of flutter-speed ratio with Mach number for wing 430. V and V_R are both calculated for the density indicated.

112
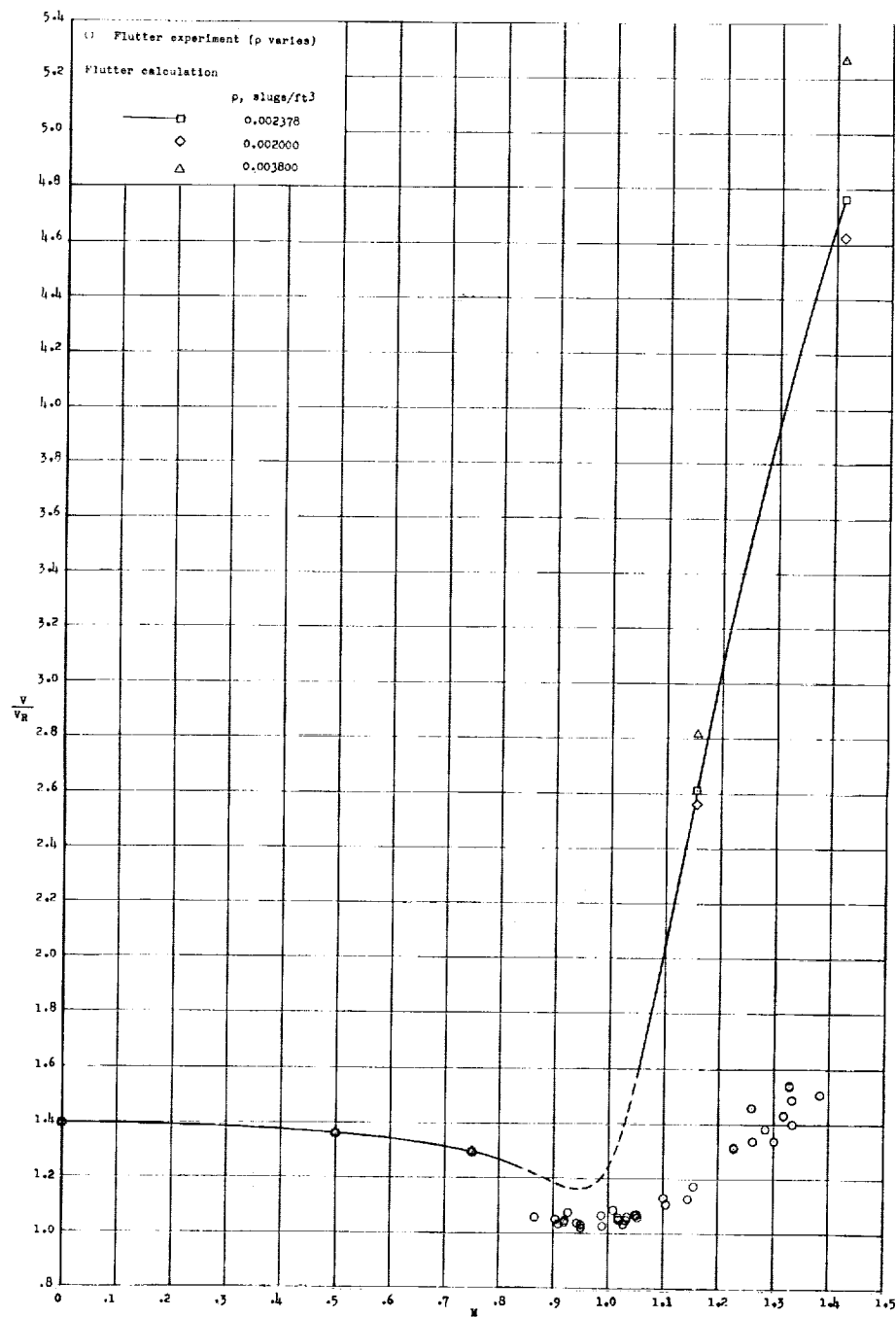
Figure 88.- Effect of density changes on the variation of flutter-speed
ratio with Mach number for wing 400. V and V_R are both calculated
for the density indicated.
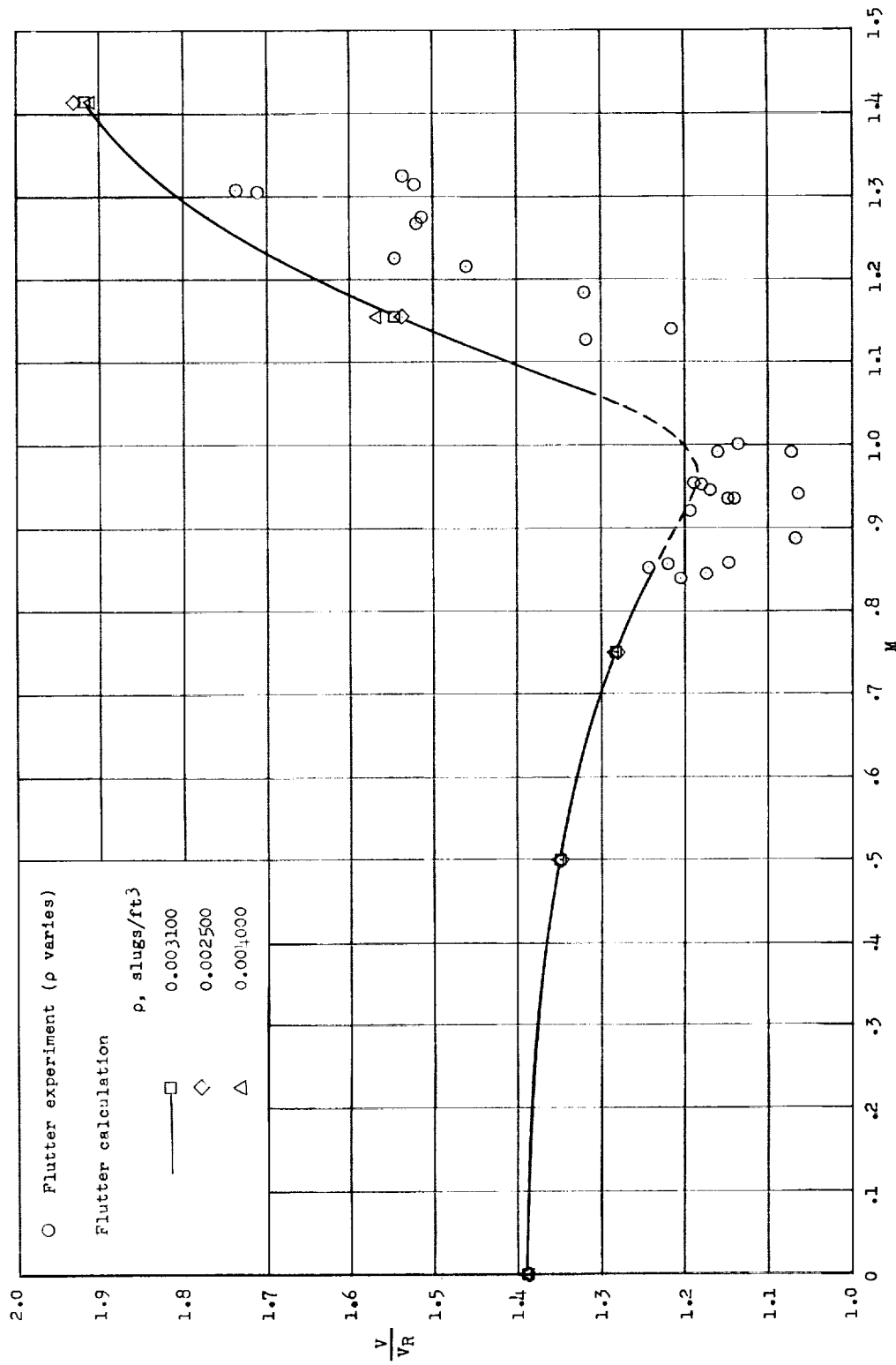
Figure 89.- Effect of density changes on the variation of flutter-speed ratio with Mach number for wing 400R. V and V_R are both calculated for the density indicated.

Figure 90.- Effect of density changes on the variation of flutter-speed ratio with Mach number for wing 4451. V and V_R are both calculated for the density indicated.

Figure 91.- Effect of density changes on the variation of flutter-speed ratio with Mach number for wing 4001. V and V_R are both calculated for the density indicated.

Figure 92.- Effect of density changes on the variation of flutter-speed
ratio with Mach number for wing 7001. V and V_R are both calcu-
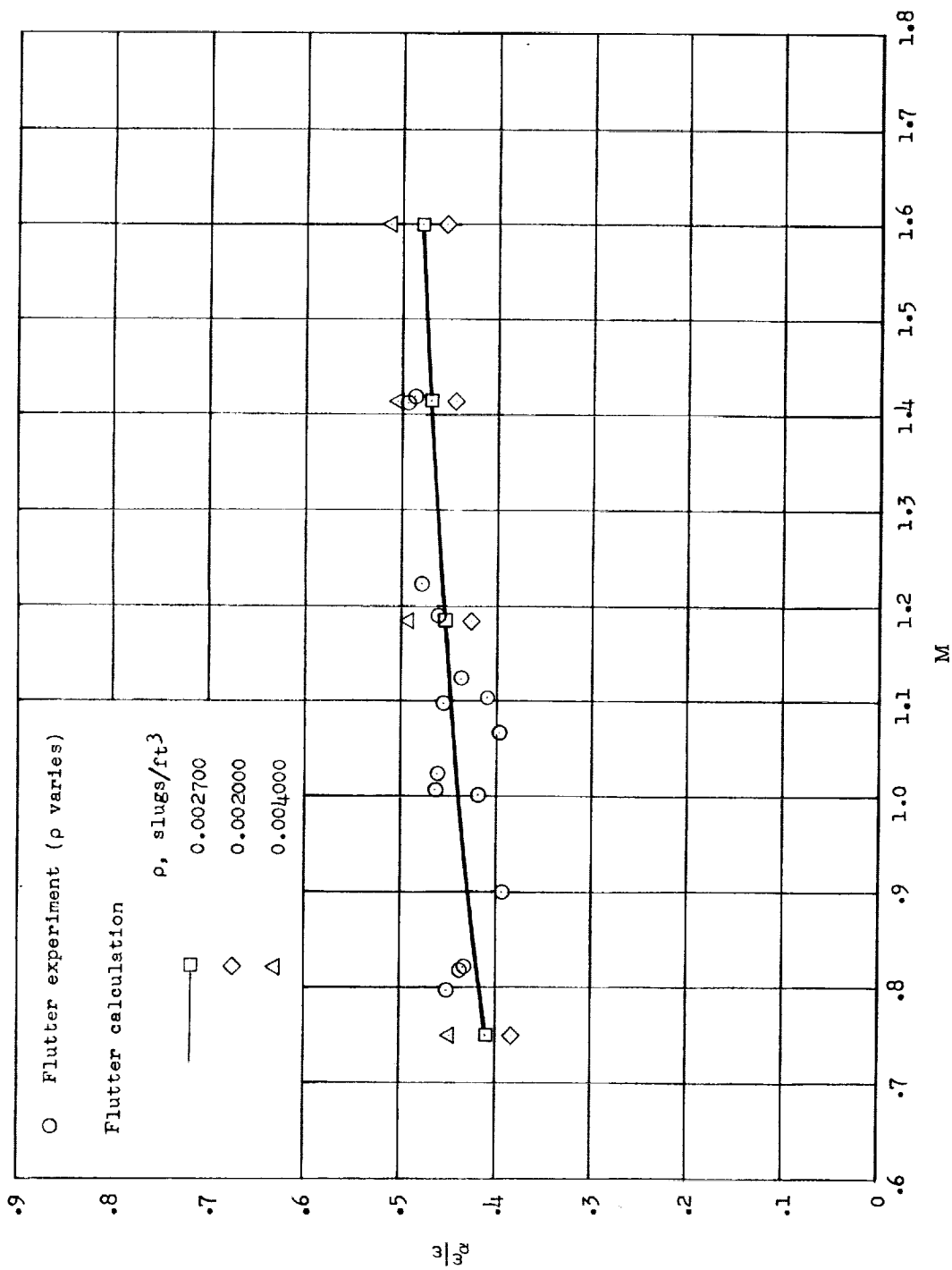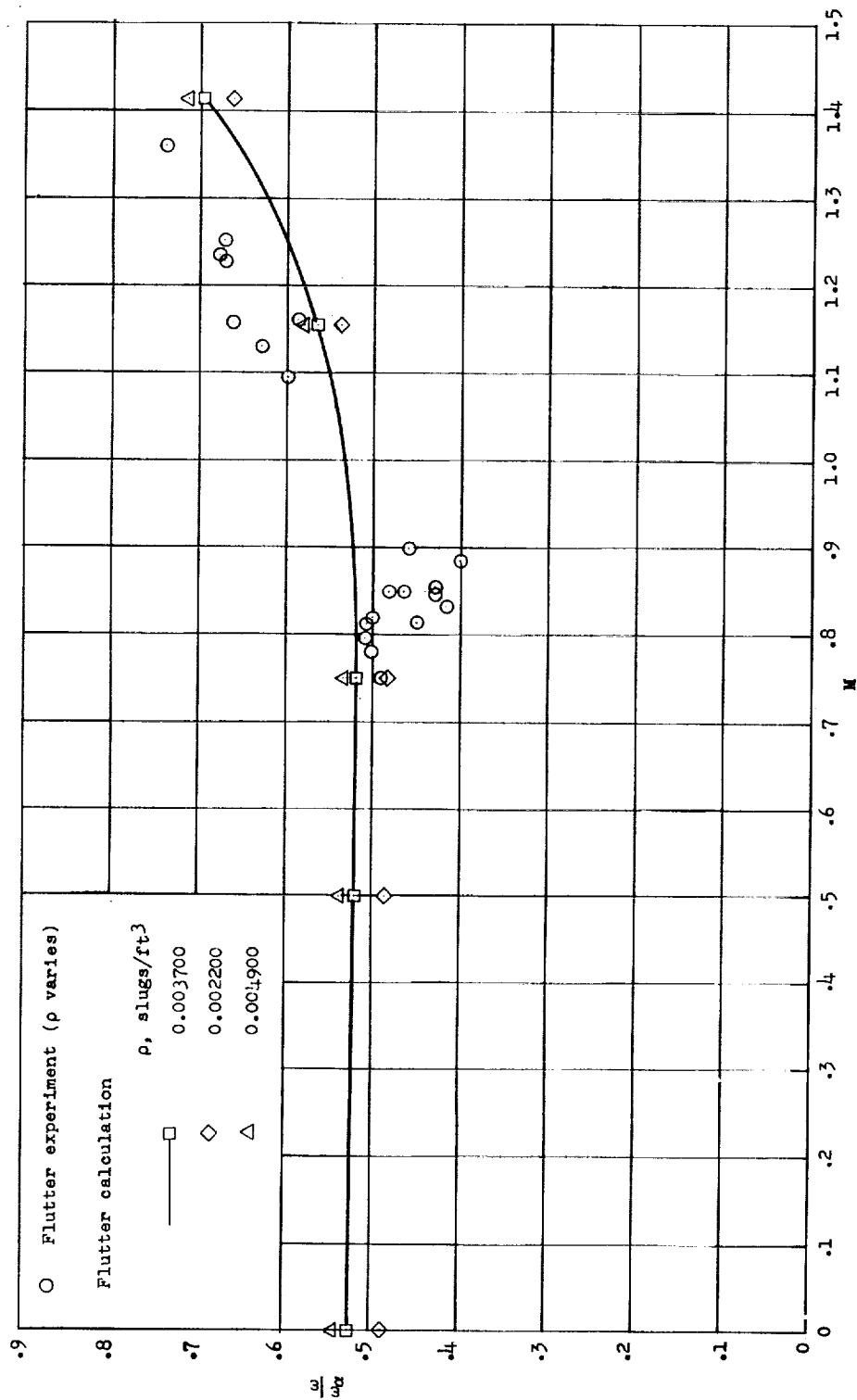lated for the density indicated.

L-464

Figure 93.- Effect of density changes on the variation of flutter frequency with Mach number for wing 445. ω_α = 2,192 radians/sec.
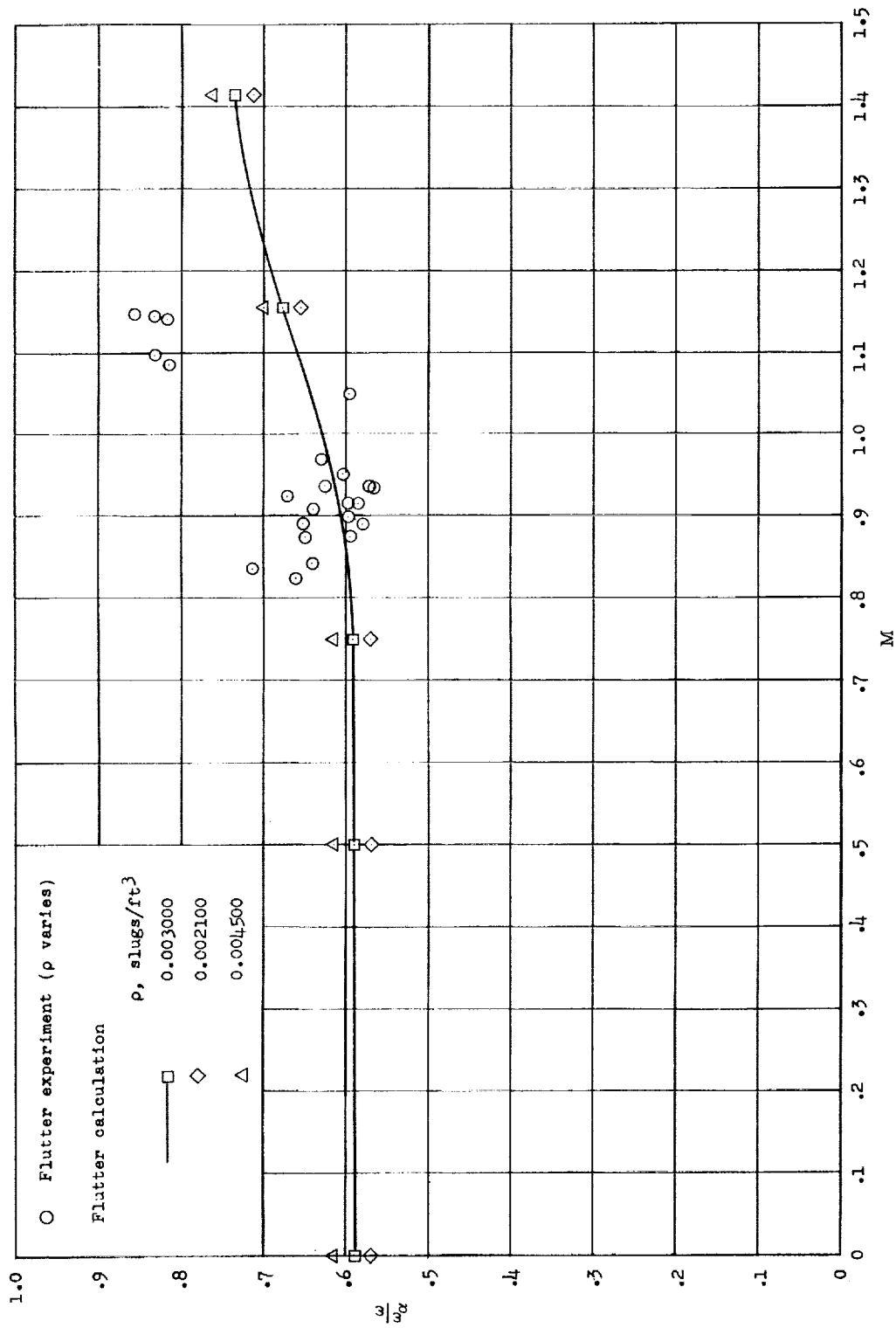
Figure 94.- Effect of density changes on the variation of flutter frequency with Mach number for wing 445F. $\omega_\alpha = 1,144$ radians/sec.

L-464
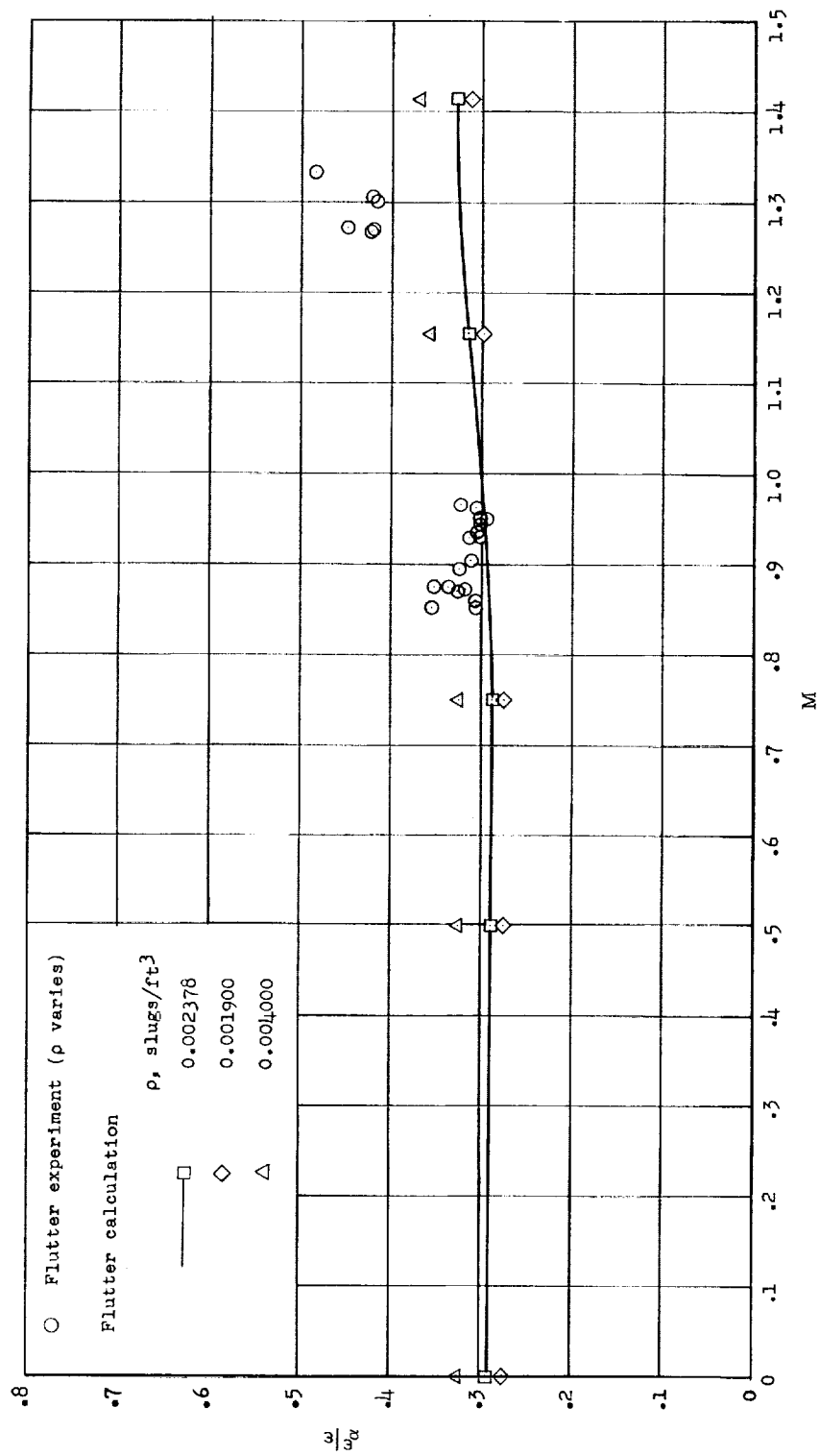
Figure 95.- Effect of density changes on the variation of flutter frequency with Mach number for wing 445R. ω_α = 2,306 radians/sec.
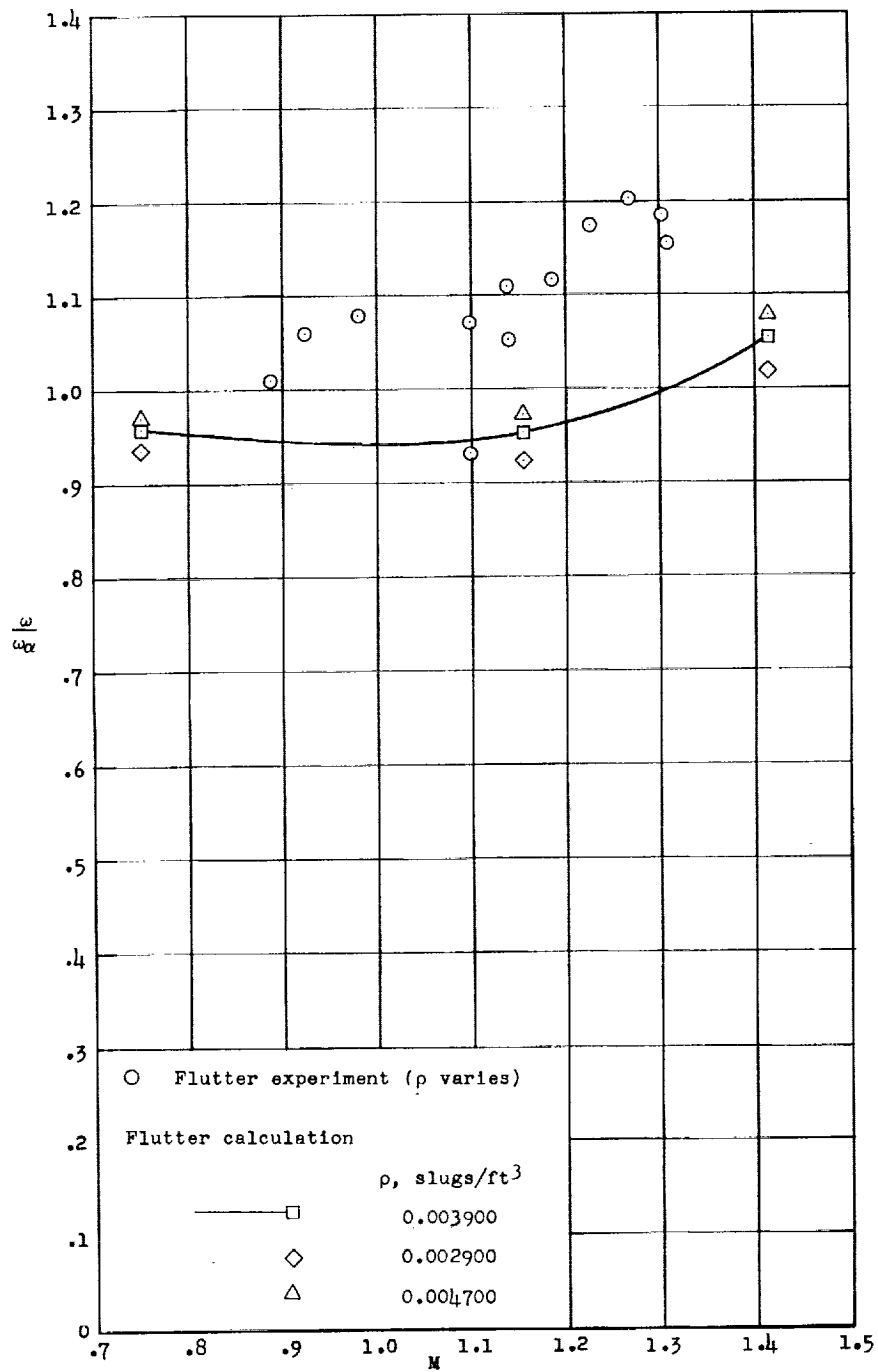
Figure 96.- Effect of density changes on the variation of flutter frequency with Mach number for wing 245. ω_α = 1,665 radians/sec.
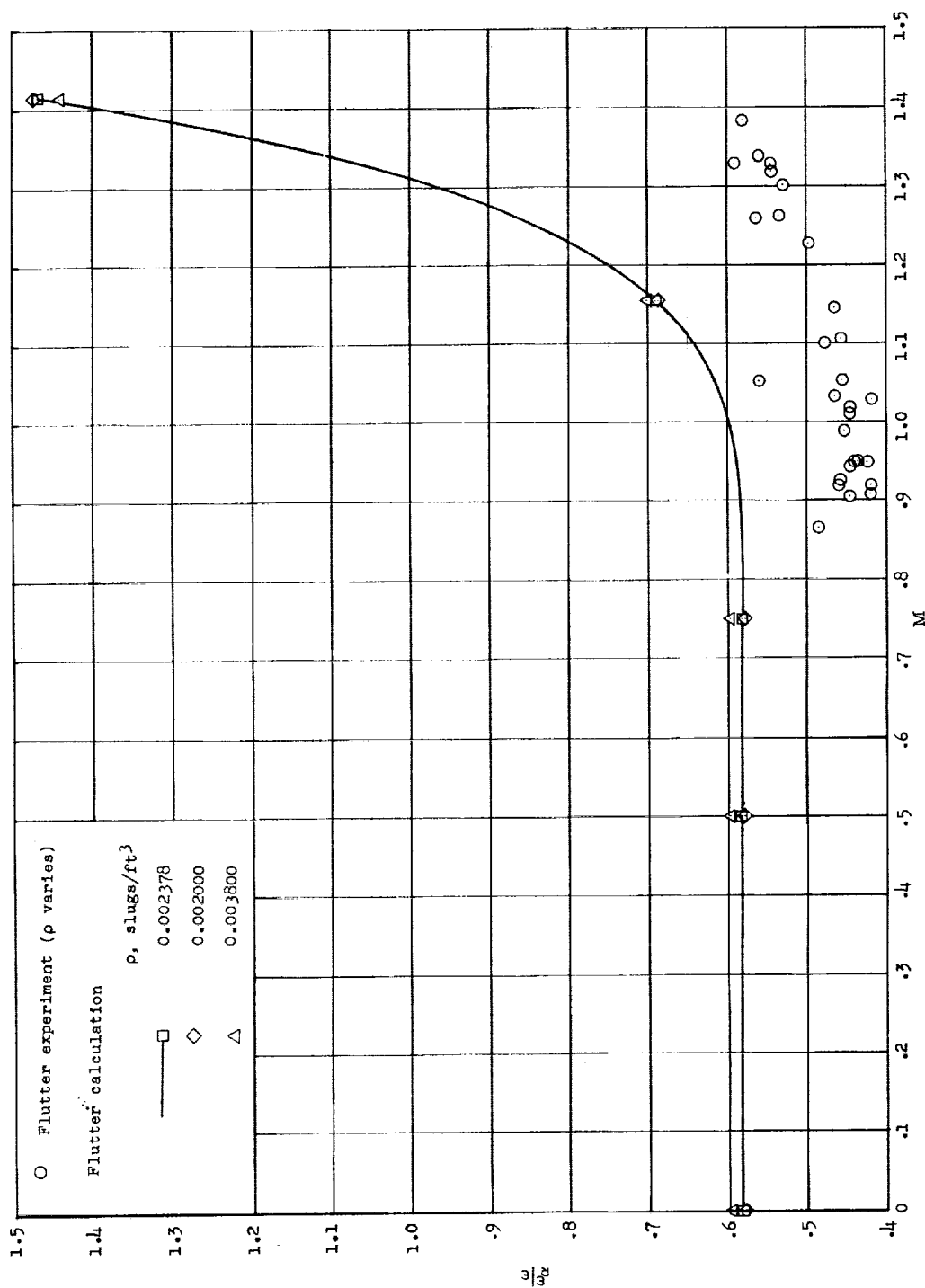
L-464
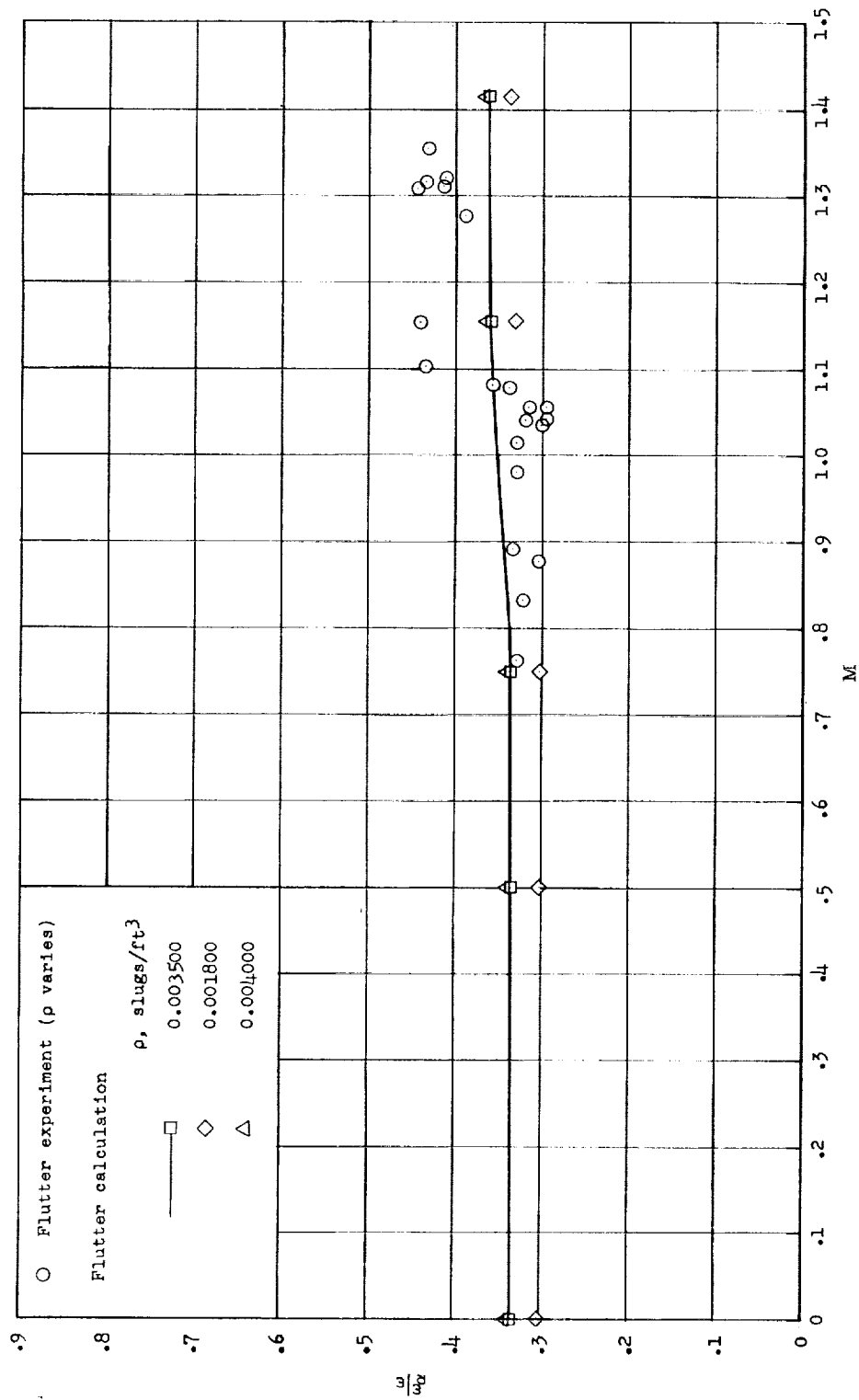
Figure 97.- Effect of density changes on the variation of flutter frequency with Mach number for wing 645. $\omega_\alpha = 3{,}173$ radians/sec.

Figure 98.- Effect of density changes on the variation of flutter frequency with Mach number for wing 452. $\omega_\alpha = 2,300$ radians/sec.
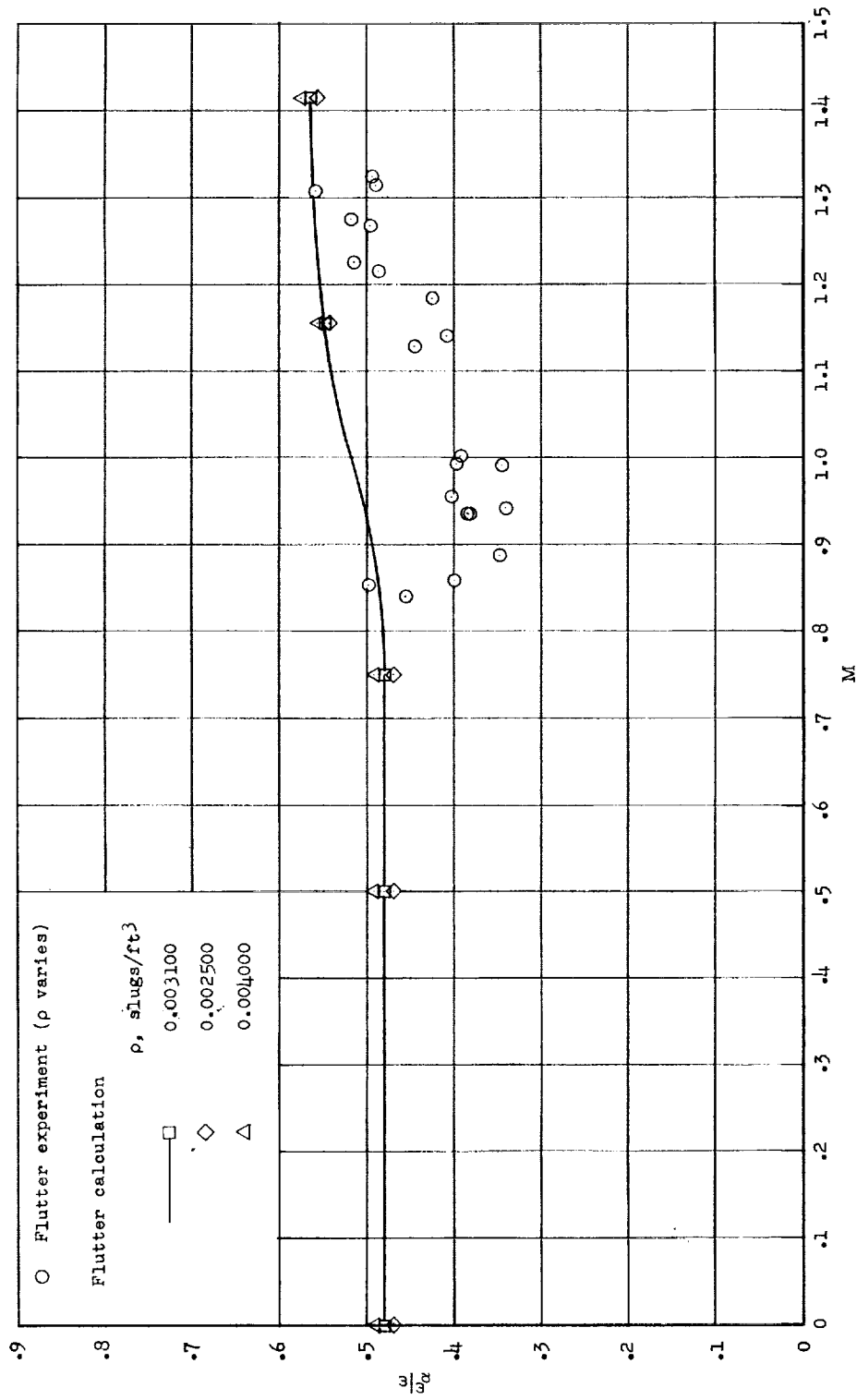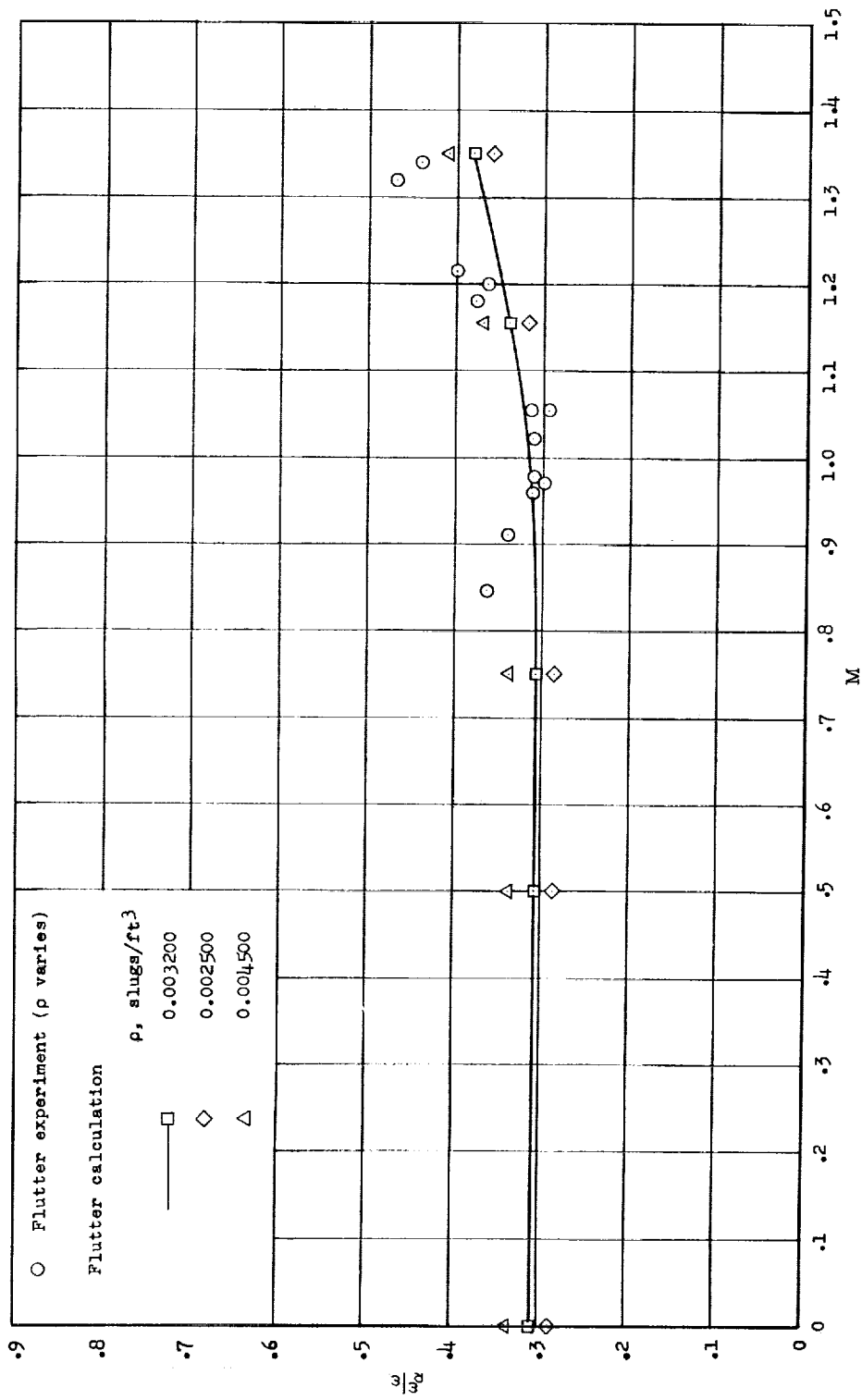
L-464

Figure 99.- Effect of density changes on the variation of flutter frequency with Mach number for wing 430. $\omega_\alpha = 2{,}158$ radians/sec.

Figure 100.- Effect of density changes on the variation of flutter frequency with Mach number for wing 400. $\omega_\alpha = 2,463$ radians/sec.
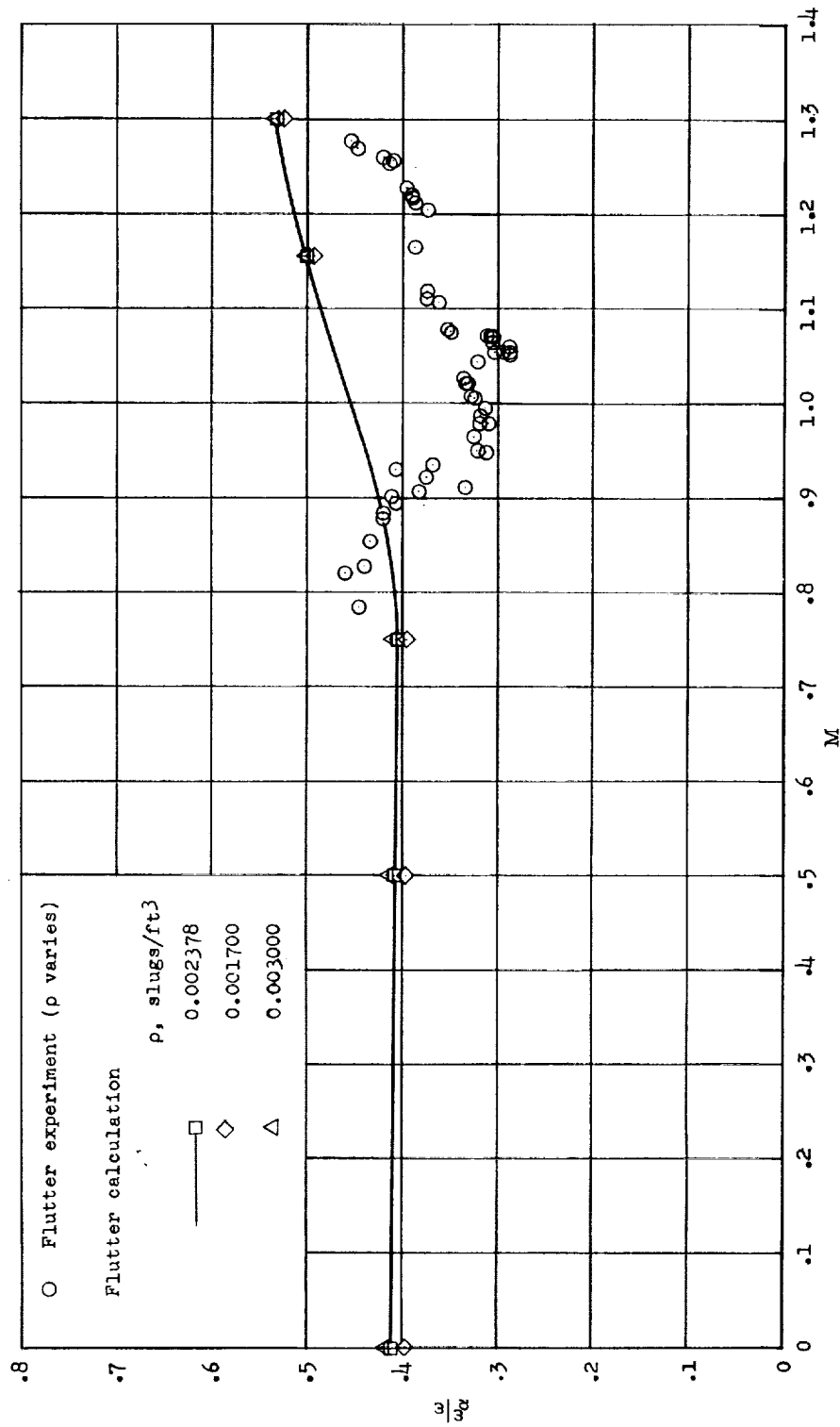
L-464

Figure 101.- Effect of density changes on the variation of flutter frequency with Mach number for wing 400R. $\omega_\alpha = 1,982$ radians/sec.

Figure 102.- Effect of density changes on the variation of flutter frequency with Mach number for wing 4451. $\omega_\alpha = 2,352$ radians/sec.

Figure 103.- Effect of density changes on the variation of flutter frequency with Mach number for wing 4001. $\omega_\alpha = 2,048$ radians/sec.
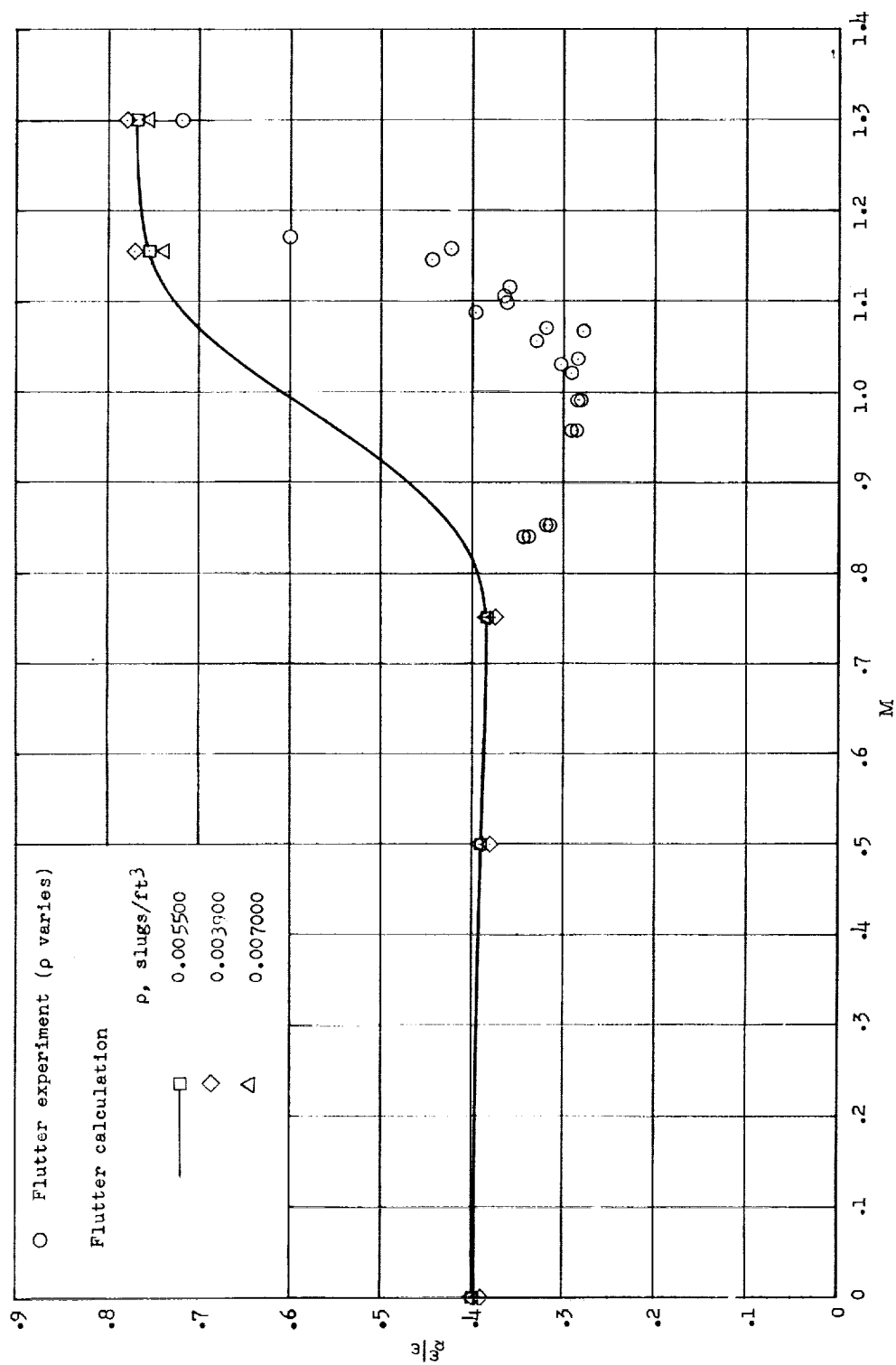
128

Figure 104.— Effect of density changes on the variation of flutter frequency with Mach number for wing 7001. $\omega_\alpha = 2{,}271$ radians/sec.
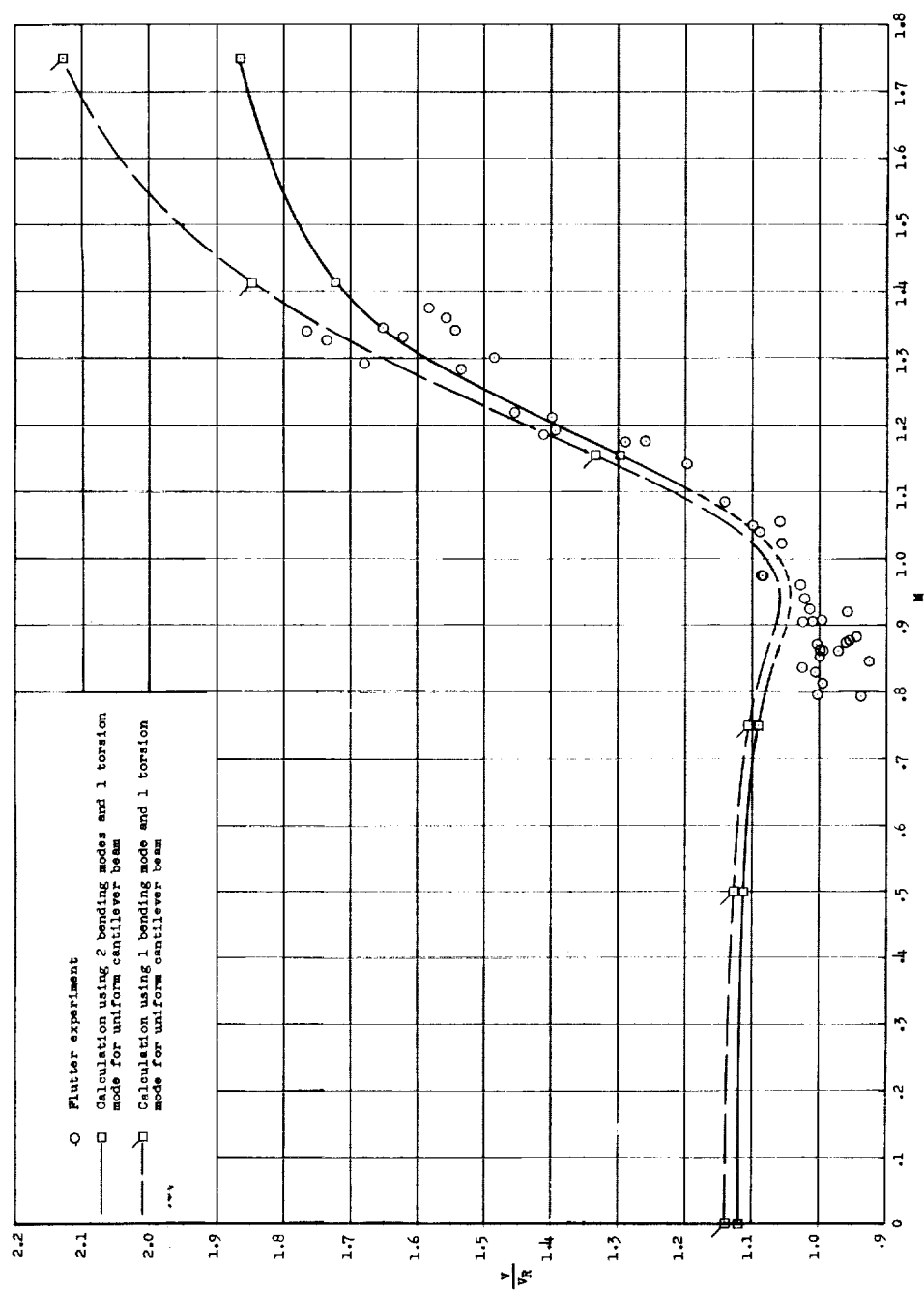
L-464

L-464

Figure 105.- Effect on calculated flutter speed of the number of modes employed. Wing 445; $\frac{\omega_{h_1}}{\omega_\alpha} = 0.1876$; $\frac{\omega_{h_2}}{\omega_\alpha} = 1.037$; V_R (three modes) = 735.0 ft/sec; V_R (two modes) = 762.6 ft/sec.
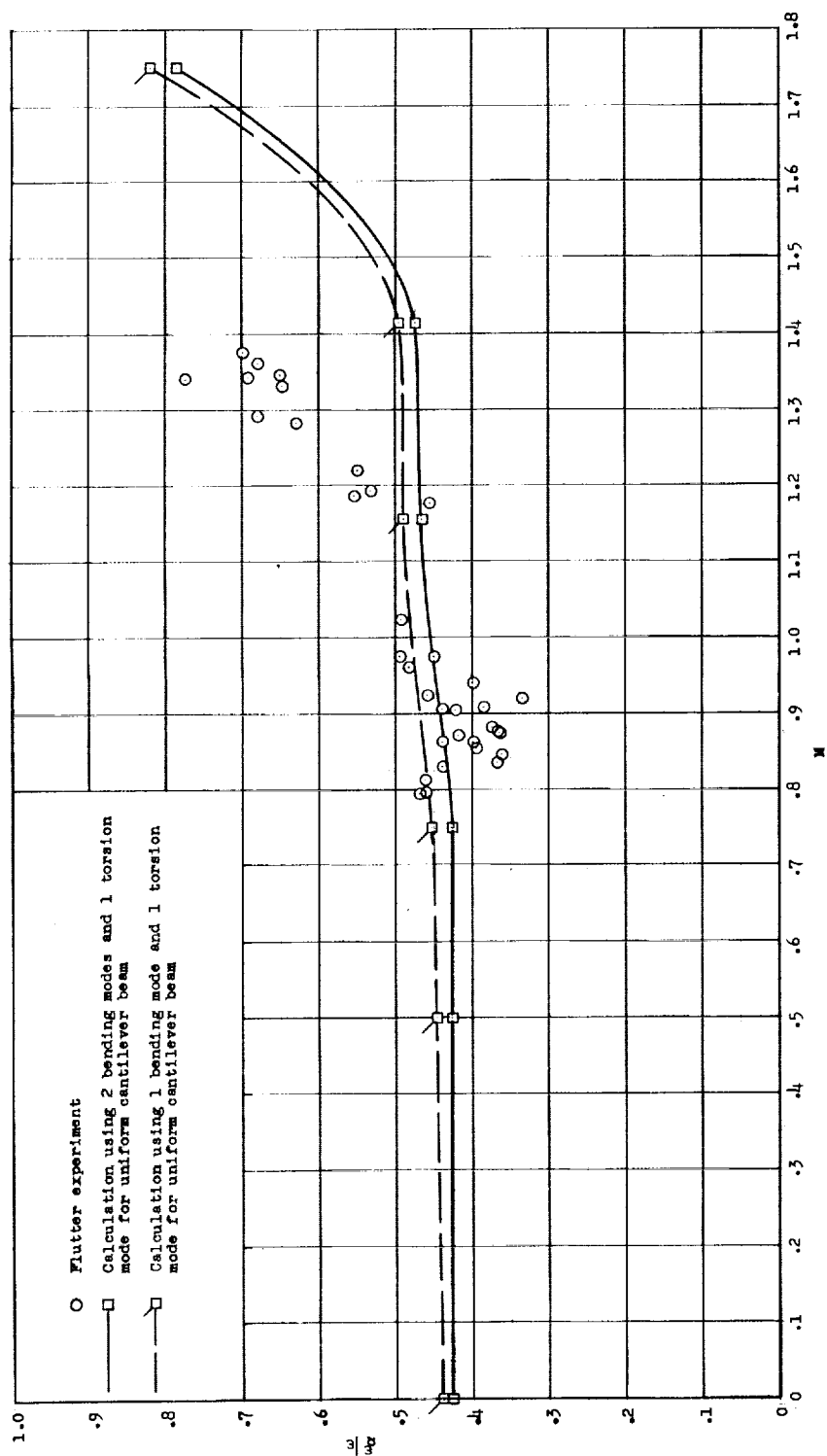
Figure 106.- Effect on calculated flutter frequency of the number of modes employed. Wing 445;

$$\frac{\omega_{h_1}}{\omega_\alpha} = 0.1876; \quad \frac{\omega_{h_2}}{\omega_\alpha} = 1.037; \quad \omega_\alpha = 2,192 \text{ radians/sec.}$$

L-464